

---

The University of Melbourne

Doctor of Philosophy

---

The electrochemical regeneration of  
granular activated carbons *in situ* of  
permeable reactive barriers

---

Rebecca Victoria McQuillan

0000-0003-4147-8353

A thesis submitted in total fulfilment of the requirements for the  
degree of Doctor of Philosophy

Department of Chemical Engineering

February 2021

---

---

---

---

## Abstract

Permeable reactive barriers have proven to be an effective and cost efficient remediation technique for the clean-up of petroleum hydrocarbon contaminated sites in extreme regions such as the Antarctic. The materials within these barriers, namely granular activated carbon, decontaminate migrating groundwaters via adsorption processes and prevent further spread of pollutants into the environment. However, with long operational periods, the activated carbon becomes saturated and is no longer effective at capturing contaminants. In an effort to prevent this, this thesis investigated the possibility of using *in situ* electrochemical treatments as a means of regenerating the activated carbon in these barriers such that the continuous replacement of saturated material is not necessary.

Aqueous phase studies were first conducted to assess which electrochemical reactions aid in the degradation of solubilized petroleum hydrocarbons. Due to the natural presence of chloride and iron at the contaminated sites in the Antarctic and sub-Antarctic, the active chlorine and electro-Fenton pathways were chosen. Similarly, naphthalene, a high priority pollutant for removal in these regions, was chosen as a model compound to investigate the efficacy of the selected reactions. Upon application of an electric current in a near-saturated naphthalene solution, both reaction pathways achieved full contaminant removal within 3 hours of treatment. Further analysis showed that the naphthalene was electrochemically transformed into species of lesser toxicity with minimal energy usage that is appropriate for use in remote regions. Varying operational conditions were assessed to determine the underlying mechanism for which naphthalene was removed, and a dynamic kinetic model was developed for each reaction that could accurately predict treatment outcomes over a range of reagent concentrations, treatment timeframes, and applied electric currents.

Due to the success for which the active chlorine and electro-Fenton pathways degraded naphthalene in the aqueous phase, the reactions were applied to naphthalene loaded granular activated carbon to determine the extent of regeneration that could be achieved. Regardless of the reaction applied, only 30 % regeneration could be achieved under any of the regenerative trials conducted, indicating that only the exterior surface of the porous granular activated carbon was likely being regenerated. As the micropores within the activated carbon were essentially unaffected by electrochemical treatments, macroporous or non-porous materials may be better suited for achieving high regeneration efficiencies.

Although complete regeneration of the activated carbon was not reached, the developed technology can still prolong the longevity for which granular activated carbon can perform within permeable reactive barriers; over four cycles of treatment, the exterior surface was continually restored and freed up adsorptive sites for further adsorption processes. Thus, an ideal method for applying electrochemical treatments *in situ* of existing permeable reactive barriers is recommended.



---

### Declaration

I hereby declare that the thesis titled “The electrochemical regeneration of granular activated carbons *in situ* of permeable reactive barriers” has not been previously submitted to any other institution or university. I certify that this thesis is solely comprised of my own work, and all information and literature used have been accurately cited. The thesis is less than 100,000 words in length, exclusive of tables, bibliographies and appendices.

---

Rebecca Victoria McQuillan  
Department of Chemical Engineering  
The University of Melbourne



---

## Publications Arising from This Thesis

### *Journal Articles:*

Chapter 2 has resulted in the following publication:

**R. V. McQuillan**, G.W. Stevens, K.A. Mumford, The electrochemical regeneration of granular activated carbons: A review, *Journal of Hazardous Materials*, 355 (2018) 34–49.

Chapter 4 has resulted in the following publication:

**R. V. McQuillan**, G.W. Stevens, K.A. Mumford, Electrochemical removal of naphthalene from contaminated waters using carbon electrodes, and viability for environmental deployment, *Journal of Hazardous Materials*, 383 (2020) 121244.

Chapter 5 has resulted in the following publication:

**R. V. McQuillan**, G.W. Stevens, K.A. Mumford, Assessment of the electro-Fenton pathway for the removal of naphthalene from contaminated waters in remote regions, *Science of the Total Environment*, 762 (2021) 143155.

### *Conference Presentations:*

**R. V. McQuillan**, G.W. Stevens, K.A. Mumford, Electrochemical regeneration of adsorbent materials within permeable reactive barriers, presented at the International Conference on Ion Exchange (ICIE). (2018) Yogyakarta, Indonesia

---

---



---

## Acknowledgements

I would first like to express my sincere gratitude to my principle supervisor, Professor Geoffrey W. Stevens. Although the PhD has been difficult, your knowledge and sense of humour have made the past few years an incredibly fun learning experience, both inside and outside of the PhD. I cannot thank you enough for all of your invaluable support and guidance, for reminding me of what is important, and for continuing to inspire and challenge me. I would also like to express my appreciation to my co-supervisor, Associate Professor Kathryn A. Mumford, for always supporting me in my endeavours. Thank you for always being in my corner and for introducing me to your passions for environmental sustainability and remediation; it has made this PhD a once in a lifetime opportunity. I am incredibly appreciative of your guidance throughout this work and for helping me transition into the next phase of my career. To my committee chair, Professor David Shallcross, thank you for your continuous support and feedback.

To all of my colleagues in the Department of Chemical Engineering, thank you for making this journey memorable. I would like to especially acknowledge Jack Churchill for his friendship, enthusiastic presence in the lengthy lab and office hours endured, and for his continuous insight and laughter over the last few years. Additional thanks go to Dr Alex Duan and Dr Augustine Doronila for all of your analytical assistance, and to Michael Zammit for your help in fabricating experimental devices.

To the members of the remediation team at the Australian Antarctic Division, I also extend a huge thanks. I especially recognize Tim Spedding for kindly welcoming me into your team, Greg Hince and Dr. Lauren Wise for all of your help with laboratory equipment and data analysis, Robbie Kilpatrick and Jeremey Richardson for making Macquarie Island a smooth and unforgettable experience, and Deborah Terry for all of the support and fun you provided at Casey Station. It has been an absolute pleasure working with all of you. I would also like to acknowledge the financial support of the Australian Antarctic Science projects 4029 and 4036 and the Melbourne Research Scholarship.

And lastly, to all of my family and friends in both Australia and the United States who have stood by me and provided me with encouragement when I needed it most. I am especially grateful to my parents, David and Camille, who have supported me in my studies abroad and provided me with feedback, insight, and unconditional love. To Caris, I could not have endured the many obstacles I faced without your companionship, spirited nature, and unrelentless love; for that I extend my deepest gratitude.



---

## Table of Contents

Abstract .....	i
Declaration .....	iii
Publications Arising from This thesis.....	v
Acknowledgements .....	vii
Table of Contents .....	ix
List of Figures .....	xv
List of Tables.....	xix
<b>1 Introduction .....</b>	<b>1</b>
1.1 Introduction.....	3
1.2 Background Literature.....	5
1.2.1 Antarctic Petroleum .....	5
1.2.2 Antarctic PRB Material .....	6
1.3 Methods of GAC Regeneration .....	7
1.3.1 Thermal .....	7
1.3.2 Chemical .....	8
1.3.3 Microbial .....	8
1.3.4 Electrochemical .....	9
1.3.5 Assessment of Regeneration Techniques .....	10
1.4 Research Objectives .....	10
<b>2 Literature Review.....</b>	<b>13</b>
2.1 Introduction.....	15
2.2 Regenerative Mechanism.....	15
2.2.1 Enhanced Desorption .....	16
2.2.1.1 Effects of pH .....	16
2.2.1.2 Ionized Species .....	17
2.2.1.3 Electrodesorption.....	18
2.2.2 Decomposition of Contaminant Species .....	19
2.2.2.1 Electrochemical Reactions .....	19
2.2.2.2 Desorbed versus Adsorbed Contaminants.....	24
2.2.3 Electrocoagulation .....	28
2.3 Operational Considerations .....	29
2.3.1 Reactor Configuration .....	29

---

2.3.1.1	Fixed Bed .....	29
2.3.1.2	Fluidized Bed .....	31
2.3.1.3	Undivided versus Divided Cell .....	32
2.3.1.4	Cathodic versus Anodic Regeneration .....	32
2.3.2	Operating Parameters .....	34
2.3.2.1	Current Density .....	34
2.3.2.2	Electrolyte .....	38
2.3.2.3	Treatment Time .....	39
2.3.2.4	pH .....	40
2.4	Industrial Application .....	41
2.5	Research Required for Implementation in Antarctic PRBs .....	43
<b>3</b>	<b>Materials and Analytical Methods.....</b>	<b>45</b>
1.1	Chemical Reagents .....	47
3.1	Experimental Materials .....	47
3.1.1	Petroleum Hydrocarbon Source.....	47
3.1.1.1	Laboratory Studies (Naphthalene) .....	47
3.1.1.2	Feasibility Trials (Special Antarctic Blend diesel) .....	48
3.1.2	Granular Activated Carbon.....	49
3.2	Analytical Techniques.....	49
3.2.1	High Performance Liquid Chromatography.....	49
3.2.2	Gas Chromatography – Mass Spectrophotometry.....	49
3.2.3	Gas Chromatography – Flame Ionization Detector.....	50
3.2.4	Ultraviolet / Visible Spectrophotometry.....	50
3.2.5	Sieving .....	50
3.2.6	pH, Oxidation-Reduction Potential, Electrical Conductivity.....	50
<b>4</b>	<b>Electrochemical Treatment of Naphthalene Contaminated Waters via Active Chlorine.....</b>	<b>51</b>
4.1	Introduction.....	53
4.2	Experimental .....	54
4.2.1	Reagents.....	54
4.2.2	Electrochemical Reactor.....	54
4.2.3	Mass Transfer Characterization .....	55
4.2.4	Analytical Methods.....	55

---

4.3	Results and Discussion .....	55
4.3.1	Unenhanced Anodic Oxidation .....	55
4.3.2	Kinetic Model Theory .....	58
4.3.3	Active Chlorine Pathway .....	60
4.3.3.1	Effect of Applied Current.....	60
4.3.3.2	Effect of NaCl Concentration.....	63
4.3.3.3	Energy Requirements .....	65
4.3.3.4	By-Product Identification .....	67
4.4	Conclusions.....	69
<b>5</b>	<b>Electrochemical Treatment of Naphthalene Contaminated Waters via Electro-Fenton .....</b>	<b>71</b>
5.1	Introduction.....	73
5.2	Experimental .....	74
5.2.1	Reagents.....	74
5.2.2	Electrochemical Reactor.....	75
5.2.3	GAC Electrode Fabrication .....	75
5.2.4	Analytical Methods.....	76
5.3	Results and Discussion .....	76
5.3.1	Control Studies .....	76
5.3.1.1	Adsorption.....	76
5.3.1.2	Volatilization.....	77
5.3.1.3	Anodic Oxidation .....	77
5.3.1.4	Aeration.....	78
5.3.1.5	Hydrogen Peroxide Production .....	78
5.3.2	Kinetic Model Theory .....	79
5.3.3	Electro-Fenton Pathway.....	82
5.3.3.1	Effect of Iron Concentration.....	82
5.3.3.2	Effect of Applied Current.....	84
5.3.3.3	Energy Requirements .....	85
5.3.3.4	By-Product Identification .....	89
5.4	Conclusions.....	91
<b>6</b>	<b>Electrochemical Regeneration of Naphthalene Contaminated Granular Activated Carbon.....</b>	<b>93</b>
6.1	Introduction.....	95

---

---

6.2	Experimental .....	96
6.2.1	Reagents .....	96
6.2.2	Desorption Studies .....	96
6.2.3	Electrodesorption Studies .....	97
6.2.4	Electrochemical Regeneration Reactor .....	98
6.2.4.1	Calculating Regeneration Efficiency .....	99
6.2.5	GAC Electrical Conductivity .....	100
6.2.6	Analytical Methods .....	101
6.3	Results and Discussion .....	101
6.3.1	Desorption .....	101
6.3.2	Electrodesorption .....	102
6.3.3	Adsorption Isotherm .....	102
6.3.4	GAC Conductivity .....	104
6.3.5	Electrochemical Regeneration .....	107
6.3.5.1	Regenerative Treatments .....	107
6.3.6	Kinetic Model .....	117
6.4	Conclusions .....	119

## **7 The Application of Electrochemical Treatments for the Regeneration of Granular Activated Carbon *in situ* of Permeable Reactive Barriers in the Antarctic .....**

121

7.1	Background .....	122
7.2	Electrochemical Treatment Design .....	123
7.2.1	Initial Considerations .....	123
7.2.1.1	Seasonal Timing .....	123
7.2.1.2	Solid Contaminant Loading .....	124
7.2.1.3	Bed Conductivity .....	124
7.2.1.4	Electrochemical Reactions .....	125
7.2.1.5	Electrode Placement .....	126
7.3	Field Trial .....	129
7.3.1	Methodology .....	129
7.3.1.1	Media Sampling .....	129
7.3.1.2	Water Sampling .....	129
7.3.2	Construction .....	130
7.4	Results and Discussion .....	131
7.5	Conclusions .....	134

---

<b>8</b>	<b>Concluding Remarks</b> .....	135
8.1	Thesis Summary .....	137
8.2	Recommendations for Future Work .....	138
	<b>References</b> .....	141
	Appendix A: Supplementary Data .....	159
	Appendix B: Data Analysis .....	163
	Appendix C: MATLAB Code .....	167

---



---

## List of Figures

<b>Figure 1.1:</b> Available techniques used for the remediation of petroleum hydrocarbon spills, as a function of time and cost .....	3
<b>Figure 1.2:</b> Schematic of an in situ PRB capturing a plume of contaminated groundwater.....	4
<b>Figure 1.3:</b> Techniques used for the regeneration of saturated activated carbons .....	7
<b>Figure 2.1:</b> Regenerative mechanisms involved in the electrochemical regeneration of GAC ..	16
<b>Figure 2.2:</b> Representation of the cathodic production of hydroxyl radicals via the Fenton reaction at the cathode surface in the presence of catalytic iron .....	24
<b>Figure 2.3:</b> The evolution of phenol in the aqueous solution as a function of time when electrochemically treating phenol loaded GAC at variable currents .....	25
<b>Figure 2.4:</b> Polarization of adsorbent particles within an electrochemical cell, causing particles to undergo dynamic adsorption, electrochemical oxidation, desorption, and regeneration ...	27
<b>Figure 2.5:</b> Different types of reactor configurations used during the electrochemical treatment of GAC.....	30
<b>Figure 2.6:</b> Typical regeneration efficiency achieved with increasing treatment time .....	40
<b>Figure 2.7:</b> Wastewater treatment system developed by Arvia Technology .....	41
<b>Figure 3.1:</b> Breakdown of petroleum hydrocarbons in the n-C <sub>1</sub> to n-C <sub>40</sub> range .....	48
<b>Figure 4.1:</b> Schematic of the electrochemical cell used.....	55
<b>Figure 4.2:</b> Naphthalene evolution as a function of time when treated at 0 and 40 mA of electric current.....	57
<b>Figure 4.3:</b> Current-voltage curve for the electrochemical cell when scanning from 0 – 5 V. ...	59
<b>Figure 4.4:</b> Normalized naphthalene concentration versus time at varying applied electric currents .....	61
<b>Figure 4.5:</b> Model predictions of active chlorine concentration as a function of time and applied current.....	63
<b>Figure 4.6:</b> Normalized naphthalene concentration as a function of time at varying NaCl electrolyte concentrations .....	64
<b>Figure 4.7:</b> Specific energy consumption when altering the applied current within a 0.1 M NaCl electrolyte and altering the NaCl concentration when operating at a constant applied current of 100 mA .....	66

---

<b>Figure 4.8:</b> Evolution of naphthalene and associated by-products on the resulting HPLC-DAD chromatograms as a function of time during the electrochemical treatment of a naphthalene contaminant solution at 100 mA within a 0.1 M NaCl electrolyte.....	68
<b>Figure 5.1:</b> Schematic of electrochemical cell used for the electrochemical treatment of naphthalene contaminated water .....	75
<b>Figure 5.2:</b> Naphthalene evolution as a function of time when treated within an electrochemical cell at 0 mA (volatilization), 5 mA (anodic oxidation + volatilization), and in the presence of aeration (aeration + anodic oxidation + volatilization) .....	77
<b>Figure 5.3:</b> Hydrogen peroxide production versus time when operating at various electric currents .....	78
<b>Figure 5.4:</b> Normalized naphthalene concentration versus time during the electro-Fenton reaction at varying iron(II) concentrations in a 0.05 M Na <sub>2</sub> SO <sub>4</sub> electrolyte at 5 mA .....	82
<b>Figure 5.5:</b> Comparison of the kinetic model and experimental data describing the % naphthalene removed after 1 hour of treatment at varying iron(II) concentrations. The subplot represents model predictions when volatilization pathways are not considered (i.e. in field deployment applications). .....	84
<b>Figure 5.6:</b> Normalized naphthalene concentration versus time during the electro-Fenton reaction at varying electric currents with a constant iron(II) concentration of 0.1 mM .....	85
<b>Figure 5.7:</b> Specific energy consumption for naphthalene removal when altering the iron(II) concentration at a constant 5 mA of electric current and applied electric current at a constant iron(II) concentration of 0.1 mmolduring the electro-Fenton pathway in a 0.05 M Na <sub>2</sub> SO <sub>4</sub> electrolyte. ....	86
<b>Figure 5.8:</b> Comparison of hydrogen peroxide production against time when utilizing a graphite rod versus a GAC-PVDF electrode .....	88
<b>Figure 5.9:</b> Evolution of naphthalene and associated by-products on the resultant HPLC-DAD chromatograms as a function of time during electro-Fenton treatments at 5 mA and an iron(II) concentration of 0.1 mmol, and the predicted removal timeframes of 1,4-naphthoquinone...	89
<b>Figure 6.1:</b> Schematic diagram of the experimental setup used for electrodesorption tests....	97
<b>Figure 6.2:</b> Schematic diagram of the laboratory scale PRB used for the electrochemical regeneration of GAC.....	98
<b>Figure 6.3:</b> Schematic of the methodology for calculating the regeneration efficiency of electrochemically regenerated GAC .....	99
<b>Figure 6.4:</b> Kinetics of naphthalene adsorption onto GC1200 GAC.....	103

---

---

<b>Figure 6.5:</b> Freundlich, Langmuir and Linear adsorption isotherms describing naphthalene adsorption onto GC1200 GAC .....	104
<b>Figure 6.6:</b> Bed resistance at varying external pressures; the subplot is a zoomed in view of resistances from 1 kPa and above, and the corresponding bed conductivity as a function of externally applied pressure.....	105
<b>Figure 6.7:</b> Conductivity of GAC as a function of bed density .....	106
<b>Figure 6.8:</b> Regeneration efficiencies as a function of applied electric current for the active chlorine and electro-Fenton pathways when undergoing two hours of electrochemical treatment .....	108
<b>Figure 6.9:</b> Regeneration efficiencies as a function of time for the active chlorine and electro-Fenton pathways.....	110
<b>Figure 6.10:</b> Schematic of hydroxyl radicals oxidizing adsorbed contaminants in a micropore vs mesopore .....	111
<b>Figure 6.11:</b> Naphthalene batch adsorption data fitted to the three-stage kinetic model .....	112
<b>Figure 6.12:</b> Linearized, first-order decay rates of hydrogen peroxide against time in the presence of varying concentrations of GAC, and the first-order decay rate as a function of GAC concentration.....	114
<b>Figure 6.13:</b> Regeneration over five cycles of adsorption followed by regeneration for the active chlorine and electro-Fenton reaction pathways. The predicted regeneration, assuming the same amount of externally adsorbed naphthalene is removed with each cycle, is also shown .....	115
<b>Figure 6.14:</b> Schematic of how a reduced isotherm underestimates the amount of adsorbate removed from the GAC surface .....	116
<b>Figure 7.1:</b> Schematic of the PRB indicating the materials used within each zone and the flow direction of ground water .....	122
<b>Figure 7.2:</b> Updated zones and materials used within the PRB.....	123
<b>Figure 7.3:</b> Resistivity of the GAC bed when mixed with varying amounts of zeolite .....	125
<b>Figure 7.4:</b> Electric fields for varying electrode arrangements.....	127
<b>Figure 7.5:</b> Relationship between bed resistance and bed length, and relationship between cell voltage and electric current at varying interelectrode distances .....	128
<b>Figure 7.6:</b> Ideal electrode array for obtaining uniform current distribution over a large volume of GAC in situ of a PRB .....	129

---

<b>Figure 7.7:</b> Layout and location of electrodes, electrical connections, and sample points pre- and post-treatment.....	131
<b>Figure 7.8:</b> Pre-treatment solid loadings of TPH and naphthalene at a depth of 30 – 45 cm ..	132
<b>Figure 7.9:</b> Pre-treatment solid loading of TPH and naphthalene at a depth of 45 – 60 cm....	132
<b>Figure A.1:</b> GC-FID detection of active chlorine by-products at 0, 3, 15, and 120 minutes of treatment .....	160
<b>Figure A.2:</b> Effect of ethanol concentration on naphthalene removal .....	160
<b>Figure A.3:</b> Model predictions of species concentrations against time during the electro-Fenton reaction pathway .....	160
<b>Figure A.4:</b> Thermal gravimetric analysis – fourier transform infrared detection (TGA-FTIR) of naphthalene desorption from GC1200 GAC .....	161
<b>Figure A.5:</b> Conductivity of aqueous NaCl solutions as a function of concentration at room temperature .....	161
<b>Figure A.6:</b> Molecular structures and relative sizes of naphthalene, water, hypochlorous acid, and hydroxyl radicals. The scale of a micropore is also shown .....	161
<b>Figure A.7:</b> Post-treatment solid TPH loadings (mg/kg) at a depth of 30 – 45 cm .....	162
<b>Figure A.8:</b> Post-treatment solid naphthalene loadings (mg/kg) at a depth of 30 – 45 cm .....	162
<b>Figure A.9:</b> Post-treatment solid TPH loadings (mg/kg) at a depth of 45 – 60 cm .....	162
<b>Figure A.10:</b> Post-treatment solid naphthalene loadings (mg/kg) at a depth of 45 – 60 cm ...	162
<b>Figure B.1:</b> Calibration curve for naphthalene detection via HPLC-DAD at 275 nm.....	164
<b>Figure B.2:</b> Calibration curve for naphthalene detection via HPLC-DAD at 254 nm.....	164
<b>Figure B.3:</b> Calibration curve for 1-naphthol detection via HPLC-DAD at 275 nm .....	164
<b>Figure B.4:</b> Calibration curve for 1,4-naphthoquinone detection via HPLC-DAD at 230 nm ....	165
<b>Figure B.5:</b> Calibration curve for H <sub>2</sub> O <sub>2</sub> detection via UV/Vis at 409 nm .....	165
<b>Figure B.6:</b> GC-FID chromatogram for TPH detection - blank.....	165
<b>Figure B.7:</b> GC-FID chromatogram for TPH detection – blank recovery .....	166
<b>Figure B.8:</b> GC-FID chromatogram for TPH detection – PRB sample.....	166

---

## List of Tables

<b>Table 1.1:</b> Estimated mass fractions for components found within Special Antarctic Blend (SAB) diesel .....	5
<b>Table 1.2:</b> Comparison of the available GAC regenerative techniques against desirable criteria for regeneration operations.....	10
<b>Table 2.1:</b> Standard reduction potentials and reduction reactions for oxidizing agents often used for the destruction of aqueous organic pollutants .....	22
<b>Table 2.2:</b> Regeneration efficiencies (RE) of GAC achieved when operating electrochemical cells with various additives for the promotion of varying reaction pathways.....	28
<b>Table 2.3:</b> Regeneration efficiencies (RE) of GAC achieved when operating electrochemical cells under the same operating conditions in fixed and fluidized bed configurations .....	31
<b>Table 2.4:</b> Regeneration efficiencies (RE) of GAC achieved when polarizing the GAC either anodically or cathodically, in both undivided and divided electrochemical cells .....	33
<b>Table 2.5:</b> Studied electrochemical regenerations of GAC .....	35
<b>Table 2.6:</b> Regeneration efficiencies (RE) of GAC achieved when operating electrochemical cells at various current densities and applied voltages .....	37
<b>Table 2.7:</b> Regeneration efficiencies (RE) of GAC achieved when operating electrochemical cells with varying electrolytes .....	39
<b>Table 3.1:</b> Chemical reagents, detailing their respective supplier, purity, and purpose for the production of this thesis .....	47
<b>Table 3.2:</b> Physical characteristics of naphthalene .....	48
<b>Table 3.3:</b> Characteristics of Acticarb GC1200 GAC .....	49
<b>Table 4.1:</b> Known and experimentally determined parameters used within the proposed kinetic model .....	60
<b>Table 4.2:</b> Comparison between experimental data and the kinetic model for the various applied currents .....	63
<b>Table 4.3:</b> Comparison between experimental data and the kinetic model for the various NaCl concentrations .....	65
<b>Table 4.4:</b> Mass spectrophotometry results detailing the by-products formed when electrochemically treating naphthalene solutions in a 0.1 M NaCl electrolyte at 100 mA/cm <sup>2</sup> . 69	

---

<b>Table 5.1:</b> Mathematical comparison between the experimental H <sub>2</sub> O <sub>2</sub> production data and the kinetic model.....	79
<b>Table 5.2:</b> Known and experimentally determined parameters used within the proposed mathematical model .....	81
<b>Table 5.3:</b> Mathematical comparison between the experimental data and kinetic model for varying iron(II) concentrations.....	83
<b>Table 5.4:</b> Mathematical comparison between the experimental data and nonlinear kinetic model for varying applied electric currents .....	85
<b>Table 6.1:</b> Freundlich, Langmuir, and Linear isotherm parameters and fit for naphthalene adsorption onto GC1200 GAC .....	104
<b>Table 6.2:</b> Determined parameters of the three-stage kinetic model and its goodness of fit to the experimental data .....	113
<b>Table 6.3:</b> Efficiency parameter for the active chlorine and electro-Fenton pathways, and the root mean square error (RMSE) of the model when predicting treatment outcomes at varying currents and timeframes.....	119
<b>Table 6.4:</b> Average cell voltages and energy consumptions when regenerating the GAC for two hours .....	119
<b>Table 7.1:</b> Ideal operating conditions for promotion of the active chlorine and electro-Fenton reactions in situ of a PRB.....	126
<b>Table 7.2:</b> Fluctuations in electric current over the 8 days of treatment.....	133

---

# CHAPTER 1

---

## Introduction

This chapter provides the background information relevant to the work contained within this thesis. It introduces the occurrence of fuel spills in the Antarctic and the need for developing remediation methods that can be deployed in its remote and extreme environments. It also identifies the motivations and research objectives for the work that follows.

---





## 1.1 Introduction

Antarctic and sub-Antarctic regions have received an increasingly large human presence in the last two centuries. Due to an historical lack of environmental awareness, this has resulted in numerous cases of loss and damage to the environment such as abandoned rubbish and tip sites, the introduction of invasive species, and the on-going occurrence of fuel spills [1]. Of these, petroleum hydrocarbon spills are considered to be the most threatening to human health and surrounding ecosystems due to the fact that they persist in the environment for centuries and seasonally affect sensitive environmental receptors [2]. The Antarctic continent itself is predicted to have between 1 – 10 million m<sup>3</sup> of petroleum contaminated soils [3], while the sub-Antarctic Macquarie Island has had several spills in the last sixty years amounting up to 10,000 L [4]. Despite a growing awareness of the negative impacts these spills can cause, the continual need and transport of petroleum fuels on all Australian Antarctic and sub-Antarctic research stations results in additional spills with time. The most recent Macquarie Island spill occurred in 2002 and resulted in 180 metric tons of contaminated soil [4], while a spill releasing over 4,000 L occurred at Casey Station on main Antarctica in 2015 [5].

With increasing awareness of the long-term environmental impacts associated with petroleum spills, The Protocol on Environmental Protection to the Antarctic Treaty (1991) mandates that all Antarctic activities are to be “cleaned up” by the generator of the waste [1]. Although the extent to what “cleaned up” means is ill-defined, it is dictated that all waste needs to be removed unless greater adverse environmental impacts will result. Similar legislation exists within the Tasmanian State Government regarding the sub-Antarctic Macquarie Island; the *Environmental Management and Pollution Control Act* (1994) states there is a duty to protect the environment and inhibit serious or material environmental harms resulting from pollutants [6]. This includes contaminated soil and groundwater, the presence of free phase petroleum, as well as the discovery of a previously discharged pollutant. To meet these regulatory requirements, the Australian Antarctic Division (AAD) and its collaborators have, in the last 20 years, put great efforts into developing technologies that aid in the remediation of these Polar Regions.

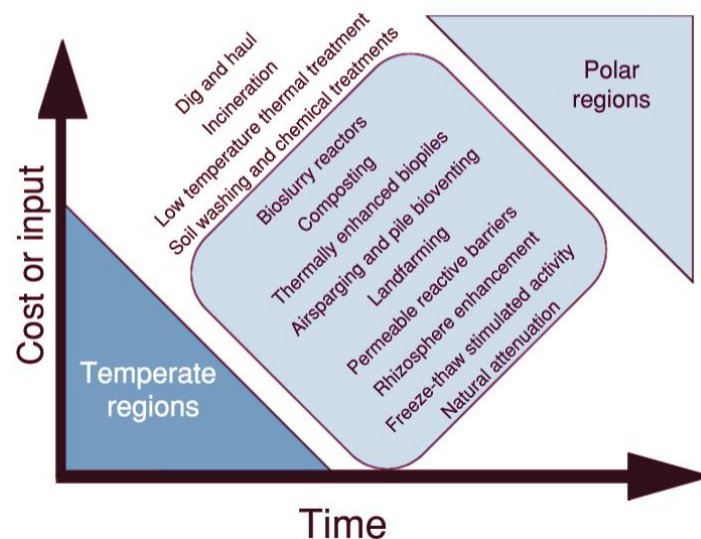


Figure 1.1: Available techniques used for the remediation of petroleum hydrocarbon spills, as a function of time and cost. The boxed techniques are considered to be most practical for remediation of Polar Regions [7].

Petroleum spills in cold climates, in comparison to temperate regions, are believed to cause more damage to the ecosystem as the cold temperatures, quick migration rates, toxic contaminants, and lack of indigenous nutrients slow natural attenuation rates [8]. This allows petroleum concentrations to remain high for several decades and disperse into larger areas with time [7]. Consequently, engineering and scientific intervention is required to help remediate these regions. Of the techniques often used in petroleum spill remediation efforts, illustrated in Figure 1.1, few are practical for deployment in Polar Regions. The *ex situ* methods used in temperate regions, such as dig-and-haul, generally have high transportation costs associated with them, while bulk extraction methods can exceed the damage received in the initial spill [7]. For these reasons, *in situ* methods are preferred for use in Polar Regions.

*In situ* permeable reactive barriers (PRB) were deployed at both the Casey and Macquarie Island research stations in 2005 and 2014 respectively [9,10]. With this technique, reactive and adsorptive materials are placed in the path of a migrating and contaminated groundwater. As the groundwater flows through the barrier, Figure 1.2, contaminants are either adsorbed onto the reactive material surface or transformed into less toxic compounds prior to being discharged into the surrounding environment. The implementation of such PRBs in the Antarctic and sub-Antarctic have proven to be a low-cost and effective method of preventing the migration of spilled petroleum hydrocarbons into areas of ecological significance [9,11].

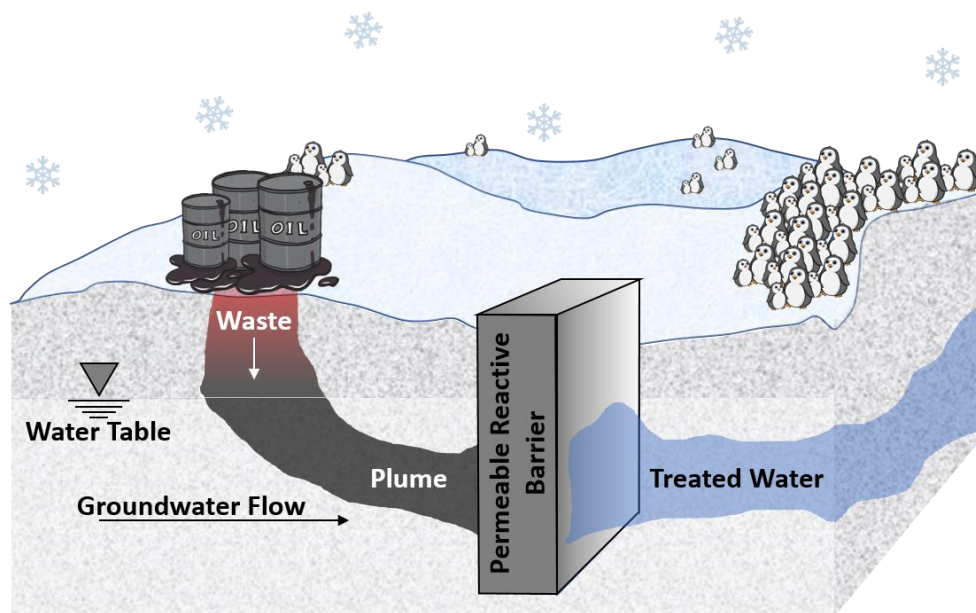


Figure 1.2: Schematic of an *in situ* PRB capturing a plume of contaminated groundwater.

However, the use of PRBs as a remediation technique is an incomplete system. Although contaminant plumes are immobilized, the captured pollutants degrade at a slower rate than they are taken up and the reactive material eventually becomes saturated over time. This renders the PRB ineffective and results in bed breakthrough, enabling petroleum hydrocarbons to spread into surrounding areas. When this occurs, two management options exist. The first is to excavate and dispose of the exhausted PRB substrate and replace it with fresh material. However, this is a lengthy and costly process and the disposal of the spent material into landfill leads to the possibility of contaminants leaching into the environment [12]. A more economical option is to regenerate the saturated material, allowing it to be used for several cycles of

adsorption and regeneration. This would ultimately extend the life of installed PRBs and is the basis of the work within this thesis.

## 1.2 Background Literature

### 1.2.1 Antarctic Petroleum

The main petroleum fuel used at Antarctic and sub-Antarctic research stations is Special Antarctic Blend (SAB) diesel. SAB is unique diesel in that the heavy and waxy end of components have been removed so that it has improved performance in cold climates [13]. The estimated mass fractions of the modified diesel are displayed in Table 1.1 where a majority of the components are aliphatic hydrocarbons in the n-C<sub>10</sub> to n-C<sub>16</sub> range. As this diesel mixture is the main source of power on Antarctic research stations, abundant amounts are stored on station. Regrettably, a history of poor fuel management and unnoticed leaks in pipes and storage tanks has led to numerous spills at all Australian research stations. Historic spills have also been discovered in these regions and have contained aviation turbine kerosene [5] and standard diesel and lube oils that are commonly used during station operations [13].

Table 1.1: Estimated mass fractions for components found within Special Antarctic Blend (SAB) diesel [4]

Equivalent Carbon Number	Mass Fraction
<i>Aliphatics</i>	
5-6	0
6-8	0
8-10	0.095
10-12	0.358
12-16	0.343
16-21	0.00187
<i>Aromatics</i>	
Benzene	0
Toluene	0
8-10	0.024
10-12	0.0981
12-16	0.083
16-21	0.00012
21-35	0

The hydrocarbons detailed in Table 1.1 are nonpolar and hydrophobic, giving SAB a low solubility of about 7 mg/L in aqueous solutions [4]. Following a fuel spill of this diesel type, its low solubility promotes its accumulation onto organic materials involving the processes of adsorption and partitioning [14]. With this pathway they easily accumulate within carbon-based materials and the food chain, causing toxic effects to environmental receptors [15]. In sandy materials that are largely devoid of natural organic matter and have minimal interaction with hydrophobic compounds, little adsorption processes take place. In these instances, light contaminants that have been spilled (having a lower density than water) migrate through sandy particulates and solubilize into or accumulate on top of the water table in the form of free phase light non-aqueous phase liquid (LNAPL). Hence, following a petroleum spill, surface runoff results in both the dispersion of dust particles containing adsorbed hydrocarbons and the movement of contaminated groundwater. Both of these processes promote the migration and spread of hydrocarbon compounds into larger areas [3].

The migration of such hydrocarbons is worsened by the fact that they are generally unreactive and will persist in the environment for decades. Although photochemical oxidation reactions can promote the degradation of hydrocarbons present on surface waters and soils, subsurface contaminations are devoid of light [14]. In this instance, hydrocarbon breakdown relies heavily on biodegradation processes as natural chemical degradation reactions are deemed insignificant for hydrocarbon destruction [14]. Unfortunately, biodegradation rates are limited in the extreme environments of Antarctic and sub-Antarctic regions, it being estimated that the half-life of the spilled hydrocarbons at Macquarie Island are in the order of tens to hundreds or years [4]. Thus, permeable reactive barriers have been implemented to immobilize contaminant plumes and limit the environmental consequences.

### 1.2.2 Antarctic PRB Material

Extensive work has been conducted regarding the use of reactive materials in PRBs for hydrocarbon capture in Antarctic and sub-Antarctic regions [9,10,16–19]. Hornig et al. [16] investigated three possible materials for deployment in cold climate PRBs, those being activated carbon, surfactant modified zeolite, and MYCLEX coated sand. On a mass basis it was found that granular activated carbon (GAC) was able to adsorb the greatest quantity of hydrocarbons from aqueous solutions. This was attributed to its large surface area, microporous structure, and high degree of surface reactivity caused by the presence of surface oxide groups and inorganic impurities [11,16]. However, it was uncertain whether its lack of structural strength could withstand the seasonal freeze-thaw regimes present in Antarctic regions. In contrast, it was shown that surfactant modified zeolite could adsorb more hydrocarbons on a surface area basis, attributed to its surfactant coating; zeolite itself is not known to effectively adsorb hydrocarbons [16]. It was concluded that modified zeolite materials may be more advantageous for use in cold climates as they do not undergo the same shrink-swell behaviour exhibited by GAC particles.

The investigated materials were field deployed in a permeable reactive barrier that was installed at Casey Station, Antarctica in the 2005/2006 summer season. The barrier was comprised of five sections running parallel to one another, in which migrating groundwater passed through a combination of materials in varying sequential orders [19]. Materials such as GAC, zeolite, sand, and various fertilizers (eg. Maxbac, Zeopro, and ammonium loaded zeolite) were implemented to promote both hydrocarbon capture and microbial growth to promote biodegradation of the captured contaminants. Following a five-year operational period, the PRB was excavated and analysed. In all cases, the highest concentration of captured hydrocarbons was found on the GAC substrate, demonstrating its ability to contain and immobilize migrating hydrocarbon plumes [11]. Although no breakthrough of contaminants could be perceived, the hydraulic permeability within the barrier was highly restricted due to the disintegration of GAC particles over the five-year operational period. This is highly undesirable as the hydraulic performance within a PRB must be maintained such that flow does not bypass the barrier, the appropriate residence times are achieved to ensure full contaminant uptake, and aqueous solutions can drain freely into the external environment. For these reasons, it was recommended that when GAC is to be installed within Antarctic PRBs for contaminant immobilization, it should be mixed with more robust materials such that hydraulic permeability is maintained [11]. Mumford et al. [11] identified that the zeolite would be a good option as it showed considerably less signs of disintegration after five years of operation. Taking this into account, all future PRBs such as the one installed at Macquarie Island in 2014, were comprised of a GAC/zeolite mixture in order to uphold hydraulic conductivity [9]. As zeolites are not considered to be significant in hydrocarbon capture and immobilization, the key substrate to be regenerated within Antarctic PRBs is GAC.

### 1.3 Methods of GAC Regeneration

The regeneration of GAC aims to restore the original adsorptive capacity of the GAC by removing contaminants that have accumulated onto the carbon surface, while damaging the carbon as little as possible [20]. This ensures that the adsorbent can undergo several cycles of adsorption and regeneration and make it economical for continuous use. To date, several methods of GAC regeneration exist, displayed in Figure 1.3. The available techniques can be broken down into two main categories: 1) desorption, where the adsorbate is displaced from the solid into a liquid phase, and 2) decomposition, whereby contaminant materials are degraded and completely removed from the system. When considering environmentally sensitive areas such as the Antarctic and sub-Antarctic, decomposition techniques are favoured such that desorbed pollutants do not migrate into areas of ecological significance, while simultaneously avoiding secondary treatments of the resulting leachate. Coinciding with this, a process that is cost and energy efficient, gives GAC a long operational life, and can be performed *in situ* is desired.

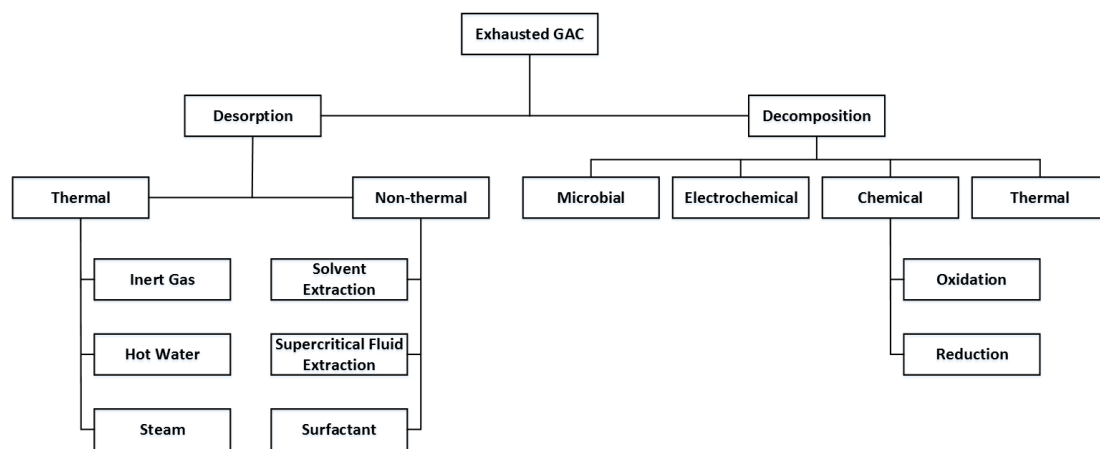


Figure 1.3: Techniques used for the regeneration of saturated activated carbons. Decomposition methods are generally preferred over desorption methods such that secondary treatments are avoided

#### 1.3.1 Thermal

Starting in the 1950s, thermal regeneration has become the most commonly used regeneration technique for GAC in industrial applications, as large quantities of GAC can be treated in relatively short time frames. With this method, exhausted GAC is placed into a purpose built furnace that operates at temperatures between 700 – 1000 °C [21] such that adsorbed contaminants are volatilized from the material surface, rendering it clean. Although this process can restore over 90 % of the original GACs adsorptive capacity, the large temperature requirements typically prohibit this process from being performed *in situ* for most applications. Similarly, the energy costs associated with the high operational temperatures, approximately 600 USD (year 1998 dollars)/m<sup>3</sup> of GAC [22], make it uneconomical for small scale processes where less than 910 kg of GAC are treated each day [23]. Costs increase further due to the fact that thermal treatments results in up to 20 % of the carbon being lost to attrition and oxidation, requiring compensation and replacement after each regenerative cycle. A bench scale study conducted by Bañuelos et al. [24] aimed to thermally regenerate 40 g of GAC saturated with orange dye at 900 °C for two hours. Following five cycles of treatment, 87.5 % of the GAC material had been lost due to burn off. Similar results have been obtained for other types of GAC and model contaminants [25–27]. Such outcomes increase costs by having to compensate for these losses with fresh material, as well as reduce the longevity of the GAC indicating that it is not sustainable for long term use.

In addition to this, the original adsorptive capacity of the GAC is often not restored during this process as the extreme heat alters the original surface chemistry and porous texture of the GAC material. It has been observed that during adsorbate burn off, characteristic micropores are widened and ultimately hinder the ability of GAC to remove small contaminants out of aqueous solutions [28]. Surface smoothing and the development of a hydrophilic exterior have also been detected, implying that this treatment method would not be effective for reuse in the containment of hydrophobic compounds such as hydrocarbons [24].

### 1.3.2 Chemical

As a means of finding an alternative to thermal treatments, Martin and Ng [29] were one of the first to conduct an extensive study analysing chemical regeneration of carbon materials. With this method, chemical solvents are introduced *in situ* or *ex situ* to either increase the solubility of adsorbed contaminants to promote desorption into an aqueous phase, or oxidize the contaminants to an innocuous form. A variety of organic (encourages desorption) and inorganic (promotes oxidation) compounds were investigated and it was determined that desorption agents (e.g. acetone, acids/bases, surfactants) were more effective than oxidizing agents. However, regeneration rates were highly variable and remained below 70 % in most cases [29]. A study conducted a decade later determined that regenerative rates remained low as up to 15 % of the pores within the GAC microstructure become blocked with residual chemicals [30], ultimately hindering its performance for continuous use. Furthermore, the use of strong extraction solvents in environmental situations is becoming increasingly unacceptable as it only serves as a means of transferring contaminants from a solid to liquid phase that generally requires secondary treatments [21].

In an attempt to avoid this, oxidizing agents such as chlorine, ozone, persulphates and peroxides can be used to promote both desorption and degradation (or complete mineralization) of adsorbed contaminants. However, the purchasing and handling of oxidizing agents can make this treatment uneconomical for continuous use, and may also result in losses to the adsorbent capacity of the GAC [21]. Bañuelos et al. [24] demonstrated that the application of an oxidizing mixture of hydrogen peroxide and iron to saturated GAC resulted in numerous cracks and pits along the GAC surface, as it could not withstand the highly oxidative environment.

### 1.3.3 Microbial

Biological treatments have also been considered as an alternative to previously established regenerative methods. In this instance, the *in situ* growth of microorganisms on or near the GAC surface is promoted such that microbial populations metabolize and biodegrade adsorbed organic compounds. The low cost, low energy, and environmentally friendly nature of this technique makes it superior in comparison to other treatment methods, however, that is not to say it is not met with its own limitations. The extent to which regeneration can progress in these systems is strongly limited by several variables. Continuous nutrient delivery (e.g. oxygen, nitrogen) is generally required to support the formation of biofilms outside of their native environment [31]. Thus, although the longevity of the GAC is increased, continuous nutrient addition cannot be avoided which may increase costs and manual labour over long operational periods. This is an important consideration, as long operational times are inevitably endured due to the slow growth rate of microbial communities, especially in the extreme environments experienced in Polar Regions. Similarly, biological treatments are not always feasible. The microbial pathway is dependent on the biodegradability of contaminants, as well as the manifestation of the appropriate microbial communities that are capable of degrading the pollutants encountered [32]. Regarding petroleum hydrocarbons, it is observed that light *n*-

alkanes are preferentially biodegraded, followed by branched and cyclic alkanes, and finally aromatics and polar compounds [2,10]. This often leaves behind residual aromatic and more complex compounds that are more toxic and take extensive timeframes to be degraded.

Despite these limitations, bioregeneration of GAC materials within Antarctic PRBs has shown to be an effective treatment method [9–11,31]. After five years of operation, it was detected that the immobilized fuel within the Casey Station PRB showed signs of microbial degradation, and at a greater extent than the surrounding soils [10]. This provided evidence that the nutrient enriched environment within the fabricated PRBs (e.g. heat, nitrogen, oxygen) are a working treatment option for petroleum contaminated groundwaters in Polar Regions. However, the slow growth rate of microbial communities and seasonal lag phase experienced in Antarctic regions limits the extent of bioregeneration achieved. Variations in temperature, pH, availability of nutrients, and insufficient contact between microorganisms and adsorbed contaminants within the GAC micropores all limit the rate and efficiency for which microbes can proliferate [10]. Similarly, too strong an adsorption of hydrocarbons onto GAC surface make them largely inaccessible for microbial degradation [10]. These factors, combined with the likelihood that biofilm formation may block adsorption sites on the GAC and hinder its long-term use, give rise to low and slow regeneration rates. Ongoing research is currently being conducted to sidestep these limitations and improve upon the microbial growth and degradation rates observed in Antarctic regions; it is essential that degradation rates surpass adsorption rates such that bed breakthrough is prevented.

#### 1.3.4 Electrochemical

A more recently developed technology, electrochemical regeneration, involves the placement of saturated GAC between two oppositely charged electrodes. Upon applying a low current across the GAC bed, desorption and degradation of adsorbed contaminants is observed. Although relatively less studied in the literature, it is anticipated that this regenerative technique can be applied either *in situ* or *ex situ*. Narbaitz and Cen [33] were one of the first to study this technique, utilizing a 1-litre electrochemical reactor to regenerate 1.2 g of phenol saturated GAC. Following five hours of treatment, the GAC was 95 % regenerated, with consecutive treatments resulting in only a 2 % loss of adsorptive capacity per cycle due to minor carbon loss. As these results exceeded the outcomes of other regenerative methods, in terms of adsorptive capability and prolonged use, it gave merit to conduct further research in the field. In the present day, numerous researchers have acquired similar results, reaching regeneration rates greater than 90 % in a matter of hours [12,24,34–37]. Furthermore, the low energy consumption associated with this method, roughly \$39 (2008 USD dollars)/ton of GAC treated, minimizes operational costs in comparison to alternative treatment methods; this corresponds to about 4 % of the price of fresh GAC [37] making it financially viable for long-term use. Additional benefits of this treatment include the absence of external chemicals (reducing cost, handling issues, and potential environmental damage), low operational costs, and negligible attrition of the GAC particles.

However, much of the research surrounding electrochemical regeneration has focused on GAC saturated with highly soluble and ionisable phenolic compounds and dyes. With the exception of García-Otón et al. [34] and Bañuelos et al. [38], little research has been conducted regarding desorption-limited petroleum hydrocarbons. These two studies, utilizing toluene as a model compound, reached regeneration rates of greater than 95 % in less than 3 hours of electrochemical treatment, suggesting it may be effective for PRB regeneration. However, there still lacks a clear understanding of the fundamental mechanisms and optimum operating

conditions involved with this treatment process when different contaminants are encountered. Furthermore, it remains unclear as to whether or not this treatment process is applicable or economical for the treatment of both large quantities and field loaded GAC [28].

### 1.3.5 Assessment of Regeneration Techniques

Based on the existing methods available for GAC regeneration, summarized in Table 1.2, electrochemical treatments are deemed to have the greatest potential for *in situ* application in Antarctic PRBs as they supersede thermal and chemical treatments in terms of cost, energy requirements, regeneration rates and time considerations. Although microbial methods are proven to be the most cost efficient with minimal energy input, the slow kinetics associated with it are generally not adequate to ensure acceptable regeneration timeframes and avoid PRB bed breakthrough. Thus, electrochemical methods will be further investigated as a means of replacement and/or enhancement to the biological processes that already occur within installed Antarctic and sub-Antarctic PRBs.

Table 1.2: Comparison of the available GAC regenerative techniques against desirable criteria for regeneration operations.

Criterion	Thermal	Chemical	Microbial	Electrochemical
Low Cost	✗	✗	✓	✓
Low Energy	✗	✓	✓	✓
<i>In situ</i>	✗	✓	✓	✓
Regeneration Efficiency	> 90 %	< 70 %	8 - 100 %	> 90 %
Comments	≤ 20 % loss of carbon per cycle, not economical for small scale	≤ 15 % micropore blockage, requires secondary treatment	Long lag phase, slow degradation rates, requires nutrient addition	Not applied at large scale, kinetics not well understood

However, the limited understanding regarding the kinetics and underlying mechanism of electrochemical regeneration, as well as the feasibility of applying it to large scale processes, is currently hindering its deployment in field applications. Furthermore, the capability of utilizing electrochemical techniques to treat petroleum hydrocarbon saturated GAC in both temperate and Polar Regions has not been established. These gaps in the literature need to be addressed with further research, in the hope of answering one overarching research question: are electrochemical treatments feasible for the *in situ* regeneration of PRB materials in Polar Climates? The investigation of this question forms the basis of the work presented and discussed in the thesis that follows.

### 1.4 Research Objectives

The primary aim of this thesis was to determine the feasibility and applicability for which electrochemical treatments can aid in the regeneration of petroleum hydrocarbon saturated GAC. Above all, the treatment of saturated GAC *in situ* of permeable reactive barriers in environmentally sensitive Polar Regions was considered. In order to achieve this, it was important to first gain an understanding of the fundamental mechanisms and theory regarding electrochemical regenerative treatments. Following this, the feasibility of applying such a treatment to PRB saturated GAC was investigated.

To address this objective, the following thesis is organized into the following eight chapters:



**Chapter 1** provides an introduction and the relevant background information regarding the research problem being addressed. It also outlines the motivations and objective of the work in the thesis that follows.

**Chapter 2** summarizes the literature pertaining to the electrochemical regeneration of granular activated carbons. It includes an overview of the research conducted to date, as well as a discussion of the underlying theory and fundamentals of the regenerative treatment. Lastly, limitations, prospects, and residual unknowns of the treatment method are identified.

**Chapter 3** details the materials and analytical methods that are used throughout the thesis and experimental chapters that follow.

**Chapter 4** begins to investigate the types of electrochemical reactions that are effective for the treatment of petroleum hydrocarbon contaminated waters. The active chlorine pathway is studied, and varying operating parameters are considered such as applied current density, salinity, and treatment time. A kinetic model is also proposed that can predict treatment outcomes.

**Chapter 5** continues to look at plausible electrochemical reactions that are effective for petroleum hydrocarbon treatments. The electro-Fenton reaction is investigated under varying operational conditions including applied electric current and iron concentration, and a kinetic model is proposed that can accurately predict treatment outcomes.

**Chapter 6** examines how the active chlorine and electro-Fenton reaction pathways can be used for the regeneration of a bed of hydrocarbon contaminated granular activated carbons. The underlying mechanism and kinetics of the treatment process are examined to ultimately determine whether electrochemical regeneration is deployable for Antarctic remediation efforts.

**Chapter 7** discusses the possibility of field deploying the technology for the *in situ* treatment of an Antarctic permeable reactive barrier. Complex diesel mixtures, the possibility of scale-up, deployment considerations, and a field-trial are discussed.

**Chapter 8** provides the concluding statements of the work contained within the thesis and provides suggestions and recommendations for future work.



---

# CHAPTER 2

---

## Literature Review

This chapter summarizes the literature surrounding the electrochemical regeneration of granular activated carbons. This includes an overview of the research conducted to date, discussion of the underlying fundamentals and theory of the regenerative treatment, as well as comparing the varying types of reactor configurations and operating conditions that affect regeneration outcomes. From this discussion, limitations and future prospects associated with electrochemical methods are identified with specific regard for deployment within Antarctic permeable reactive barriers.

*This chapter has resulted in the following publication:*

**McQuillan, R. V.,** Stevens, G. W., & Mumford, K. A.. The electrochemical regeneration of granular activated carbons: A review. *Journal of Hazardous Materials*, 355 (2018), 34–49.

---



## 2.1 Introduction

The need for developing a technology that can effectively regenerate exhausted granular activated carbons (GAC) extends well beyond permeable reactive barriers (PRB) and environmental remediation efforts. The large surface area, microporous structure, and increased surface reactivity associated with GAC [11,16] makes it one of the most powerful adsorbent materials used in purification processes. In the present day, industries such as oil and gas, pharmaceutical, and wastewater treatment are now incorporating increasing amounts of GAC into their manufacturing processes. With increasing amounts of legislation being placed on environmental protection, product quality, and liquid and gas emissions, the global demand for activated carbon continues to increase nearly 10 % annually from its global consumption of 4.28 million tons in 2012 [39].

Although proven to be highly effective, the leading shortcoming of GAC is the limited lifetime for which it can perform. Upon reaching its adsorptive capacity, it is no longer effective and is most often sent for disposal and replaced with fresh material. However, the continuous material change out that results is not financially viable, and the disposal of exhausted material into landfill leads to the possibility of toxic contaminants leaching into the environment [12]. A more economical and environmentally sound option is to regenerate the material such that it can be used for several cycles of adsorption and regeneration.

Several regenerative techniques are extensively covered in the literature and are currently applied in industrial applications. As detailed in Chapter 1, this includes thermal [40], chemical [29,41], and microbial methods [42]. However, these methods are met with limitations such as high energy consumption and carbon attrition [27], pore blockage and the requirement for secondary treatments [43], and slow regeneration rates [32], respectively.

In an attempt to overcome these restrictions, attention is being turned towards a relatively newer technology, electrochemical regeneration, at which saturated GAC is placed between two oppositely charged electrodes. Upon application of an electric current, both desorption and degradation processes of the adsorbed contaminants is observed. Researchers have acquired high GAC regeneration rates in a matter of hours, making this technology seem highly advantageous [34,36,44]. However, the literature has had limited discussion surrounding this technology, and as such, its development has progressed very slowly. The following review aims to present 1) the theory of electrochemical regeneration, 2) summarize what research has been done related to the electrochemical treatment of activated carbons, and 3) identify limitations and future engineering prospects associated with the technology. Such an understanding is critical prior to investigating the feasibility of applying such a technology towards PRB applications.

## 2.2 Regenerative Mechanism

The application of an electric current across an exhausted bed of granular activated carbon results in two main regenerative processes. First, enhanced desorption from the GAC surface commences, Figure 2.1(A)–(C), and results in an adsorbent free of contaminant species. Second, electrochemical reactions occurring at the electrodes and polarized GAC particles stimulate the degradation of contaminant species, completely removing them from the system, Figure 2.1(D). An ideal electrochemical regenerative process will promote both mechanisms such that further treatments of desorbed compounds can be avoided. The following sections describe in further detail the regenerative mechanisms depicted in Figure 2.1.

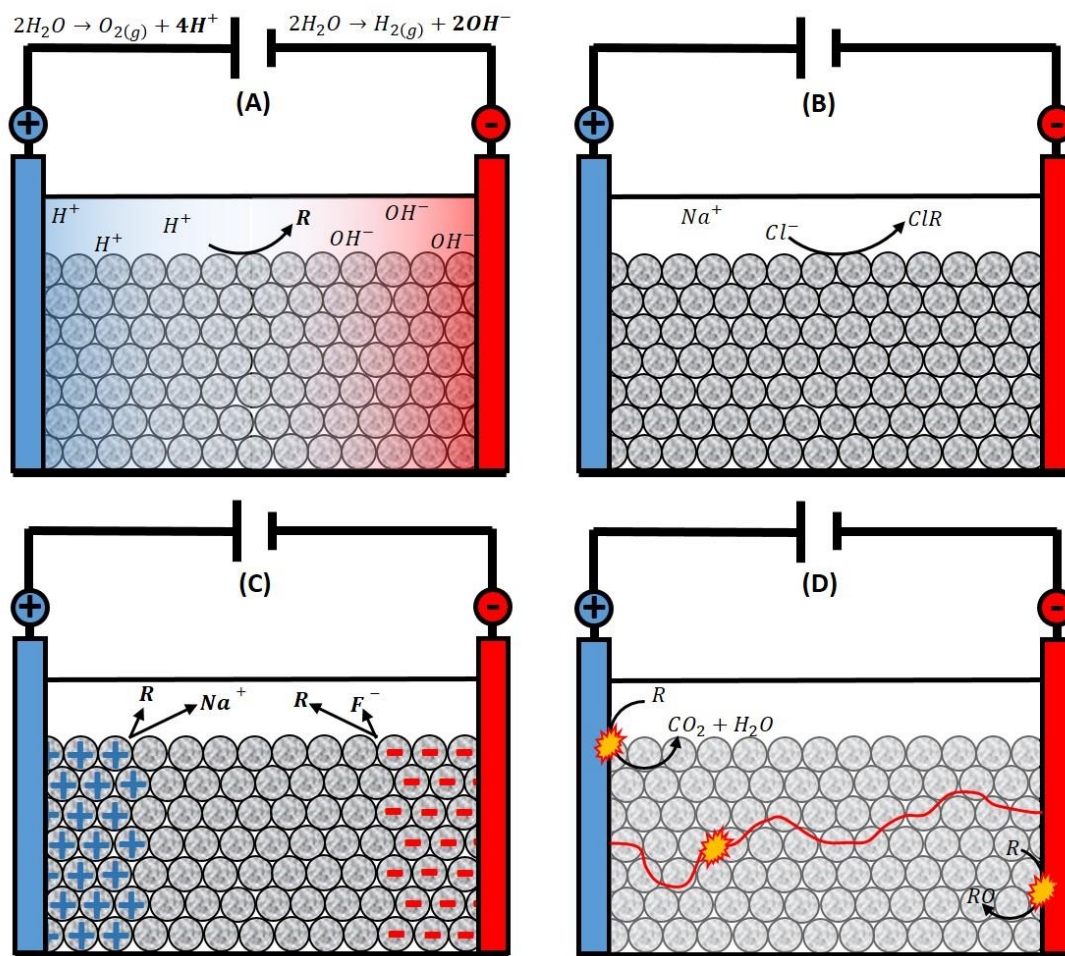
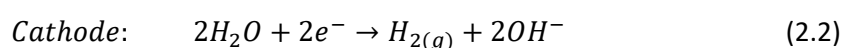
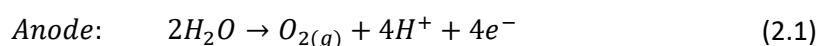


Figure 2.1: Regenerative mechanisms involved in the electrochemical regeneration of GAC. A) Enhanced desorption due to changes in local pH, B) Enhanced desorption due to local changes in salinity concentration, or adsorbate reacting with ionized species to produce a less readily adsorbed compound, C) Electrodesorption whereby species are repelled from the charged GAC surface, and D) Oxidation/degradation reactions occurring at either the electrodes or polarized GAC particles.

## 2.2.1 Enhanced Desorption

### 2.2.1.1 Effects of pH

Within an electrolytic cell, electrons are transported between two electrodes via an external power supply. This results in the development of a positively charged anode, where oxidation reactions occur, and a negatively charged cathode, where reduction reactions occur; the electrolyte in close vicinity to each of these electrodes is known as the anolyte and catholyte respectively. Most often aqueous solutions are utilized as the electrolyte, and upon application of an electric current, electrolysis reactions of water into hydrogen and oxygen become the principle reactions at the cathode and anode respectively [45]. Simultaneous to the production of gaseous species, acidic protons ( $H^+$ ) and basic hydroxyl ions ( $OH^-$ ) are generated as described by Equations (2.1) and (2.2). These reactions quickly form an acidic and basic front within an electrolytic cell.



Regarding the regeneration of exhausted GAC, such changes in pH are sometimes enough to shift the adsorptive equilibria between the adsorbate and adsorbent and promote desorption processes. Karimi-Jashni and Narbaitz [46] demonstrated that when a phenol loaded GAC was electrochemically treated, the catholyte had developed a pH of 12 within two hours of treatment and resulted in a regeneration efficiency 30 % greater than that of the pH 2 anolyte. It was postulated that dissociated phenol compounds at high pH values (greater than its pKa of 9.99) undergo enhanced desorption due to increased electrostatic repulsive forces between adjacently adsorbed anionic compounds and anionic functional groups on the GAC surface [47]. Competitive adsorption with hydroxyl ions and the increased solubility of organic compounds with increasing pH are also known to encourage desorption processes [48]. In contrast, acidic environments decrease the solubility of organic compounds, and neutralize the functional groups on the GAC surface (e.g. carboxylic acids); the reduction in electrostatic repulsive forces promotes the adsorption of compounds onto the solid GAC surface [48]. Based on this reasoning, Karimi-Jashni and Narbaitz [46] concluded that the electrochemical regeneration of GAC is largely dependent on the creation of extreme pH values within the electrolytic system. Similar conclusions were reached by Berenguer et al. [49] who demonstrated that high pH values promoted desorption due to increased solubility of contaminants and amplified electrostatic repulsions between ionized compounds and the GAC surface.

However, electrogenerated protons and hydroxyl ions migrate via electromigration to the oppositely charged electrode and neutralize the pH fronts that have developed through the formation of water [50]. As protons have an ionic mobility nearly 1.8 times that of hydroxyl ions [45], longer operational periods result in an overarching acidic front within the system and decrease the pH of the catholyte if the electrolyte and adsorbent material do not have a large buffering capacity; this outcome is assuming the operation of an undivided cell in which an ionic membrane is not present to restrict the migration of molecules to and from the catholyte and anolyte regions. Such results may limit the extent to which the system pH can be modified to promote the desorption of contaminants and regeneration of GAC during electrochemical regenerative treatments, as alkaline conditions may be challenging to preserve.

Although several authors claim that the electrochemical regenerative process is solely dependent on pH modifications, limited kinetic studies have been conducted to evidence this. In other words, it is unknown if the rate of desorption at extreme pH values is sufficient to have a leading effect, in comparison to chemical reactions, during the short electrochemical treatment times of a few hours. In addition to this, pH dependencies will limit this form of treatment to compounds that dissociate within solution and increase electrostatic repulsions with the GAC surface. This is inconsistent with the findings of García-Otón et al. [34] who regenerated a GAC loaded with toluene to 98 %; as toluene does not disassociate, it is unlikely that the regenerative process was due to increased repulsive forces arising from an ionized toluene compound.

#### 2.2.1.2 Ionized Species

In addition to the migration of  $H^+$  and  $OH^-$  ions within an electrochemical system, other ionic species within the electrolyte exhibit the same behaviour. The most commonly used electrolyte, sodium chloride (NaCl), readily dissociates into sodium cations,  $Na^+$ , and chloride anions,  $Cl^-$ . Upon application of an electric potential, the positively and negatively charged ions migrate to the cathode and anode respectively. Zhang et al. [51,52] detected that the increased concentration of sodium ions at the cathode began to react with phenol species adsorbed onto the GAC surface to form sodium phenate. As this compound is water soluble and not readily

adsorbed by activated carbon, desorption processes commenced and the GAC surface was regenerated [29,51]. Through this reaction pathway, it was found that GAC within the sodium enriched catholyte reached a regeneration of 20 % higher than when located in the chloride rich anolyte. A comparable study attempting to electrochemically regenerate chromium (VI) loaded GAC, found that the increased chloride concentration at the anode resulted in the formation of a more soluble anionic chromium (VI) species, and in turn, promoted desorption from the GAC surface [53]. Thus, although electrochemical treatments have the capability of converting adsorbed species into a less readily adsorbed compound, it is highly specific to the adsorbate and reactive species present within the electrolyte.

Changes in electrolyte salinity can also shift the adsorptive equilibria between the adsorbate and adsorbent to promote desorption. A study conducted by Arafat et al. [54] examined the adsorptive capacity of aromatic compounds (phenol, benzene and toluene) on GAC at varying salt concentrations. It was demonstrated that increasing the potassium chloride (KCl) concentration from 0.05 M to 0.5 M resulted in a 1.6-fold increase in the adsorptive capacity of the GAC. This was attributed to  $K^+$  ions aiding in the neutralization of the GAC surface and phenolic compounds, limiting the magnitude of electrostatic repulsive forces between the adsorbate and adsorbent, as well as between adjacently adsorbed molecules [54]. It is also likely that the increased salt concentrations reduced the solubility of the organic compounds in the aqueous phase and promoted their adsorption onto the GAC surface.

### 2.2.1.3 *Electrodesorption*

When an electric potential is applied across a conductive material such as GAC, oppositely charged compounds migrate towards the charged surface where they are held in place via a strongly formed double electric layer [55]. Upon removing the electric field, the charged compounds are released from the interface and diffuse back into the bulk solution. This progression of steps, named electrosorption and electrodesorption, ultimately enhance the rate and capacity for sorption processes on a given material. It has several advantages over other ion exchange methods, as the adsorption and desorption process are fully reversible and no external chemicals are required for surface regeneration [55]. For these reasons, it is now being looked to as an alternative treatment to industrial desalination processes.

The same principle applies when considering the regeneration of exhausted GAC. GAC is characterized as a semi-conductor that holds surface charge, and the application of an electric potential through the material results in a charged surface and subsequent electrostatic repulsion of similarly charged species. Bán et al. [22] demonstrated that applying a negative potential to a carbon surface decreased the amount of cations adsorbed, and inversely increased the amount of adsorbed anions (the opposite occurred when a cathodic potential was applied). It was also realized that uncharged molecules are most strongly adsorbed at, and close to, a potential of zero charge, while they become desorbed at increasingly higher positive and negative potentials via displacement by solvent dipoles [22]. This implies that electrodesorption processes are not only limited to ionized, disassociated compounds. However, the extent of GAC regeneration that can be achieved via this mechanism alone, regarding uncharged species, has not yet been investigated.

Regarding charged adsorbates, Bain et al. [56] utilized an anionic charged GAC substrate to investigate the electrosorption of cationic arsenic out of an aqueous solution. Upon reversing the polarity to a cathodic potential, 100 % regeneration of the GAC was achieved, and the original arsenic concentration in the aqueous solution was restored [56]. The results indicated



that arsenic was not converted to other compounds during treatment, and instead merely displaced between the solid and liquid phases via electrostatic repulsive forces. Berenguer et al. [49] also applied this theory to regenerate a phenol loaded GAC; upon applying a 1.0 A cathodic current to an exhausted GAC holding negatively charged phenol species, an 80 % regeneration efficiency was achieved. Several other authors have utilized this technique with activated carbon materials to clean aqueous solutions contaminated with fluoride [57], arsenic [58], brine [55], aromatic compounds [22], and copper [59].

## 2.2.2 Decomposition of Contaminant Species

Although desorption processes alone are considered to be a regenerative process, it is beneficial for contaminants to also be oxidized into a non-toxic product, or completely mineralized and removed from the system; this would avoid secondary treatments of the resulting leachate solution. During the electrochemical treatment of GAC, oxidation and decomposition reactions may occur through one of three main reaction pathways: i) direct electron transfer between the anode surface and pollutant species, ii) indirect oxidation via electrogenerated hydroxyl radicals within a thin layer near the anode surface, and iii) indirect oxidation via electrogenerated oxidizing species such as active chlorine species ( $\text{HOCl}$ ,  $\text{OCl}^-$ ,  $\text{Cl}_2$ ) and hydrogen peroxides [60]. The following section reviews the types of reactions that are likely to occur during electrochemical treatments, as well as where in the system they are likely to occur during a GAC regenerative process.

### 2.2.2.1 Electrochemical Reactions

#### 2.2.2.1.1 Direct Anodic Oxidation

Direct oxidation, or the direct transfer of electrons from a solubilized substance to an electrode surface, occurs at the anode within an electrochemical cell. Contaminant species first migrate to and are adsorbed onto the anode surface, where direct electron transfer results in an oxidized compound. This reaction is described by Equation (2.3), where  $R_{ads}$  is the organic compound adsorbed on the anode surface,  $P_{ads}$  is the oxidized product, and  $z$  is the number of electrons transferred [61].



Generally, direct oxidation is not considered to be a key oxidizing mechanism for the treatment of wastewaters contaminated with organic compounds as it has extremely slow kinetics [61] and yields poor degradation of organic species [62]. Analysis of the thermodynamics also reveals that the direct oxidation of water to form oxygen, 1.23 V vs a Standard Hydrogen Electrode (SHE), becomes difficult to avoid and decreases the probability of other compounds undergoing direct electrolysis at the anodic surface. With increasing operational time and the promotion of direct oxidation, the catalytic activity of anodes has also shown to decrease with time due to the formation of organic radicals that polymerize on the electrode surface [63]; this is commonly referred to as the poisoning effect, and ultimately hinders the expected performance regarding wastewater decontamination processes [61]. For these reasons, indirect oxidation is considered to be much more effective for the purposes of electrochemical treatments.

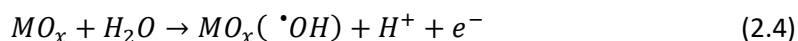
#### 2.2.2.1.2 Indirect Anodic Oxidation

Indirect oxidation involves the oxidation of pollutants via an intermediate electrogenerated active species including active chlorine, ozone, hydrogen peroxides and hydroxyl radicals. Such reagents are electrogenerated *in situ* at the electrode surface and utilized immediately in the destruction of contaminant species in the bulk solution [64]. This type of treatment has been

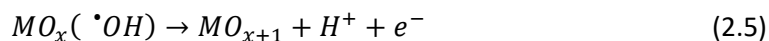
applied extensively to treat varying types of wastewaters contaminated with organics and ammonia [65,66], polyaromatic hydrocarbons [67], dyes, paper mill waste, phenolic compounds [68] as well as mixtures of organic contaminants [69]. Although this mechanism can proceed via a number of electrogenerated intermediate species (being largely dependent on the types of salts present in the electrolyte or wastewater), it is in general agreement that electrogenerated hydroxyl radicals are the superior pathway under which organic compounds are indirectly electrochemically degraded.

The hydroxyl radical,  $\cdot\text{OH}$ , is the second most powerful oxidizing agent known, characterized by a standard reduction potential of 2.87 V versus SHE. The high instability and low selectivity of these radicals enables them to degrade a wide range of organic pollutants, often until complete mineralization into  $\text{H}_2\text{O}$  and  $\text{CO}_2$  is achieved. The degradation and mineralization reactions that transpire with these radicals are due to i) dehydrogenation, or abstraction of a hydrogen atom to form water, ii) hydroxylation, or electrophilic addition to a non-saturated bond, or iii) electron transfer and subsequent redox reactions [70]. Depending on the quantity of hydroxyl radicals generated, degradation reactions will propagate until water and carbon dioxide constituents are reached, or all radicals combine with each other.

The oxidizing strength of hydroxyl radicals and the ease at which they are formed have made them a fundamental tool for the treatment of contaminated wastewaters. Put simply, the oxidation of water at the anodic surface, denoted  $\text{MO}_x$  in Equation (2.4), results in the formation of hydrogen ions and hydroxyl radicals, which can in turn, react with organic pollutants in the nearby vicinity [71,72].



Depending on the anode material, the electrogenerated radicals will either physisorb or chemisorb onto the anode surface. Anodic materials such as platinum (Pt), iridium oxide ( $\text{IrO}_2$ ), graphite, and ruthenium oxide ( $\text{RuO}_2$ ) are considered to be 'active' anodes, and are characterized by the existence of higher oxidation states [61]. As hydroxyl radicals have a strong affinity to these sites, they will chemically adsorb onto the anode surface to create a higher oxide material, denoted  $\text{MO}_{x+1}$  in Equation (2.5). Although higher oxide materials have a lower reduction potential in comparison to standalone hydroxyl radicals, they are still capable of converting organic substances, denoted R in Equation (2.6), into an oxidized form; this type of reaction is generally referred to as electrochemical oxygen transfer reaction (EOTR).

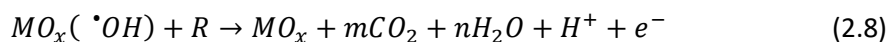


As presented by Equation (2.6), the main shortcoming of using active anodes is that the hydroxylation reaction pathway often results in an oxygenated product,  $\text{RO}$ , rather than an alkyl radical that will undergo further reactions to reach complete mineralization. Depending on the treatment requirements, however, achieving organic conversion over complete combustion may be considered sufficient if the formation of more biodegradable products is desired; this is especially true of wastewaters containing toxic compounds that are recalcitrant to microbial treatments. For instance, the formation of carboxylic acids may be considered an adequate result and will ultimately save on energy requirements and treatment times in comparison to achieving complete mineralization via electrochemical methods alone. A second limitation

associated with the use of active anodes is that the formation of hydroxyl radicals is in competition with oxygen formation via the higher oxide anodic material, demonstrated in Equation (2.7). The preferential formation of oxygen gas will ultimately decrease the energy efficiency endured with increasing treatment times. For these reasons, non-active anodes generally achieve better performance when electrochemically combusting aqueous organic species for complete removal [73].

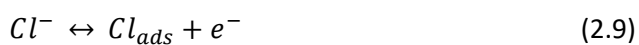


Non-active anodes include materials such as lead dioxide (PbO<sub>2</sub>), tin dioxide (SnO<sub>2</sub>), and boron-doped diamond (BDD). Higher oxidation states are not present on these materials, and as a result, hydroxyl radicals will instead physisorb to their surface. As no chemical transformation of the radicals transpires in this instance, the adsorbed radical species maintains its high oxidizing potential and quickly degrades nearby organic species. This reaction pathway is shown via Equation (2.8) where  $m$  is the number of carbon atoms in the organic compound,  $R$ ; it is common for these reactions to take place until complete mineralization has been reached. Non-active anodes are also understood to have a higher oxygen overpotential, meaning there is less competition with the formation of gaseous oxygen; the increased electric potential required beyond the thermodynamic requirement of 1.23 V vs SHE for oxygen evolution [74] is greatest on non-active anodes, and thus results in increased concentrations of hydroxyl radicals in comparison to active anodes [61]. Although non-active anodic materials generally incur higher capital cost, they are more energy efficient and are thus favoured for the electrochemical degradation of organic species.



As an alternative to hydroxyl radicals, several other oxidizing agents can be electrochemically generated *in situ* for the purposes of indirect electrochemical conversion and combustion processes. The speciation of oxidizing species formed is largely dependent on the existing ions in the supporting electrolyte or wastewater being treated. Table 2.1 outlines the standard reduction potentials of the most commonly used oxidizing agents for the decontamination of wastewater contaminated with organic compounds [70].

Of the species listed in Table 2.1, the most commonly used electrolyte in electrochemical processes, sodium chloride, is recognized to play a large role in indirect oxidation reactions. Upon dissociating in aqueous medium, the positive sodium cations and negative chlorine anions are drawn to the cathode and anode respectively and undergo their relevant reduction and oxidation reactions. At the anode this results in the production of active chlorine species such as free chlorine (Cl<sub>2</sub>), hypochlorous acid (HOCl), or hypochlorite ions (OCl<sup>-</sup>), as shown via Equations (2.9)-(2.12). These highly oxidizing species are known to enhance the degradation and decomposition of organic species during electrochemical treatments, independently or simultaneously to degradation reactions occurring via hydroxyl radicals [36,65,75].



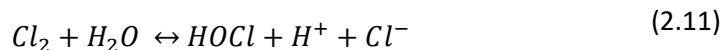
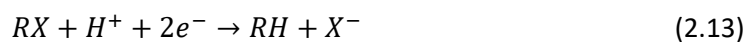


Table 2.1: Standard reduction potentials and reduction reactions for oxidizing agents often used for the destruction of aqueous organic pollutants [70]

Oxidizing Agent	Reduction Reaction	E°/V vs SHE
Fluorine	$F_{2(g)} + 2H^+ + 2e^- \rightarrow 2HF$	3.05
	$F_{2(g)} + 2e^- \rightarrow 2F^-$	2.87
Hydroxyl Radical	$\cdot OH + H^+ + e^- \rightarrow H_2O$	2.87
Sulfate Radical Anion	$SO_4^{\cdot-} + e^- \rightarrow SO_4^{2-}$	2.80
Ferrate Ion	$FeO_4^{2-} + 8H^+ + 3e^- \rightarrow Fe^{3+} + H_2O$	2.60
Ozone	$O_{3(g)} + 2H^+ + 2e^- \rightarrow O_{2(g)} + H_2O$	2.20
Peroxodisulfate Ion	$S_2O_8^{2-} + 2e^- \rightarrow 2SO_4^{2-}$	2.01
Hydrogen Peroxide	$H_2O_2 + 2H^+ + 2e^- \rightarrow 2H_2O$	1.763
Permanganate Ion (I)	$MnO_4^- + 4H^+ + 3e^- \rightarrow MnO_{2(s)} + 2H_2O$	1.67
Hydroperoxyl Ion(I)	$HO_2^{\cdot} + H^+ + e^- \rightarrow H_2O_2$	1.65
Permanganate Ion (II)	$MnO_4^- + 8H^+ + 5e^- \rightarrow Mn^{2+} + 4H_2O$	1.51
Hydroperoxyl Ion (II)	$HO_2^{\cdot} + H^+ + e^- \rightarrow H_2O_2$	1.44
Dichromate Ion	$Cr_2O_7^{2-} + 14H^+ + 6e^- \rightarrow 2Cr^{3+} + 7H_2O$	1.36
Chlorine	$Cl_{2(g)} + 2e^- \rightarrow 2Cl^-$	1.358
Manganese Dioxide	$MnO_2 + 4H^+ + 2e^- \rightarrow Mn^{2+} + 2H_2O$	1.23
Oxygen	$O_{2(g)} + 4H^+ + 4e^- \rightarrow 2H_2O$	1.229
Bromine	$Br_{2(l)} + 2e^- \rightarrow 2Br^-$	1.065

The speciation and oxidizing power of electrogenerated active chlorine relies heavily on the pH of the solution. At pH values of 2 and below,  $Cl_2$  is the predominate species with a standard reduction potential of 1.36 V vs SHE [70]. The electrogenerated  $Cl_2$  remains dissolved in solution until supersaturation drives the formation of gaseous chlorine, and will oxidize contaminants in the bulk of solution [76]. Hypochlorous acid (HOCl), on the other hand, dominates at a pH between 2 and 7, while hypochlorite ions ( $OCl^-$ ) dominate at pH values greater than 8 [77]. These compounds have standard reduction potentials of 1.49 and 0.89 vs SHE respectively [78], making them powerful tools for wastewater treatment applications. One concern exists, however, with the use of active chlorine species; that more toxic, chlorinated organic species may be formed during the reaction pathways. In this instance, secondary treatments or longer treatment times may be required to promote the reduction of chlorinated organics at the cathode, Equation (2.13) [76].

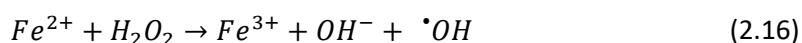


### 2.2.2.1.3 Indirect Cathodic Oxidation

Although reduction reactions at the cathode are generally used in wastewater treatment for the removal of heavy metal ions,  $M^{n+}$ , via deposition, Equation (2.14) [68], they can also be utilized for the treatment and removal of organic compounds.



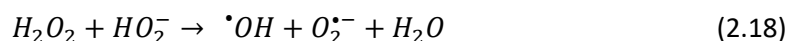
This generally occurs via indirect oxidation using electrogenerated hydrogen peroxides ( $H_2O_2$ ) as an intermediate species. As shown by Equation (2.15), a two-electron reduction of dissolved oxygen can take place at the cathode to form  $H_2O_2$ . This reaction is relatively easy to promote as the reduction of oxygen can take place at a wide range of pH values, and is favoured on inexpensive steel and carbon electrodes [49]. Although  $H_2O_2$  itself is considered to be a strong oxidizing agent, having a reduction potential of 1.76 V vs SHE, it is limited in the types of organic species it can attack; its slow reaction rate makes it insignificant in the oxidation of organic components [79]. However, secondary reactions can be promoted that transform the peroxides into the more powerful oxidizing agents such as hydroxyl radicals. This is achieved in the presence of metal catalysts such as iron, Fe(II), and is commonly referred to as the Fenton reaction, Equation (2.16). This reaction has been used extensively for the treatment of contaminated ground waters and industrial waste streams containing pollutants such as amines, dyes, pharmaceuticals, pesticides, surfactants, explosives, and several other types of organic compounds [70,80–83]. Fenton-like reactions, instead using catalysts such as copper, cobalt or manganese, have also been shown to be effective in the production of hydroxyl radicals from electrogenerated hydrogen peroxides [68].



The last few decades have shown promise in utilizing the electro-Fenton approach, and it is in many ways considered advantageous to the traditional Fenton approach (conventional mixing of  $H_2O_2$  and Fe) as it negates the need for handling and purchasing dangerous peroxides, yet still reaches high degradation rates [70]. Rather, in the electrochemical method, all that is required is the clean reagent, an electron. Another benefit of the electro-Fenton method is that the precipitation of iron sludge is avoided; only small catalytic quantities of soluble iron are required, amounts commonly found in ground waters, as the iron is continuously regenerated at the cathode surface, shown by Equation (2.17).



In the absence of iron or alternative metal catalysts, it has been shown that  $H_2O_2$  can be further reduced at the cathode to form hydroxyl radicals, Equation (2.18), or transformed in the presence of a GAC surface within a three-phase system [76,84]. The efficacy of the later reaction, however, is dependent on the amount of adsorbate present on the GAC surface, where higher quantities of adsorbed compounds reduce the number of surface active sites available for  $H_2O_2$  transformation [85].



The possible pathways for the cathodic generation of hydroxyl radicals and subsequent Fenton reaction for the mineralization of contaminants in aqueous systems is depicted in Figure 2.2. Utilizing this method, several works have successfully treated water contaminated with hydrocarbons [15,82,86,87], resulting in by-products such as ketones and aldehydes, pharmaceuticals [88], phenolic compounds [89], as well as chlorinated aromatic compounds [90]. It is assumed that intermediate products formed during this process are susceptible to further degradation if continuous oxidants are generated [79].

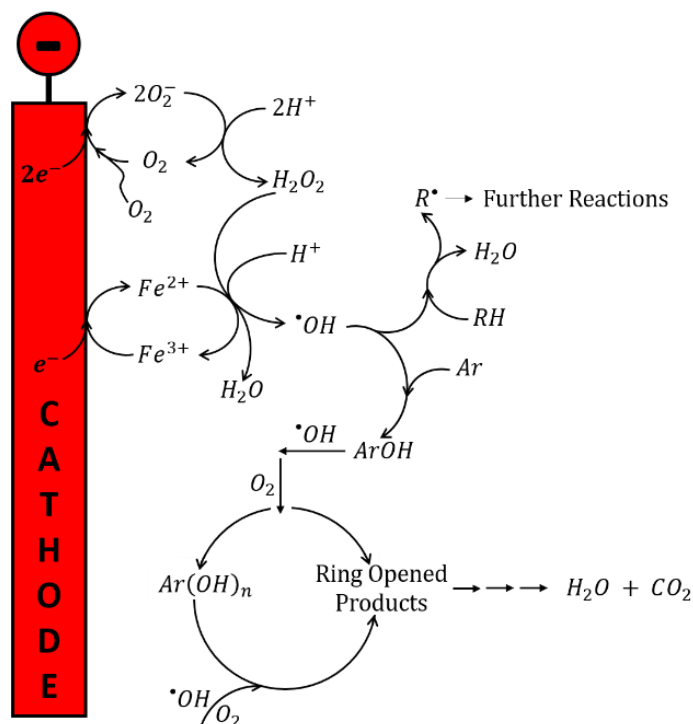


Figure 2.2: Representation of the cathodic production of hydroxyl radicals via the Fenton reaction at the cathode surface in the presence of catalytic iron. 'RH' refers to an unsaturated compound, while 'Ar' is an aromatic compounds undergoing mineralization, adapted from [70]

## 2.2.2.2 Desorbed versus Adsorbed Contaminants

### 2.2.2.2.1 Desorbed Contaminants

Regarding the use of electrochemical reactions to aid in the regeneration of exhausted GAC, many researchers claim that regeneration is ruled firstly by enhanced desorption from the GAC surface, followed by degradation reactions at the electrodes [33,37,49,84]. A study of where this pathway was plausible was conducted by García-Otón et al. [34], whereby electrochemical methods were used to regenerate a toluene loaded GAC. Following electrochemical treatment, a mixture of toluene, benzyl alcohol, benzoic acid and benzaldehyde were detected within the electrolyte, providing evidence that toluene was undergoing degradation reactions. When the experiment was repeated, but the previously used platinum anode was replaced with gold, an anodic material not known to oxidize toluene, no oxidized intermediates were detected in solution. This implied that oxidation reactions were occurring solely at the anode following desorption from the GAC surface.

Several other researchers investigating the electrochemical regeneration of GAC have observed similar behaviour [51,52,91]. By monitoring the aqueous phase contaminant concentration during electrochemical treatment time, such as shown in Figure 2.3, an immediate increase in pollutant concentration is observed, indicative of desorption processes occurring, followed by a decrease in concentration, representative of degradation reactions taking place. This commonly observed development is largely indicative of a desorption-dependent process, with the time lag between desorption and degradation processes being due to mass transfer within the treatment cell. It is noted, however, that some authors come to this conclusion via monitoring the aqueous phase total organic carbon (TOC) or chemical oxygen demand (COD) with time [91]. In such instances, it is unknown if the measured organic concentrations are representative of a

desorbed contaminant from the GAC surface, or an oxidized species converted at the working electrode or polarized GAC surface (discussed more in section 2.2.2.2).

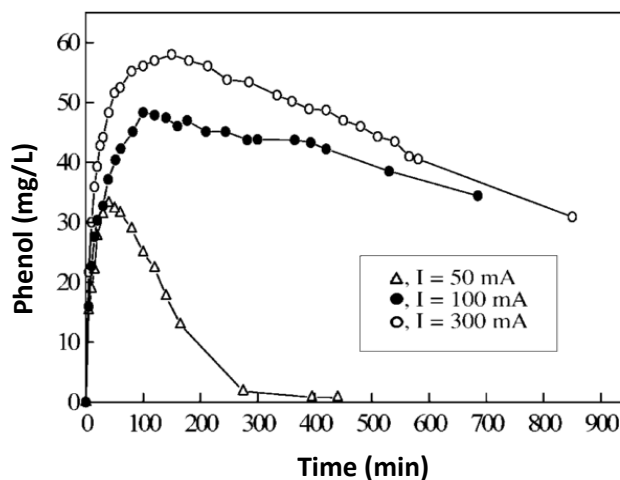


Figure 2.3: The evolution of phenol in the aqueous solution as a function of time when electrochemically treating phenol loaded GAC at variable currents. In all cases, an immediate increase in phenol is seen, indicative of desorption, followed by a decrease in phenol, indicative of oxidation processes occurring [52].

Weng and Hsu [37] also concluded that electrochemical regeneration of GAC is desorption dependent. In their study, GAC regeneration neared 91.1 %, yet no signs of oxidation or degradation were seen within the electrolyte. Thus it was concluded that the high regeneration rate was attributed to desorption processes alone [37]. Conversely, this conclusion was based on the fact that TOC levels linearly increased with time, and no decrease was detected; it should be considered that this may be due to inadequate treatment time or applied electric potential.

Unfortunately, an electrochemical cell that relies on desorption followed by oxidation at the electrodes will incur mass transfer limitations regarding both intra-particle diffusion from the GAC pores, as well as bulk mass transfer to the electrode surface. This is because oxidation reactions involving direct electron transfer and hydroxyl radicals are believed to occur within the Nernst diffusion layer of the electrode surface, less than 50  $\mu\text{m}$  thick, and not in the bulk of solution [36,61]. Such mass transfer limitations becomes increasingly evident when contaminant concentrations within the aqueous phase are low [36].

#### 2.2.2.2 Adsorbed Contaminants

Other researchers have identified that upon placing conductive particles within an electric field in an electrochemical cell, such as shown in Figure 2.4, the particles become polarized and act as microelectrodes where redox reactions take place. Such polarization induces particles to undergo dynamic adsorption, electrochemical catalytic oxidation, desorption, in addition to adsorbent regeneration [68] as Faradaic reactions can occur on the surface of the microelectrodes where contaminant species are adsorbed [12]; such Faradaic reactions include those described in the previous sections, given that the appropriate compounds are present within the system.

Such an electrochemical system that utilizes conductive particles between two electrodes, whether they be GAC, iron, aluminium, conductive ceramic or steel, is generally referred to as a three-dimensional electrochemical reactor (TDER). It is considered to be superior to the standard two-dimensional cell due to the increased area of the electrode surface that decreases

energy consumption, enhances mass transfer, and provides an increased number of active sites at which oxidizing agents can be electrogenerated [78]. More specifically, TDERs utilizing GAC as microelectrodes have proven to be effective for the treatment contaminated aqueous solutions including refinery wastewaters [92], dyes [78], phenol wastes [93], formic acid [94], and several other organic and inorganic containing wastes [68]. Although the capabilities of TDERs have been demonstrated for the decontamination of aqueous solutions, commonly reaching contaminant removal efficiencies more than double its 2D counterpart, less influence has been placed on adsorbent regeneration. If this reaction pathway can be promoted *in situ*, it would be largely beneficial for electrochemical GAC regenerative methods.

Several researchers have demonstrated that the placement of GAC particles between working electrodes results in greater quantities of electrogenerated hydrogen peroxides and oxidizing agents. For example, Bañuelos et al. [95] observed that cathodically polarizing 0.3, 0.5, and 1.0 g of GAC resulted in H<sub>2</sub>O<sub>2</sub> concentrations of 3, 6.3, and 8.9 mM in the bulk solution respectively; it was concluded that this was a result of the increase in active sites upon which oxygen reduction could take place, Equation (2.15). Polcaro et al. [96] observed similar results, demonstrating that increasing the amount of activated carbon within the system resulted in increased oxidation reactions and greater removal of chlorophenol pollutants from a contaminated wastewater supply. It was concluded that this was not due to adsorption processes alone, as increases in activated carbon concentration (from 2 to 13 g/L) resulted in reductions in the ratio of aromatic to aliphatic compounds during treatment; this implied that enhanced degradation reactions were occurring on GAC microelectrodes [96]. Similarly, Wei et al. [92] showed that polarized GAC particles could more than double the chemical oxygen demand (COD) removal of an oil refinery wastewater in comparison to its two-dimensional equivalent. Studies such as these quickly show the capacity for which microelectrodes can enhance the decontamination of contaminated waters, and with this reasoning, it is plausible to suggest that the same mechanism should enable quicker regeneration rates of contaminated GAC surfaces.

When promoting the electrogeneration of hydrogen peroxides on the surfaces of microelectrodes such as GAC, the extent of reaction is dependent on the amount of dissolved oxygen (DO) present in the system. Increasing the DO content of the aqueous phase results in a linear increase in H<sub>2</sub>O<sub>2</sub> production, attaining concentrations 10 times the amount when aeration is not present [95]; a limit is ultimately reached due to oxidation reactions and degradation of H<sub>2</sub>O<sub>2</sub> at the anode. Sowimya et al. [78] had similar findings, showing that aeration of the aqueous phase resulted in increased oxidant levels and greater pollutant removal, from 40 to 76 %, due to the increase in electrogenerated oxidants on the GAC surface.



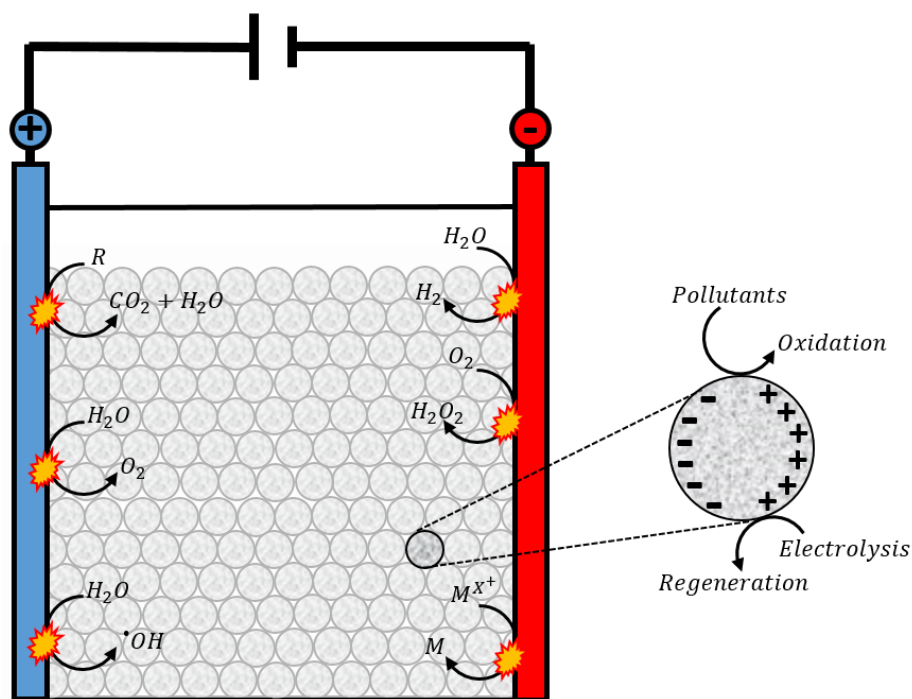
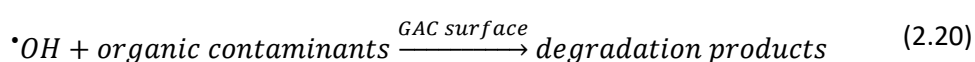


Figure 2.4: Polarization of adsorbent particles within an electrochemical cell, causing particles to undergo dynamic adsorption, electrochemical oxidation, desorption, and regeneration.

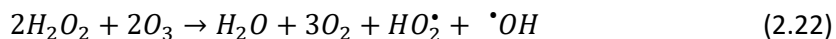
Microelectrode GAC particles not only aid in the production of  $H_2O_2$ , but also act as a catalyst for the decomposition of hydrogen peroxides into highly oxidizing hydroxyl radicals, the simplified mechanisms being shown in Equations (2.19) - (2.21) [84]. In this instance, hydroxyl radicals form on or near the GAC surface and are in much closer proximity to any adsorbed contaminants (in comparison to the working anode). This results in contaminant removal at the GAC surface, and in turn, quicker GAC regeneration due to the decrease in mass transfer limitations.



Taking advantage of this reaction pathway, Bañuelos et al. [38] mixed GAC with an iron-loaded ion-exchange resin (1:10 w/w) such that as  $H_2O_2$  formed on the GAC surface, the Fenton reaction quickly followed as stated in Equation (2.16). Upon loading the GAC with toluene and commencing electrochemical treatments, oxidation by-products of toluene were observed within the column, and the GAC was nearly 100 % regenerated in the first run [38]. Furthermore, subsequent loading and regeneration treatments only showed a 2 % loss in efficiency for each cycle. When the study was performed without iron-loaded resin, little regeneration was seen and toluene was shown to build up within the system, contradicting the notion that GAC alone is an effective catalyst for the production of hydroxyl radicals.

As an alternative to the Fenton reaction, other authors have introduced ozone into the electrochemical reactor for the purposes of converting electrogenerated peroxides into hydroxyl radicals at the GAC surface [91], described by Equation (2.22). Zhan et al. [91] used this method in an attempt to overcome the irreversible adsorption commonly observed with phenol

loaded carbons; previous studies have shown that up to 40 % of phenol is irreversibly bound, limiting the amount of desorption processes that can proceed during regenerative treatments [97]. Following electrochemical treatment with the introduction of ozone, however, the carbon was nearly 90 % regenerated, and maintained a regeneration efficiency of 72 % after 12 cycles of treatment. Other additives such as oxygen, for increased H<sub>2</sub>O<sub>2</sub> production, and steel anodes, for simultaneous electrocoagulation processes have also been tried; these are summarized in Table 2.2.



Promoting direct oxidation reactions on the surface of anodic polarized GAC has also been tried and tested, however, this has resulted in less favourable results. Zhou & Lei [84] claim that anodic oxidation reactions on GAC particles are more likely to lead to the formation of oxygen and carbon dioxide, rather than the formation of hydroxyl radicals or direct electron transfer to contaminant species. This is not unexpected, as direct oxidation of organic substances has been shown to be minor in comparison to indirect oxidation processes, as discussed in Section 2.2.2.1.1.

Table 2.2: Regeneration efficiencies (RE) of GAC achieved when operating electrochemical cells with various additives for the promotion of varying reaction pathways.

Adsorbent / Amount	Pollutant	Additive	Treatment Time [hr]	RE [%]	Ref.
Lignitic GAC, 1.0 g	Toluene	Iron for Fenton reaction Control (no iron introduced)	1.0	98 0	[38]
Activated Carbon Fibre, 0.5 g	Phenol	Ozone for hydroxyl radical formation Control (no ozone introduced)	3.0	89 68	[91]
GAC, 160 cm <sup>3</sup>	Phenol	Use of steel anode for simultaneous electrocoagulation processes	-	80	[98]
Woody GAC, 3.0 g	<i>p</i> -nitrophenol	Oxygen sparging (for enhanced H <sub>2</sub> O <sub>2</sub> production) Control (no oxygen sparging)	0.5	95 85	[84]

### 2.2.3 Electrocoagulation

Electrocoagulation processes may occur simultaneously to the electrochemical reactions occurring within an electrolytic cell and aid in the removal of contaminant species. In this instance, easily oxidisable anodic materials such as iron, steel and aluminium, are used and sacrificed during electrochemical treatments. With increasing operational time the metals dissolve into the bulk solution in the form of divalent and trivalent metals ions where they quickly react with water to form metal hydroxides such as Fe(OH)<sub>2</sub>, Fe(OH)<sub>3</sub>, and Al(OH)<sub>3</sub> [98,99]. Such hydroxides are continuously produced during treatment and coagulate hydrophobic and particulate contaminants in the aqueous phase to form insoluble complexes that precipitate out of solution. Gong et al. [99] demonstrated that this type of treatment could remove 86 % of the polyaromatic hydrocarbons (PAHs) present in a contaminated water supply. Although degradation of the contaminant species was observed, analysis of the produced and settled iron sludge showed that some of the PAHs had merely adsorbed onto the precipitate [99]. With this result, secondary treatments, such as solid-liquid separation, would be required. Regarding the

electrochemical regeneration of GAC, Cañizares et al. [98] utilized a sacrificial steel anode to electrocoagulate desorbed phenol compounds out of solution. In the first cycle, a regeneration efficiency of 80 % was reached for the GAC, however, declined to 65 % in a fourth cycle of regeneration; this is likely due to GAC pores becoming blocked with precipitate, and lowering regeneration efficiencies upon continuous use.

### 2.3 Operational Considerations

Although the electrochemical regeneration of GAC is known to be a functional treatment, research to date has focused primarily on variations in reactor configuration and operating parameters, with research groups utilizing different types of GAC and model contaminants. Although this makes it difficult to gain an understanding of the underlying mechanism, kinetics, and possibility of scale up, the following section aims to summarize and compare how various operating parameters used during the electrochemical regeneration of GAC affect the outcomes achieved. A discussion of the various operating parameters is also presented.

#### 2.3.1 Reactor Configuration

##### 2.3.1.1 Fixed Bed

Fixed beds, depicted in Figure 2.5A, involve the fixation of adsorbent particles on, or between, the working anode and cathode. This configuration has been utilized by several researchers due to the ease of control, enhanced current efficiency, and large surface area to volume ratio that results [68]. The simplicity of the design is also advantageous when scaling-up the reactor. Most often, the adsorbent material is placed in contact with either the anode or cathode as to avoid short circuiting and subsequent decreases in current and degradation efficiencies [100]. To avoid short circuiting, Brown et al. [101] separated the adsorbent material and counter electrode via a microporous membrane, while Wei et al. [92] took an alternative approach by placing a mixture of GAC and non-conducting ceramic particles within the reactor. A similar concept, used by Wang et al. [102], introduced alternating layers of GAC and cellulose acetate coated GAC (GAC-AC) to avoid direct contact between the GAC particles and working electrodes; this configuration resulted in increases in contaminant removal and current yield, with simultaneous decreases in power consumption compared to a standard three-dimensional electrode reactor in which GAC alone was utilized at the particle electrode.

Other researchers have placed the adsorbent material in contact with both anode and cathode simultaneously and have still achieved favourable regeneration efficiencies. Weng and Hsu [37] and Sun and Liu [35] used this configuration to treat waste water treatment plant and phenol loaded GAC and reached regenerations of 91.1 and 94 % respectively. Wang and Balasabramanian [12] also used this configuration and reached a regeneration efficiency of 100 % for the treatment of over 6 kg of exhausted GAC; upon analysing the resulting current efficiencies (i.e. the ratio of current passed to the amount of targeted pollutant removed), it was found that it would quickly decrease when operating at large currents (indicative of short circuiting occurring), but would maintain a high efficiency when operating at low currents.

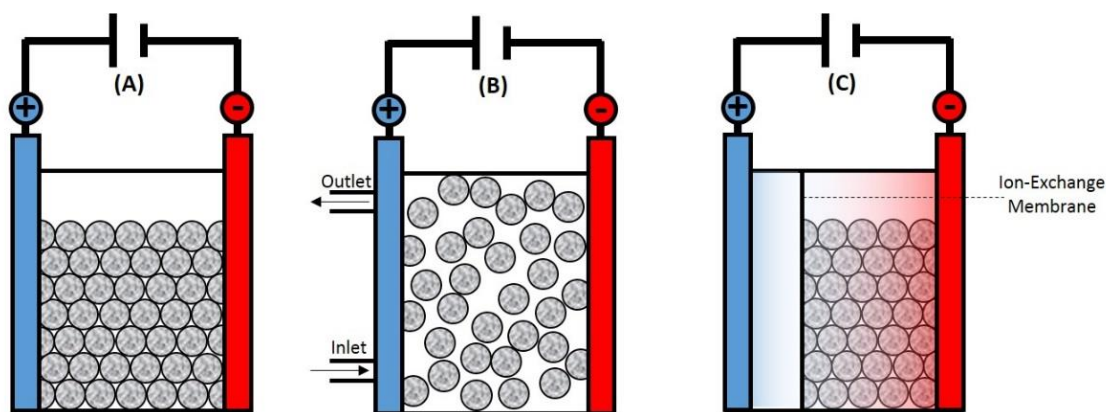


Figure 2.5: Different types of reactor configurations used during the electrochemical treatment of GAC. A) Fixed bed reactor in which the GAC is fixed in place and in contact with the anode and/or cathode, B) Fluidized bed reactor in which the GAC is fluidized via the flow of air or electrolyte, and C) A divided cell in which an ion-exchange membrane is utilized to separate the anodic and cathodic compartments.

The leading limitation with fixed bed configurations is restricted mass transfer. This can be overcome via semi-batch mode operation or the implementation of electrolyte mixing and/or aeration. Mixing may be advantageous to desorption processes, due to the increased concentration gradients between the GAC surface and bulk solution, and current efficiency, due to the quick removal of high resistance electrogenerated gases [47]. Some instances in which enhanced mixing has enhanced GAC regeneration efficiencies are presented in Table 2.3. However, when the desorption of contaminants from the GAC surface is pH dependent, the mixing of anolyte and catholyte can hinder the formation of high and low pH fronts at the electrodes. A study by Karimi-Jashni and Narbaitz [47] showed that mixing was detrimental to the desorption of phenol loaded GAC, as high pH values were not reached.

#### 2.3.1.1.1 'Microconductor Principle'

It is also understood that if the applied electric field is large enough, the fixed bed of conductive particles does not need to be in contact with either the working anode or cathode and will instead become polarized due to the shift in electric charge within the system. This type of mechanism is well explained by the 'microconductor principle', described by Rahner et al. [103]. It was used to demonstrate why, in the presence of an electric field, immobile organic compounds that are largely unaffected by electrokinetic processes are still removed from contaminated soil matrices when undergoing electrokinetic treatment. It claims that removal is not dependent on electrokinetic transport, but rather on the polarization of conductive particles or films within the soil (e.g. weathered rocks and minerals). Upon being polarised, microelectrodes are formed and initiate the redox reactions that aid in the breakdown of immobilized contaminants [103].

The idea was simulated by embedding a platinum wire within an epoxy resin, upon which an electric field was applied across the material via two external electrodes [103]. With the introduction of the electric field, current was seen to flow through the platinum wire, thus becoming a microconductor. However, whether or not induced polarized microconductors will form is dependent on the gradient of the electric field,  $E$ , calculated by Equation (2.23) where  $U_{external}$  is the applied electric potential and  $L$  is the distance between the working electrodes.

$$E = \frac{U_{external}}{L} \quad (2.23)$$

Upon placing a microconductor within the electric field, the potential difference over the microconductor itself,  $\Delta U_{microconductor}$ , is given by Equation (2.24), where  $l$  is the length of the microconductor.

$$\Delta U_{microconductor} = E \times l \quad (2.24)$$

For Faradaic redox reactions to occur at the surface of the microelectrodes, the potential difference over the microconductor needs to be sufficient enough to overcome the resistances of the system [104,105]. The electric field that enables this to occur is referred to as the critical electric field and is highly dependent on the matrix being treated and the types of microconductors present. Once applied, redox reactions commence and are thought to enhance contaminant removal via i) direct oxidation at the microconductor surface, ii) oxidation by induced radicals, or iii) accelerating microbiological activity by improving the conditions of the micro-environment [103].

### 2.3.1.2 Fluidized Bed

Fluidized reactors, depicted in Figure 2.5B, where adsorbent materials are not fixed in place and rather mobilized via the flow of air or electrolyte, have also been investigated. Although mass transfer is greatly increased in these reactors, current distribution across the reactor becomes non-uniform and unstable, lowering current efficiencies and making scale-up more difficult [68]. Similarly, contact between the electrode and adsorbent material is not guaranteed and may hinder regeneration efficiencies. Despite this, fluidized reactors have in several cases shown to be superior to fixed beds, as summarized in Table 2.3.

Table 2.3: Regeneration efficiencies (RE) of GAC achieved when operating electrochemical cells under the same operating conditions in fixed and fluidized bed configurations. Where <sup>a</sup> refers to the 'stripping efficiency', quantifying the amount of contaminant desorption during electrochemical treatment.

Adsorbent / Amount	Pollutant	Bed Type	RE [%]	Ref.
WV-A1100 GAC, 0.2 g (Fixed) 5.7 g (Fluidized)	Toluene	Fixed	98 <sup>a</sup>	[34]
		Fluidized	95 <sup>a</sup>	
Coconut Shell GAC, 0.3 g	Phenol	Fixed	78.8	[51]
		Fluidized	85.2	
Coconut Shell GAC, 7.5 g	Phenol	Fixed	73	[52]
		Fluidized	83	
Woody GAC, 3.0 g	<i>p</i> -nitrophenol	Fluidized		[36]
		1.25 L/min	79.2	
		1.75 L/min	85.2	
		3.25 L/min	87.3	
		3.75 L/min	83.1	

Zhou and Lei [36] and Berenguer et al. [49] utilized fluidized reactors in the electrochemical regeneration of exhausted GAC and reached regeneration efficiencies of 90 and 80 % respectively. Zhou and Lei [36] attributed the high regeneration efficiency to the GAC particles being able to come into close proximity with the anode, in which hydroxyl radicals could oxidize adsorbed species. By increasing the electrolyte flowrate in the fluidized reactor, pollutant removal rates increased from 85.4 to 96.8 % when operated for 1.5 hours [36]. Zhang et al. [52] also showed that mixing to promote particle fluidization within the electrochemical cell could

reach regeneration efficiencies 10 % higher than when the GAC was fixed onto the cathode surface. However, bubbling and fluidization within the reactor can lead to non-uniform current distributions and high ohmic drops, which in turn leads to higher energy consumption [72].

To overcome the limitations associated with fluidized beds, Liu et al. [106] proposed using a novel spouted bed reactor in which a moving packed bed is formed. With this arrangement, simultaneous adsorption of contaminants and regeneration of the adsorbent material occur within the same vessel; the spouted bed promotes turbulent regions in which adsorption processes can occur, whilst zones of moving packed bed allow a continuous conductive pathway for regeneration currents to pass [106]. Increased mass transfer and decreased energy consumption associated with fluidized and packed beds respectively, is achieved. It was found that increasing the liquid flowrate from 4.61 to 11.61 ml/s and promoting greater movement in the reactor (i.e. transforming a fixed bed into a fluidized bed), the contaminant removal rate in the liquid phase increased from 64.8 to 98.9 %, despite operating at the same current of 0.5 A. This is representative of a more energy efficient process.

### 2.3.1.3 *Undivided versus Divided Cell*

A divided cell, depicted in Figure 2.5C, utilizes an ion-exchange membrane to prevent the transfer of anions and/or cations between the anolyte and catholyte compartments; this also avoids species that are oxidized at the anode migrating to and becoming reduced at the cathode. Thus, this type of reactor configuration is especially useful when trying to maintain high concentrations of oxidizing agents. Studies have shown that regenerating phenol loaded GAC within a divided cell can reach slightly higher regeneration efficiencies due to maintaining the catholyte pH at 12 to promote desorption processes [46,107]. In contrast, Berenguer et al. [49] claims that the consumption and degradation of desorbed phenol at the counter-electrode in an undivided cell would lead to greater shifts in equilibrium and enhance regeneration rates. This was confirmed in a study in which the cathodic regeneration of spent GAC reached higher regeneration in all cases when an undivided cell was utilized [49]. Similar findings were obtained by Narbaitz and Cen [33], where although cathodic treatment achieved greater GAC regeneration, residual pollutant was detected in the aqueous phase. In contrast, anodic treatments left little to no residual pollutant within the electrolyte due to the increased oxidizing conditions. Based on these results, an undivided cell would be favourable such that desorption processes could occur at the cathode, upon which desorbed contaminants can migrate to and be oxidized at the anode. Other things to consider are the high cost of ion exchange membranes, difficulty in setting up, and the hindered removal of gases. For these reasons, Narbaitz and Karimi-Jashni [107] ultimately recommended that undivided cells are more practical. Table 2.4 compares the regeneration efficiencies of GAC when utilizing undivided and divided reactors.

### 2.3.1.4 *Cathodic versus Anodic Regeneration*

It is generally agreed that the cathodic regeneration of granular activated carbon (i.e. placing the material in contact with the cathode) results in better regeneration efficiencies than anodic regeneration [33,49]; several examples of this are summarized in Table 2.4.

Zhang [51] showed that the cathodic regeneration of a phenol saturated GAC achieved regeneration efficiencies 20 % higher than that of anodic regeneration. However, it was observed that residual phenol was seen in solution following cathodic treatment, whereas none was seen during anodic regeneration. This is most likely due to mass transfer limitations between the pollutant and the anode and/or electrogenerated oxidizing species, and suggests that cathodic treatment achieves greater desorption rates, whilst anodic treatment achieves

higher degradation rates. Similar results were seen in a study by Narbaitz and Cen [33], however it was concluded that such a limitation can be overcome by extending treatment times, and allowing greater mixing between the electrode compartments.

In an attempt to gain the advantages of both cathodic and anodic treatments, Narbaitz and Cen [33] experimented with changing the polarity of the GAC halfway through regenerative treatment. Although the regeneration efficiencies were not found to be superior in any way, less residual phenol was seen in the aqueous phase following the regenerative treatment [33]. This suggests that anodic oxidation and generated oxidizing species play a key role in degradation of organic compounds.

*Table 2.4: Regeneration efficiencies (RE) of GAC achieved when polarizing the GAC either positively or negatively, in both undivided and divided electrochemical cells. Where <sup>a</sup> is constant voltage operation, <sup>b</sup> is constant current operation, and <sup>c</sup> refers to the 'stripping efficiency', quantifying the amount of contaminant desorption during electrochemical treatment.*

Adsorbent / Amount	Pollutant	Cell Type	Adsorbent Polarity	Time [hr]	RE [%]	Ref.	
WV-A1100 GAC 0.2 g	Toluene	Undivided	Anodic <sup>a</sup> , +3V	3	99 <sup>c</sup>	[34]	
			Cathodic <sup>a</sup> , -2V		100 <sup>c</sup>		
			Cathodic <sup>b</sup> , 500 mA		98 <sup>c</sup>		
F-400 GAC 1.2 g	Phenol	Undivided	Cathodic <sup>b</sup> , 50 mA	3	85	[33]	
			Anodic <sup>b</sup> , 50 mA		80		
			Simultaneous Anodic and Cathodic <sup>b</sup> , 50 mA		86 / 80		
			Reversed (Anodic to Cathodic) <sup>b</sup> , 50 mA		70		
			Reversed (Cathodic to Anodic) <sup>b</sup> , 50 mA		81		
207A GAC 2.0 g	Phenol	Undivided	Cathodic <sup>b</sup> , 1.0 A	3	81	[49]	
			Anodic <sup>b</sup> , 1.0 A		39		
		Divided	Cathodic <sup>b</sup> , 1.0 A		57		
			Anodic <sup>b</sup> , 1.0 A		49		
Coconut Shell GAC, 0.3 g	Phenol	Undivided	Cathodic <sup>b</sup> , 50 mA	5	78	[51]	
			Anodic <sup>b</sup> , 50 mA		56		
Filtrisorb F-400 GAC, 1.2 g	Phenol	Undivided	Cathodic <sup>b</sup> , 50 mA	25	78	[46]	
			Anodic <sup>b</sup> , 50 mA		59		
		Divided	Cathodic <sup>b</sup> , 50 mA		10		72
			Cathodic <sup>b</sup> , 50 mA		78		

It has also been shown that the polarity of the adsorbent material can affect the resulting surface chemistry of the adsorbent following treatment. Through the use of temperature programmed desorption experiments, it was demonstrated that the anodic treatment of GAC can result in an increasing amount of oxygen surface groups adhered to the adsorbent surface [34]. This is not favourable when trying to selectively adsorb hydrophobic compounds, such as hydrocarbons, out of an aqueous solution that can form polar bonds with the aqueous phase. When cathodically treated, the opposite occurred and the oxygen content on the GAC had decreased; this could ultimately improve the selectivity towards hydrophobic hydrocarbons if used as a preparatory method [34]. Similar findings were detected by Li et al. [108] whereby GAC material was pre-treated with electrolysis to see how its adsorptive capacity would be affected. Anodic and cathodic pre-treatments resulted in the oxidation and reduction of functional groups (i.e. phenol, quinones) on the GAC surface, and upon being placed in contaminant solution, simultaneous adsorption and degradation reactions occurred due to the presence of highly

reductive surface groups [108]; reduced GAC proved to have the greatest degradation abilities, followed by untreated GAC, and lastly oxidized GAC. This coincides with the findings of García-Otón et al. [34], stating that cathodic polarized GAC is more favourable for the continuous use of GAC.

### 2.3.2 Operating Parameters

Similar to variations in reactor configuration, the operating parameters of the electrochemical cells utilized for the regeneration of GAC are diverse and demonstrate that small changes in operating conditions largely affect the GAC regeneration outcomes that are achieved. Such operating conditions and outcomes are summarized in Table 2.5, and are discussed in further detail in the following sections.

#### 2.3.2.1 Current Density

Current density is a key parameter during electrochemical treatments, as it is the driving force for contaminant degradation and controls the rate of Faradaic reactions occurring on any given electrode surface. Thus, with increases in applied current there is an increased rate of direct and indirect reaction pathways, such as those described in 2.2.2. The same applies for GAC regeneration and, as summarized in Table 2.6, it is well recognized that increases in current density result in increases in GAC regeneration efficiency and decreases in treatment time [12,35,98,109]. For example, a study by Sun et al. [35] showed that regeneration efficiencies of GAC could reach 90 % when operating for 180 minutes at 1 A, versus 98 % in 100 minutes when operating at 3 A, ultimately saving on time and energy consumption.

Such increases in regeneration rates are attributed to the increased rate of oxidation reactions and  $\cdot\text{OH}$  formation that result with the greater ionic transport through the cell [47]. Simultaneously, increases in applied current result in an increased applied electric potential, in the form of voltage, and cause the GAC surface to maintain a higher surface charge that increases electrostatic repulsions between the GAC surface and contaminant and promote desorption [91].

Notably, the extent of enhancement caused by increasing current density is dependent on mass transfer within the electrochemical cell. If oxidation reactions are not mass transfer limited (i.e. not dependent on compounds migrating from the bulk solution to the electrode surface), increases in current density lead to increases in pollutant removal rate [74,76]. In contrast, if oxidation reactions are mass transfer limited, increases in current will instead enhance parasitic side reactions such as oxygen production, decreasing current efficiency whilst increasing energy costs [74,76].



Table 2.5: Studied electrochemical regenerations of GAC. 'A' is anode material, 'C' is cathode material, 'E' is electrolyte, 'I' is applied current, and \* refers to a treatment where electrocoagulation processes are simultaneously occurring.

Pollutant	Operating Conditions	Time [hr]	RE [%]	Ref.	
Phenol	A: Pt, C: Pt/AC, E: 1 % NaCl, I: 100 mA Undivided Cell, Fixed Bed	2.5	95	[33]	
	A: Pt/Ti, C: Steel/AC, E: 0.5 M NaOH, I: 1.0 A Undivided Cell, Fluidized Bed	3.0	80	[49]	
	A: Pt, C: Pt/AC, E: 1 % NaCl, I: 50 mA Undivided Cell, Fluidized Bed	5.0	85.2	[51]	
	A: Pt, C: Pt/AC, E: 0.1 M NaCl, I: 50 mA Undivided Cell, Fixed Bed	25.0	77, 77, 64	[110]	
	A: Pt, C: Pt, E: 0.1 M NaCl, I: 50 mA Divided Cell, Fixed Bed	10	80	[46]	
	A: Ti, C: Ti, E: 1.0 g/L Na <sub>2</sub> SO <sub>4</sub> , I: 2.0 A Undivided Cell, Fixed Bed	2.0	94	[35]	
	A: Pt, C: Pt, E: 2.0 % NaCl, I: 100 mA Undivided Cell, Fluidized Bed	5.0	86	[52]	
	A: *Steel/AC, C: SS, E: Acid-Phenol Waste, I: 1.0 A Undivided Cell, Fixed Bed	-	80	[98]	
	A: Pt, C: Carbon-PTFE, E: 0.05 M Na <sub>2</sub> SO <sub>4</sub> , I: 400 mA Undivided Cell, Fixed Bed	3.0	89	[91]	
	A: BDD, C: Pt, E: 0.1 M Na <sub>2</sub> SO <sub>4</sub> , I: 0.215 A/cm <sup>2</sup> Undivided Cell, Fluidized Bed	1.0	59.5	[97]	
	A: Pt/Ti, C: Pt/Ti, E: 3.0 % NaCl, I: 1.6 A Undivided Cell, Fixed Bed	2.0	100	[44]	
	<i>p</i> -nitrophenol	A: PbO <sub>2</sub> , C: SS, E: 5 g/L NaCl, I: 4 mA/cm <sup>2</sup> Undivided Cell, Fluidized Bed	1.5	90	[84]
		A: PbO <sub>2</sub> , C: SS, E: 5 g/L NaCl, I: 4 mA/cm <sup>2</sup> , pH 3 Undivided Cell, Fluidized Bed	1.5	92.1	[36]
Toluene	A: Pt, C: Ni/AC, E: 0.5 M NaOH, I: 500 mA Undivided Cell, Fluidized Bed	3.0	98	[34]	
	A: Pt/Ti, C: GAC, E: 0.05 M Na <sub>2</sub> SO <sub>4</sub> , I: 0.55 V Undivided Cell, Fixed Bed	1.0	98	[38]	
Natural Organic Matter	A: Pt, C: Pt, E: 1.0 % NaCl, I: 0 – 4.4 mA/cm <sup>2</sup> Divided Cell, Fixed Bed	5.0	8 - 20	[28]	
Waste Water Treatment Plant	A: Graphite, B: Graphite, E: 0.1 M NaCl, I: 5 V/cm Undivided Cell, Fixed Bed	24.0	91.1	[37]	
Orange II Dye	A: Carbon Cloth, C: Ti/AC, E: 0.05 M Na <sub>2</sub> SO <sub>4</sub> Undivided Cell, Fixed Bed	1.0	90	[24]	
4,4'-diamino stilene-2,2'-disulfonic acid wastewater	A: SnO <sub>2</sub> /Ti, C: SS, E: 5 % (w/w) Na <sub>2</sub> SO <sub>4</sub> , I: 200 A/m <sup>2</sup> Undivided Cell, Fixed Bed	3.0	100	[12]	
Bentazone	A: Pt, C: Ag/AC Cloth, E: 0.01 M Na <sub>2</sub> SO <sub>4</sub> , I: 1700mV Undivided Cell, Fixed Piece of Activated Carbon Cloth	3.0	90	[111]	
Halogenated disinfection by-products	A: Pt, C: Graphite/AC, E: 100 mM phosphate buffer, I: 1000 mV Undivided Cell, Fixed Bed	6.0	> 90	[108]	
Chromium (VI)	A: SS, C: SS, E: 2 % NaCl, I: 0.1 V/cm Undivided Cell, Fluidized Bed	1.0	69.9	[53]	
EDTA	A: Graphite/AC, C: Graphite, E: 1.39mS/cm Na <sub>2</sub> SO <sub>4</sub> , I: 200 mA Undivided Cell, Fixed Bed	1.0	95	[112]	

After a particular current density is exceeded, regeneration efficiencies tend to stabilize, or sometimes decline, due to an increased amount of side reactions occurring. Possible side reactions include solvent breakdown, particularly towards the formation of hydrogen and oxygen at the electrodes. The generation of air bubbles, which have infinite electrical resistance, further decrease the transfer efficiency of current in the cell and limit the amount of oxidation reactions that occur [33]. Similarly, gaseous bubbles may block adsorption and desorption sites on the porous GAC structures [113]. Lower regeneration efficiencies at higher currents may also be observed due to the conversion of  $H_2O_2$  back to oxygen at high voltages, Equation (2.25), hindering the formation of hydroxyl radicals [78], or hydroxyl radicals themselves being transformed back to oxygen at high currents [112]. In general, operating at increased voltages increases the likelihood for which electrogenerated oxidizing species may be reduced at the counter electrode. For example, Brown et al. [101] observed that the regeneration efficiency of a carbon based adsorbent steadily increased with increasing current, but then began to decrease when the current density exceeded a set value of  $20 \text{ mA/cm}^2$ . Additional advantages of operating a regenerative cell at lower currents is the prevention of oxidizing the GAC surface and altering the microporous structure [12], as well as extending the life of the electrodes [92].



The energy consumption associated with increased current densities, calculated by Equation (2.26), also needs to be considered; where  $E$ ,  $E_{cell}$ ,  $I$ , and  $t$  are the energy consumption (kWh), average cell voltage (V), applied current (A), and treatment time (h) respectively. Thus, it is crucial to find a balance between energy consumption and regeneration efficiency when operating an electrochemical cell, and it is generally uneconomical to strive for small increases in oxidation rates when large increases in cell voltage arise [98]. A more detailed analysis on energy consumption involves Equation (2.27), where the specific energy consumption,  $E_{sp}$ , per quantity of pollutant removed is calculated; here,  $E_{cell}$  is the average cell voltage (V),  $V$  is the volume of solution being treated (L) and  $\Delta R$  is the change in pollutant concentration (g/L) during the applied treatment time.

$$E = E_{cell} \times I \times t \quad (2.26)$$

$$E_{sp} = \frac{E_{cell} I t}{V \Delta R} \quad (2.27)$$

Table 2.6: Regeneration efficiencies (RE) of GAC achieved when operating electrochemical cells at various current densities and applied voltages.

Adsorbent / Amount	Pollutant	Applied Current	Treatment Time [hr]	RE [%]	Ref.
F-400 GAC, 1.2 g	Phenol	10 mA	5	76	[33]
		30 mA		88	
		50 mA		92	
		100 mA		93	
207A GAC, 2.0 g	Phenol	0.2 A	3	72	[49]
		0.5 A		75	
		1.0 A		80	
		1.5 A		78	
		2.0 A		77	
Field Spent GAC, 15.0 g	Waste Water Treatment Plant	1 V/cm	12	66.0	[37]
		3 V/cm		70.1	
		5 V/cm		74.4	
Coconut Shell GAC, 0.3 g	Phenol	15 mA	5	72	[51]
		30 mA		76	
		50 mA		78	
		80 mA		86	
F-400 GAC, 1.2 g	Phenol	10 mA	25	62	[110]
		30 mA		65	
		50 mA		77	
		100 mA		76	
GAC, 6283.2 g	4,4'-diamino stilene-2,2'-disulfonic acid wastewater	200 A/m <sup>2</sup>	1	38	[12]
		675 A/m <sup>2</sup>		95	
		2533 A/m <sup>2</sup>		98	
GAC, -	Phenol	1.0 A	3	97	[35]
		2.0 A		90	
		3.0 A		98	
Coconut Shell GAC, 7.5 g	Phenol	50 mA	5	86.0	[52]
		100 mA		86.2	
		300 mA		86.8	
Jacobi GAC, 1.0 g	Natural Organic Matter	0 mA	5	10	[28]
		50 mA		17	
		100 mA		15	
		200 mA		17	
Activated Carbon Fibre, 0.5 g	Phenol	100 mA	4	62	[91]
		200 mA		73	
		300 mA		81	
		400 mA		88	
		500 mA		88	
Picacarb 830 GAC, 1.0 g	Chromium (VI)	1.0 V	1	68.2	[53]
		1.5 V		69.1	
		2.0 V		69.8	
GAC, 1.0 g	Phenol	0.4 A	2	42	[44]
		0.8 A		90	
		1.6 A		88	
		2.4 A		99	

### 2.3.2.2 Electrolyte

With the exception of naturally conductive wastewaters and materials, the addition of electrolytes is necessary to allow ions and electric current to flow. Due to its accessibility, solubility and low cost, the most commonly used electrolyte is sodium chloride. Narbaitz and Cen [33] remarked that increasing NaCl concentrations from 0.1 to 1.0 % (w/w) linearly increased the resulting regeneration efficiency of GAC; this phenomenon has also been confirmed by other research groups [36,51]. This is likely due to the increase in electrolyte conductivity which enables more current to flow and increases the rate of oxidation reactions. In conjunction with this, electrogenerated chlorine species, Equations (2.9) - (2.12), may promote the degradation of organic contaminants in solution. Higher NaCl concentrations also result in greater variances in pH in the anolyte and catholyte; as pH aids in the desorption of some organic pollutants from GAC, this may enhance regeneration [47].

Beyond a concentration of 1 % (w/w) NaCl, no further increases in regeneration of adsorbent materials has been seen. This may be due to active chlorine consuming some of the produced hydroxyl radicals, Equation (2.28), and lowering degradation rates [36].



A drawback of using sodium chloride as an electrolyte is that it can result in the chlorination of organic compounds which may have an increased toxicity. In this case, longer treatment times would be required to degrade the formed compounds [110]. Similarly, toxic intermediate products can be avoided if the formation of hypochlorite and hypochlorous acid are prevented by maintaining low pH levels [36]. In contrast, a study by Li et al. [108] showed that chlorinated by-products could also be degraded, where greater than 90 % of halogenated by-products present were removed within 6 hours of cathodic treatment.

The use of alternative electrolytes such as sodium bicarbonate ( $NaHCO_3$ ), sodium sulphate ( $Na_2SO_4$ ), and sodium acetate ( $CH_3COONa$ ), summarized in Table 2.7, have also been tested but have resulted in significantly lower regeneration efficiencies [33,34,51]. Narbaitz and Cen [33] and Wei et al. [92] claim this to be due to bicarbonate ions acting as scavengers to radicals within solution, hindering the oxidation rate of organic pollutants.

Table 2.7: Regeneration efficiencies (RE) of GAC achieved when operating electrochemical cells with varying electrolytes. Where <sup>a</sup> refers to the 'stripping efficiency', quantifying the amount of pollutant desorbed from the GAC surface during treatment.

Adsorbent / Amount	Pollutant	Electrolyte	pH	Treatment Time [hr]	RE [%]	Ref.
F-400 GAC, 1.2 g	Phenol	0.01 % NaCl	-	5	77	[33]
		0.1 % NaCl			84	
		1.0 % NaCl			90	
		5.0 % NaCl			90	
		1.0 % NaHCO <sub>3</sub>			64	
		1.0 % Na <sub>2</sub> SO <sub>4</sub>			82	
		1.0 % CH <sub>3</sub> COONa			84	
WV-A1100 GAC, 0.2 g	Toluene	0.5 M NaOH	-	3	98 <sup>a</sup>	[34]
		2.0 M Na <sub>2</sub> CO <sub>3</sub>			96 <sup>a</sup>	
		0.5 M Na <sub>2</sub> CO <sub>3</sub>			92 <sup>a</sup>	
		0.5 M Na <sub>2</sub> SO <sub>4</sub>			94 <sup>a</sup>	
207A GAC, 2.0 g	Phenol	0.5 M NaOH	13.5	3	80	[49]
Field Spent GAC, 15.0 g	Waste Water Treatment Plant	0.1 M NaOH	-	48	75.1	[37]
		Tap Water			74.6	
Coconut Shell GAC, 0.3 g	Phenol	1.0 % NaCl	-	5	78.8	[51]
		1.0 % Na <sub>2</sub> CO <sub>3</sub>			66.5	
		1.0 % NaHCO <sub>3</sub>			57.7	
		1.0 % Na <sub>2</sub> SO <sub>4</sub>			65.5	
F-400 GAC, 1.2 g	Phenol	0.1 M NaCl	2	25	56	[46]
			12		83	
GAC, 1.0 g	Phenol	3.0 % NaCl	-	2	90	[44]
		0.5 M NaOH			82	
		Distilled Water			42	
GAC, 5.0 g	Reactive Black B	-	2	1.0	75	[78]
			3		75	
			4		55	
			8.13		36	

### 2.3.2.3 Treatment Time

It is consistently shown that longer treatment times results in greater GAC regeneration [12,33,37,49,114]. If the regenerative mechanism of spent adsorbents is desorption followed by oxidation, this suggests that there is a mass transfer limitation between the desorption of the contaminant at the GAC surface and its oxidation at the electrode surface [33]. Thus, with longer treatment times, more desorption and subsequent oxidation reactions can take place. However,

this would also result in increased energy consumption, Equations (2.26) and (2.27), and altering of the GAC surface becomes more likely [110]. Regeneration efficiencies of adsorbent materials also tend to stabilize after a characteristic period of time, as shown in Figure 2.6. Berenguer et al. [49] postulated this may be due to oxidation by-products adsorbing onto the GAC surface and blocking pores, and in turn, preventing full regeneration from being reached. It may also be explained by irreversible adsorption of contaminants onto the GAC surface, in which higher regeneration efficiencies are more difficult to achieve due to limited desorption processes occurring.

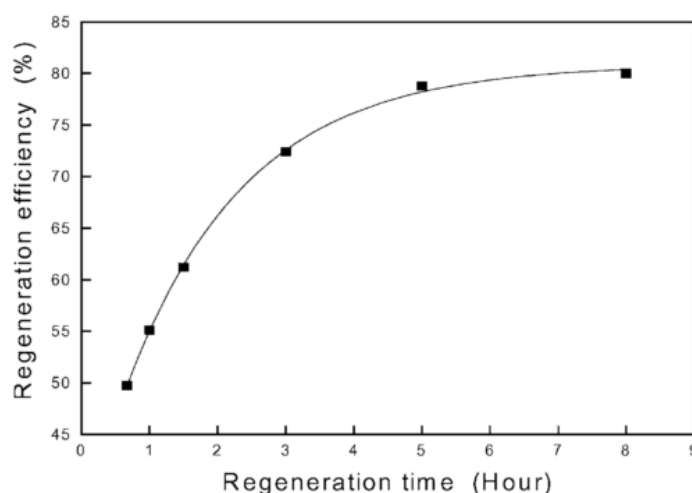


Figure 2.6: Typical regeneration efficiency achieved with increasing treatment time. The plot depicted is representative of the electrochemical regeneration of a phenol saturated GAC [51]

With regeneration rates such as that shown in Figure 2.6, towards the end of the treatment time it is observed that large inputs of energy are needed to gain small increases in regeneration efficiency (i.e. the same energy input needed to progress from 0 to 75 % regeneration is the same needed to progress from 75 to 80 %). This makes the process uneconomical when striving for small increases in regeneration efficiency. In an attempt to overcome this, some researchers have treated aqueous wastes streams with electrochemical methods as a form of pre-treatment for further biodegradation processes. In this scenario, full mineralization is no longer the desired result, and instead, increasing the biodegradability of contaminants becomes the main objective. For example, the conversion of complex, toxic compounds to more biodegradable carboxylic acids and alcohols is considered an adequate outcome and saves on overall energy usage.

Utilizing electrochemical GAC regeneration as a pre-treatment for biological regeneration of the adsorbent material has not yet been explored in the literature. However, it is known that electrochemical treatments are effective at removing high levels of organic carbon, decreasing toxicity, and increasing the biodegradability of contaminants [15,92]. Hou et al. [115] has shown that when utilizing a combined electro/bio system for the treatment of a contaminated water source, the biological portion accounted for up to 40 % of the total carbon removal. Such results indicate that a combined electro/bio treatment for the purposes of GAC regeneration may be a viable option for future engineering prospects; this has yet to be investigated.

#### 2.3.2.4 pH

The pH within an electrochemical cell affects the adsorptive capacity of contaminants, speciation of electrogenerated compounds, electrosorption/electrodesorption processes, and

the rates at which oxidizing reactions occur. Although these processes work separately from one another, it is generally understood that high pH values enhance desorption, while low pH values enhance oxidation reactions. For example, the Fenton reaction requires an acidic environment, in the pH range of 2 – 4, for oxidizing hydroxyl radicals to be formed [80]. Upon being generated, the standard reduction potential of the electrogenerated hydroxyl radicals is much higher in acidic conditions, 2.8 V versus SHE, in comparison to alkaline media, 1.55 V versus SHE [62]. This may give reason as to why several researchers have seen lower regeneration efficiencies when operating at increased pH values. Other possibilities are that acidic conditions limit oxygen formation at the anode, Equation (2.1), and improve the current efficiency of the system [116],  $\text{H}_2\text{O}_2$  stability decreases in basic conditions, and the formation of bicarbonate ions in alkaline solutions act as radical scavengers [78].

In contrast, some researchers have had success with regenerating GAC within alkaline conditions. Berenguer et al. [49] reached GAC regeneration efficiencies slightly higher than 80 % when operating at a pH value greater than 13. This may be due to either enhanced electrodesorption of disassociated contaminants [43], or that unprotonated species are more easily oxidized than their protonated counterparts [76]. For all these reasons combined, Karabacakoglu and Öznur [53] recommend operating an electrochemical regenerative cell at the highest possible acidic pH value.

#### 2.4 Industrial Application

The large-scale implementation for the electrochemical regeneration of GAC has not yet been implemented, largely due to a lack of understanding and optimisation of the treatment process. However, a technology operating on a similar principle has recently been developed by Arvia Technology Ltd., whereby contaminant adsorption and electrochemical destruction occur within a single cell. The Arvia Organics Destruction Cell™ (ODC), depicted in Figure 2.7, passes contaminated wastewater through a bed of proprietary Nyex™ particles that adsorb contaminant organic compounds. Once the adsorbent becomes saturated, a low electric voltage is passed through the material to oxidize and destroy any adsorbed contaminants, simultaneously regenerating the adsorbent whilst producing an effluent with decreased chemical oxygen demand, colour, and micropollutant levels [117–120]. It is proposed that this technology is applicable to several industries for the continuous treatment of generated wastewaters including chemical, pharmaceutical, mining, food and beverage, and oil and gas.

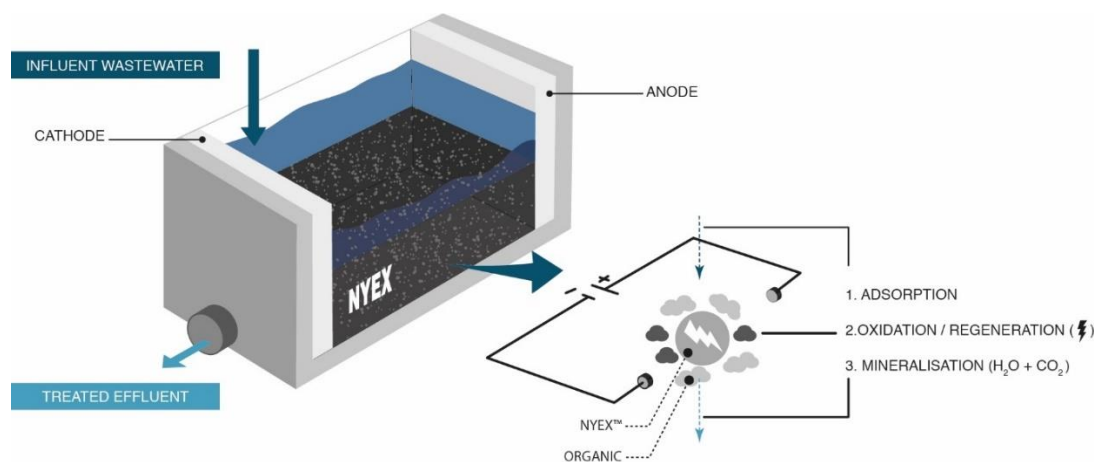


Figure 2.7: Wastewater treatment system developed by Arvia Technology, combining both adsorption and advanced oxidation processes within a single unit [117]

The Nyex™ adsorbent material utilized within the ODC™ is a non-porous carbon material developed to overcome the slow adsorption and desorption processes associated with traditional GAC materials; this results in much quicker treatment times as the process is no longer reliant on slow intra-particle diffusion processes [101]. Similarly, the lack of microporosity results in greater electrical conductivity and a decreased surface area, about 0.14 % of traditional GAC. Although its adsorptive capacity is greatly decreased, it can in turn be fully anodically regenerated within ten minutes of treatment, proving to be superior to GAC regeneration [101]. Further work has been conducted on this technology to show that it can effectively treat waters contaminated with phenol [121], dyes [101], atrazine [114], chlorinated compounds [122], and can be effectively scaled up [123].

A comparable technology, developed by Eko Harden Technologies Oy, uses electrochemical treatments to promote the *in situ* remediation of contaminated soils. The manufactured EKOGRID™, abbreviated for *ElectroKinetic Oxidation*, utilizes a combination of electrokinetics, electrochemical reactions, and enhanced biodegradation processes to breakdown and mineralize immobile contaminants adsorbed onto soil particles [124]. Although the matrix in this instance is much less conductive than GAC, the same types of mechanisms and reactions are promoted to achieve complete pollutant removal and remediation.

The EKOGRID™ operates on a pulsed voltage profile that continuously reverses polarity; this results in the formation of electroosmotic forces in opposing directions and initiates the back and forth movement of water. As charged ions shift within the wet soil matrix and soil particles charge and discharge with each voltage pulse, Faradaic reactions occur on the surface of the soil particles, as is observed within a GAC matrix, and result in the formation of oxygen, oxidizing agents and hydroxyl radicals [124]. Such oxidizing species subsequently breakdown nearby contaminants within the soil system, whilst increased oxygen levels enhance the natural rate of biodegradation processes occurring. This technology has been deployed and shown to be successful in over ten countries worldwide, aiding in the remediation of soils contaminated with aliphatic and aromatic hydrocarbons, chlorophenols, and crude oils [125].

Analogous technologies have been designed by GeoTechnik GmbH, whereby an electric voltage is introduced across a contaminated soil mass with the aim of degrading harmful substances at the place at which they are adsorbed (i.e. not reliant on electrokinetic transport) [126]. The design proposes that any wet soil matrix acts as a diluted electrochemical reactor, with redox reactions occurring at all interfaces between the soil particles and soil water [103,127]. The natural capacitive nature of the soils and extent of redox reactions is further increased when microconductors within the soil are present, such as conductive minerals and films that include iron, manganese or titanium compounds [103]. Ultimately, it is claimed that the occurrence of such redox reactions within the soil subsurface are able to break down toxic organic substances into non-harmful by-products such as water and carbon dioxide.

The systems described above are directly analogous to a PRB-like system, under which the same redox reactions may occur at the conductive GAC-groundwater interface. Therefore, the success of the treatments described give promise to the viability of designing a regenerative GAC treatment for *in situ* PRB treatment. Moreover, the increased conductivity of the GAC in comparison to contaminant soils is believed to achieve much quicker treatment time, in a matter of days, versus a matter of months.



## 2.5 Research Required for Implementation in Antarctic PRBs

This chapter demonstrates that electrochemical treatments are an effective method for the regeneration of exhausted GAC. The high regeneration efficiencies, short treatment times, low energy consumption and *in situ* capabilities make it beneficial for use in environmental remediation efforts such as PRB regeneration. However, the development of this technology has progressed slowly since its initial exploration two decades ago and it is not ready for field deployment.

Research to date has predominantly focused on variations in reactor configurations and operating parameters, with research groups utilizing different types of GAC and model contaminants. Little focus has been put towards the functional aspects of the treatment process, such as the underlying mechanism and kinetics, and is currently delaying process optimization and scale up. With further research, an understanding needs to be gained on the effects varying operating parameters have on treatment outcomes, as well as determining the regeneration pathways and electrogenerated active species that will enhance degradation processes for target compounds. Studies to date have been limited to contaminant compounds such as phenolics and dyes that are characterized by high aqueous solubility and the capacity to disassociate at extreme pH values. As such, the regenerative process is claimed to be heavily reliant on desorption processes and it is unknown if electrochemical treatments would have the same effect on GAC materials saturated with hydrophobic compounds (e.g. petroleum hydrocarbons) that are largely limited by desorption and disassociation processes. This needs to be investigated to determine if this treatment is applicable to the remediation of petroleum contaminant sites and materials such as those faced in Antarctic PRBs.

Recent industrial progressions have shown that non-porous materials are effective for use in combined adsorption-electrochemical treatment systems. A key example of this is the Organics Destruction Cell™ developed by Arvia Technology, whereby electric currents are utilized to continuously regenerate carbon based adsorbent materials. However, the use of such materials within PRBs in both temperate and Polar regions may not be practical as they have limited adsorption capacities and may not ensure contaminant dispersal is avoided. Rather, the design of a system in which both adsorption and regeneration of GAC can occur in the same vessel is ideal and is the focus of this thesis.

The following chapters address some of the prevailing questions in the literature regarding the electrochemical regeneration of GAC, while also placing focus on the feasibility of regenerating Antarctic PRB substrate materials. Firstly, as desorption processes alone are not a sufficient result in environmental applications, a methodical approach is taken to identify what types of electrochemical reactions and electrogenerated active species aid in the decomposition of petroleum hydrocarbon compounds commonly detected in Antarctic PRBs. Due to the natural presence of chloride and iron at the contaminated sites in the Antarctic, the active-chlorine and electro-Fenton pathways are considered. At a more general level, this analysis demonstrates the importance of selecting a suitable electrolyte and presents a procedure for which it can be identified. Secondly, insoluble and hydrophobic petroleum compounds are utilized as a model contaminant in this work to assess whether electrochemical treatments are applicable for the regeneration of Antarctic PRB materials; this simultaneously sheds light on how insoluble contaminants respond to electrochemical methods where desorption and disassociation processes are limited. And lastly, a systematic evaluation is undertaken to identify the underlying kinetics and mechanisms for which GAC is electrochemically regenerated; enhanced desorption, electrodesorption, and electrochemical oxidation processes are considered, and the

relative degree to which they aid in GAC regeneration is determined. Altogether, longstanding questions in the literature concerning the mechanism and optimization of the treatment process are answered, and the practicality of using electrochemical techniques to regenerate contaminated GAC within Antarctic PRBs is addressed.

---

# **CHAPTER 3**

---

## Materials and Analytical Methods

This chapter describes the materials and analytical methods used throughout the thesis that follows. Specific experimental designs are detailed in the chapters in which they are used.

---



### 3.1 Chemical Reagents

All chemicals used throughout this thesis were either analytical or gradient grade and used as received from the supplier; relevant chemicals are detailed in Table 3.1. For the preparation and carrying out of all experimental and cleaning procedures, reverse osmosis (RO) water was used. For analytical procedures, academic grade Milli-Q (Millipore, resistivity > 18 MΩ cm<sup>-1</sup>) was utilized.

Table 3.1: Chemical reagents, detailing their respective supplier, purity, and purpose for the production of this thesis.

Chemical	Formula	Supplier	Purity [%]	Use in Thesis
Acetone	(CH <sub>3</sub> ) <sub>2</sub> CO	BJ Honeywell	100	TPH extraction, Cleaning
Acetonitrile	CH <sub>3</sub> CN	BJ Honeywell	≥ 99.9	HPLC carrier
pH Buffer	pH 4, 7, 10	Chem-Supply	-	pH probe calibration
Decon90	-	Decon	100	Cleaning
Dichloromethane	CH <sub>2</sub> Cl <sub>2</sub>	RCI Lab Scan	≥ 99.9	TPH Extraction
Ethanol	C <sub>2</sub> H <sub>5</sub> OH	Chem-Supply	100	Cleaning, dissolving naphthalene
Helium	He	Coregas	99.99	GC carrier
Hexane	C <sub>6</sub> H <sub>14</sub>	RCI Labscan	95	TPH/Naphthalene extraction
Hydrogen Peroxide	H <sub>2</sub> O <sub>2</sub>	Chem-Supply	30	H <sub>2</sub> O <sub>2</sub> calibration
Hydromatrix	-	Agilent	100	TPH extraction
Ferrous sulfate heptahydrate	FeSO <sub>4</sub> •7H <sub>2</sub> O	Chem-Supply	99.5	Electrolyte
Naphthalene	C <sub>10</sub> H <sub>8</sub>	Sigma-Aldrich	99	Hydrocarbon source
1-Naphthol	C <sub>10</sub> H <sub>8</sub> O	Sigma-Aldrich	≥ 99	By-product detection
1,4-Naphthoquinone	C <sub>10</sub> H <sub>6</sub> O <sub>2</sub>	Sigma-Aldrich	97	By-product detection
Potassium Ferricyanide	K <sub>3</sub> Fe(CN) <sub>6</sub>	Chem-Supply	99	Mass Transfer Characterization
Potassium Ferrocyanide	K <sub>4</sub> Fe(CN) <sub>6</sub>	Sigma-Aldrich	≥ 98.5	Mass Transfer Characterization
Sodium Chloride	NaCl	Chem-Supply	99	Electrolyte
Sodium Hydroxide	NaOH	Chem-Supply	99	pH adjustment
Sodium Sulphate	Na <sub>2</sub> SO <sub>4</sub>	Chem-Supply	99	Electrolyte
Special Antarctic Blend diesel	-	BP	100	Hydrocarbon source
Sulfuric Acid	H <sub>2</sub> SO <sub>4</sub>	Scharlau	95 – 97	pH adjustment
Titanium Oxysulphate	TiOSO <sub>4</sub>	Sigma-Aldrich	1.9 – 2.1	H <sub>2</sub> O <sub>2</sub> Detection

More detailed descriptions on the use and purpose of each chemical is given throughout the chapters that follow.

### 3.2 Experimental Materials

#### 3.2.1 Petroleum Hydrocarbon Source

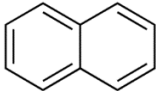
##### 3.2.1.1 Laboratory Studies (Naphthalene)

Although the contaminated sites at Australian Antarctic Research stations are comprised of a complex mixture of Special Antarctic Blend (SAB) diesel, kerosene, and lube oils, a single petroleum compound was used to investigate and model the efficacy of electrochemical treatments towards petroleum hydrocarbons. How such treatments affect complex hydrocarbon mixtures, such as SAB, is addressed later in a feasibility study.

Of the compounds present in SAB diesel, aromatic compounds are believed to have the greatest toxicity and are the least susceptible to biodegradability; this makes them a high priority compound for removal in the contaminated sites present in the Antarctic and sub-Antarctic. Thus, one of the more prevalent aromatic compounds within SAB, naphthalene, was chosen as

a model compound. In addition to its toxicity, the strong  $\pi$ - $\pi$  interactions between naphthalene and granular activated carbon make it an interesting compound of choice as this limits its desorption capabilities from the GAC surface. If electrochemical treatments are proven effective in regenerating a highly toxic, not easily biodegraded, or readily desorbed compound, it is hopeful that the process can be applied to complex mixtures of hydrocarbons. The details of naphthalene are detailed in Table 3.2.

Table 3.2: Physical characteristics of naphthalene.

Chemical Formula	Chemical Structure	Molecular Weight [g/mol]	Solubility [mg/L]
C <sub>10</sub> H <sub>8</sub>		128.174	31

One of the major limitations of utilizing naphthalene is its limited solubility; dissolving naphthalene crystals into water takes several days to dissolve. To counteract this in subsequent experimental work, a concentrated stock solution was first prepared in ethanol. Adequate dilution of the stock solution was performed in RO water, leaving all final synthetic naphthalene solutions with an alcohol concentration of less than 0.2 % v/v. As slight recrystallization is seen during the dilution into water, the solution was mixed on a magnetic stirrer for 24 hours to ensure complete dissolution.

### 3.2.1.2 Feasibility Trials (Special Antarctic Blend diesel)

Special Antarctic Blend (SAB) diesel is the main form of fuel used and spilled at Australian research stations. As shown by Figure 3.1, it is mostly comprised of hydrocarbons in the n-C<sub>10</sub> to n-C<sub>16</sub> range. However, when looking at contaminated sites in the Antarctic and sub-Antarctic, there is an historic presence of aviation turbine kerosene (ATK), diesels, and lubrication oils that are also likely to present during analysis. The sum of all petroleum-based hydrocarbons is referred to as Total Petroleum Hydrocarbons (TPH), comprising hydrocarbons in the n-C<sub>9</sub> to n-C<sub>40</sub> range such as shown in Figure 3.1. During the analysis of contaminated GAC substrates extracted from Antarctic PRBs, contaminant concentrations are thus reported in TPH.

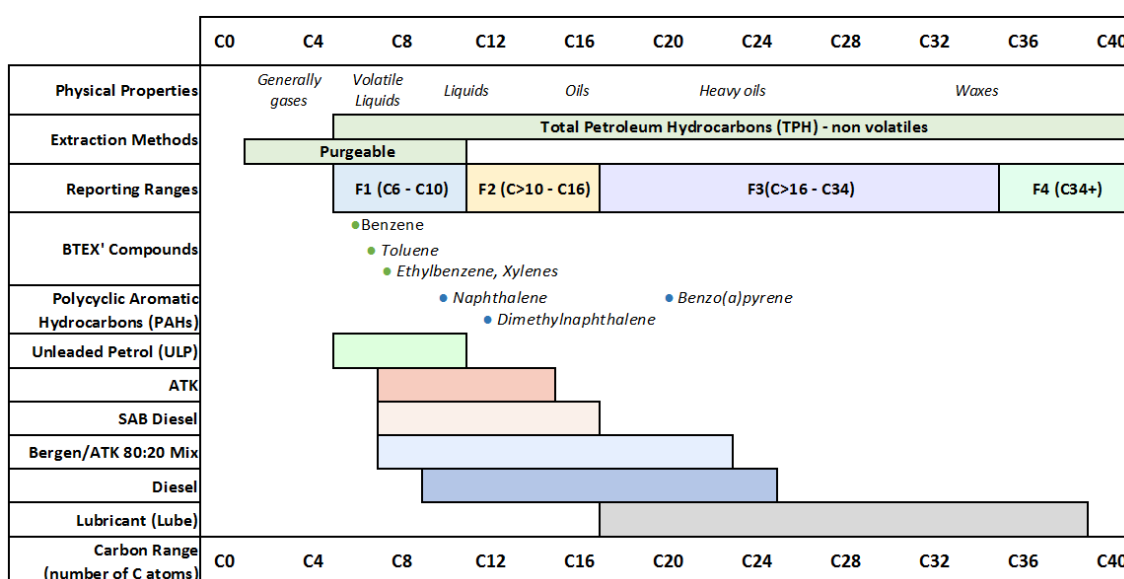


Figure 3.1: Breakdown of petroleum hydrocarbons in the n-C<sub>1</sub> to n-C<sub>40</sub> range.

### 3.2.2 Granular Activated Carbon

The model adsorbent material used in this study is limited to granular activated carbons that are utilized by the Australian Antarctic Division; this includes GAC supplied by Activated Carbon Technologies Pty Ltd. The GAC of choice generally implemented in Antarctic PRBs is GC1200, and thus will be utilized to model the electrochemical treatments in the thesis that follows. The characterisation of this type of GAC is detailed in Table 3.3.

Table 3.3: Characteristics of Acticarb GC1200 GAC. †Indicates properties provided by [128]

Material Property	Acticarb GC1200
Source Material	Coconut Husk
Activation Method	Steam Activated
Mesh Size†	4 x 8, 6 x 12, 12 x 40
BET Surface Area (m <sup>2</sup> /g)†	1137
Total Pore Volume (cm <sup>3</sup> /g)†	0.458
Micropore Fraction [%]†	100
Mesopore Fraction [%]†	0
Contact pH†	10.71 ± 0.09
Point of zero charge (pH <sub>pzc</sub> )†	5.70 ± 0.37

Prior to using this GAC in experimental runs, the desired particle size was obtained by utilizing a stack of ASTM 2007 sieving trays in order of decreasing mesh size. Particle size in the range of 1.70 – 2.36 mm was used for all subsequent studies such that variations in data were kept to a minimum. Following sieving, the GAC was washed several times in RO water to remove ash and fines, and then placed in an oven at 105 °C for 24 hours until a constant weight was obtained. Following drying, the GAC was kept in a sealed glass bottle with a Teflon-lid to avoid adsorption of contaminants or moisture from the air onto the GAC surface.

### 3.3 Analytical Techniques

#### 3.3.1 High Performance Liquid Chromatography

An Agilent 1200 Series High Performance Liquid Chromatography (HPLC) was used to determine the solubilized naphthalene concentrations within aqueous solutions, before, during and after electrochemical treatments. Analysis was performed using a ZORBAX Eclipse XBD-C<sub>18</sub>, 3.5 μm, 3.0 x 150 mm column under the following chromatographic conditions: an acetonitrile and water mixture with a ratio of 60:40 v/v and a mobile phase flowrate of 1.0 ml/min; room temperature (20 °C); sample injection volume of 20 μl, isocratic elution mode and a run time of 6 minutes. UV-Visible detection was performed with a diode array detector (DAD) at a wavelength of 275 nm, with naphthalene eluting at 3.1 minutes.

The HPLC was calibrated by preparing a naphthalene stock solution with a concentration of 30 mg/L in acetonitrile. Sample injection volumes between 0.1 and 25 μl were analysed on the HPLC to form a calibration curve consisting of the mass of naphthalene (x 10<sup>6</sup> g) versus the integrated peak area on the chromatogram (x 10<sup>5</sup>). The calibration curve was performed in duplicate and resulted in an R<sup>2</sup> value greater than 0.99.

#### 3.3.2 Gas Chromatography – Mass Spectrophotometry

An Agilent gas chromatograph (GC 6890) coupled with mass spectroscopy (MS 5973N) was utilized to detect and identify by-product species generated during electrochemical treatments. 5 ml aqueous phase samples were taken from the electrochemical reactor at various timepoints and extracted for 5 minutes via vigorous shaking with 5 ml of hexane in a Teflon-caped 40 ml

headspace vial. Following extraction, 2  $\mu\text{l}$  samples of the organic layer were injected into the GC with the following chromatographic conditions: helium carrier gas operating at 1.3 ml/min at a split injection ratio of 1:20 and temperature of 300 °C; the oven had an initial temperature of 50 °C that was held for 3 minutes, and then ramped at a rate of 18 °C until a temperature of 300 °C was reached and held for 10 minutes. Under these conditions, naphthalene was found to elute at 8.66 minutes, with all new by-product peaks being identified with the Wiley Spectral MS Library.

### 3.3.3 Gas Chromatography – Flame Ionization Detector

Gas Chromatography coupled with a Flame Ionization Detector (GC-FID) was used to determine the TPH, SAB, and naphthalene concentrations on exhausted GAC materials. A 4 g solid sample was extracted on an Accelerated Solvent Extraction (ASE) Dionex 200; to each unprocessed sample, Hydromatrix (calcined diatomaceous earth) was added to act as a drying agent, along with 1 ml of internal standard. The standard utilized was a mixture of 1,4-dichlorobenzene, *p*-terphenyl, and deuterated tetracosane ( $\text{C}_{24}\text{D}_{50}$ ) at 50 mg/L, and cyclooctane and bromoeicosane at 250 mg/L in dichloromethane (DCM). Following sample preparation, the ASE was operated at 1,500 psi with the following runtime characteristics: heat 6 minutes, static 3 minutes, 125 °C set temperature, flush at 20 % volume, purge for 60 seconds, with a total of 2 cycles utilizing a 1:1 v/v DCM : acetone solvent.

Following extraction, the organic portion of the samples were measured using an Agilent 6890N GC-FID with a split/splitless injector. With a 3.0 ml/min helium carrier gas, 1  $\mu\text{l}$  of the extract was injected (5:1 pulsed split) at 310 °C. The oven temperature was started and held at 36 °C for 3 minutes, and then increased to 320 °C at a ramping rate of 18 °C/min; the temperature of the FID detector was set to 330 °C. The resulting TPH, SAB, and naphthalene concentrations in the organic extracts were determined using calibration curves generated from standard solutions; they were measured using the ratio of total detector response of the hydrocarbons to the internal standard peak response.

### 3.3.4 Ultraviolet / Visible Spectrophotometry

Ultraviolet/visible (UV/Vis) spectrophotometry was conducted on an Agilent Cary 300 spectrophotometer to determine the hydrogen peroxide ( $\text{H}_2\text{O}_2$ ) concentration within aqueous solutions. The titanium(IV) oxysulfate ( $\text{TiSO}_4$ ) method was used, whereby 0.14 ml of a 1.9 – 2.1 %  $\text{TiSO}_4$  solution was mixed with 1.4 ml of aqueous sample. Upon mixing, a yellow-coloured  $\text{Ti-H}_2\text{O}_2$  complex formed and the sample was measured on the UV/Vis at a wavelength of 409 nm.

The UV/Vis was calibrated by preparing  $\text{H}_2\text{O}_2$  standard solutions from a concentrated 30 w/w%  $\text{H}_2\text{O}_2$  stock solution.  $\text{H}_2\text{O}_2$  concentrations between 0.6 and 163 mg/L were prepared and analysed on the UV/Vis to form a calibration curve consisting of the hydrogen peroxide concentration (mg/L) versus the absorbance (-). The calibration curve was performed in duplicate and resulted in an  $R^2$  value greater than 0.99.

### 3.3.5 Sieving

Prior to use, the desired particle size of the GAC was obtained by utilizing a stack of ASTM 2007 sieving trays in order of decreasing mesh size. The stack was manually shaken for 5 minutes, and the resulting particles in the size range of 1.70 – 2.36 mm was used for all studies.

### 3.3.6 pH, Oxidation-Reduction Potential, Electrical Conductivity

The pH of aqueous solutions was measured using an InLab Versatile pH (Mettler Toledo). Prior to use, the pH probe was calibrated with pH 4, 7, and 10 buffer solutions.



---

# CHAPTER 4

---

## Electrochemical Treatment of Naphthalene Contaminated Waters via Active Chlorine

This chapter examines the active chlorine electrochemical reaction pathway and its effectiveness for the degradation and removal of solubilized naphthalene within contaminated waters.

*This chapter has resulted in the following publication:*

**McQuillan, R. V.**, Stevens, G. W., & Mumford, K. A.. Electrochemical removal of naphthalene from contaminated waters using carbon electrodes, and viability for environmental deployment. *Journal of Hazardous Materials*, 383 (2020) 121244.

---



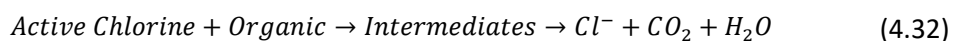
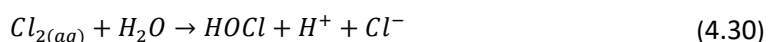
#### 4.1 Introduction

Chapter 1 discussed the methods available for GAC regeneration, comprising desorption and decomposition pathways, and concluded that decomposition methods are favoured for use in environmental applications. This is due to the fact that desorption alone results in leachates that require secondary treatment; when considering the *in situ* application within PRBs, this may also enable desorbed contaminants to disperse into the surrounding environment.

In order to achieve decomposition pathways, the appropriate electrochemical reactions need to be promoted; this is dependent on the target pollutants and composition of the wastewater being treated. Promoting ineffective reactions that fail to generate the appropriate oxidizing agents has led many to the conclusion that desorption is the main mechanism at which electrochemical regenerative methods succeed (refer to Chapter 2). Therefore, prior to investigating GAC regeneration itself, this chapter begins by identifying the electrochemical reactions that assist the breakdown of petroleum hydrocarbon species commonly seen at the contaminated sites of the Antarctic and sub-Antarctic. Without degradation reactions occurring during *in situ* PRB treatments, electrochemical methods may not be appropriate for field deployment applications.

When considering remediation efforts in coastal regions, such as the ice-free zones of Antarctica, contaminated groundwaters present with a high salinity. This is due to the periodic inundation of seawater during extreme high tides that leaves surface waters and soils with high concentrations of chloride ions [3,129]. Due to the natural presence of chloride within these contaminated sites, it becomes feasible to promote the ‘active chlorine’ electrochemical pathway, known to be effective in the oxidation and breakdown of several aqueous organic compounds [76,77,130–133].

This pathway occurs via three sequential reactions, described by Equations (4.29) - (4.31). First, chloride ions ( $Cl^-$ ) in the bulk solution migrate to the anode and undergo electrochemical transformation to form solubilized chlorine ( $Cl_{2(aq)}$ ). Second, the generated chlorine re-enters the bulk solution where it is rapidly transformed into either hypochlorous acid (HOCl) or hypochlorite ions ( $OCl^-$ ) depending on the pH of the system;  $Cl_{2(aq)}$  dominates at a pH levels of 2 and below, HOCl between a pH of 3 and 8, and  $OCl^-$  in more alkaline conditions.



The resulting oxidizing mixture of  $Cl_2$ , HOCl, and  $OCl^-$  is generally referred to as ‘active chlorine’, where all three species are capable of oxidizing and breaking down organic species, shown by Equation (4.32). HOCl is deemed to be the most oxidizing and useful product in wastewater treatment processes, making it beneficial to operate between slightly acidic and neutral conditions [77,134]. Through this reaction pathway, waters contaminated with textile effluents [60,135,136], nitrates and ammonium [65,137], pharmaceuticals [138], and phenolics [139,140] have successfully been treated.

This chapter focuses on the ability of the active chlorine pathway to degrade petroleum hydrocarbons commonly seen in Antarctic contaminated sites. The fuels that are used and

spilled in these regions are generally modified mixtures in which the heavy and waxy end components have been removed to improve its performance in cold climates [13]. Through such modification, the BTEX compounds (benzene, toluene, ethylbenzene and xylene) that commonly present in temperate climates have a limited presence in these regions [4]. However, aromatic compounds are still believed to have the greatest toxicity and are the least susceptible to biodegradation processes, indicating that they will persist in the environment for long periods of time. Thus, one of the more prevalent aromatic compounds, naphthalene, was chosen as a model contaminant to examine the efficacy of the active chlorine pathway. Varying operational parameters are considered such as the applied electric current, hydrodynamic conditions, and saline concentrations, and a kinetic model is proposed that can accurately predict treatment outcomes under all experimental conditions tested. This will ultimately make scale-up more conceivable and shed light on what types of reactions would be effective for the regeneration of carbon substrate materials such as granular activated carbon. It is noted that granular activated carbon electrodes themselves could not be used for this study as their high porosity and adsorptive capacity made it difficult to distinguish between naphthalene removal due to active chlorine degradation in the bulk solution and adsorption processes onto the carbon surface; adsorption alone was observed to achieve full naphthalene removal in as little as one hour of treatment

## 4.2 Experimental

### 4.2.1 Reagents

The analytical reagents used within this chapter are detailed in Table 3.1. Sodium chloride (NaCl), sodium sulphate ( $\text{Na}_2\text{SO}_4$ ), and potassium ferricyanide ( $\text{K}_3\text{Fe}(\text{CN})_6$ ) were purchased from Chem-Supply and used as received. Potassium ferrocyanide ( $\text{K}_4\text{Fe}(\text{CN})_6$ ) and solid naphthalene were purchased from Sigma-Aldrich. Reverse osmosis (RO) water was used for the preparation of all solutions, except for naphthalene in which a concentrated stock solution was prepared in ethanol (EtOH) due to its low solubility in water. Adequate dilution of the EtOH stock solution was performed in RO water, leaving all final synthetic naphthalene solutions with an alcohol concentration of less than 0.2 % v/v.

### 4.2.2 Electrochemical Reactor

Electrochemical experiments were carried out in an undivided glass cell with a capacity of 250 ml, depicted in Figure 4.1. Commercially available cylindrical carbon rods (8 mm  $\varnothing$ , Jaycar) were used as the single anode and cathode, placed 20 mm apart and vertically parallel to one another. The electrodes were connected to a MP3087 (PowerTech) DC regulated power supply (0 – 32 V, 0 – 3 A) and operated under galvanostatic conditions at room temperature (23 °C); during experiments, temperatures were found to fluctuate  $\pm 1$  °C. Due to the absence of a reference electrode, all reported voltages are representative of the cell potential. The solution was continuously agitated with a magnetic stirrer to ensure ample mixing and guarantee that sampling events were unaffected by concentration gradients within the solution. For each experimental run, 200 ml of a synthetic 20 mg/L naphthalene solution within a supporting NaCl electrolyte at various concentrations (0.01, 0.025, 0.05 and 0.1 M) was introduced into the cell giving each electrode a submerged geometrical surface area of 10.3 cm<sup>2</sup>. The reactor was covered to minimize the effects of naphthalene volatilization, with a small opening to allow for sampling and equilibration with atmospheric pressure. Upon application of an electric current (40, 70, 100 or 160 mA), 150  $\mu\text{l}$  aqueous samples were taken at various time points and analysed for naphthalene concentration against time. The resulting by-products, pH, and cell voltage were also examined. All experimental runs were conducted at least twice to test for repeatability.

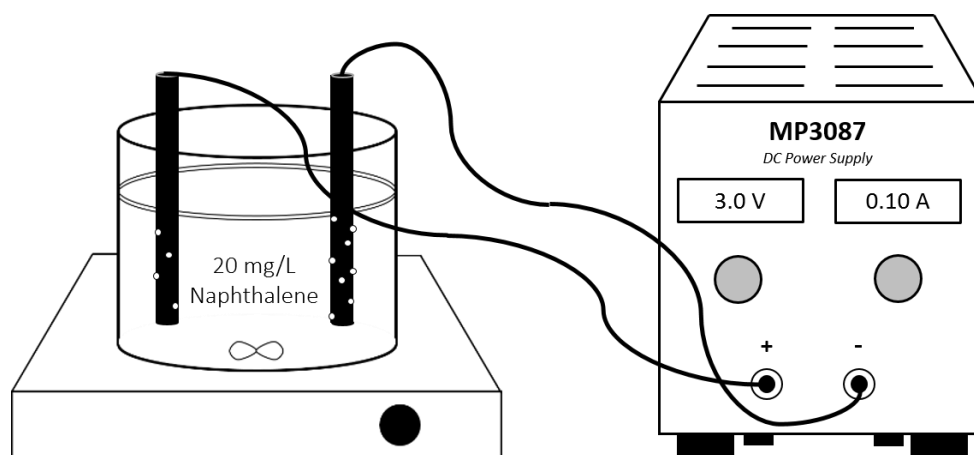


Figure 4.1: Schematic of the electrochemical cell used.

#### 4.2.3 Mass Transfer Characterization

The mass transfer behaviour within the hydrodynamic conditions of the reactor was characterized by the well-established limiting-current technique of the potassium ferro/ferricyanide couple [141,142]; this procedure evaluates the diffusion rate of electroactive species migrating from the bulk solution to the electrode surface where it undergoes electrochemical transformation. Within a 0.5 M Na<sub>2</sub>SO<sub>4</sub> supporting electrolyte, a 1 mM solution of K<sub>4</sub>Fe(CN)<sub>6</sub> was oxidized in the presence of excess 0.1 M K<sub>3</sub>Fe(CN)<sub>6</sub> to ensure that the cathodic reduction never became the limiting reaction. The same electrochemical reactor detailed in Figure 4.1 and 200 ml of solution were utilized, and a cell voltage sweep ranging from 0 – 5 V was applied. For each applied voltage, the electrical current was given ample time to stabilize and the steady-state readings were recorded. The resulting current-voltage (I-E) curve allowed for the determination of the limiting current,  $I_{lim}$  (A), and in turn, the mass transfer coefficient,  $k_m$  (m/s) of the electrochemical cell as detailed by Equation (4.33) [74].

$$I_{lim} = zFAk_mC^b \quad (4.33)$$

Here,  $z$  is the number of electrons involved in the anodic oxidation reaction,  $F$  is Faraday's constant (96,485 C/mol),  $A$  is the area of the electrode (m<sup>2</sup>), and  $C^b$  is the bulk concentration of the reactant (mol/m<sup>3</sup>).

#### 4.2.4 Analytical Methods

Naphthalene concentration was monitored using High Performance Liquid Chromatography (HPLC) whilst Gas Chromatography coupled with Mass Spectroscopy (GC-MS) was used to detect and identify by-product species generated during electrochemical treatments; these are described in Chapter 3.

### 4.3 Results and Discussion

#### 4.3.1 Unenhanced Anodic Oxidation

Prior to investigating the effect that electrogenerated active chlorine has on naphthalene removal, the ability of the implemented carbon anode to oxidize naphthalene was assessed. As detailed in Chapter 2, solubilized organic compounds can be electrochemically degraded via three main pathways: i) direct electron transfer at the anode, ii) electrogenerated hydroxyl radicals at the anode, or iii) indirection oxidation in the bulk solution due to generated oxidizing species such as active chlorine and peroxides [132–134,143]. Of these, direct oxidation is not known to play a significant role as it has slow kinetics towards organic compounds [61,62], whilst

oxidation with hydroxyl radicals at the anode surface is considered to be the most effective. Such radicals are formed at the anode during the dissociation of water (refer to Chapter 2) and are capable of fully mineralizing a variety of organic compounds [71]. However, expensive “non-active” anodic materials such as boron-doped diamond (BDD) are needed to avoid the chemisorption of radicals onto the anodic surface [133,143] which makes them unavailable for organic destruction. Although highly efficient, such electrode materials are limited to small scale processes due to their increased cost and have thus been disregarded for this study. Instead, inexpensive, “active” carbon electrodes that are more practical for field deployment have been implemented; they also better mimic the types of reactions that will occur on granular activated carbon during electrochemical regenerative treatments.

To test the capability for which the active carbon anode used in this work promotes degradation pathways i) and ii), an inert 0.1 M Na<sub>2</sub>SO<sub>4</sub> electrolyte was used. As sodium sulphate is electrochemically inert in this system, no bulk oxidizing agents (e.g. persulphate compounds, S<sub>2</sub>O<sub>4</sub><sup>2-</sup>) are generated that would promote degradation pathway iii); non-active anodes with high oxygen overpotentials such as BDD and PbO<sub>2</sub> [133,144] are required for their production. Similarly, the formation of hydrogen peroxides via the electrochemical transformation of dissolved oxygen at the cathode surface was considered and measured via the TiSO<sub>4</sub> method [145,146], but no detectable amounts were produced at any of the experimental conditions trialled. Thus, any naphthalene removed in these conditions would be due to direct oxidation or reactions with hydroxyl radicals chemisorbed at the anodic surface.

The cell was first operated in the absence of an electric current to act as a volatilization control. As naphthalene is one of the more volatile polycyclic aromatic compounds [147], its evaporation needs to be quantified to fully understand its removal from the system. Similarly, carbon is a known adsorptive material and any adsorption processes onto the carbon electrode surfaces will affect its removal rate; this was measured via a second control conducted in a closed vial with no headspace to prohibit any naphthalene volatilization. Following the control runs, the cell was operated at 40 and 100 mA to test for hydroxyl radical formation and subsequent naphthalene removal at the varying electric currents. The results are shown in Figure 4.2 where the experimental data is fitted to an exponential first-order kinetic fitting.

Over a 48 hour period, no detectable amount of naphthalene was adsorbed onto the electrode surfaces. This is believed to be due to the unidirectionally-oriented carbon fibres and binding agent used to hold the carbon electrodes together, limiting the amount of micropores available for organic adsorption. In contrast, naphthalene volatilization was measured to occur at a steady first-order rate of  $7.3 \times 10^{-5} \text{ s}^{-1}$ , which was enhanced upon application of an electric current. A constant current of 40 mA increased the overall naphthalene removal rate to  $1.7 \times 10^{-4} \text{ s}^{-1}$ , removing 70 % of the naphthalene within 2 hours of treatment. Due to the active nature of the anode, this increase in removal is attributed to naphthalene reacting with small amounts of chemisorbed hydroxyl radicals at the anode surface. HPLC analysis was used to confirm that such electrochemical transformation of the solubilized naphthalene was occurring.

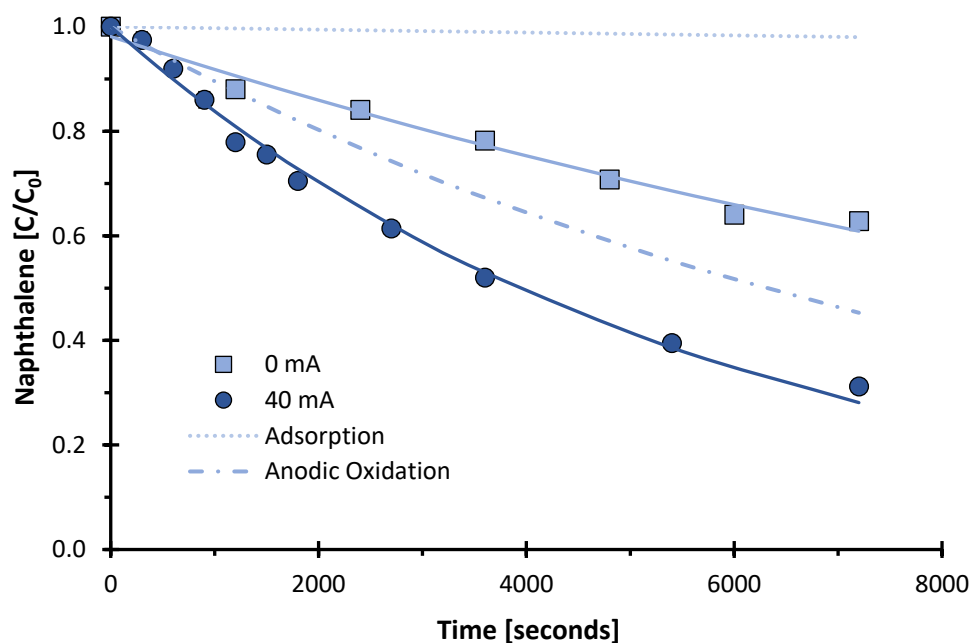


Figure 4.2: Naphthalene evolution as a function of time when treated at 0 and 40 mA of electric current. Points are experimental data whilst solid lines are a first-order fitting. The dashed lines are representative of losses due to adsorption and calculated losses due to anodic oxidation alone.

HPLC chromatograms showed a single by-product that eluted at 1.2 minutes, continuously increasing in size simultaneous to naphthalene disappearance, indicative of a direct electrochemical transformation process. The anodic oxidation rate itself was calculated by taking the difference between the 40 mA and volatilization removal rates and found to be  $9.3 \times 10^{-5} \text{ s}^{-1}$ , approximately 1.3 times faster than the evaporative rate. This rate, presented by the dashed line in Figure 4.2, is critical to identify when considering the *in situ* treatment of groundwaters. As naphthalene volatilization is significantly slowed at subsurface levels of 10 cm and greater, (nearly 13-fold) [148] it will have negligible effects on overall removal, indicating that without promotion of the active chlorine pathway, environmental remediation efforts would rely solely on hydroxyl radical formation at the anode surface.

Although this is feasible, extremely long treatment times would be required to obtain sufficient removal of naphthalene species. The extrapolated data from Figure 4.2 suggests timeframes over 800 hours of treatment would be needed to reach contaminant levels low enough to protect 95 % of marine species as required by the 'Australian and New Zealand Guidelines for Fresh and Marine Water Quality' [149]. Operating the cell at higher electric currents, such as 100 mA, did not increase naphthalene removal rates, likely due to the occurrence of parasitic side reactions starting to occur, such as oxygen and hydrogen gas evolution, rather than hydroxyl formation at the increased cell potentials [135].

HPLC analysis identified the generated by-product as 1-naphthol, a hydroxylated naphthalene species and a recognized product formed during naphthalene and hydroxyl radical reactions [150]. Prolonged treatment times did not present any further by-product species, and 1-naphthol concentrations were not seen to decrease. This indicates that naphthalene is only partially oxidized by the active anode used in this work, and no further oxidation of the generated 1-naphthol occurs. This is commonly observed and described in the literature when

using active electrodes, exemplifying why non-active electrodes are more beneficial for this type of reaction pathway.

As anodic oxidation only enables the transformation of naphthalene into 1-naphthol, not an acceptable end result in environmental applications [149], an enhanced treatment process using indirect bulk oxidation methods is required to obtain efficient, quick removal rates, as well as naphthalene conversion into a lesser toxic form. A new set of experiments was conducted to address whether electrogenerated active chlorine species on carbon anodes enable naphthalene degradation in a more efficient manner. Several experimental criteria were assessed including degree of naphthalene removal, associated kinetics, energy consumption and efficiency, and by-products formed during electrochemical treatment.

#### 4.3.2 Kinetic Model Theory

To model the active chlorine reaction pathway, it is assumed that naphthalene removal occurs via two main mechanisms: a first-order volatilization,  $k_{vol}$  ( $s^{-1}$ ), and a second-order reaction with electrogenerated active chlorine species,  $k_{rxn}$  ( $M^{-1} s^{-1}$ ). This is described by Equation (4.34), where  $[N]$  and  $[AC]$  are the concentrations of naphthalene and active chlorine species respectively (M). The first-order volatilization rate was experimentally measured in Section 4.3.1 and assumed to be constant at  $7.3 \times 10^{-5} s^{-1}$ . Although the temperature of the electrochemical cell was seen to fluctuate  $\pm 1$  °C during experimental trials, this variation was assumed to have negligible effects on the volatilization rate. No other temperatures were studied in this work, however previously published works have shown that temperatures ranging a span of 35 °C (between 25 - 60° C) had insignificant effects on the abatement of organics when utilizing the active chlorine pathway [135].

$$\frac{d[N]}{dt} = -k_{vol}[N] - k_{rxn}[N][AC] \quad (4.34)$$

Although the anodic oxidation of naphthalene was seen to occur within  $Na_2SO_4$  electrolyte to form 1-naphthol (refer to Section 4.3.1), this reaction was not detected when chloride ions were introduced into the system. This is due to chloride ions being preferentially reacted at the anode surface and limiting the amount of naphthalene that could undergo direct oxidation, discussed more in Section 4.3.3.1.

The time dependence of active chlorine concentration is described by its generation at the anode surface (expected to follow Faraday's law), and its consumption via reduction at the cathode surface and second-order reaction with naphthalene. These three terms are represented on the right-hand side of Equation (4.35) respectively where  $I$  is the applied current (C/s),  $\varepsilon$  is the current efficiency, or fraction of current going towards active chlorine production,  $n$  is the number of electrons required to electrogenerate active chlorine,  $F$  is Faraday's constant (C/mol),  $V$  is the volume of solution undergoing treatment (L),  $a$  is the specific area of the electrode,  $A/V$  ( $m^{-1}$ ), and  $k_m$  is the mass transfer coefficient of electroactive species within the electrochemical reactor (m/s). For simplification of the model, the production of active chlorine is assumed to be a single-step reaction at the anode encompassing Equations (4.29) - (4.31), and its reduction at the cathode surface is assumed to be mass transfer limited (i.e. dependent on the diffusion of active chlorine species from the anode to the cathode surface, represented by the  $ak_m$  term); this is a well-supported assumption due the quick rate at which active chlorine oxidants are reduced at cathode surfaces [139,151]. The reaction of active chlorine species with by-products formed during the treatment are also not considered.



$$\frac{d[AC]}{dt} = \frac{\varepsilon I}{nFV} - ak_m[AC] - k_{rxn}[N][AC] \quad (4.35)$$

The mass transfer coefficient of the electrochemical cell,  $k_m$ , is determined via the limiting-current technique of the widely used potassium ferro/ferricyanide redox couple [141,142]. The cell voltage was scanned from 0 - 5 V, and the resulting I-E plot is depicted in Figure 4.3.

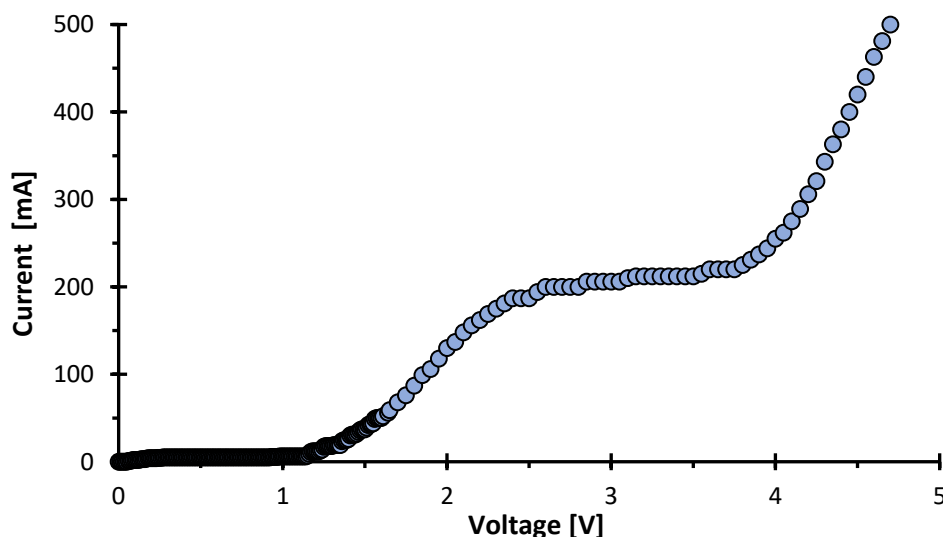


Figure 4.3: Current-voltage curve obtained for the electrochemical cell when scanning from 0 – 5 V, where ‘V’ is the cell voltage.

No electric current is observed to pass in the cell voltage range of 0 – 0.92 V. Beyond this, Faradaic reactions of the ferri/ferro redox couple commence and increase in the range of 0.92 – 1.34 V. The slow growth of current in this range suggests that the concentration of the redox couple near the electrode surfaces is not significantly different from the bulk solution, and that the rate of electrochemical reaction is strictly limited by the amount of current being passed through the system - a charge transfer controlled process [74,152]. With further increases in cell voltage, the current rises at a quickened rate until a stable current is reached at 2.85 V. Between 2.85 and 3.5 V, there are negligible increases in current in relation to the changes in applied voltage as shown by the plateau in Figure 4.3. This steady current, observed at 212 mA, is representative of the limiting current,  $I_{lim}$ , at which the oxidation of  $K_4Fe(CN)_6$  at the anode becomes strictly dependent on its diffusive mass transport from the bulk solution to the anode surface - a mass transfer controlled process [74,152]. Under these conditions, the concentration of  $K_4Fe(CN)_6$  at the anode is effectively zero meaning increases in current will have no effect on its oxidation rate. It is also under these conditions that the determined  $I_{lim}$  can be used to determine the mass transport coefficient within the reactor,  $k_m$ , via Equation (4.33); it has been calculated to be 0.0021 m/s for the electrochemical reactor used in this work. It is noted that the current increases that are observed at 4.0 V and beyond are due to formation of hydrogen gas on the cathodic surface [153].

Considering the two kinetic equations that aim to describe naphthalene removal under the active chlorine reaction, Equations (4.34) and (4.35), the  $I$ ,  $n$ ,  $F$ ,  $V$ , and  $a$  parameters are known and constant, whilst the  $k_{vol}$  and  $k_m$  parameters are determined experimentally and independently from one another; they describe the operating temperature and hydrodynamics of the reactor respectively. All known parameters are summarized in Table 4.1, leaving the

specific reaction rate between naphthalene and active chlorine,  $k_{rxn}$ , and the current efficiency,  $\varepsilon$ , as the fitting parameters of the model. Under all experimental conditions trialled,  $k_{rxn}$  should be constant to validate the kinetic model, whilst  $\varepsilon$  is assumed to be dependent on the chloride concentration within the system [151], discussed further in Section 4.3.3.2.

Table 4.1: Known and experimentally determined parameters used within the proposed kinetic model.

$k_{vol}$ ( $s^{-1}$ )	$I$ ( $C/s$ )	$n$ (-)	$F$ ( $C/mol$ )	$V$ ( $L$ )	$a$ ( $m^{-1}$ )	$k_m$ ( $m/s$ )
$7.30 \times 10^{-5}$	0.04, 0.07, 0.10, or 0.16	2	96,485	0.2	5.15	0.0021

To determine the validity of the model and the efficacy of the active chlorine pathway for the degradation of solubilized naphthalene species, the electrochemical reactor was operated at varying electric currents (0 – 220 mA) and sodium chloride concentrations (0.01 – 0.2 M). Following acquisition of the data, the ODE15S multistep solver of MATLAB® is used to solve the system of ordinary differential equations (ODEs), and the NLINFIT tool is used to minimize the difference between the experimental data and model equations using a least squares method estimation. From this, the values of the  $k_{rxn}$  and  $\varepsilon$  parameters can be determined, and the kinetic model validated.

### 4.3.3 Active Chlorine Pathway

#### 4.3.3.1 Effect of Applied Current

Enhanced bulk oxidation experiments to promote the active chlorine pathway were conducted utilizing a 0.1 M NaCl supporting electrolyte at a series of electric currents ranging 40 – 220 mA. The resulting normalized naphthalene concentration ( $C/C_0$ ) as a function of time and applied current is shown in Figure 4.4, where it is seen that naphthalene removal was significantly increased when the active chlorine pathway is promoted. In all cases, removal commenced immediately and continued until entirely removed from the system. Full removal was detected at timeframes nearing 1.0, 1.5, 2.0, and 2.5 hours for applied electric currents of 160 mA, 100 mA, 70 mA, and 40 mA respectively, and removal rates were up to 12 and 9 times greater than those observed in the volatilization control and anodic oxidation processes alone. Compared to the 800 hours required for anodic oxidation alone, the active chlorine pathway is clearly superior towards naphthalene oxidation as the electrogenerated active chlorine species quickly attack and aid in the breakdown of naphthalene in the bulk solution, Equations (4.29) - (4.32).

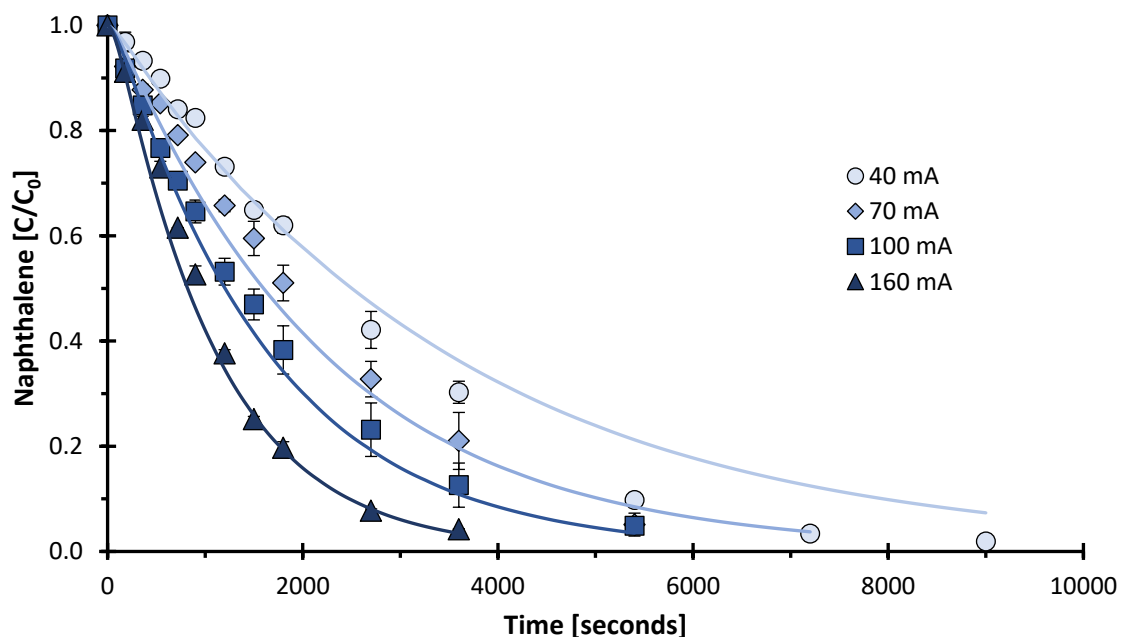


Figure 4.4: Normalized naphthalene concentration versus time at varying applied electric currents. Points are experimental data whilst lines are the fitted kinetic model.

Under all applied currents, the Australian regulations for marine water contaminant concentration were reached [149], where the rate of naphthalene removal linearly increased with increasing electric currents. For example, 70 %, 79 %, 88 %, and 96 % of the naphthalene was removed from the system within 1 hour of treatment when operating at currents of 40 mA, 70 mA, 100 mA, and 160 mA respectively. These results agree with Faraday's law of electrolysis, the first term in Equation (4.35), stating that the rate at which a substance reacts at an electrode surface is directly proportional to the amount of current passed. Thus, with more active chlorine being electrogenerated at the anode, Equations (4.29) - (4.31), it is expected that naphthalene removal rates will be increased.

Currents beyond 160 mA (i.e. 220 mA) did not enhance the naphthalene removal rates. This phenomena is commonly observed in electrochemical systems when the overall removal kinetics become limited by the mass transfer of chloride ions diffusing from the bulk electrolyte to the anode surface - a mass transfer controlled process [74]. In such cases, further increases in current will not enhance reaction rates for active chlorine production as there is a limited supply of solute at the electrode which can undergo electrochemical reaction. Rather, increases in current will go towards unproductive side reactions such as oxygen gas evolution, Equation (4.36), and limit the amount of effective current passed for active chlorine production [61,154].



Although the potential required for oxygen evolution, 1.23 V/Standard Hydrogen Electrode (SHE), is lower than that required for chlorine production, 1.36 V/SHE, the two electron reaction to form chlorine, Equation (4.29), has much faster kinetics than the four electron reaction towards oxygen production [155]. This indicates that at lower electric currents and cell potentials, chlorine evolution is kinetically favoured. This is especially true of carbonaceous anodes that have a low overpotential for chlorine evolution and a higher overpotential for oxygen formation; at increasing NaCl concentrations the formation of oxygen becomes almost completely inhibited [156]. The results of Figure 4.4 are consistent with this understanding

where increases in current result in increases in active chlorine production; this continues until a current of 160 mA is reached, beyond which any further electrons introduced into the system go towards oxygen evolution at the anode. Table 4.2 summarizes the increase in cell voltages at the varying applied currents within this work.

The kinetic favouring of active chlorine production may also explain why no detectable amount of 1-naphthol was observed during promotion of the active chlorine pathway, as was seen in the Na<sub>2</sub>SO<sub>4</sub> trials; the discharge of chlorine at the anode inhibits the hydroxylated reactions of hydroxyl radicals from occurring [60,76,80,155]. This suggests that anodic oxidation does not contribute to naphthalene degradation during promotion of the active chlorine pathway, and has thus not been included in the kinetic model.

The limiting removal rate observed at 160 mA equates to an applied current density of 15.5 mA/cm<sup>2</sup> of electrode surface area and is the maximum rate per square unit at which active chlorine species can be produced at the carbon anode used in this work. Further increases in naphthalene removal rates would only occur via increases in electrode surface area that would overcome the mass transfer limitation from the bulk solution to the electrolytic surface. A prime example of this is using a 3D electrode, such as a bed of granular activated carbon, that greatly increases the space-time yield and electrode area-volume ratio [68]. This is investigated in Chapter 6.

At all applied currents, naphthalene concentrations were seen to follow an exponential decrease with time as is commonly observed in the literature [60,64,65,136]. A pseudo-first order kinetic analysis is generally used to model this behaviour, as it is assumed that the concentration of electrogenerated active chlorine is much greater than the concentration of organics. This assumption suggests that active chlorine concentration is independent of time and assumes a constant apparent removal rate,  $k_{app}$ , Equation (4.37). However, in reality active chlorine concentrations will start from a concentration of zero and gradually increase with time at a rate proportional to the amount of electric current put into the system; this indicates that organic removal rates will be slow initially but increase with time as the concentration of active chlorine increases. The first-order model also makes it difficult to predict naphthalene removal rates at varying current densities and experimental conditions not studied, as  $k_{app}$  fluctuates with reactor configuration, hydrodynamic conditions, and operating parameters [60,65,137,153,157,158]. The kinetic model proposed in Section 4.3.2 aims to overcome such limitations.

$$r = -k_{rxn}[AC][Organic] \cong -k_{app}[Organic] \quad (4.37)$$

Thus, the suitability of the kinetic model was tested by fitting Equations (4.34) and (4.35) to the data in Figure 4.4. Through this, the second-order reaction rate between naphthalene and active chlorine was determined to be  $k_{rxn} = 2.2 \text{ M}^{-1}\text{s}^{-1}$ . Although the reaction rate between active chlorine and naphthalene has not been documented, the determined value is within the range expected for active chlorine reacting with aromatic organic compounds [77]. With the determined reaction rate, the model was seen to fit the experimental data to a high accuracy, detailed in Table 4.1, despite changes in applied electric current in the range of 0 – 160 mA.

Table 4.2: Comparison between experimental data and the kinetic model for the various applied currents. The root mean squared error (RMSE) and average cell voltages are listed.

Current [mA]	$k_{rxn}$ [ $M^{-1} s^{-1}$ ]	RMSE	Average Cell Voltage [V]
0		0.020	0.0
40	2.2	0.049	4.2
70		0.040	4.7
100		0.030	5.3
160		0.040	6.4

The dynamic model shows similar levels of accuracy in comparison to the first-order analyses that have been conducted in the literature, but has the added benefit of being able to accurately predict naphthalene removal despite changes in applied electric current. This is largely a result of the model predicting variations in active chlorine concentration as a function of the applied current and time, such as shown via Figure 4.5; concentrations gradually increase from an initial concentration of zero until a maximum value is reached due to the combined effects of its generation, dependent on the applied electric current, and its removal due to reactions with naphthalene and reduction at the cathode surface as described by Equation (4.35). As depicted, increasing the current up to 160 mA is beneficial for increased organic destruction, as the steady state active chlorine equilibrium concentration is maximized.

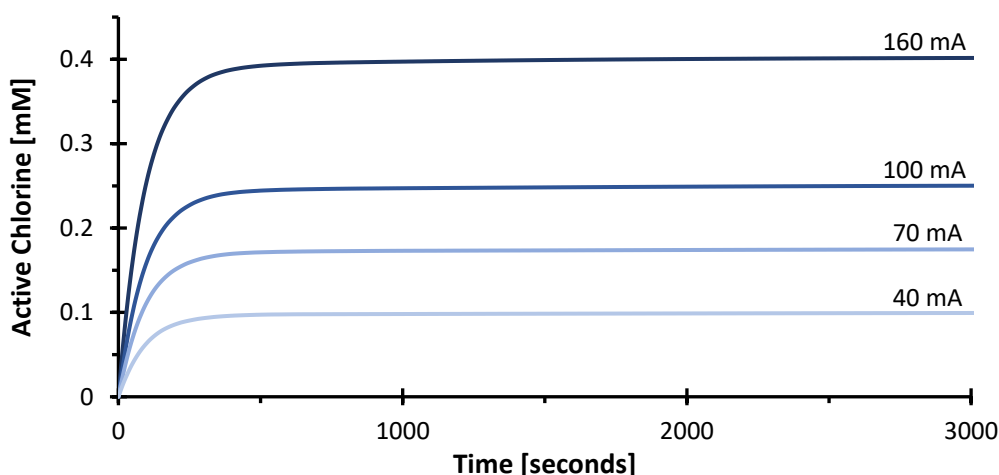


Figure 4.5: Model predictions of active chlorine concentration as a function of time and applied current.

#### 4.3.3.2 Effect of NaCl Concentration

A second set of experiments was conducted to investigate how electrolyte concentration affects treatment outcomes, and to assess if the proposed model could account for such variations in the system. It is expected that when less chloride is present within the system, less active chlorine would be electrogenerated due to the limited solute available at the anode to undergo transformation; this would, in turn, reduce naphthalene removal rates. To investigate this, initial NaCl concentrations were varied between 0.01 M, 0.025 M, 0.05 M, and 0.1 M whilst the applied electric current was held constant at 100 mA in all cases.

The results in Figure 4.6 show naphthalene removal rates are greatly affected by the starting electrolyte concentration, and more so in comparison to changes in the applied current. For example, 55 %, 65 %, 83 %, and 87 % of naphthalene was removed in the first hour of treatment when being electrochemically treated in the presence of 0.01 M, 0.025 M, 0.05 M, and 0.1 M NaCl, highlighting the significance that chloride ions have on the removal process. This is

expected as increased concentrations will result with greater amounts of chloride available at the anode surface that can go towards active chlorine production [74,159]. Simultaneous to this, the increased ionic conductivity of the electrolyte with increasing chloride concentrations resulted in a significant reduction in the required cell voltage, tabulated in Table 4.3. Thus, increased amounts of NaCl have the added benefit of increasing removal rates whilst reducing energy consumption, a beneficial result for application in environmental scenarios. Chloride concentrations beyond 0.1 M (i.e. 0.2 M) had no further effects on naphthalene removal rates, as it is likely that the system began operating within a charge-transfer controlled process [74,152]. Such an observation is commonly seen in the literature where a maximum electrolyte concentration is reached [135,136,160], and further increases in concentration only contribute to reducing energy consumption rather than aiding in contaminant removal rates.

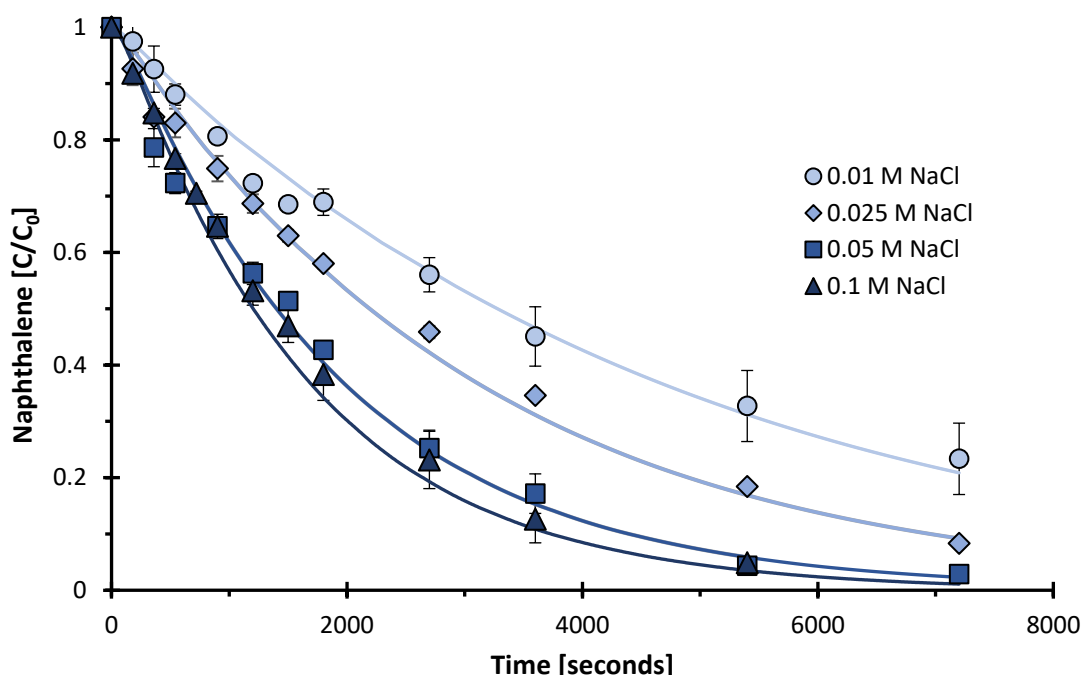


Figure 4.6: Normalized naphthalene concentration as a function of time at varying NaCl electrolyte concentrations. Points are experimental data whilst lines are the fitted kinetic model.

In order to maintain the targeted applied current at decreased chloride concentrations, it is likely that oxygen evolution becomes more competitive at the anode surface. For example, in the case of 0.01 M NaCl, the limited availability of chloride at the anode will reduce the amount of current going towards active chlorine production, and cause some to go towards oxygen gas evolution, Equation (4.36); these two reactions are known to occur simultaneously in electrochemical systems [155]. In contrast, increased NaCl concentrations will favour the electrogeneration of active chlorine due to the faster kinetics at the anode surface, discussed in Section 4.3.3.1. To account for these variations in the kinetic model, the current efficiency term,  $\varepsilon$ , is introduced and accounts for the fraction of current going towards active chlorine production.

Through fitting the model equations to the data in Figure 4.6, a linear correlation between the current efficiency and the starting chloride concentration was observed and described by Equation (4.38). As expected, increases in chloride concentration were seen to increase the fraction of current going towards active chlorine production. Equation (4.38) suggests that the maximum current efficiency,  $\varepsilon = 1$ , occurs at a chloride concentration of 0.059 M, beyond which

no further increases in efficiency are obtained. Interestingly, this is in good agreement with a study conducted by Polcaro et al. [151] that also identified that the current efficiency for chloride oxidation reached 1 when a chloride concentration of 0.06 M was reached.

$$\varepsilon = 14.53[NaCl]_0 + 0.14, \quad 0.01 < [NaCl]_0 < 0.2 \quad \text{and} \quad 0 < \varepsilon < 1 \quad (4.38)$$

It is assumed that the efficiency term is only dependent on the initial chloride concentration,  $[NaCl]_0$ , and not time as its concentration is expected to remain fairly constant during treatment timeframes. This was deemed an acceptable assumption since chloride ions are used in the production of active chlorine species, they are also regenerated via active chlorine reduction at the cathode, Equations (4.39) and (4.40), and through reaction with naphthalene species, Equation (4.32).



Substituting Equation (4.38) into Equation (4.35) of the kinetic model showed that the model could accurately predict treatment outcomes despite variations in chloride concentrations; the mathematical goodness of fit is detailed in Table 4.3. In agreement with the results in Section 4.3.2, a  $k_{rxn}$  value was still found to be  $2.2 \text{ M}^{-1}\text{s}^{-1}$ , validating the model equations described within this work. The proposed model can accurately predict treatment outcomes over a large range of electric currents (0 – 220 mA) and chloride concentrations (0 – 0.2 M).

Table 4.3: Comparison between experimental data and the kinetic model for the various NaCl concentrations. The root mean squared error (RMSE) and average cell voltage are tabulated.

NaCl [M]	$k_{rxn} [\text{M}^{-1} \text{s}^{-1}]$	$\varepsilon [-]$	RMSE	Average Cell Voltage [V]
0.010	2.2	0.28	0.025	17.7
0.025		0.50	0.028	9.9
0.050		0.86	0.034	7.0
0.100		1.0	0.030	5.3

The accuracy of the proposed kinetic model is believed to be advantageous over those presented in the literature where pseudo first-order kinetics are commonly assumed, as it can account for variations in operating conditions. Similarly, the literature generally uses the efficiency term,  $\varepsilon$ , as an empirical fitting parameter of the model or encompasses it in the  $k_{app}$  reaction rate [65,66,69,137,139,157,161,162]. This work has identified the current efficiency is correlated with the starting chloride concentration, allowing the model to describe and predict treatment outcomes over a range of operating conditions.

#### 4.3.3.3 Energy Requirements

One of the main inhibitors of utilizing electrochemical technologies for the treatment of contaminant wastewaters, particularly in environmental applications, is the practicality for which it can be scaled. Large treatment volumes require large electrode areas and increased energy consumption, both of which may be impractical when using expensive anodic materials or treating waters in remote regions where resources are limited. To address these limitations, this work has firstly shown that expensive anode materials are not necessary and capital expenditure can be greatly reduced via implementing cheap carbon electrodes for bulk

oxidization pathways. However, operational costs still need to be assessed to ensure energy efficiency is not compromised when utilizing a less effective material.

The specific energy consumption,  $E_{sp}$  (kWh/kg), was calculated for each experimental trial to determine the energy usage per unit of naphthalene removed. This was done using Equation (4.41) where  $E_{cell}$  is the average cell voltage (V) that remained mostly constant with each trial,  $I$  is the applied current (A),  $t$  is the treatment time (hr),  $V$  is the volume of solution treated (L), and  $\Delta N$  is the quantity of naphthalene removed from the system (g/L). The specific energy consumption to reach full naphthalene removal was considered.

$$E_{sp} = \frac{E_{cell}It}{V\Delta N} \quad (4.41)$$

Figure 4.7 shows that the energy consumption is highly dependent on both the applied electric current and electrolyte concentrations. With increasing electric currents, more energy per unit of naphthalene degraded was consumed due to the greater voltages required to operate the cell, detailed in Table 4.2. Currents of 40 mA, 70 mA, 100 mA, to 160 mA resulted in specific energy requirements of 104 kWh/kg, 150 kWh/kg, 219 kWh/kg, and 303 kWh/kg respectively, nearly tripling the energy consumption in the range of currents investigated. Despite this, increasing the applied current simultaneously increases the rate of naphthalene removal, indicating that there is a trade-off between treatment timeframes and energy consumption. A compromise might be reached via implementing a modulated current [61,163], where the current is gradually decreased in accordance with the organic contaminant concentration; this aims to limit the amount of surplus active chlorine produced to save on energy consumption, however, this has not been assessed in this study.

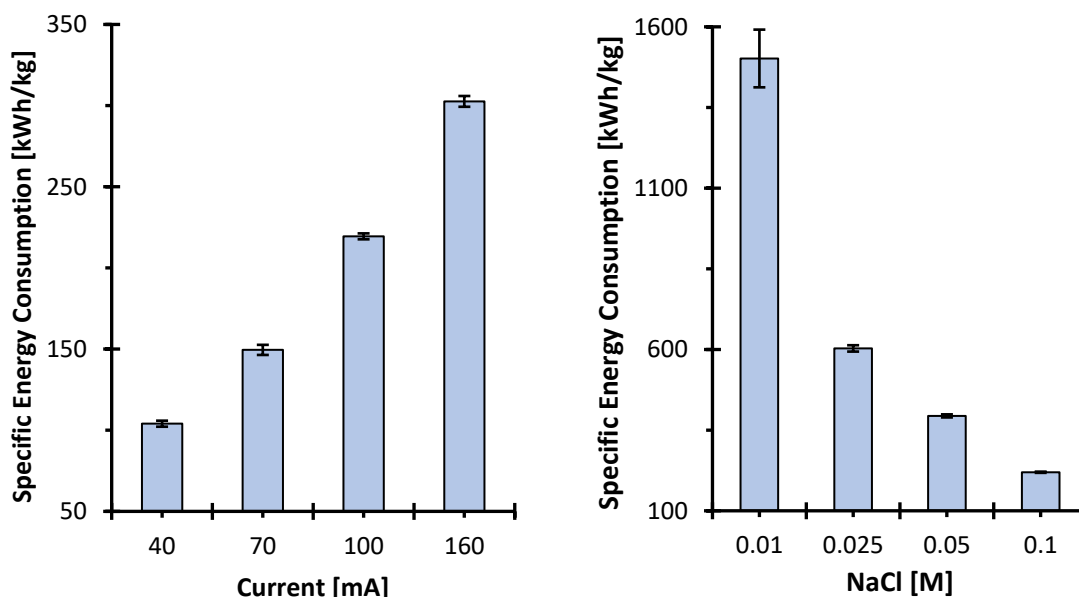


Figure 4.7: (Left) Specific energy consumption when altering the applied current within a 0.1 M NaCl electrolyte and (right) altering the NaCl concentration when operating at a constant applied current of 100 mA.

In contrast, increases in chloride concentration greatly reduced the resultant energy consumption whilst simultaneously increasing removal rates. Energy usage could be reduced 7-fold by increasing the chloride concentration from 0.01 to 0.1 M; energy requirements of 1,502



kWh/kg, 603 kWh/kg, 394 kWh/kg, and 219 kWh/kg were reported when utilizing NaCl concentrations of 0.01 M, 0.025 M, 0.05 M, and 0.1 M respectively. At the same time, full naphthalene removal is expected within 4, 2.8, 1.9, and 1.5 hours for each respective chloride concentration. This is explained by the increased presence of ions within the system that reduce the electrical resistance within the cell, resulting in a lowered applied voltage needed to drive the desired current, refer to Table 4.3. The combined effects of decreased voltages and increases in chloride concentration that enhance the current efficiency ultimately allow a greater effective current to be passed per unit of naphthalene removed.

It is interesting to note that because the maximum current efficiency is achieved around 0.06 M NaCl, increasing the NaCl concentration from 0.05 to 0.1 M had only a small effect on the overall naphthalene removal rate, shown in Figure 4.6. However, this change in NaCl concentration almost halved the amount of energy required, reducing it from 394 to 219 kWh/kg. This is a beneficial finding when considering the environmental remediation of coastal regions that present with high salinities, such as the Antarctic, as seawater is comprised of a chloride concentration nearing 0.6 M. In this instance, the active chlorine pathway should be able to be promoted effectively, whilst greatly reducing the required energy requirements.

Not considering capital expenditure, the data from this work estimates that 104 kWh of energy can remove one kg of solubilized naphthalene when operating at 40 mA; this corresponds to an operating cost nearing AUD \$1.05 per m<sup>3</sup> of a naphthalene saturated water supply (assuming Tasmanian electricity prices of 32.59 ¢/kWh and a naphthalene saturation level of 31 mg/L). It is difficult to compare these results to other works that have utilized electrochemical methods to treat wastewaters due to differences in experimental conditions. However, the energy usage in this work has utilized less than one-tenth of the energy consumed relative to studies utilizing BDD anodes for aqueous organic destruction [135,164]. Although non-active BDD anodes are considered to be the most effective for hydroxyl radical formation and wastewater treatment, this work has shown that their energy consumption can be outperformed via the chloride-mediated oxidation pathway on the active electrodes used. The low energy requirements and quick treatment times make this treatment highly favourable for use in environmental remediation efforts; it is presumed that such low energy requirements could be supplied by either diesel or solar power in remote environmental applications, such as those presented in the Antarctic and other comparable Polar Regions.

#### 4.3.3.4 By-Product Identification

A prevalent concern with utilizing active chlorine degradation techniques is the possibility of generating chlorinated by-products that may be more toxic than the starting compound. To investigate this, HPLC and GC/MS were utilized to determine what electrochemical transformations the solubilized naphthalene was undergoing during treatment.

Figure 4.8 shows the HPLC chromatograms that presented with treatment time, where the naphthalene concentration, peak (I) eluting at 3.1 minutes, exponentially decreased in the first 1.5 hours of treatment. The simultaneous nature at which three main by-product peaks evolve (II-IV) indicates that a direct electrochemical transformation process is occurring. Unlike the results of the inert sodium sulphate electrolyte, no naphthol peaks were detected as all of the effective current was likely going towards active chlorine and/or oxygen production, discussed in Section 4.3.3.1. GC/MS was able to identify the by-products being formed and the summarized results are tabulated in Table 4.4.

GC/MS analysis revealed that the first and main reaction that naphthalene undergoes is its mono-chlorination to form 1-chloro- and 2-chloronaphthalene species, associated with the shoulder peaks of compounds II and III in Figure 4.8; this is consistent with similar studies in the literature describing naphthalene degradation in the presence of chloride ions [67,144,165]. Such by-products are due to the highly oxidizing HOCl species undergoing electrophilic substitution on the electron dense aromatic naphthalene structure [77], illustrating the effectiveness of the active chlorine pathway. The concentration of the mono-chlorinated species continued to increase until a maximum concentration was reached nearing the 60-minute mark whereby 87 % of the initial naphthalene had undergone transformation.

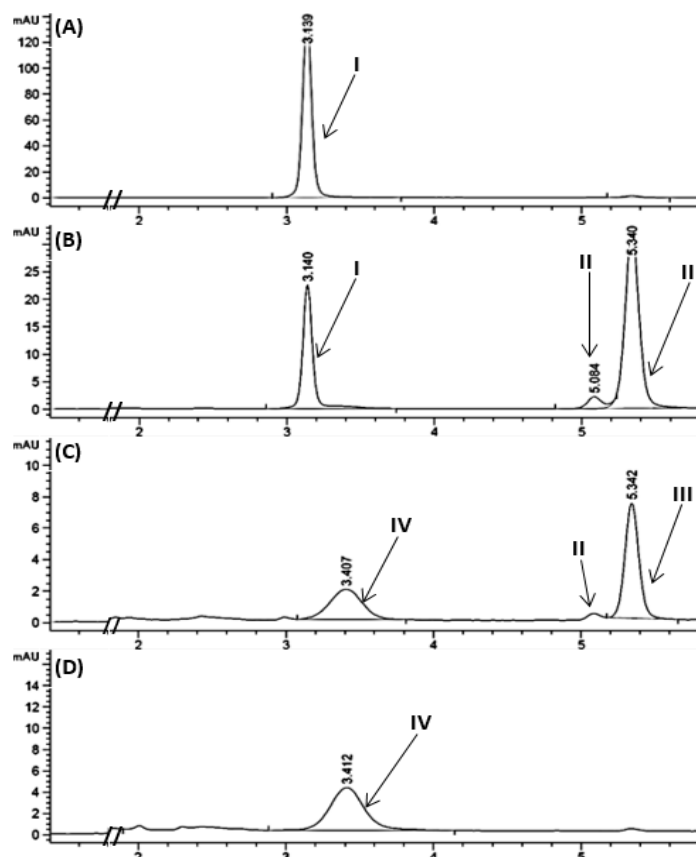


Figure 4.8: Evolution of naphthalene and associated by-products on the resulting HPLC-DAD chromatograms (detection at 275 nm) as a function of time during the electrochemical treatment of a naphthalene contaminant solution at 100 mA within a 0.1 M NaCl electrolyte. Where (A) is the stock solution pre-treatment, (B) is at 30 minutes, (C) is at 90 minutes, and (D) is at 180 minutes.

Such chlorinated compounds are known to be toxic to aquatic organisms, making their generation a cause for concern, especially when considering environmental applications. However, prolonged treatment time (refer to Figure 4.8C – D) showed that their concentration began to decrease following the 60-minute mark, and continued to do so until they were fully removed from the system within 180 minutes of treatment. This is a crucial finding as even though toxic by-products are being generated through the active chlorine pathway, they are further degraded and removed from the system. This is in agreement with other studies showing that the electrochemical chlorine mediated pathway can achieve up to 95 % removal of the total chemical oxygen demand in organic contaminated waters [135]. Similar works have shown that chlorinated aromatic compounds undergo subsequent oxidation to form ring opened products, removing all chlorinated hydrocarbons in the process [67,165,166].

During the reduction and ultimate removal of the mono-chlorinated naphthalene species, a new chromatographic peak (IV) formed and eluted at 3.4 minutes, likely comprising breakdown by-products of the monochlorinated species. Through GC/MS analysis, the broadened peak shown in Figure 4.8D was found to be comprised of a variety of by-products including oxygenated naphthalene species such as naphthoquinone, 1,4-naphthoquinone-2,3-oxide, and small quantities of 1,2-dichloronaphthalene; the GC chromatograms presented in Appendix A.1 better display their evolution with time. The occurrence of oxygenated compounds suggests that during the initial attack of naphthalene via hypochlorous acid, the single electron transfer process produces a radical cation which then undergoes nucleophilic substitution from water to form oxygenated naphthalene compounds such as those previously described [167]. Such by-products were only seen at low concentrations for a limited time, and upon their detection 100 % of the naphthalene had been removed from the system. Interestingly, no trichloronaphthalene species were detected.

The presence of toxic dichloro-naphthalene species in peak (IV) is not considered to be an appropriate result for treatment in environmental regions. However, the formation of oxygenated products such as 1,4-naphthoquinone-2,3-oxide provides evidence that the chlorinated species continue to undergo electrochemical transformation. With further treatment time, chromatographic peaks continued to decrease until no detectable peaks were seen at 240 minutes and beyond on either HPLC or GC/MS instrumentation. It is assumed that the oxygenated naphthalene compounds underwent further ring opening and degradation to form compounds such as carboxylic acids and alcohols as noted by others [165,168]. With this in mind, it is concluded that if sufficient timeframes are used (up to 4 hours of treatment) the active chlorine pathway promoted on active carbon electrodes is a promising technique for use in environmental remediation efforts, as all toxic products are removed from the system.

*Table 4.4: Mass spectrophotometry results detailing the by-products formed when electrochemically treating naphthalene solutions in a 0.1 M NaCl electrolyte at 100 mA/cm<sup>2</sup>.*

Peak	HPLC Retention Time (min)	GC/MS Retention Time (min)	Molecular Ion, M <sup>+</sup>	Identification
I	3.1	8.65	128	Naphthalene
II / III	5.1 / 5.3	10.30	162	1-chloronaphthalene / 2-chloronaphthalene
IV	3.4	10.5 / 11.2 / 11.6	158 / 174 / 196	Naphthoquinone / 1,4-naphthoquinone 2,3-oxide / 1,2-dichloronaphthalene

#### 4.4 Conclusions

This chapter has identified that electrochemical methods are a possible and deployable technology for the treatment of contaminated groundwaters in Polar Regions, such as the Antarctic, where resources and manual labour are limited. It was specifically shown that the active chlorine pathway can aid in the remediation of petroleum hydrocarbon spills, where the high priority pollutant, naphthalene, can be fully degraded and removed from a contaminant water supply within 1-3 hours of treatment. Such results support the notion that decomposition pathways can be achieved when electrochemically regenerating GAC, which is addressed in Chapter 6.

To aid in the scalability and ultimate deployment of this technology in environmental efforts, this work showed that inexpensive carbon materials are an effective alternative to the expensive anodic materials generally used in electrochemical processing, such as BDD and  $\text{PbO}_2$ . Not only does the carbon greatly reduce capital expenditure, but it uses about one tenth of the energy in comparison to BDD options when promoting bulk oxidation methods. The high efficiency and low energy requirements suggest that this treatment is a feasible treatment option for deployment in remote environmental regions, including the *in situ* treatment of carbonaceous PRB substrate materials.

A kinetic model was proposed that can accurately describe naphthalene removal via the active chlorine pathway under a variety of operating conditions. Removal rates were seen to be highly dependent on two critical parameters: applied electric current and saline concentration. The efficacy of the proposed kinetic model indicates that reproducing the active chlorine pathway in environmental applications is one step closer.

One existing concern associated with the active chlorine pathway is that it results in the formation of toxic chlorinated by-products. However, this work has shown that increased treatment times were able to subsequently remove any toxic by-products from the system. With prolonged treatment up to 4 hours, all detectable naphthalene and generated by-products were removed. If deploying this treatment in environmental efforts, it would need to be ensured that appropriate residence times are achieved to ensure toxicity levels are not increased at the site being handled.

---

# CHAPTER 5

---

## Electrochemical Treatment of Naphthalene Contaminated Waters via Electro-Fenton

This chapter investigates the electro-Fenton electrochemical pathway and its effectiveness for the degradation and removal of solubilized naphthalene within contaminated waters.

*The chapter has resulted in the following publication:*

**McQuillan, R. V.,** Stevens, G. W., & Mumford, K. A.. Assessment of the electro-Fenton pathway for the removal of naphthalene from contaminated waters in remote regions. *Science of the Total Environment*, 762 (2021) 143155.

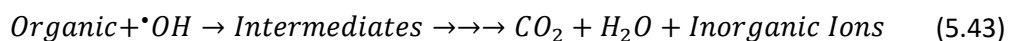
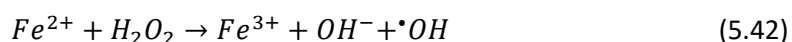
---



## 5.1 Introduction

Chapter 4 identified that the active chlorine pathway is an effective treatment for removing naphthalene from contaminated waters. It also proved to be a low cost and deployable option for remediation efforts in coastal regions, such as the Antarctic, due to the natural presence of high salinity waters. Despite this, it was shown that chlorinated hydrocarbons may elute into the surrounding environment if adequate treatment timeframes are not utilized. As sufficient timeframes cannot always be guaranteed in field deployment scenarios (i.e. extreme weather events, delays or loss of resources, etc), an alternative electrochemical pathway, known as the electro-Fenton reaction, is considered in this chapter.

The well-known and traditional Fenton reaction, Equation (5.42), where hydroxyl radicals are generated from externally added Fenton reagents, iron(II) and hydrogen peroxide, has been extensively used to treat contaminated wastewaters [70,83,169]. The generated hydroxyl radicals ( $\cdot\text{OH}$ ) have a substantially large reduction potential of 2.87 V vs the standard hydrogen electrode (SHE) [70] and are capable of oxidizing a variety of organic compounds such as aromatics, dyes, pharmaceuticals, and pesticides [62,170]; exceptions to this include carbon tetrachloride, chloroform, hexachloroethane, and freons [171]. If susceptible to the hydroxyl radical pathway, however, the oxidizing power of such radicals often results in the complete mineralization of organic and organometallic compounds, resulting in water, carbon dioxide, and inorganic ions as products [70], Equation (5.43); this is believed to leave little, to no, residual toxic compounds [172,173].



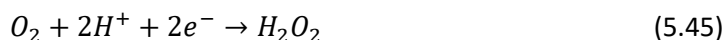
Despite the success the Fenton reaction has had for the treatment of wastewaters, it has a number of drawbacks. The first of these is the large quantities of hydrogen peroxide and iron reagents required to achieve full contaminant removal; not only does this make the process uneconomical, but the handling of large amounts of oxidizing agents creates safety concerns. The traditional Fenton reaction also results in large quantities of precipitated iron(III) sludge that requires secondary separation and treatment.

The electro-Fenton process is able to overcome these limitations via two methods: 1) hydrogen peroxide is electrogenerated *in situ* and therefore manual handling and addition of strong oxidizing reagents is not necessary, and 2) only small amounts of iron(II) ( $\text{Fe}^{2+}$ ) are required as the produced ferric iron ( $\text{Fe}^{3+}$ ) in Equation (5.42) is continuously transformed back to its ferrous state at the cathode surface, Equation (5.44), avoiding the formation of iron sludge.



Although not reliant on the external addition of chemicals, the electro-Fenton pathway is reliant on the presence of dissolved oxygen ( $\text{O}_2$ ) and small quantities of  $\text{Fe}^{2+}$ , typically in the millimolar concentration range. Upon application of an electric current under these conditions, a sequence of reactions occur starting with the two-electron reduction of  $\text{O}_2$  at the cathode surface to form hydrogen peroxide ( $\text{H}_2\text{O}_2$ ), Equation (5.45). When ferrous ions are present the peroxide is transformed into the more powerful oxidizing agent, the hydroxyl radical, making them available for organic destruction, Equation (5.42). The regeneration of  $\text{Fe}^{2+}$  via a single-electron reduction

at the cathode, Equation (5.44), suggests that the electro-Fenton reaction can occur continuously until the desired treatment outcomes have been reached.



The necessary iron concentration for this pathway is frequently naturally present in contaminated soils and subsequent groundwaters, making it a plausible treatment option for environmental remediation efforts. A majority of researchers declare an optimal  $Fe^{2+}$  concentration between 0.1 – 1.0 mM, depending on the reactor configuration and electrode materials used [70]. Other studies have shown that the reaction will occur at iron concentrations outside of this range, but at a lower rate and efficiency [174,175].

Regarding application efforts in the sub-Antarctic Macquarie Island, where a number of petroleum hydrocarbon spills have occurred in the last century, the electro-Fenton process is a feasible option due to the naturally high iron content found in the local soils and groundwaters. Following the installation of a permeable reactive barrier (PRB) at Macquarie Island in 2014, annual measurements indicated that groundwaters entering the PRB had an iron content ranging 0.03 – 17.0 mg/L [9], well within the range required for the Fenton reaction to commence. The iron concentration within the PRB was found to accumulate and be even higher, fluctuating between 10 – 200+ mg/L over a two year period [9]. For these reasons, the electro-Fenton pathway becomes a realistic approach for carrying out the *in situ* treatment of petroleum compound species observed at contaminant sites in the sub-Antarctic. Prior to field deployment, however, an understanding of the reaction efficiency, underlying mechanisms and practicality for the treatment of petroleum hydrocarbons needs to be obtained.

Accordingly, this chapter continues to investigate the types of reactions that may be promoted on carbon substrates for the environmental clean-up of petroleum hydrocarbon contaminated sites in the Antarctic. The electro-Fenton pathway is considered, and similar to Chapter 4, naphthalene was chosen as the model contaminant. Varying operational parameters are considered such as applied electric current and iron concentration, and a kinetic model is proposed that is able to predict treatment outcomes under all experimental conditions investigated.

## 5.2 Experimental

### 5.2.1 Reagents

The analytical reagents used within this chapter are detailed in Table 3.1. Sodium sulphate ( $Na_2SO_4$ ) and ferrous sulphate heptahydrate ( $Fe_2SO_4 \cdot 7H_2O$ ) were purchased from Chem-Supply and used as received. Solid naphthalene, polyvinylidene fluoride (PVDF, MW  $\sim 530,000 \text{ g mol}^{-1}$ ) and N,N-dimethylformamide (DMF) were purchased from Sigma-Aldrich, whilst sulfuric acid ( $H_2SO_4$ ) was supplied by Scharlau. Acticarb GC1200 Granular activated carbon (GAC) was supplied from Activated Carbon Technologies Pty Ltd and graphite sheet (DSN 530) was provided by Suzhou Dasen Electronics Material Co. Titanium(IV) oxysulfate solution (1.9 – 2.1 %) was used as received from Sigma-Aldrich for the purpose of hydrogen peroxide detection. Reverse osmosis (RO) water was used for the preparation of all solutions, except for naphthalene in which a concentrated stock solution was prepared in ethanol (EtOH) due to its low solubility in water. Adequate dilution of the EtOH stock solution was performed in RO water, leaving all final synthetic naphthalene solutions with an alcohol content of less than 0.2 % v/v; this was not found to have a detectable effect on naphthalene degradation, shown in Appendix A.2.



### 5.2.2 Electrochemical Reactor

Electrochemical experiments were carried out in an undivided glass cell, Figure 5.1, having a capacity of 250 ml. A single cylindrical carbon rod (8 mm  $\varnothing$ , Jaycar) was used as anode and vertically placed in the centre of the cell. Five cylindrical graphite rods (6.3 mm  $\varnothing$ , AlfaAesar) were used as cathodes in a circular array surrounding the anode. The cathodes were placed 10 mm away from the anode and vertically parallel to one another. A MP3087 (PowerTech) DC regulated power supply (0 – 32 V, 0 – 3 A) was connected to the electrodes and all experimental runs were operated under galvanostatic conditions at room temperature (23 °C); temperatures within the reactor were found to fluctuate  $\pm 1$  °C during treatment timeframes. Due to the absence of a reference electrode, all reported voltages are representative of the cell potential. The solution was continuously agitated with a magnetic stirrer to ensure ample mixing and guarantee that sampling events were unaffected by concentration gradients within solution. For each experimental run, 200 ml of a synthetic 20 mg/L naphthalene solution within an inert 0.05 M Na<sub>2</sub>SO<sub>4</sub> electrolyte was introduced into the cell giving the anode and cathodes a submerged geometrical surface area of 12.1 and 32.2 cm<sup>2</sup> respectively. The electrolyte was saturated with oxygen, nearing 8 mg/L, prior to experiments by sparging the electrolyte with 1.25 L/min of air for several hours via a Dymax AP700 air pump; the reactor was continuously supplied with air at this rate for the duration of each experiment. The pH of the electrolyte was adjusted to 2.6 by the addition of 1.0 M H<sub>2</sub>SO<sub>4</sub>, within the optimal range for the Fenton reaction to commence [70], and a catalytic amount of Fe<sup>2+</sup> (0.1, 0.2, or 2.0 mM) was added immediately prior to the commencement of an electric current. The reactor was covered with a Teflon-lined lid to minimize the effects of naphthalene volatilization, with a small opening to allow for sampling and equilibration with atmospheric pressure. Upon application of an electric current (1, 2, 3, or 5 mA), 150  $\mu$ l aqueous samples were taken at various time points and analysed for naphthalene concentration against time. The resulting by-products formed, pH, and cell voltage were also examined. All experimental runs were conducted in duplicate to test for repeatability.

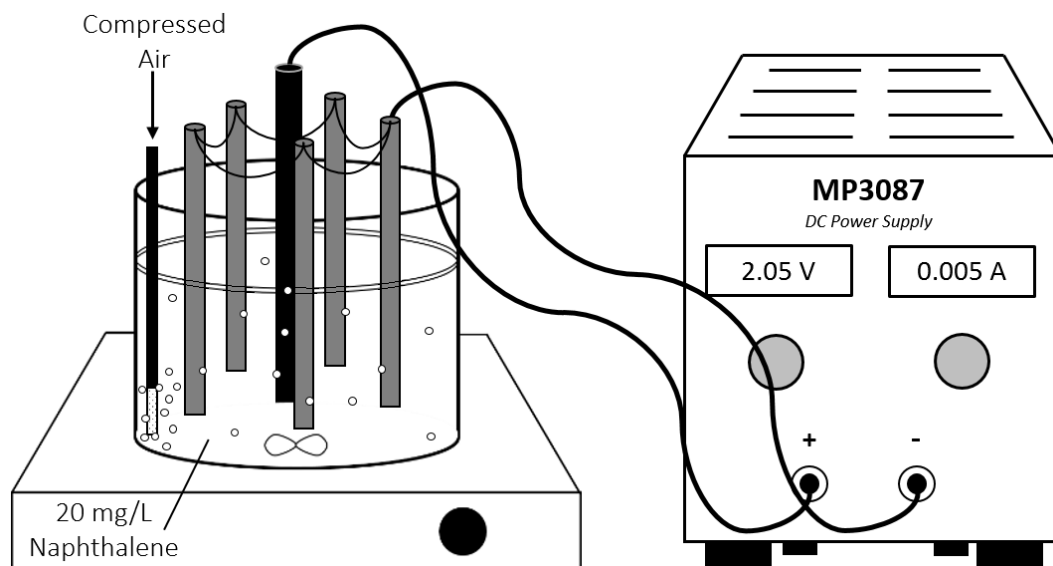


Figure 5.1: Schematic of electrochemical cell used for the electrochemical treatment of naphthalene contaminated water.

### 5.2.3 GAC Electrode Fabrication

GAC-PVDF electrodes were fabricated by first dissolving PVDF in DMF at 100 °C until fully dissolved. Following complete dissolution, the GAC was ground in an electric grinder for 2

minutes to form a fine powder and then added to the stirring PVDF/DMF solution, maintaining a ratio of 1:10 PVDF to GAC. The slurry was stirred at 100 °C for 2 hours to ensure a homogenous mixture, after which the temperature was increased to 150 °C to evaporate off excess solvent. Upon reaching the desired viscosity, about an 80 % reduction in volume, the slurry was thinly cast onto a graphite sheet and placed into a 100 °C oven for two hours, followed by a vacuum oven set to 80 °C for 12 hours; this ensured that all excess DMF was removed. The resultant plate electrode was cut to the desired dimensions and used as cathode in the electrochemical reactor.

#### 5.2.4 Analytical Methods

Naphthalene concentration was monitored using High Performance Liquid Chromatography (HPLC), whilst hydrogen peroxide concentration was analysed using UV/Vis spectrophotometry as described in Chapter 3. HPLC and Gas Chromatography coupled with Mass Spectroscopy (GC-MS) were used to detect and identify by-product species during electrochemical treatments. The pH of the studied aqueous solutions was measured using an InLab Versatile pH probe (Mettler Toledo).

### 5.3 Results and Discussion

#### 5.3.1 Control Studies

The electrochemical cell was characterized to 1) understand the varying pathways naphthalene is removed from the system without commencement of the electro-Fenton reaction; analogous to the active chlorine studies in Chapter 4, this includes adsorption of naphthalene onto the carbonaceous electrodes, volatilization, and partial oxidation at the anodic surface, and 2) determine if the key Fenton reagent, hydrogen peroxide, could be electrogenerated in the experimental setup being utilized.

##### 5.3.1.1 Adsorption

The literature surrounding the electro-Fenton technique generally employs highly porous, 3D, carbonaceous electrodes for the *in situ* generation of H<sub>2</sub>O<sub>2</sub> such as carbon felts [90,176–179], carbon-polytetrafluoroethylene (PTFE) [180,181], reticulated vitreous carbon (RVC) [176,182,183], activated carbon fibres (ACF) [184–186], carbon sponge [187,188], gas-diffusion electrodes (GDE) [95,189–191], and carbon nanotubes (CNT) [190,192,193]. The large surface areas of these materials are beneficial for the electrogeneration of hydrogen peroxide as it overcomes the mass-transfer limitation of low concentrations of dissolved oxygen in the bulk aqueous solution, approximately 8 mg/L, reaching the cathodic surface [194]. Similarly, the oxygen-containing functional groups present on these carbonaceous substrates (i.e. -COOH, C-O-C) aid in the catalysis of the two-electron reduction of oxygen to form greater quantities of H<sub>2</sub>O<sub>2</sub> [195]. Their electrochemical stability and high overpotential toward water discharge [70] further make them beneficial for use in electro-Fenton processes. However, such 3D electrodes could not be used in this work as it made it difficult to distinguish between naphthalene removal due to electro-Fenton degradation in the bulk solution and adsorption processes onto the carbon surface; adsorption alone was observed to achieve full naphthalene removal in as little as one hour of treatment.

To minimize adsorption effects, non-porous, graphite rods were used as cathode material in the electrochemical reactor. Adsorption of naphthalene onto the electrodes was examined in a closed vial with no headspace to prohibit volatilization. Over a 24-hour period insignificant amounts of naphthalene were removed from the liquid phase via adsorption processes; this is

likely due to the non-porous nature of the electrodes used, limiting the surface area and micropores available for adsorption processes to occur.

### 5.3.1.2 Volatilization

Although volatile compounds such as phenols and aromatic organics are commonly used as model contaminants in the literature, volatilization effects are commonly ignored when applying the electro-Fenton pathway. This is not acceptable when using naphthalene as a target contaminant as it is one of the more volatile polycyclic aromatic compounds [147], and it is likely that volatilization will have a notable contribution to its overall removal rate. Volatilization effects were measured by operating the reactor in the absence of an electric current and external air supply. As shown by Figure 5.2, volatilization was seen to occur at a first-order rate of  $7.1 \times 10^{-5} \text{ s}^{-1}$ , in good agreement with the data presented in Chapter 4. Through volatilization alone, 20 % of the initial naphthalene species was removed within the first hour of treatment, indicating that this removal pathway cannot be ignored.

### 5.3.1.3 Anodic Oxidation

The effects of partial anodic oxidation on the active carbon anode used (discussed in more detail in Chapter 4) was assessed by applying a 5 mA electric current within an inert 0.05 M  $\text{Na}_2\text{SO}_4$  electrolyte in the absence of iron and aeration. As shown in Figure 5.2, the overall naphthalene removal rate increased to  $1.6 \times 10^{-4} \text{ s}^{-1}$  with the application of current, removing 48 % of the initial naphthalene concentration within one hour. The anodic oxidation rate itself, not including the effects of volatilization, was calculated to be  $8.6 \times 10^{-5} \text{ s}^{-1}$  by taking the difference between the anodic oxidation and volatilization controls. When considering field deployment applications, this is the critical rate to identify as volatilization will have minimal effects in subsurface levels of 10 cm and greater where contaminated groundwaters are generally found [148]. Varying the applied current from 1 – 100 mA did not show any fluctuation in the anodic oxidation rate, consistent with previous studies [196]. This is likely due to the anodic oxidation rate being dependent on the mass transfer of naphthalene species to the anodic surface; in this instance, increases in current will go towards parasitic side reactions such as the formation of oxygen gas rather than naphthalene oxidation itself as there is a limited amount of solute at the anode surface to undergo electrochemical transformation [61,154,163].

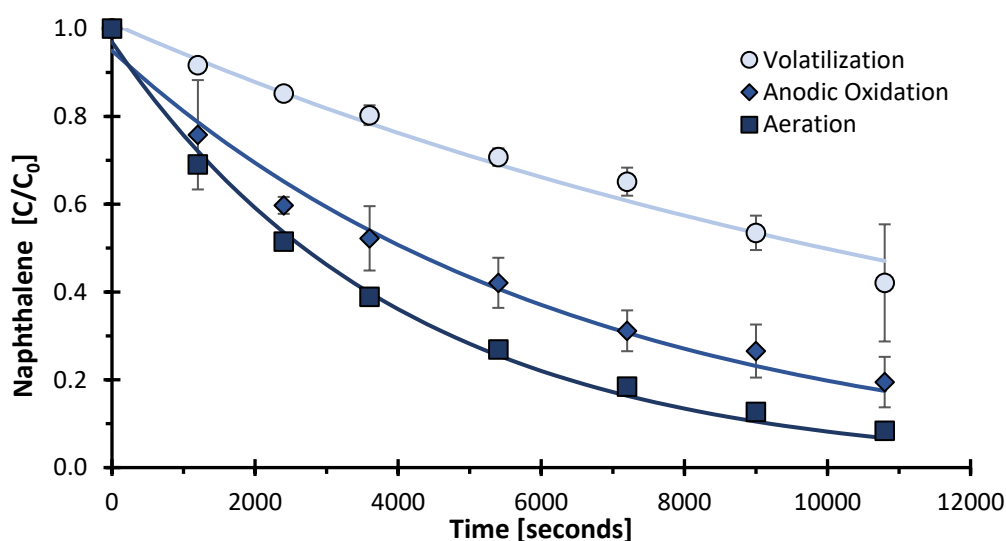


Figure 5.2: Naphthalene evolution as a function of time when treated within an electrochemical cell at 0 mA (volatilization), 5 mA (anodic oxidation + volatilization), and in the presence of aeration (aeration + anodic oxidation + volatilization). Points are experimental data whilst solid lines are first-order fittings.

#### 5.3.1.4 Aeration

Due to the low solubility of oxygen in aqueous solution, near 8 mg/L, the literature expresses the need for aeration during electro-Fenton treatments to better allow the electrogeneration of hydrogen peroxide [70,80]. However, due to the volatile nature of naphthalene, it is likely that sparging the solution will enhance its volatilization rate. This is commonly observed with organic compounds due to the greater surface area of the liquid/air interface that results; with an increase in interfacial area, organics such as naphthalene will partition into the gas phase at a heightened rate and be removed from the system more quickly [197]. Such a result was observed, shown in Figure 5.2, whereby the naphthalene removal rate was again increased to an overall first-order removal rate of  $2.5 \times 10^{-4} \text{ s}^{-1}$ . Not including the effects of anodic oxidation or volatilization, aeration alone was calculated to have a removal rate of  $9.0 \times 10^{-5} \text{ s}^{-1}$ . The literature does not report the enhanced removal that results during air sparging when applying the electro-Fenton pathway; this may be a problematic oversight as out of all the controls conducted, aeration was found to have the greatest effect, increasing the naphthalene removal rate by 1.5-fold.

#### 5.3.1.5 Hydrogen Peroxide Production

To confirm that the reactor could produce hydrogen peroxide with the less efficient, non-porous cathode material, currents of 1, 3 and 5 mA were applied to the 0.05 M  $\text{Na}_2\text{SO}_4$  electrolyte in the absence of naphthalene and iron. The resulting  $\text{H}_2\text{O}_2$  concentration in the bulk concentration was measured, and as shown in Figure 5.3 it was generated in all cases with a rapid increase detected upon application of an electric current. Increased concentrations of  $\text{H}_2\text{O}_2$  were detected when operating at heightened currents, in agreement with Chapter 4 and Faraday's law of electrolysis stating the rate at which a substance is formed at an electrode surface is proportional to the amount of current passed,  $r = i/nF$ . Thus, dissolved oxygen reacts at the cathodic surface at an increased rate when higher currents are applied.

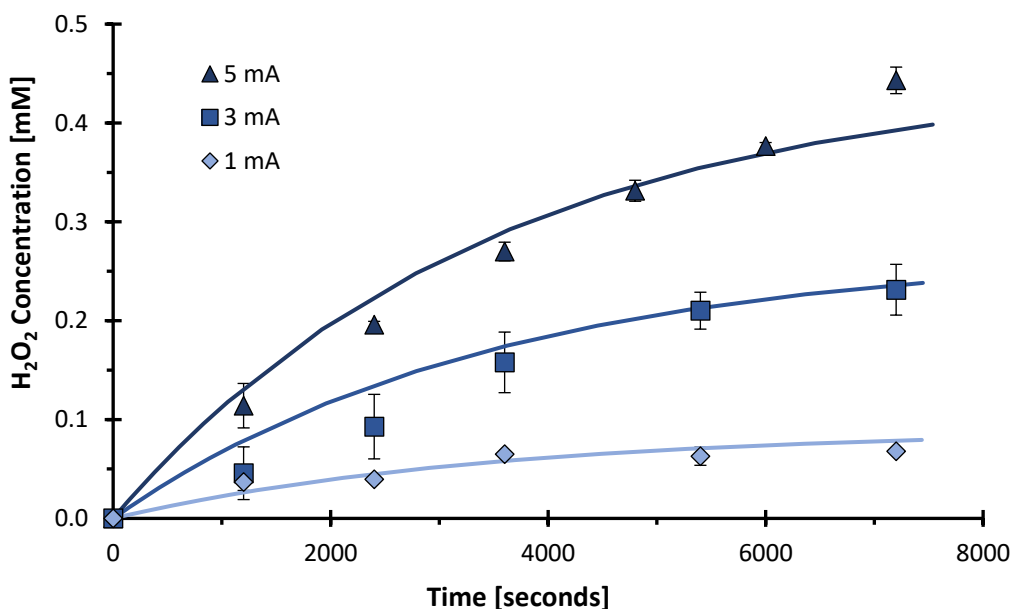
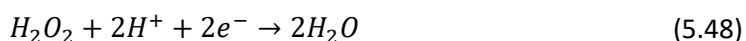


Figure 5.3: Hydrogen peroxide production versus time when operating the cell at various electric currents. Points are representative of the average values of experimental data whilst the lines are the fitted kinetic model.

The resulting  $\text{H}_2\text{O}_2$  concentrations were not seen to follow a linear increase with time but rather approached a maximum value, indicating that the generated  $\text{H}_2\text{O}_2$  is breaking down

simultaneously to being generated at the cathodic surface. This is an expected result, as it is well understood in the literature that  $H_2O_2$  undergoes spontaneous self-decomposition in aqueous solutions, Equation (5.46), particularly when inorganic ions, ultraviolet light, and metallic compounds are present, or the container is open to atmospheric conditions (i.e. not in a closed, well-sealed container) [198]. Electrogenerated hydrogen peroxide may also diffuse towards the anode surface and undergo a two-electron oxidation to form oxygen, Equation (5.47), [146], or in some cases undergo a further two-electron reduction at the cathode to form water, Equation (5.48) [176]. With such removal pathways occurring, a maximum  $H_2O_2$  concentration is often observed [146,174,176].

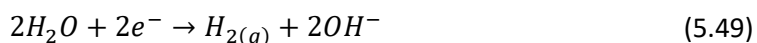


The removal rate ( $k_{removal}$ ) of  $H_2O_2$  within the system (discussed more in Section 5.3.2), was assumed to be proportional to the  $H_2O_2$  concentration, and its first-order removal rate determined to be  $2.9 \times 10^{-4} s^{-1}$ , in good agreement with decay rates reported elsewhere in the literature [198,199]. The determined rate of removal was fitted to the experimental data in Figure 5.3, and the goodness of fit is detailed in Table 5.1 where it is found to describe the experimental results well; root mean square errors (RMSE) of 0.028 or lower were achieved in all cases.

Table 5.1: Mathematical comparison between the experimental  $H_2O_2$  production data and the kinetic model; the root mean square error (RMSE) is tabulated.

Current [mA]	$k_{decay} [s^{-1}]$	RMSE
1		0.007
3	$2.9 \times 10^{-4}$	0.021
5		0.028

Operating the reactor at currents above 5 mA had no increased effect on  $H_2O_2$  production. This is likely due to the reactor entering a mass-transfer limited regime where the production rate of  $H_2O_2$  is dependent on the mass transfer of oxygen from the bulk solution to the cathode surface [74]. Thus, increases in current and associated cell potentials go towards hydrogen gas production, Equation (5.49), and limit the amount of  $H_2O_2$  that may be produced [70,80]. This is expected as applied potentials of 0.7 V/SHE are required for hydrogen peroxide production, whilst hydrogen gas production will commence at an increased potential nearing 0.83 V/SHE [70,200]. To avoid hydrogen production and preserve energy efficiency, the reactor was operated at currents of 5 mA or lower during all electro-Fenton treatments.



### 5.3.2 Kinetic Model Theory

To model the electro-Fenton pathway, it is assumed that naphthalene removal occurs via four main mechanisms: a first-order volatilization rate,  $k_{vol} (s^{-1})$ , a first-order anodic oxidation rate,  $k_{ano} (s^{-1})$ , a first-order aeration rate,  $k_{aer} (s^{-1})$ , and a second-order reaction rate between

naphthalene and electrogenerated hydroxyl radicals in the bulk solution,  $k_1$  ( $M^{-1} s^{-1}$ ). This is described by Equation (5.50) where  $[N]$  and  $[OH]$  are the concentrations of naphthalene and hydroxyl radicals in the bulk solution (M).

$$\frac{d[N]}{dt} = -(k_{vol} + k_{ano} + k_{aer})[N] - k_1[N][OH] \quad (5.50)$$

The  $k_{vol}$ ,  $k_{ano}$ , and  $k_{aer}$  terms were measured experimentally in Section 5.3.1, and are assumed to remain constant at  $7.1 \times 10^{-5} s^{-1}$ ,  $8.6 \times 10^{-5} s^{-1}$ , and  $9.0 \times 10^{-5} s^{-1}$  respectively. Although volatilization rates will noticeably alter with changes in temperature, fluctuations in reactor temperature were negligible in the timeframes considered ( $\pm 1^\circ$  during 3 hours of treatment).

The concentration of hydroxyl radicals varies with time, depending on its generation and consumption rates described in Equation (5.51); here,  $k_2$  is the rate of Fenton's reaction ( $M^{-1} s^{-1}$ ),  $[Fe^{2+}]$  and  $[H_2O_2]$  are the concentrations of iron(II) and electrogenerated hydrogen peroxide (M),  $k_3$  is the rate at which iron scavenges hydroxyl radicals ( $M^{-1} s^{-1}$ ), and  $k_4$  is the rate at which hydroxyl radicals consume hydrogen peroxide ( $M^{-1} s^{-1}$ ). Of these terms, Fenton's reaction is well understood and has a known reaction rate of  $k_2 = 63 M^{-1} s^{-1}$  [70,89,130], whilst  $Fe^{2+}$  is known to scavenge hydroxyl radicals to form  $Fe^{3+}$  at a much quicker rate of  $k_3 = 3.2 \times 10^8 M^{-1} s^{-1}$  [70,130], represented by Equation (5.52). The reaction between  $H_2O_2$  and  $\cdot OH$  is reported to be  $k_4 = 3.3 \times 10^7 M^{-1} s^{-1}$  [174]. Although further hydroxyl radical scavenging reactions exist, such as their self-decay to form hydrogen peroxide, they have not been included within the kinetic model as their low bulk concentration and short timeframe for which they exist limit their occurrence [70].

$$\frac{d[OH]}{dt} = k_2[Fe^{2+}][H_2O_2] - k_3[Fe^{2+}][OH] - k_4[H_2O_2][OH] - k_1[N][OH] \quad (5.51)$$



Hydrogen peroxide concentrations, as discussed in Section 5.3.1.5, fluctuate with time and will directly affect the number of radicals generated for naphthalene degradation. Its generation at the cathode surface and consumption through the Fenton reaction, decomposition, and reaction with hydroxyl radicals are expressed by Equation (5.53) where  $\epsilon$  is the current efficiency (i.e. fraction of current going towards hydrogen peroxide generation),  $I$  is the applied current ( $C s^{-1}$ ),  $n_1$  is the number of electrons utilized in the reduction of dissolved oxygen to form  $H_2O_2$ ,  $F$  is Faraday's constant ( $C mol^{-1}$ ),  $V$  is the volume of the reactor (L), and  $k_{removal}$  is the previously determined removal rate of hydrogen peroxide ( $s^{-1}$ ).

$$\frac{d[H_2O_2]}{dt} = \frac{\epsilon I}{n_1 F V} - k_2[Fe^{2+}][H_2O_2] - k_{removal}[H_2O_2] - k_4[H_2O_2][OH] \quad (5.53)$$

The change in  $Fe^{2+}$  concentration as a function of time is modelled and described by Equation (5.54), where it is consumed through the Fenton reaction and scavenging of hydroxyl radicals. As discussed in Section 5.1, one of the main benefits of the electro-Fenton pathway is that  $Fe^{2+}$  is regenerated during electro-Fenton treatments due to the single electron reduction of  $Fe^{3+}$  species at the cathode surface, Equation (5.44). This is represented by the last term in Equation

(5.54) where  $Fe^{2+}$  is regenerated at a rate proportional to the applied electric current; here,  $n_2$  is the number of electrons required for  $Fe^{2+}$  regeneration.

$$\frac{d[Fe^{2+}]}{dt} = -k_2[Fe^{2+}][H_2O_2] - k_3[Fe^{2+}][OH] + \frac{(1 - \varepsilon)I}{n_2FV} = -\frac{d[Fe^{3+}]}{dt} \quad (5.54)$$

Due to the low concentrations and acidic medium used, it is assumed that  $Fe^{3+}$  does not precipitate out of solution during treatment and is thus in equilibrium with  $Fe^{2+}$  species as described by Equation (5.54); an example of the equilibrium values predicted by the model are shown in Appendix A.2 and seen to be in good agreement with the literature [174]. It is also assumed that only two reactions occur at the cathode surface, those being the generation of hydrogen peroxide and regeneration of iron(II) species. Hydrogen gas evolution is not considered, and as discussed in Section 5.3.1.5, currents were limited to 5 mA to prevent its generation; this is a reasonable assumption as hydrogen peroxide production and iron regeneration occur at lower applied potentials than hydrogen gas production, 0.7 and 0.77 V/SHE versus 0.83 V/SHE respectively. Thus, the kinetic model assumes that the applied electric current is distributed between these two reactions, described by the  $\varepsilon$  and  $(1 - \varepsilon)$  terms in Equations (5.53) and (5.54), and is dependent on the relative concentrations of dissolved oxygen and  $Fe^{3+}$  in the system.

As dissolved oxygen and  $Fe^{3+}$  compete for space on the cathode surface to undergo electrochemical transformation, low concentrations of  $Fe^{3+}$  allow a greater portion of the current to go towards hydrogen peroxide generation, whilst higher  $Fe^{3+}$  concentrations will consume an increasing proportion of the current [201]. Thus, the correlation between current efficiency and the relative concentrations of dissolved oxygen and iron(III) is described by Equation (5.55), where the current efficiency evolves with the changing  $Fe^{3+}$  concentration,  $[Fe^{3+}]$  (M), during treatment. Consistent with the works of others, only the oxidation of water into oxygen gas was considered at the anode, and the dissolved oxygen concentration was assumed to remain constant as the solution was saturated prior to treatment and continuous aeration was provided [89,201].

$$\varepsilon = \frac{[O_2]}{[O_2] + [Fe^{3+}]} \quad (5.55)$$

Considering the five transient expressions that comprise the kinetic model, (5.50), (5.51) and (5.53) - (5.55), the  $k_2, k_3, k_4, I, n_1, n_2, F$  and  $V$  terms are known and constant, whilst the  $k_{vol}, k_{ano}, k_{aer}$ , and  $k_{removal}$  terms are measured experimentally and independently from one another; all parameters and their respective values are summarized in Table 5.2. The specific reaction rate between naphthalene and hydroxyl radicals,  $k_1$ , and the evolving current efficiency,  $\varepsilon$ , are the only unknown parameters;  $k_1$  should be constant for all experimental conditions trialled to validate the model, whilst  $\varepsilon$  will vary based on the initial iron(II) and evolving iron(III) concentrations during treatment.

Table 5.2: Known and experimentally determined parameters used within the proposed mathematical model.

$k_2$ ( $M^{-1}s^{-1}$ )	$k_3$ ( $M^{-1}s^{-1}$ )	$k_4$ ( $M^{-1}s^{-1}$ )	$I$ (C/s)	$n_1/n_2$ (-)	$F$ (C/mol)	$V$ (L)	$k_{vol}$ ( $s^{-1}$ )	$k_{ano}$ ( $s^{-1}$ )	$k_{aer}$ ( $s^{-1}$ )	$k_{removal}$ ( $s^{-1}$ )
63	$3.2 \times 10^8$	$3.3 \times 10^7$	0.001, 0.003, or 0.005	2/1	96,485	0.2	$7.1 \times 10^{-5}$	$8.6 \times 10^{-5}$	$9.0 \times 10^{-5}$	$2.9 \times 10^{-4}$

To determine the validity of the proposed model, as well as determine the effectiveness for

which the electro-Fenton pathway may aid in the degradation of solubilized naphthalene species, the electrochemical reactor was operated at varying currents (0 – 5 mA) and iron concentrations (0 – 2 mM). The ODE15S multistep solver of MATLAB® was used to solve the system of ordinary differential equations (ODEs), and the NLINFIT tool used to minimize the difference between the experimental data and model equations using a least squares method estimation. From this, the values of  $k_1$  and  $\varepsilon$  were determined.

### 5.3.3 Electro-Fenton Pathway

#### 5.3.3.1 Effect of Iron Concentration

The concentration of the first Fenton reagent,  $\text{H}_2\text{O}_2$ , was already observed to be dependent and controlled by the applied electric current. The effect of the second Fenton reagent,  $\text{Fe}^{2+}$ , was investigated by varying its concentration between 0 – 2 mM whilst maintaining an optimal current of 5 mA. Upon application of current, the naphthalene concentration was monitored against time to determine if the electro-Fenton reaction would commence and aid in naphthalene degradation.

The normalized naphthalene concentrations ( $C/C_0$ ) as a function of initial iron concentration and time are shown in Figure 5.4, where it is seen that naphthalene removal is significantly enhanced in the presence of iron; this is attributed to the commencement of the electro-Fenton reaction, Equation (5.42), whereby generated hydroxyl radicals attack the solubilized naphthalene in the bulk solution, Equation (5.43). For example, an initial iron concentration of 0.1 mM more than doubled that rate of naphthalene removal in comparison to the control (where only volatilization, aeration, and anodic oxidation occur), and reached complete removal within 2.5 hours of treatment. This suggests that the electro-Fenton pathway is a plausible option for the treatment of naphthalene contaminated waters in remedial applications. Although the control achieves a noticeable amount of removal in this timeframe, it is reiterated that in field applications volatilization pathways will have minimal effects and a larger fraction of the contaminant removal would be attributed to the electro-Fenton reaction itself.

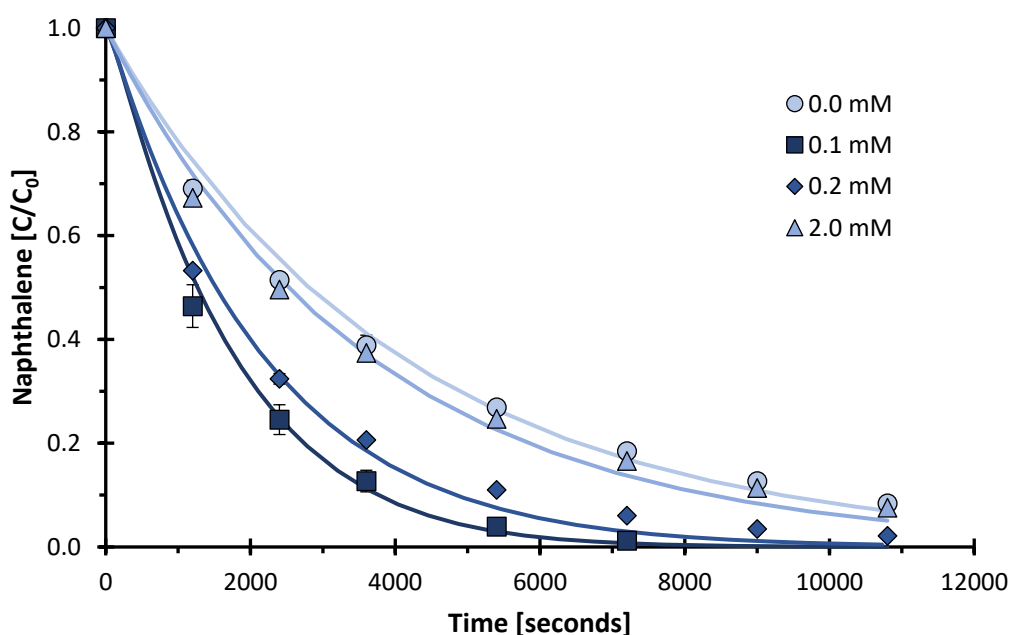


Figure 5.4: Normalized naphthalene concentration versus time during the electro-Fenton reaction at varying iron(II) concentrations in a 0.05 M  $\text{Na}_2\text{SO}_4$  electrolyte at 5 mA. Points are representative of experimental data, whilst the lines are the fitted kinetic model.



Initial iron concentrations of 0.2 mM and 2.0 mM were also seen to achieve naphthalene degradation and removal, but at a much lower efficiency in comparison to the 0.1 mM trial. For example, 89 %, 79 %, and 70 % of the naphthalene was removed in the first hour of treatment when initial iron concentrations of 0.1 mM, 0.2 mM, and 2.0 mM were used. Such reduction in removal is due to the increased  $\text{Fe}^{2+}$  concentrations scavenging greater amounts of hydroxyl radicals, Equation (5.52), and reducing the oxidizing power of the bulk solution. This is a prominent inhibitory reaction, as hydroxyl radicals will react with  $\text{Fe}^{2+}$  at a heightened rate of  $3.2 \times 10^8 \text{ M}^{-1}\text{s}^{-1}$  and limit the extent to which naphthalene can be oxidized [70,130]. Thus, smaller quantities of  $\text{Fe}^{2+}$  are desirable for achieving high efficiencies during electro-Fenton treatments. Regardless, the results demonstrate that initial iron concentrations of 0.1 mM, 0.2 mM and 2.0 mM can all reach acceptable levels of naphthalene, as mandated by The Australian regulations for marine water contaminant concentration [149], in timeframes of 2.2, 3.1, and 5.7 hours of treatment.

The five ODE's of the kinetic model (Equations (5.50), (5.51), and (5.53) - (5.55)) were fitted to the data in Figure 5.4, and the value of  $k_1$  was determined to be  $1.1 \times 10^8 \text{ M}^{-1} \text{ s}^{-1}$ . Although the liquid phase reaction rate between naphthalene and hydroxyl radicals has not been previously reported, this is within the range estimated for the reaction rate between hydroxyl radicals and aromatic compounds,  $10^8 - 10^{10} \text{ M}^{-1}\text{s}^{-1}$  [70,89]. Using this reaction rate, the model was seen to fit the data with high accuracy at the varying iron concentrations trialed in Figure 5.4; the mathematical fit is detailed in Table 5.3 where RMSEs of 0.07 or lower were achieved in all cases. Similarly, the correlation between the current efficiency and evolving  $\text{Fe}^{3+}$  concentrations enabled treatment outcomes to be accurately predicted when considering initial iron(II) concentrations in the range of 0.0 to 2.0 mM, validating the model equations used.

Table 5.3: Mathematical comparison between the experimental data and kinetic model for varying iron(II) concentrations; the root mean square error (RMSE) and average cell voltages are tabulated.

$\text{Fe}^{2+}$ Concentration [mM]	$k_1$ [ $\text{M}^{-1}\text{s}^{-1}$ ]	RMSE	Average Cell Voltage [V]
0.0		0.01	2.2
0.1	$1.1 \times 10^8$	0.07	2.1
0.2		0.04	2.0
2.0		0.06	1.9

With the determined reaction rate constant,  $k_1$ , and current efficiencies validated, the proposed kinetic model can predict treatment outcomes to a high accuracy despite variations in iron concentration; this can aid in determining ideal treatment conditions. Figure 5.5, for example, shows the predicted percentage of naphthalene removed following one hour of treatment at varying iron concentrations, revealing that the optimal iron concentration to use in the electro-Fenton system is 0.06 mM. This is slightly lower than the findings commonly reported in the literature, nearing 0.1 – 0.2 mM [70], however, a study investigating the electro-Fenton oxidation of phenanthrene [175], a polycyclic aromatic compound similar to naphthalene, reported having an optimal concentration of 0.05 mM  $\text{Fe}^{2+}$ , in good agreement with the results found herein.

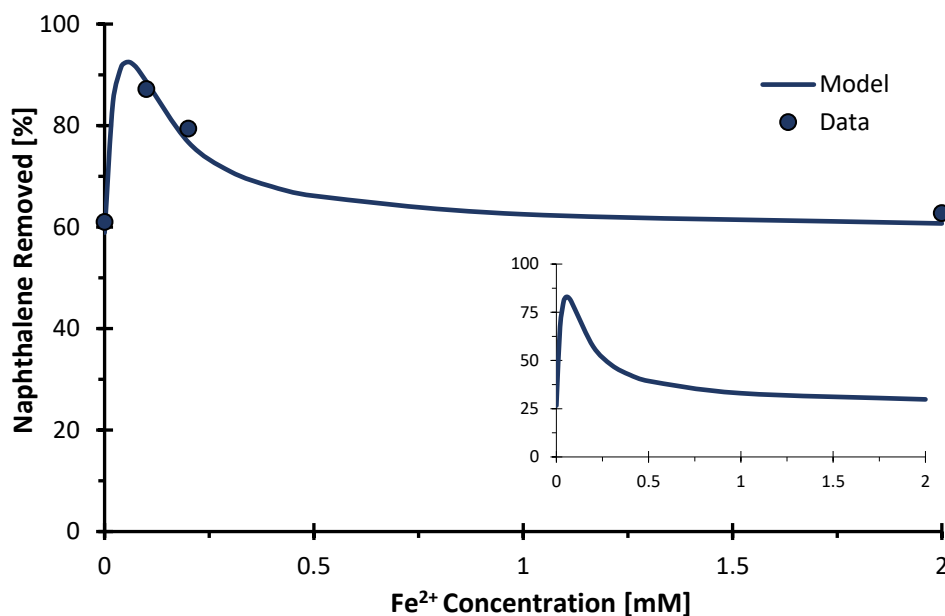


Figure 5.5: Comparison of the kinetic model and experimental data describing the % naphthalene removed after 1 hour of treatment at varying iron(II) concentrations. The subplot represents model predictions when volatilization pathways are not considered (i.e. in field deployment applications).

In subsurface field applications, treatment outcomes would differ vastly from these results as volatilization would have minimal effects on the removal of groundwater contaminants; the subplot of Figure 5.5 aims to represent this where the effects of volatilization are ignored. Here it is seen that in the presence of 0.06 mM iron(II) the electro-Fenton reaction reaches 83 % removal in one hour of treatment, whilst only 27 % is removed in the absence of iron (relying solely on anodic oxidation). Thus, despite the system used herein only increasing the naphthene removal rate 2.4-fold in comparison to the controls, it is predicted that in field deployment applications, naphthalene would be removed over 6 times as fast than when relying solely on anodic oxidation; this better demonstrates the magnitude for which the electro-Fenton reaction can aid in environmental remediation efforts.

### 5.3.3.2 Effect of Applied Current

A second set of experiments was conducted to determine if the proposed model can predict treatment outcomes when changes in applied current occur. Considering the results of Section 5.3.1.5, it is expected that with increasing currents up to 5 mA, faster removal rates would result due to the increased amounts of electrogenerated hydrogen peroxide. To investigate this, currents of 2 and 5 mA were studied whilst leaving the iron concentration constant at 0.1 mM.

The results shown in Figure 5.6 confirm that the rate of naphthalene removal is affected by changes in applied electric current, where faster rates of removal are detected at increased electric currents. As discussed in Section 5.3.1.5, this is due to the higher currents converting dissolved oxygen into H<sub>2</sub>O<sub>2</sub> at an increased rate which is then available for the Fenton reaction to commence, Equations (5.42) and (5.43). For example, increasing the electric current from 2 to 5 mA increased the naphthalene removal rate 1.6-fold, reaching full removal within 3.5 and 2.5 hours respectively.

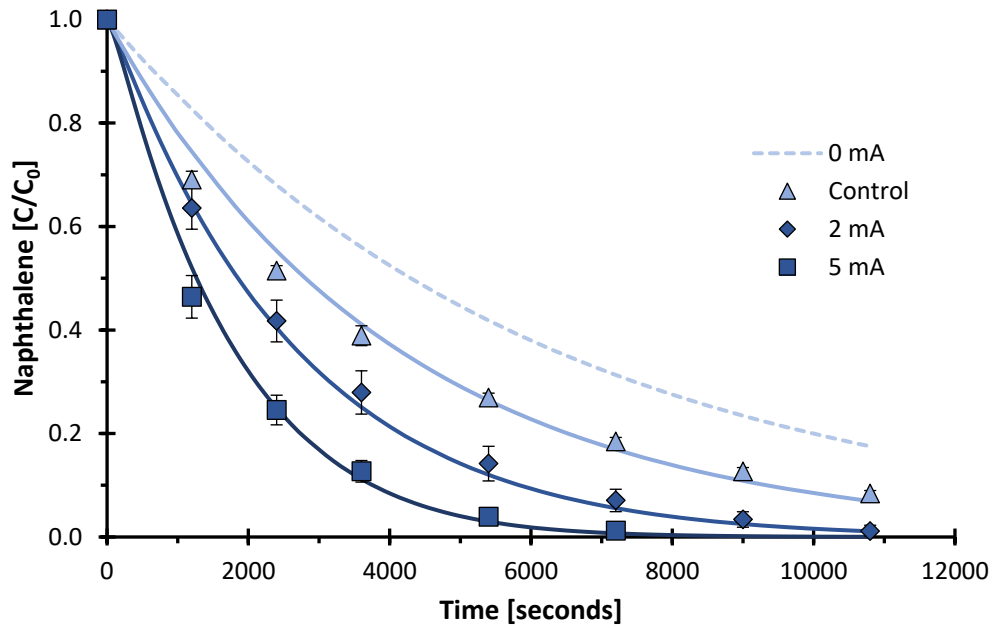


Figure 5.6: Normalized naphthalene concentration versus time during the electro-Fenton reaction at varying electric currents with a constant iron(II) concentration of 0.1 mM. Points are experimental data whilst the lines are the kinetic model 'Control' is representative of the combined volatilization/aeration and anodic oxidation pathways, whilst 0 mA is representative of volatilization/aeration pathways alone.

The previously determined reaction rate,  $k_1$ , and current efficiency correlation of the kinetic model are fitted to the data in Figure 5.6, where it is observed that they are still able to predict treatment outcomes to a high accuracy despite variations in electric current. The mathematical goodness of fit is described in Table 5.4, where the resulting accuracy further validates the model equations used in this work; the kinetic model can accurately predict treatment outcomes over a large range of iron concentrations (0 – 2 mM) and applied electric currents (0 – 5 mA).

Table 5.4: Mathematical comparison between the experimental data and nonlinear kinetic model for varying applied electric currents; the root mean square error (RMSE) and average cell voltages are tabulated.

Current [mA]	$k_1$ [ $M^{-1}s^{-1}$ ]	RMSE	Average Cell Voltage [V]
0		0.01	0.0
2	$1.1 \times 10^8$	0.03	1.9
5		0.07	2.1

### 5.3.3.3 Energy Requirements

To determine if energy requirements of this system are feasible for environmental applications, such as the Antarctic, Equation (5.56) was used to calculate the energy usage per unit of naphthalene removed, where  $E_{sp}$  is the specific energy consumption (kWh/kg),  $E_{cell}$  is the average cell voltage (V),  $I$  is the applied current (A),  $t$  is the treatment time (hr),  $V$  is the volume of solution treated (L), and  $\Delta N$  is the quantity of naphthalene removed from the system during the treatment timeframe (g/L); the specific energy consumption to reach full naphthalene removal was considered.

$$E_{sp} = \frac{E_{cell}It}{V\Delta N} \quad (5.56)$$

The results shown in Figure 5.7 demonstrate that the specific energy consumption is affected by

both changes in  $\text{Fe}^{2+}$  concentration and the applied electric current. For example, increasing the iron content from 0.1 to 2.0 mM was seen to increase the energy consumption from 5.6 to 8.0 kWh/kg per unit of naphthalene removed. Despite an increase in ions that lower electrochemical resistance and resultant cell voltage, refer to Table 5.3, an increase in specific energy is still observed due to the hindered naphthalene removal rates that result with large iron concentrations scavenging the oxidizing power of the solution. This is the opposite of the results in Chapter 4 where increases in ion concentration vastly lowered the energy requirements; however, increased quantities of chloride ions in the active chlorine pathway do not act as a scavenging reagent.

Despite this, the energy usage associated with each of the trialed iron concentrations, 5.6 kWh/kg, 6.7 kWh/kg, and 8.0 kWh/kg, remains low, and has reduced energy requirements in comparison to the active chlorine pathway. For example, the optimal conditions examined in Chapter 4 resulted in a specific energy consumption nearing 104 kWh/kg; the electro-Fenton reaction has shown to reach complete naphthalene removal in the same timeframe but uses 5.4 % the amount of energy. This is attributed to the lower cell potentials required to produce hydrogen peroxide in the electro-Fenton pathway, 0.7 V/SHE, versus 1.3 V/SHE for active chlorine production. Furthermore, once the oxidizing species are produced, naphthalene has proved to have a much faster reaction rate with hydroxyl radicals in comparison to active chlorine species,  $1.1 \times 10^8$  versus  $2.2 \text{ M}^{-1}\text{s}^{-1}$  respectively. In either case, however, the resultant energy consumptions are low enough for field deployment applications in remote regions.

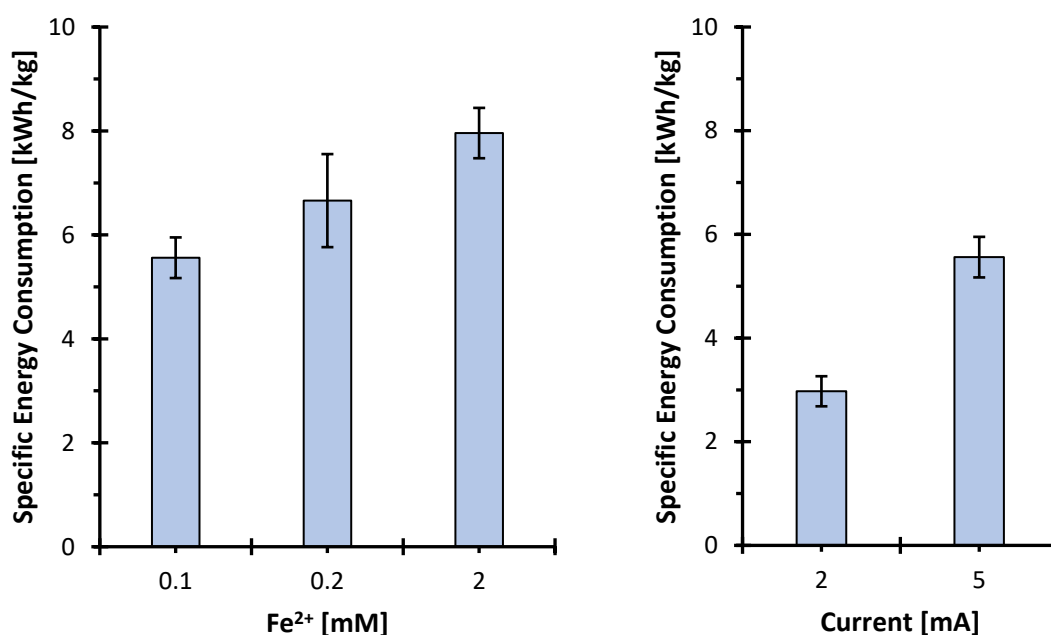


Figure 5.7: Specific energy consumption for naphthalene removal when altering the iron(II) concentration at a constant 5 mA of electric current (left) and applied electric current at a constant iron(II) concentration of 0.1 mmol (right) during the electro-Fenton pathway in a 0.05 M  $\text{Na}_2\text{SO}_4$  electrolyte.

Changes in applied current also affected specific energy consumption, with it doubling from 2.8 to 5.6 kWh/kg when increasing the current from 2 to 5 mA.; this is expected and due to the larger cell voltages required to drive the desired current, Table 5.4. Thus, there exists a trade-off between the required treatment timeframes and the amount of energy consumed, where

faster removal rates result in greater energy consumption; the optimal condition is dependent on the end user's application.

Not considering capital expenditure or the energy required for aeration, the results shown in Figure 5.7 estimate that 5.6 kWh can remove 1 kg of solubilized naphthalene when implementing the electro-Fenton reaction at a current of 5 mA in the presence of 0.1 mM Fe<sup>2+</sup>; this corresponds to an energy operating cost nearing AUD \$0.06 per m<sup>3</sup> of a naphthalene saturated water supply (assuming 2019 Australian electricity prices of 32.59 ¢/kWh and a naphthalene saturation level of 31 mg/L). In view of the extreme environments present in the sub-Antarctic, it is understood that such energy requirements are low enough to be operated via external photovoltaic panels. As described by Brillas [202], photovoltaic/electro-Fenton systems have been shown to be an effective and economical way to treat contaminated waters. Furthermore, such integrated systems can accumulate excess electricity in rechargeable batteries and enable all electrical devices (e.g. power supplies, aerators) to be continuously powered, day or night, without the need for an electricity supply [202]; such an autonomous system would be ideal for remediation efforts in remote regions such as the Antarctic.

Due to varying reactor configurations, model contaminants, and electrode materials implemented in the literature, it is difficult to compare the calculated energy requirements of this work to other publications; however, they are found to be within reasonable scale of other works that have conducted a cost-effectiveness study for the electro-Fenton reaction [194,203]. Although other studies have reported quicker removal timeframes that would further lower specific energy consumption, their treatments are often coupled with adsorption processes and the use of highly efficient, non-active anodes such as boron doped diamond (BDD) that are capable of producing hydroxyl radicals and oxidizing organic compounds at their surface [133,143,204]. The use of such anodes has been disregarded here, as the scope of this work is to implement inexpensive carbon anodes that are more practicable for field deployment applications. With this in mind, the carbonaceous electrodes used herein prove to have promising results for remediation efforts as the naphthalene is removed in short timeframes with minimal amounts of energy consumption.

The energy usage could be further reduced by overcoming the rate-limiting step of the reaction; as discussed in Section 5.3.1.5, that is the limited amount of hydrogen peroxide that can be produced on the non-porous electrodes used. Hence, without changing the anode to highly expensive materials such as BDD to increase removal rates and lower energy consumption, the cathode can instead be exchanged with a more porous material that is capable of producing larger quantities of H<sub>2</sub>O<sub>2</sub>.

To demonstrate this, the granular activated carbon (GAC) used in Antarctic remediation efforts (GC1200 GAC, as characterized in Chapter 3) was used to make a porous plate electrode as described in Section 5.2.3. This electrode, with dimensions of 14 × 6 cm, was used as the cathode in the electrochemical reactor and the resultant hydrogen peroxide concentration was monitored with time. The results are shown in Figure 5.8 where it is seen that the porous GAC electrode is capable of producing nearly twice the amount of peroxide than the original graphite rod; this is attributed to the increased surface area associated with activated carbons (1,137 m<sup>2</sup>/g for GC1200 GAC [128]), as well as the large quantity of oxygen-containing functional groups on GAC surfaces that catalyse the electrogeneration of hydrogen peroxide.

Even without surface oxygen groups, increases in electrode surface area alone are known to increase the rate of electrochemical conversion during electrochemical treatments [74], and

align with the results illustrated in Figure 5.8. This suggests that the use of 3D electrodes with substantial surface areas, such as a bed of activated carbon, would be beneficial for use in the treatment of contaminated groundwater in remote environmental regions; it would increase reaction efficiency whilst reducing treatment timeframes. Such electrodes were not used in this study as adsorption effects were too strong and prevented investigating the efficiency of the electro-Fenton reaction towards naphthalene degradation, discussed in Section 5.3.1.1. The efficiency for which GC1200 GAC produces  $\text{H}_2\text{O}_2$ , however, gives strong evidence that the electro-Fenton reaction would be effective for the regeneration of a contaminant loaded GAC. In this instance, the electrochemical production of oxidizing species can occur on the GAC surface itself, in close proximity to where contaminant species are adsorbed, and free up active adsorptive sites; this is investigated in Chapter 6.

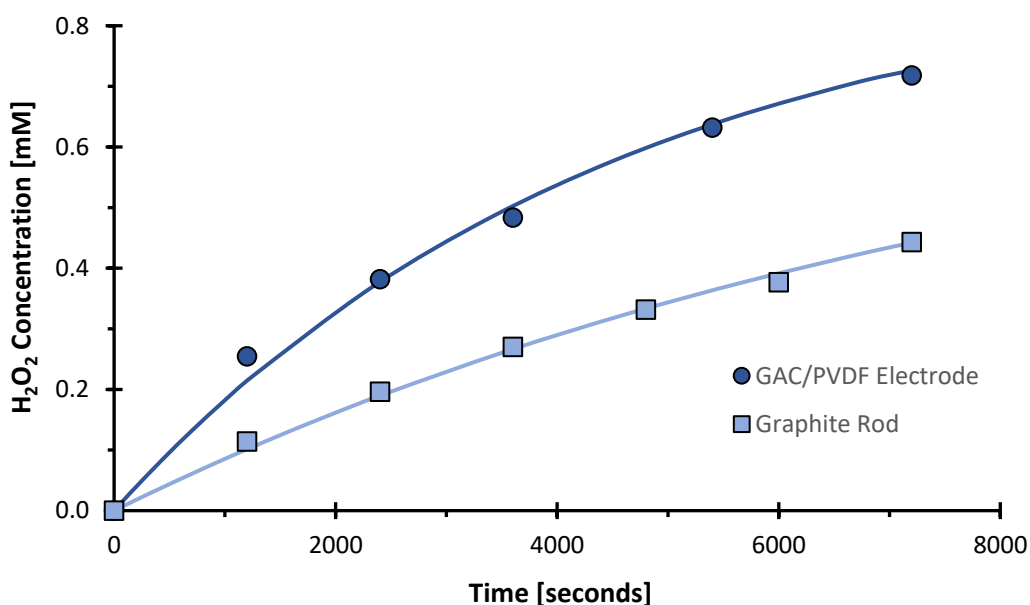


Figure 5.8: Comparison of hydrogen peroxide production against time when utilizing a graphite rod versus a GAC-PVDF electrode.

Similarly, when field deployment regions present with lower ambient temperatures, such as in the Antarctic and sub-Antarctic, the saturation point of dissolved oxygen increases and will allow for greater amounts of  $\text{H}_2\text{O}_2$  to be electrogenerated *in situ*. Although this would enhance  $\text{H}_2\text{O}_2$  production, it is important to note that such decreases in temperature may simultaneously reduce reaction rates. For example, the Fenton reaction has been shown to follow Arrhenius kinetics, where elevated temperatures nearing 30 – 35 °C are commonly reported as having optimal reaction rates [205,206] due to the enhanced kinetics and mass transfer within the system. Despite this, promotion of the Fenton reaction at decreased temperatures nearing 10 °C have still had successful contaminant removal results with high reaction efficiencies [207]. The results of Huo et al., for example, indicated that the increased stability of  $\text{H}_2\text{O}_2$  at low temperatures ultimately outweighs the adverse effects of reduced reaction rates [208]. Thus, although reaction rates may be altered with fluctuations in temperature, the model equations and underlying mechanisms identified in this work are believed to be suitable to describe a wide range of operating temperatures in both temperate and extreme environments.

### 5.3.3.4 By-Product Identification

A concern identified with the active chlorine pathway in Chapter 4 was that naphthalene was transformed into chlorinated hydrocarbons during its degradation. Although chloride ions are likely to be present in field deployment applications, a benefit of the electro-Fenton pathway is that it can commence at low enough potentials that avoid the production of active chlorine species; potentials near 0.7 V/SHE are required for the electro-Fenton pathway, whilst potentials of 1.36 V/SHE are needed for active chlorine production. Although this in itself can prevent chlorinated hydrocarbons from forming, the by-products resulting from electro-Fenton treatments were still investigated to ensure undesirable compounds were not being produced.

The HPLC analysis conducted during electro-Fenton treatment is shown in Figure 5.9, where the naphthalene peak is shown to exponentially decrease with time. Within 2.5 hours, the naphthalene is fully depleted whilst a number of small, transient peaks were seen to elute and disappear on the chromatograms with increasing time; this indicates that naphthalene and its by-products quickly undergo subsequent electrochemical transformation to form a variety of short-lived species. Due to the low concentration and transient nature of the eluting by-products, not all of the compounds could be identified. However, the first and main by-products to appear were trace amounts of 1- and 2- naphthol species, a hydroxylated naphthalene species. The formation of naphthol species is anticipated as the main reactant within the electro-Fenton system is the hydroxyl radical, known to oxidize compounds via the hydroxylation of a non-saturated bond [70]. It is also consistent with works investigating the reaction of naphthalene with hydroxyl radicals in the gaseous phase [150,209], where naphthol was found to be the first generated by-product in a series of oxidizing reactions.

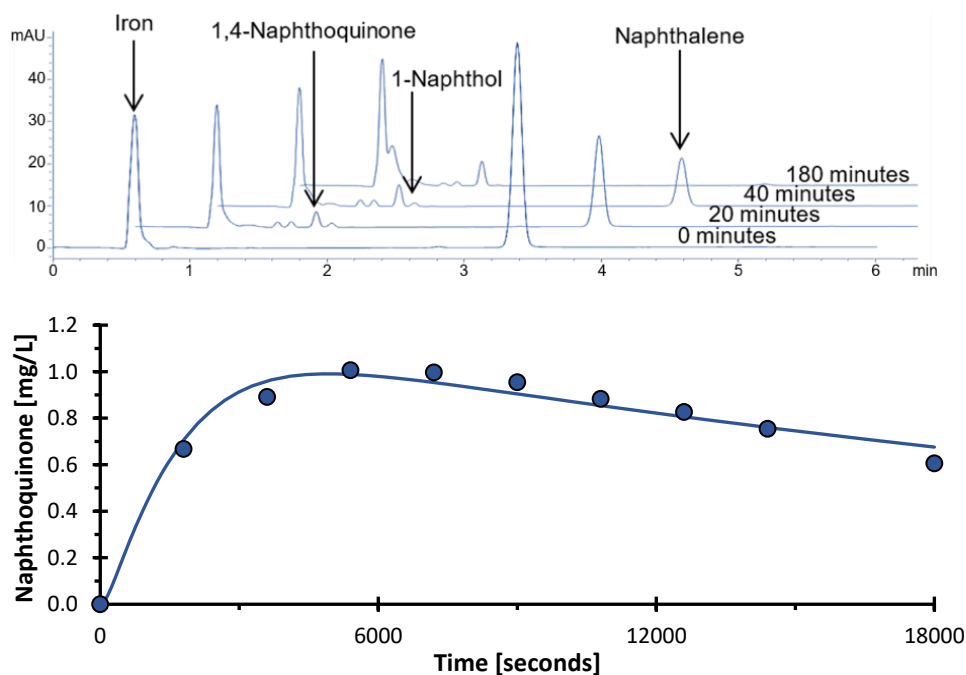


Figure 5.9: (Top) Evolution of naphthalene and associated by-products on the resultant HPLC-DAD chromatograms as a function of time during electro-Fenton treatments at 5 mA and an iron(II) concentration of 0.1 mmol, and (bottom) the predicted removal timeframes of 1,4-naphthoquinone.

The naphthol species were highly transient and seen to have a small yield relative to the disappearance of naphthalene. This is believed to be due to the naphthol species being quickly oxidized again, either through additional reactions with hydroxyl radicals or dissolved oxygen

species. Dissolved oxygen is then not only required for the electrogeneration of hydrogen peroxide, but it also aids in the propagation of the hydroxyl chain reaction [169,194], described by Equation (5.57). This pathway suggests that following the initial attack of a hydroxyl radical on an organic compound,  $R$ , an unpaired electron generally remains and enables dissolved oxygen to easily be incorporated into the structure of the organic species [209]; such reactions commonly continue until complete mineralization is reached [194].



It has been reported by others that that further oxidation between naphthol species and  $O_2$  in the gaseous phase by reaction (5.57) forms 2,3-epoxy-naphthoquinone [150] prior to forming ring-cleaved products containing end -carbonyl and -carboxylic groups such as phthalaldehydes and formylcinnamaldehydes [209]. As 2,3-epoxy-naphthoquinone was detected in small quantities through gas chromatography-mass spectroscopy (GC/MS) analysis ( $M^+$  of 174), it is plausible that naphthalene and its associated by-products were broken down via this pathway, explaining their quick disappearance on the resulting chromatograms. Comparable works that have promoted the electro-Fenton pathway for the removal of aromatic compounds have first detected polyhydroxylated derivatives, followed by a variety of ring-cleaved and ring-opened products, a majority of which are carboxylic acids [89,90,177,210–212], after which they are further degraded into  $CO_2$  and  $H_2O$  to reach complete removal. Due to the oxidizing power of electro-Fenton mediums, such by-products are reported to quickly disappear and not accumulate within solution [213]; as this was observed through the HPLC and GC/MS analysis conducted herein, it is probable that similar reaction pathways and outcomes were achieved.

An exception to this was the and long-lasting presence of 1,4-naphthoquinone within the system, produced via a simultaneous but less prevalent reaction pathway whereby a hydroxyl radical attacks the  $C_{(4)}$  position of generated 1-naphthol species [150]. Although the concentration of 1,4-naphthoquinone remained low throughout all trialed treatments, less than 1 mg/L, it proved to be much more resilient to oxidation via hydroxyl radicals in comparison to naphthalene and the other detected by-products; the slow rate of removal of this compound is depicted in Figure 5.9 where at 5 hours of treatment, 0.61 mg/L of 1,4-naphthoquinone remained.

Due to its continual presence, the observed decay of naphthoquinone was incorporated into the kinetic model, described by Equation (5.58), where  $[NQ]$  is the concentration of 1,4-naphthoquinone (M),  $\varphi$  is the fractional conversion of naphthalene to form naphthoquinone (rather than alternative by-products), and  $k_5$  is the reaction rate between naphthoquinone and hydroxyl radicals ( $M^{-1}s^{-1}$ ). Equation (5.58), in conjunction with the five ODEs of the kinetic model, was fitted to the data in Figure 5.9 and  $k_5$  was found to be  $6.5 \times 10^6 M^{-1}s^{-1}$ , two orders of magnitude slower than the reactions between hydroxyl radicals and naphthalene or iron, explaining its slow disappearance from the system. This is an expected result, as it has been reported that the half-life of hydroxyl radicals reacting with naphthalene in the gaseous phase is nearly 11-fold shorter than with 1,4-naphthoquinone (14 versus 156 hours) [214]. Pimentel et al. had analogous findings during the electro-Fenton treatment of aqueous phenol solutions, whereby 1,4-benzoquinone intermediates had much slower reaction rates with hydroxyl radicals in comparison to phenol or other by-product species generated such as hydroquinone [213].



$$\frac{d[NQ]}{dt} = \phi k_1 [N][\cdot OH] - k_5 [NQ][\cdot OH] \quad (5.58)$$

The fitted kinetic model also revealed that about 8.7 % of naphthalene species reacts to form 1,4-naphthoquinone, whereas the majority of it undergoes the quicker removal pathway described previously through Equation (5.57). Although the yield of naphthoquinone remains low during treatment, the toxicity associated with 1,4-naphthoquinone [214] may require prolonged treatment timeframes when applied in remedial applications to ensure its complete removal. However, it is also realized that 1,4-naphthoquinone is more easily biodegraded than its parent compound [214], naphthalene, suggesting that if residual amounts remain in environmental applications it is more likely to undergo biodegradation processes. Such a symbiotic process between electro-Fenton and microbial treatments would, overall, still increase the rate at which pollutants are removed from contaminated sites, and have been shown to be a successful and effective treatment option [215]. Because of this, increasing the biodegradability of contaminants is often considered a sufficient result of electrochemical treatments [15,100,186]. As the naphthalene in this work was observed to be continually hydroxylated and oxidized into less recalcitrant forms, it is believed that such treatments would be beneficial for the remediation of contaminated sites, such as in the Antarctic where biodegradation processes alone have relatively slow kinetics. Even if slight amounts of carboxylic acids or naphthoquinones remain, the partial or full substitution of methyl and hydrogen groups with carboxylic acid or esters groups will increase the biodegradability of the initially present organic and contaminant compounds, and increase the rate of contaminant removal within these regions [216].

#### 5.4 Conclusions

This chapter has identified that the electro-Fenton pathway is another possible option for the treatment of contaminated groundwaters in Polar Regions such as the Antarctic. It was specifically shown that the high priority pollutant for removal, naphthalene, can be fully removed within 3 hours of treatment whilst using minimal resources that are appropriate for field deployment scenarios. In comparison to the active chlorine results of Chapter 4, this pathway has lower energy usage and avoids the production of chlorinated compounds. Although minimal amounts of 1,4-naphthoquinone were detected, sufficient treatment times will ensure its complete removal from the system.

To aid in potential field deployment and gain an understanding of the electro-Fenton degradation pathway, a kinetic model was proposed and seen to accurately predict treatment outcomes despite variations in reactor conditions; the two main variables of the model were identified to be the iron content and applied electric current. Based on these two inputs, treatment outcomes can be predicted under a range of operating conditions, bringing the possibility of field deployment one step closer.

The rate-limiting factor of this reaction was determined to be the limited amounts of hydrogen peroxide that could be generated on the non-porous cathodes used. It is believed that this could be overcome by using 3D, porous cathodes suggesting that this treatment pathway would be suitable for the *in situ* regeneration of PRB substrate materials; this is to be investigated in the following chapter.



---

# CHAPTER 6

---

## Electrochemical Regeneration of Naphthalene Contaminated Granular Activated Carbon

This chapter investigates the effectiveness of electrochemical technologies for the regeneration of naphthalene loaded granular activated carbon. The active chlorine and electro-Fenton reaction pathways described in Chapters 4 and 5 are evaluated, and the underlying regenerative mechanism addressed.

---



## 6.1 Introduction

Chapters 4 and 5 concluded that electrochemical technologies are an effective pathway to degrade contaminants commonly found in Antarctic permeable reactive barriers; *in situ* decomposition of petroleum contaminants can be achieved with either the active chlorine or electro-Fenton pathways. In addition to this, each pathway was observed to have low energy requirements, making the technology feasible for deployment in environmental remediation efforts. This chapter aims to determine whether these reactions can be used to regenerate the granular activated carbon (GAC) material used within Antarctic and sub-Antarctic permeable reactive barriers (PRB).

A review of the literature (Chapter 2) identified four mechanisms that may take place during the electrochemical treatment of adsorbent materials:

- 1) enhanced desorption due to changes in pH,
- 2) enhanced desorption due to the presence of ionized species,
- 3) electro-desorption of charged species, and
- 4) oxidation reactions occurring at the external electrodes and/or the GAC surface itself.

Considering each of these, the change in contaminant concentration on the GAC surface and surrounding liquid will change as described by Equations (6.59) and (6.60) respectively, where  $q_i$  is the solid phase concentration of contaminant  $i$  (mg/g),  $t$  is time (s),  $r_{desorption}$  is the rate of desorption from the GAC surface due to changes in pH, ions, and/or electrostatic repulsions (mg/g/s),  $r_{oxidation,GAC}$  is the rate of oxidation reactions occurring on the GAC surface (mg/g/s),  $C_i$  is the liquid phase concentration of contaminant  $i$  (mg/L), and  $r_{oxidation,ex}$  is the rate of oxidation reactions occurring at the external electrodes (mg/g/s).

$$\frac{dq_i}{dt} = -r_{desorption} - r_{oxidation,GAC} \quad (6.59)$$

$$\frac{dC_i}{dt} = r_{desorption} - r_{oxidation,GAC} - r_{oxidation,ex} \quad (6.60)$$

Much of the literature investigating the electrochemical regeneration of GAC has focused primarily on the outcomes of treatment, leaving little discussion surrounding the regenerative mechanism itself. Due to this, there is significant discrepancy in the literature with respect to how and why electrochemical regeneration works the way it does; many authors claim it is dependent solely on desorption processes,  $r_{desorption}$ , while others claim oxidation reactions on the GAC surface,  $r_{oxidation,GAC}$ , are the driving mechanism [143]. Without a clear understanding of the underlying mechanism, scale-up and ultimate application *in situ* of PRBs is greatly hindered.

Therefore, this chapter aims to identify the underlying mechanisms and relative degree to which they aid in the electrochemical regeneration of GAC. Naphthalene is again chosen as a model contaminant, and several experimental setups are used to address how enhanced desorption, electrodesorption, and oxidation reactions alter the contaminant concentration on a pre-loaded GAC substrate. Naphthalene also proves to be an interesting compound of choice for this study as much of the literature describes studies of highly soluble compounds that are readily desorbed from adsorbent materials and aid in regeneration outcomes. As naphthalene is nearly

insoluble, it represents an appropriate surrogate for all recalcitrant contaminants that may be strongly bound to GAC; success with naphthalene will provide confidence in utilizing this technique more generally.

Since the ultimate application of this technology is for the *in situ* treatment of PRBs, desorption processes alone are not a sufficient treatment outcome as it may result in spreading contaminants into regions outside of the PRB. Thus, the active chlorine and electro-Fenton reactions are investigated to determine if complete removal, rather than mere desorption, can be achieved. Various operational parameters are studied such as applied current and treatment timeframes, and the resulting regeneration efficiencies are reported.

## 6.2 Experimental

### 6.2.1 Reagents

The analytical reagents used are detailed in Table 3.1. Sodium chloride (NaCl), sodium sulphate (Na<sub>2</sub>SO<sub>4</sub>), ferrous sulfate heptahydrate (Fe<sub>2</sub>SO<sub>4</sub>•7H<sub>2</sub>O), and hydrogen peroxide (H<sub>2</sub>O<sub>2</sub>) were purchased from Chem-Supply and used as received. Solid naphthalene and titanium(IV) oxysulfate solution (1.9 – 2.1 %) were purchased from Sigma-Aldrich, whilst sulfuric acid (H<sub>2</sub>SO<sub>4</sub>) was supplied by Scharlau. Acticarb GC1200 granular activated carbon (GAC) was supplied by Activated Carbon Technologies Pty Ltd (as characterized in Chapter 3). Reverse osmosis (RO) water was used for the preparation of all solutions, except for naphthalene in which concentrated solutions were prepared in ethanol (EtOH) due to its low solubility in water.

### 6.2.2 Desorption Studies

A set of trials were conducted to determine if desorption plays a role during electrochemical regenerative treatments. A concentrated naphthalene solution was first prepared in ethanol to reach a concentration nearing 400 mg/L. As detailed in Chapter 3, ethanol was used as solvent during GAC loading processes due to the low solubility of naphthalene in water, 31 mg/L. 40 ml of the prepared solution was placed into a 40 ml headspace vial with 1.0 g of sieved, washed, and dried GAC, and then placed onto a rotary tube mixer. The GAC was mixed for 48 hours to reach a steady solid naphthalene concentration nearing 10,600 mg/kg; this was calculated by sampling the liquid phase concentration before and after adsorption, and using Equation (6.61), where  $q_{naph}$  is the solid phase concentration (mg/g),  $C_0$  and  $C_t$  are the liquid phase concentration before and after adsorption (mg/L),  $V$  is the volume of desorption solution (L), and  $M$  is the mass of GAC (kg). A naphthalene concentration of 10,600 mg/kg was considered a reasonable solids concentration, as the GAC within Antarctic PRBs has not been reported to exceed concentrations of 6,373 mg/kg. A control was used in all cases (40 ml stock solution with no GAC) to account for losses due to volatilization or adsorption onto the vial walls.

$$q_{naph} = \frac{(C_0 - C_t) \times V}{M} \quad (6.61)$$

The loaded GAC was separated from the adsorption solution via a stainless-steel mesh and rinsed with 40 ml of RO water to remove residual ethanol; the naphthalene concentration in the 40 ml rinsate was checked to ensure the calculated solid loading concentration was accurate. The GAC was allowed to dry at 100 °C overnight to remove residual moisture from within the GAC pores prior to conducting desorption studies; thermal gravimetric analysis showed naphthalene did not desorb from the GAC surface until temperatures of 250 °C were reached (illustrated in Appendix A.3). The dried GAC was then placed into a new 40 ml headspace vial

containing 40 ml of desorption solution varying in pH and salinity to determine how fluctuating conditions affect naphthalene desorption processes. Sulfuric acid ( $H_2SO_4$ ) and sodium hydroxide (NaOH) were utilized to make desorption solutions of pH 3, 6, and 11, whilst sodium chloride (NaCl) was used to alter the salinity between 0.05, 0.1 and 1.0 M NaCl. The GAC was mixed in the desorption solution for 48 hours on a rotary tube mixer, and naphthalene desorption was monitored with time by taking 150  $\mu$ l aliquots and analysing them via HPLC. The amount of naphthalene desorbed from the solid surface,  $q_{naph,des}$  (mg/kg), could be calculated via Equation (6.62), where  $C_{t,2}$  is the aqueous phase naphthalene concentration after the desorption period (mg/L).

$$q_{naph,des} = \frac{C_{t,2} \times V}{M} \quad (6.62)$$

A desorption control was utilized in all cases (fresh GAC in 40 ml desorption solution) to ensure that the raw GAC was free of naphthalene and did not affect desorption results. All desorption studies were done in triplicate.

### 6.2.3 Electrodesorption Studies

A set of trials were conducted to investigate the role that electrodesorption plays during electrochemical regenerative treatments. In all cases, 1.5 g of GAC was loaded with naphthalene in the same manner described in Section 6.2.2 to reach a final solid phase concentration nearing 10,600 mg/kg. The loaded and dried GAC was placed into a stainless-steel mesh basket, 35 mm in height with a 12 mm internal diameter as shown in Figure 6.1; a thin nylon mesh was placed between the GAC particles and the steel basket to prevent short-circuiting from occurring. The GAC was packed down with glass wool to ensure good electrical contact between the GAC particles, and a stainless steel wire (1 mm diameter) was inserted into the centre of the GAC bed to act as a current feeder. The basket and wires were placed into a 40 ml headspace vial via two airtight holes in the Teflon-lined cap, along with 38 ml of an electrochemically inert 0.05 M  $Na_2SO_4$  electrolyte. The stainless steel wires were attached to a QJ3005T benchtop DC power supply (QJE) to charge the GAC bed to the desired surface charge, negative or positive. A small magnetic stirrer was placed in the vial to ensure good mixing.

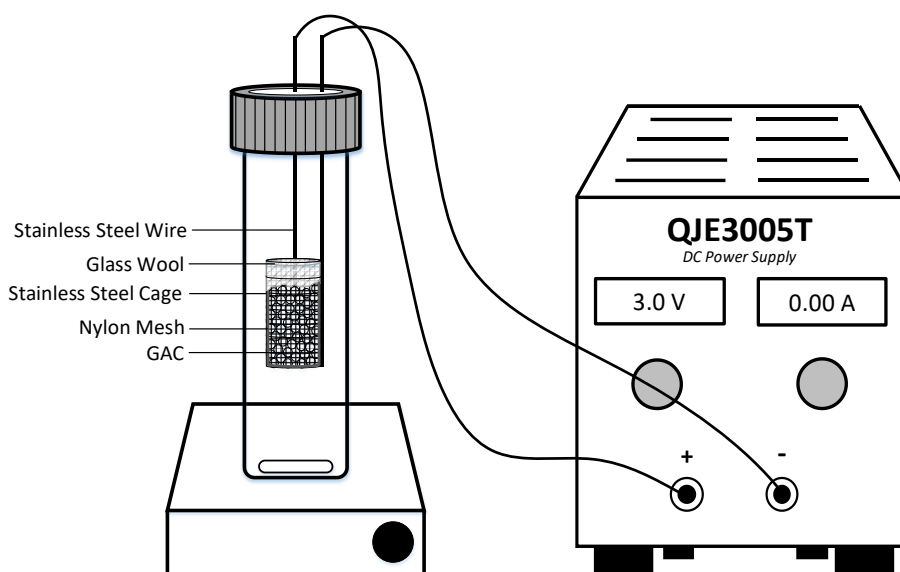


Figure 6.1: Schematic diagram of the experimental setup used for electrodesorption tests.

Positive and negative cell voltages of 0.5, 1.0, 1.5, and 2.0 V were applied to the GAC particles; cell voltages above 2.0 V were not investigated as to avoid unwanted Faradaic reactions from occurring. Each voltage was applied for 48 hours after which a 1.0 ml sample was taken and replaced with 1.0 ml of fresh electrolyte. The cell voltage was then increased, and the procedure repeated until all cell voltages were completed. The samples were tested for naphthalene concentration via HPLC analysis, and the amount of naphthalene desorbed was determined via Equation (6.62). All electro-desorption trials were done in duplicate.

#### 6.2.4 Electrochemical Regeneration Reactor

The electrochemical regeneration of GAC was conducted in a laboratory scale PRB having a GAC bed with dimensions of 20 x 20 x 20 mm. For each regenerative run, 4.0 g of dried, naphthalene loaded GAC (loaded in the same manner as Sections 6.2.2 and 6.2.3) was placed into the reactor fabricated from polyvinyl chloride, as depicted in Figure 6.2. A stainless steel cathode plate and graphite anode plate were vertically inserted into the box to surround the GAC bed, spaced 20 mm apart; each electrode had a surface area of 4 cm<sup>2</sup> in contact with the GAC bed. A thin nylon mesh separated the bed from one of the external electrodes to prevent short-circuiting and allow the bed to act as an extended surface area of the external electrode it was in direct contact with. The separator was placed between the GAC and cathode when applying a positive charge to the GAC bed to promote the active chlorine pathway, whilst it was placed between the GAC and anode when applying a negative, cathodic charge to the GAC to promote the electro-Fenton pathway.

A MP3087 DC Power Supply (PowerTech) was connected to the electrodes and operated under galvanostatic conditions at room temperature (23 °C). Due to the absence of a reference electrode, all reported voltages are representative of the cell potential. Two openings were located on the sides of the reactor to allow electrolyte to flow through the GAC bed parallel to the external electrodes, and a peristaltic pump recirculated the reactor solution (40 ml) at a rate of 11.3 ml/min through a 40 ml headspace vial; the vial was used to sample the aqueous phase (pH, naphthalene/by-products concentration), and/or aeration the solution with an Dymax AP700 air pump as required for electro-Fenton treatments.

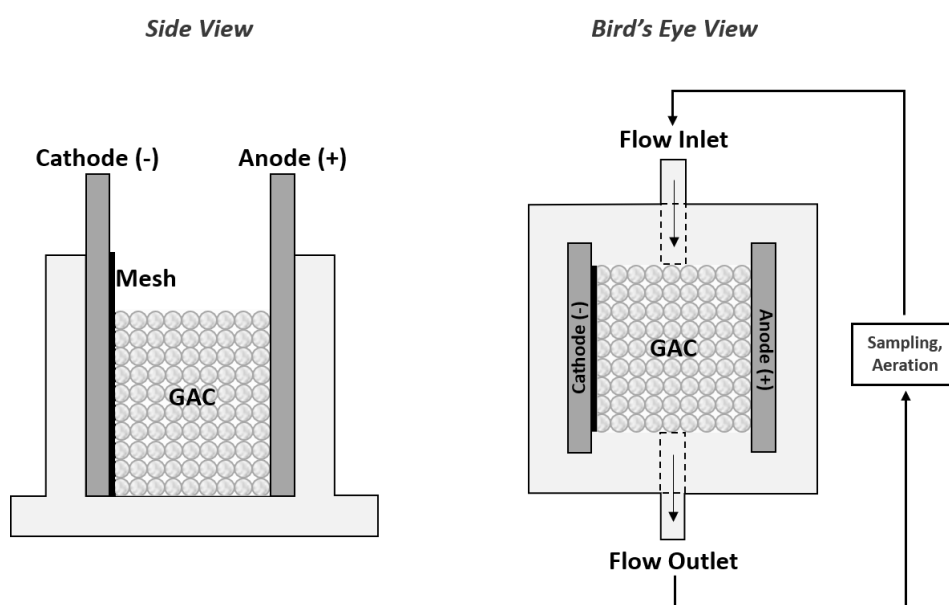


Figure 6.2: Schematic diagram of the laboratory scale PRB used for the electrochemical regeneration of GAC.



The recirculating electrolyte was adjusted based on the reaction being promoted; 0.1 M NaCl for active chlorine, and an aerated 0.05 M Na<sub>2</sub>SO<sub>4</sub> with 0.1 mM Fe<sub>3</sub>SO<sub>4</sub>•7H<sub>2</sub>O modified to a pH of 2.6 for electro-Fenton. The reactor was operated under galvanostatic conditions, after which the GAC was separated from the electrolyte via a stainless steel mesh, rinsed with 100 ml of water to remove residual salts, and dried in an oven at 105 °C overnight before determining the extent of regeneration achieved. Controls were conducted to account for any naphthalene losses and/or regeneration achieved when going through the described process, but without passing an electric current through the material. Varying electric currents (0 – 500 mA) and treatment timeframes (0 – 8 hours) were studied.

#### 6.2.4.1 Calculating Regeneration Efficiency

The aim of regenerating GAC is to restore the adsorptive capacity of the starting GAC material; this is best described through its isotherm, specifying the solid and liquid equilibrium concentrations that result between a specific adsorbent and adsorbate species [217]. Such an isotherm is shown in Figure 6.3 where a correlation between the equilibrium solid and liquid concentrations,  $Q_e$  (mg/g) and  $C_e$  (mg/L) respectively, can be seen.

The isotherm is generally used to calculate the extent of regeneration achieved (or adsorptive capacity restored) following electrochemical treatments. This is achieved through a ‘(1) batch adsorption, (2) regeneration, (3) batch re-adsorption’ method, schematically shown in Figure 6.3. With this method, the GAC is first loaded from an initial liquid concentration,  $C_0$ , to reach equilibrium concentrations of  $q_{e1}$  and  $c_{e1}$ , where the slope of the adsorption line is dependent on the solid-liquid ratio of the GAC-adsorption solution. Following initial loading, the GAC is regenerated whereby adsorbate species are removed from the GAC surface and free up active adsorptive sites and result in a solid concentration equal to  $q_{reg}$ . Because  $q_{reg}$  is not a measurable parameter, a second adsorption step is carried out under identical conditions (i.e. same  $C_0$  and solid-liquid ratio) to reach a new equilibrium concentration represented by  $q_{e2}$  and  $c_{e2}$ .

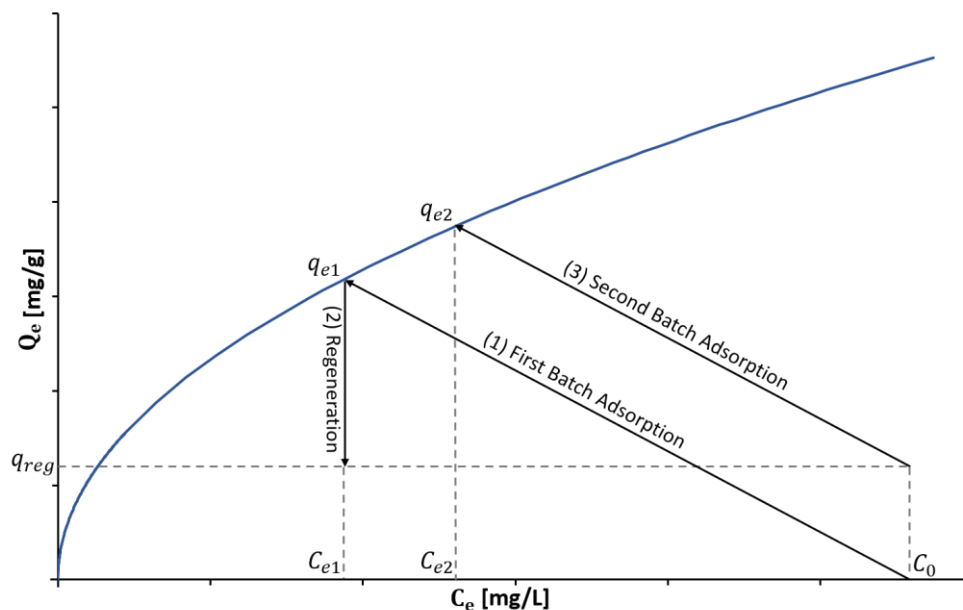


Figure 6.3: Schematic of the methodology for calculating the regeneration efficiency of electrochemically regenerated GAC.

Through this three-step process, and by measuring the liquid phase concentration at each of these steps, the regeneration efficiency or percent of adsorbate removed during treatment, can be calculated via Equation (6.63) as previously reported [218]. Here,  $V$  is the volume of solution during the adsorption steps (L),  $M$  is the mass of GAC undergoing regeneration (g), and  $K_f$  (g/L) and  $n$  (-) are the fitting constants of the Freundlich isotherm that relate the liquid concentration to the solid loading (discussed further in Section 6.3.3).

$$RE (\%) = \frac{q_{e1} - q_{reg}}{q_{e1}} \times 100 = \frac{V \left( 2C_0 - C_{e2} - C_{e1} - \frac{K_f C_{e2}^n M}{V} \right)}{q_{e1}} \times 100 \quad (6.63)$$

This methodology assumes that any loss in adsorptive capacity is due to residual adsorbate remaining on the adsorbent surface, rather than changes in adsorptive capacity that result due to alterations of the surface chemistry during treatment (i.e. a change in the shape of the isotherm). Despite these concerns, this method is believed to be the most accurate when describing partial regenerations [218]. Controls were conducted to assess the validity of this assumption by regenerating fresh GAC and assessing how its adsorptive capacity towards naphthalene was affected, and is discussed further in Section 6.3.5.1.1.

The isotherm describing the adsorptive equilibria between GC1200 GAC and naphthalene was created by preparing several naphthalene solutions in the concentration range of 25 – 2,000 mg/L. As described in the previous sections, ethanol was used as a solvent to overcome the limited solubility of naphthalene in aqueous solution; ethanol also increases the kinetics at which naphthalene adsorbs onto GAC, allowing RE calculations to be completed in a matter of days, rather than months which would be unrealistic for this study. 40 ml of each naphthalene solution was placed into a 40 ml headspace vial containing 1.0 g of GAC. The vials were mixed on a rotary tube mixer for 48 hours at a room temperature of 23 °C (sufficient time to reach steady-state equilibrium as discussed later in the Chapter), after which the aqueous phase was sampled and centrifuged at 3,000 rpm for 10 minutes to remove any fine dust that resulted during the mixing period. The supernatant was analysed via HPLC to determine the residual naphthalene in solution and to calculate the equilibrium solid loading that was achieved via Equation (6.61) where  $q_{naph}$  is equal to the equilibrium concentration,  $q_e$ . All samples were conducted in triplicate and the resulting datasets were modelled via Freundlich, Langmuir and linear isotherms. A control was used containing 40 ml naphthalene solution with no GAC to correct for volatilization and adsorption processes onto the glass vials.

Following electrochemical treatments, the regenerated GAC was reloaded under these same conditions for 48 hours and the resultant liquid equilibrium concentration,  $C_{e2}$ , was determined and used to calculate the regeneration efficiency, Equation (6.63).

### 6.2.5 GAC Electrical Conductivity

The electrical conductivity and resistivity of the GAC bed was measured at room temperature via a two-point technique as described elsewhere [219,220]. For each sample point, 4.0 g of sieved, washed, and dried GAC was placed into the electrochemical reactor and an Economy True RMS Autorange digital multimeter was used to measure the resistance across the bed of material in air. Varying pressures in the range of 0 – 55 kPa were applied to the bed by resting weights on top of the GAC; no crushing of the carbon particles or attrition could be detected within this range of applied pressures, suggesting that any detected changes in bed conductivity

are due to rearrangement of the particles themselves. Similarly, varying bed compaction levels were assessed via applying pressure with a G-clamp to reduce the bed height in increments of 0.025 cm, and the resulting bed resistance was measured; compaction levels between 0.55 g GAC/cm<sup>3</sup> (representative of uncompacted GAC) and 0.61 g GAC/cm<sup>3</sup> were measured, equivalent to a reduction in bed height of 0.175 cm.

For either method used, the conductivity of the bed,  $\sigma$  ( $\Omega^{-1} \text{ cm}^{-1}$ ), is calculated via Equation (6.64), where  $L$  is the distance between the electrodes (cm),  $R$  is the measured resistance across the bed ( $\Omega$ ), and  $A$  is the cross-sectional area of the bed (cm<sup>2</sup>) that changes as a function of bed height.

$$\sigma = \frac{L}{RA} \quad (6.64)$$

For each applied pressure or bed density considered, the bed was repacked and remeasured three times to account for unavoidable variations in bed packing and particle orientation.

### 6.2.6 Analytical Methods

Aqueous naphthalene and hydrogen peroxide (H<sub>2</sub>O<sub>2</sub>) concentrations were monitored using High Performance Liquid Chromatography (HPLC) and UV-Vis spectrophotometry respectively as described in Chapter 3. The pH of the solutions was adjusted and measured using an InLab Versatile pH probe (Mettler Toledo) calibrated with pH 4, 7, and 10 buffer solutions prior to use.

## 6.3 Results and Discussion

### 6.3.1 Desorption

Much of the literature claims that enhanced desorption is a key process during the electrochemical regeneration of GAC. Such enhancement is due to 1) local changes in pH that alter the adsorptive equilibria between the adsorbent and adsorbate or 2) the presence of ionized species that alter the adsorptive equilibria and/or react with the adsorbate to transform it into a more readily desorbed compound [143]. Despite this claim, there are limited kinetic studies showing that the rate of enhanced desorption has a leading effect during the short electrochemical treatment times of a few hours. To address this, naphthalene loaded GAC was placed into aqueous desorption solutions varying in pH (3, 6, and 11) and salinity (0.05, 0.1, and 1.0 M NaCl). The solutions were allowed to mix for 48 hours and the solution was analysed with time to determine the magnitude and rate at which enhanced desorption occurs.

Throughout the 48 hour period, no detectible quantities of naphthalene were desorbed at any of pH or salinity levels studied. This is indicative of high-affinity, favourable adsorption behaviours whereby the affinity of the adsorbate for the adsorbent enables large amounts of adsorption to occur at low equilibrium liquid concentrations [221–223]; this concurrently hinders unfavourable desorption from occurring. Such adsorption is commonly observed between GAC substrates and aromatic compounds in aqueous systems, including a variety of phenolic compounds and dyes [224] and naphthalene [222]. Ania et al. [222], for example, illustrated the high affinity of naphthalene towards GAC and reported that a solid naphthalene concentration of 10,095 mg/kg resulted in an equilibrium liquid concentration nearing  $7.0 \times 10^{-6}$  mg/L; comparable results have been observed between naphthalene and GC1200 GAC specifically [225]. Relating these results to this work, where an initial solid concentration of 10,600 mg/kg is implemented, negligible amounts of desorption would be expected.

Small levels of irreversible adsorption are also commonly observed with aromatic compounds [226] or when using thermally activated GAC such as the GC1200 GAC in this study [32]. Causes of irreversible adsorption include  $\pi$ - $\pi$  dispersion interactions between aromatics and the basal plane of the carbon surface, chemisorption of the adsorbate with surface oxygen groups, or polymerization between adjacently bound adsorbate species [226]. Regarding the adsorption of inert naphthalene, it is most probable that strong  $\pi$ - $\pi$  interactions between the pi-orbitals of the adsorbate and adsorbent limit desorption processes. Such attractive forces have been reported to have interaction energies of up to 43 kJ/mol [227], greater than non-covalent hydrogen bonds that have binding energies between 25 – 40 kJ/mol [228].

Previous studies that have observed enhanced desorption processes due to pH or salinity claim it is due to the increased electrostatic repulsions between the adsorbate and adsorbent. Berenguer et al. [49], for example, detected that 30, 45, and 60 % of the phenol adsorbate desorbed within 3 hours when placed in solutions of pH 0.2, 7.5, and 13.5 respectively. As both the phenol and surface functional groups on the GAC surface deprotonate in alkaline media ( $pK_a = 9.89$  and  $pH_{pzc} = 9$ ), the enhanced desorption was due to the increased electrostatic repulsions between the adsorbate and adsorbent [49]; likewise, deprotonated phenol has a higher solubility in aqueous solutions making it a more readily desorbed compound [49].

As naphthalene is a non-dissociative compound that is inert in nature, changes in pH and salinity are not expected to have such effects. It is therefore concluded that enhanced desorption will not play a significant role during the electrochemical regeneration of the naphthalene loaded GAC. This also answers in part, one of the prevailing gaps in the literature: how non-dissociative compounds on GAC surfaces respond to electrochemical treatments.

### 6.3.2 Electrodesorption

Electrodesorption relies on applying an electric potential, or giving charge, to the surface of the adsorbent which will 1) electrostatically repel adsorbed compounds with a similar charge, or 2) result in competitive adsorption between the adsorbate and other compounds in the aqueous solution to promote desorption. As naphthalene does not readily dissociate in solution, it will not take on a charge that would be electrostatically repelled from a charged GAC surface. However, it is possible that naphthalene could be displaced via the increased interactions between the GAC and other compounds in solution; it is reported that uncharged molecules are most strongly adsorbed at surface potentials nearing zero, and become increasingly desorbed at higher negative and positive potentials due to increased columbic interactions between the charged GAC surface and solvent dipoles, such as polar water or ionized species [22].

To investigate if such electrodesorption would have an effect on naphthalene, both negative and positive charges of 0.5, 1.0, 1.5, and 2.0 V were applied to the loaded GAC for 48 hours each. Similar to the results observed in the Section 6.2.2, however, electrodesorption trials resulted in no detectible amount of naphthalene being displaced from the GAC surface. This is likely due to the strong interactive forces between the naphthalene and GAC structures, and suggests that naphthalene displacement due to electrostatic repulsions is highly unlikely to occur during electrochemical regenerative treatments.

### 6.3.3 Adsorption Isotherm

A kinetic study was conducted to determine the time required to reach steady-state equilibrium concentrations when adsorbing naphthalene onto GC1200 GAC. In triplicate, 1.0 g of GAC was mixed on a rotary tube mixer with 40 ml of a 280 mg/L naphthalene/ethanol solution and the

naphthalene concentration was monitored with time. As shown in Figure 6.4, nearly 92 % of the equilibrium adsorptive capacity was reached within the first 7 hours of mixing, after which, adsorption rates slowed until the 48 hour mark was reached and a solid loading of 10,760 mg/kg was achieved; no further increases in solid loading were observed in the 40 hours following. Based on these results, it was concluded that 48 hours is a sufficient timeframe to reach equilibrium and obtain isotherm data for both fresh and regenerated GAC.

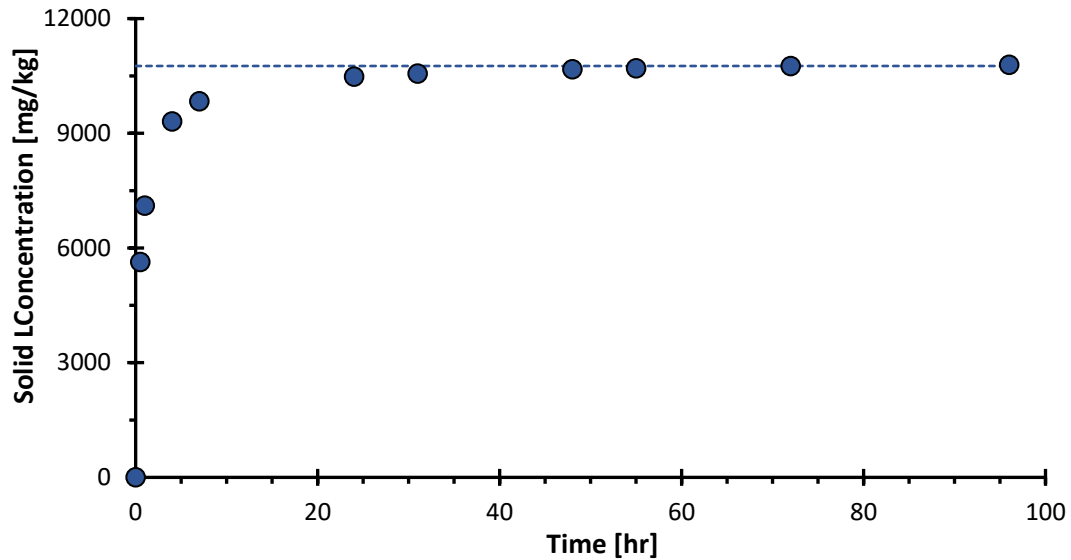


Figure 6.4: Kinetics of naphthalene adsorption onto GC1200 GAC. The dashed line presents the steady-state solid concentration achieved, 10,760 mg/kg.

The isotherm describing naphthalene adsorption onto GC1200 GAC following a 48 hour adsorption period is shown in Figure 6.5. Several isotherms were fitted to the equilibrium data to determine which best describes the naphthalene-GC1200 system. The Freundlich isotherm, Equation (6.64) where  $K_f$  (mg/L) and  $n$  (-) are fitting constants, is an empirical model applied to GAC substrates that present with heterogeneous surfaces and multilayer adsorption [217,222]. Surface heterogeneity suggests that active sorption sites vary in bonding energies, where the strongest binding sites are occupied first followed by sites with exponentially decreasing adsorption energies [217,229]. At heightened concentrations, the Freundlich isotherm also states that adsorbed molecules may attract further contaminants towards them, resulting in multilayer adsorption with no theoretical maximum concentration to be reached [230].

$$Q_e = K_f C_e^n \quad (6.65)$$

In contrast, the Langmuir isotherm, Equation (6.66) where  $q_{max}$  is the maximum adsorptive capacity of the GAC substrate (mg/kg) and  $K_l$  is a fitting parameter (L/mg), assumes monolayer coverage where there is a fixed number of active adsorptive sites that are all equal and identical; it further assumes that there is no interaction between adsorbed molecules [217,222]. Both the Langmuir and Freundlich isotherms are widely used to describe the adsorption of organic compounds onto GAC substrates.

$$Q_e = \frac{q_{max} K_l C_e}{1 + K_l C_e} \quad (6.66)$$

When low concentrations are used, the linear isotherm, Equation (6.67) where  $K_d$  is the distribution coefficient (L/kg), has also been used to describe the sorption of hydrocarbons out of aqueous solution onto GAC substrates [231]. This isotherm suggests that adsorption processes are not dependent on the initial concentration of the aqueous solution [231].

$$Q_e = K_d C_e \quad (6.67)$$

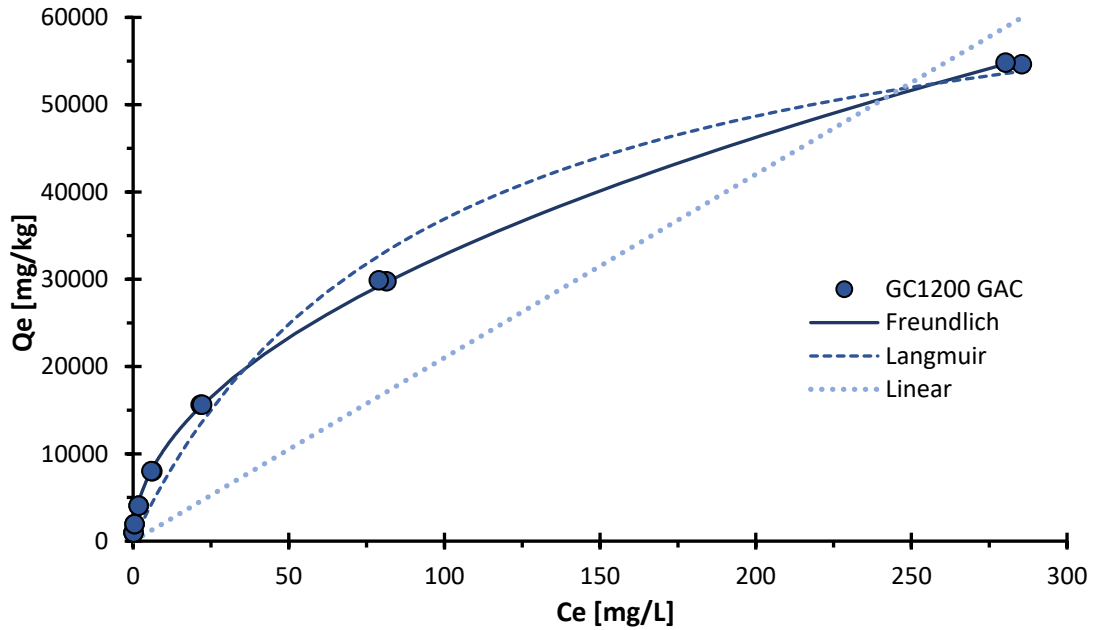


Figure 6.5: Freundlich, Langmuir and Linear adsorption isotherms describing naphthalene adsorption onto GC1200 GAC.

As shown by Figure 6.5, the Freundlich isotherm was found to have the best fit across the concentration range investigated, resulting in a  $R^2$  of 0.999. The determined Freundlich constants,  $K_f$  and  $n$ , were determined and detailed in Table 6.1; due to the accuracy at which they described the naphthalene-GC1200 system, they were used to calculate the regeneration efficiency achieved following electrochemical treatments, denoted by Equation (6.63).

Table 6.1: Freundlich, Langmuir, and Linear isotherm parameters and fit for naphthalene adsorption onto GC1200 GAC.

Isotherm	Parameters	$R^2$	RMSE
Freundlich	$K_f$ [mg/L] 3.367 $n$ [-] 0.495	0.999	0.36
Langmuir	$q_{max}$ [mg/kg] 71.470 $K_L$ [L/mg] 0.011	0.983	2.58
Linear	$K_d$ [L/kg]] 0.210	0.838	7.61

### 6.3.4 GAC Conductivity

The electrochemical reactor was designed such that the GAC bed was in direct contact with only one of the external electrodes; this allowed the electrically conductive bed to behave as an

extended electrode surface of the one it was in contact with [232]. For example, when a GAC bed is in contact with the external anode it will act as a 3D anode, whilst it will act as a 3D cathode when in contact with the external cathode [233]. Bed materials that have increased electrical conductivity are advantageous during electrochemical treatments as they increase the distance from the external electrode over which Faradaic reactions are promoted; this increases regeneration efficiencies by reducing variations in outcomes throughout the bed [101]. To ensure good electrical conductivity, performance, and a uniform passing of electric current through a GAC bed, sufficient particle-to-particle contact must be maintained; this is commonly achieved through the application of pressure to the bed material [219,234,235].

Using the fabricated electrochemical reactor, the electrical properties of the GC1200 GAC bed were monitored as a function of externally applied pressure. As illustrated in Figure 6.6, the GAC bed reported an average resistance nearing 40,000  $\Omega$  when no external pressure was applied; this is equivalent to a conductivity of  $1.1 \times 10^{-5} \Omega^{-1} \text{cm}^{-1}$ , within the range classified as a semiconductor material. Despite the bed having some electrical conductivity in this instance, it could be greatly enhanced via the application of pressure to the material. For example, incremental pressures of 1.2 and 3.7 kPa decreased the bed resistance to 900 and 140  $\Omega$  respectively, increasing the electrical conductivity 33- and 382-fold to  $3.6 \times 10^{-4}$  and  $4.2 \times 10^{-3} \Omega^{-1} \text{cm}^{-1}$ . Such improved conductivity was due to the increased number of electrical contacts that occur between the individual carbon pieces that make up the bed; this subsequently aids in the conduction of electrons from one particle to another [234,236]. In contrast, uncompacted GAC has such low mass that particle-particle contact is minimal and leaves large gaps of non-conductive air that increase the electrical resistivity of the bed [236].

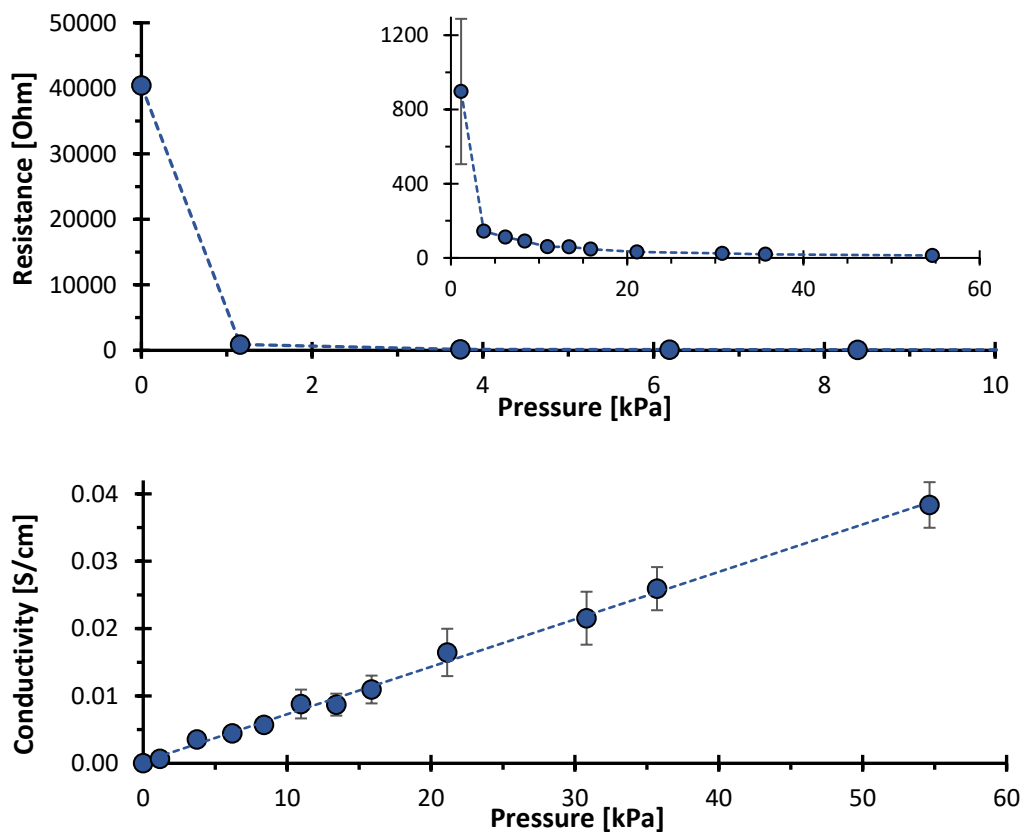


Figure 6.6: (Top) Bed resistance at varying external pressures; the subplot is a zoomed in view of resistances from 1 kPa and above. (Bottom) The corresponding bed conductivity as a function of externally applied pressure.

Figure 6.6 shows that the electrical conductivity of the bed linearly increased with increasing externally applied pressure, but at a much slower rate compared to the initial application of weight; similar observations have been observed by other investigators [235,236]. When an applied pressure of 55 kPa was reached, the bed conductivity was measured to be  $3.8 \times 10^{-2} \Omega^{-1} \text{cm}^{-1}$ , three orders of magnitude larger than the uncompacted GAC and within the expected conductivity range of GAC beds [101]. No particle attrition or crushing was detected within the range of pressures investigated, suggesting that the increased conductivity was due to enhanced contact between particles, and/or their spatial rearrangement within the bed.

Such increases in bed conductivity are advantageous during electrochemical treatments as they promote uniform regenerative outcomes throughout the bed [101]. This is partly attributed to the increased surface area-to-volume ratio of the electrode surface that enhances mass transfer within the system to allow greater amounts of oxidizing species to be electrogenerated [68,78,237]. For example, Zárate-Guzmán et al. [234] examined the electrochemical performance of a 3D GAC electrode by measuring the concentration of electrogenerated  $\text{H}_2\text{O}_2$  at varying levels of bed compaction; compacting the bed from  $0.39$  to  $0.46 \text{ g/cm}^3$  was shown to linearly increase the  $\text{H}_2\text{O}_2$  concentration from  $2.8$  to  $78 \text{ mg/L}$ , corresponding to a  $94.5\%$  increase [234]. This is comparable to the results described in Chapter 5 where greater quantities of  $\text{H}_2\text{O}_2$  were produced when using the 3D GAC-PVDF electrode compared to simple graphite rods.

As bed density is more easily measured when dealing with large quantities of GAC, such as in field deployment scenarios, varying compaction levels were also assessed in this work; the results are presented in Figure 6.7 where compaction levels between  $0.55$  and  $0.61 \text{ g GAC/cm}^3$  were considered.

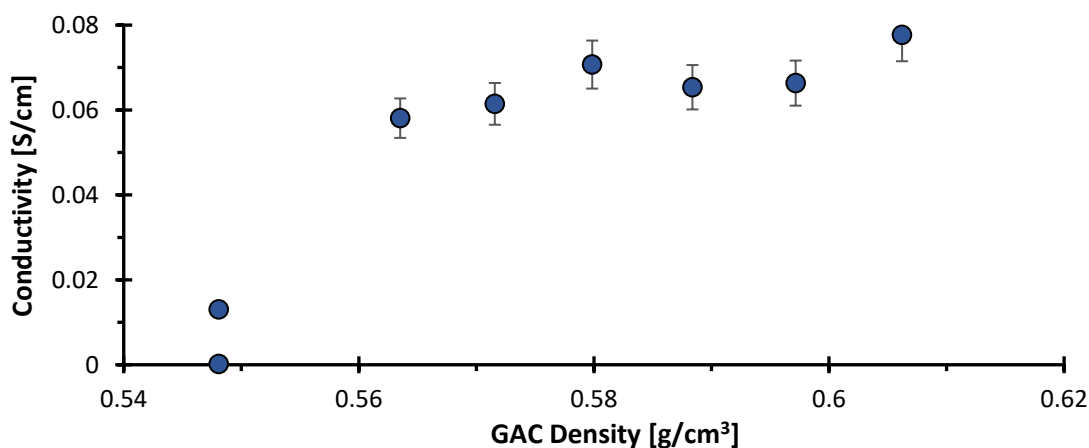


Figure 6.7: Conductivity of GAC as a function of bed density.

As predicted, compression of the material increased the electrical conductivity of the bed. Uncompacted GAC, having a density near  $0.55 \text{ g/cm}^3$ , presented with minimal conductivity as previously discussed; the initial increase in conductivity observed at  $0.55 \text{ g/cm}^3$  in Figure 6.7 is due to the added weight of the G-clamp used for compression measurements, but undetectable changes in bed height resulted. Beyond this, incremental compression of the bed was observed to increase the bed conductivity up to  $6.6 \times 10^{-2} \Omega^{-1} \text{cm}^{-1}$  when a density of  $0.58 \text{ g/cm}^3$  was reached; further increases in bed density, in the range of  $0.58 - 0.61 \text{ g/cm}^3$ , had no detectable effects. Beyond  $0.61 \text{ g/cm}^3$  (data not shown) electrical conductivities were quadrupled, reaching a conductivity near  $2.6 \times 10^{-1} \Omega^{-1} \text{cm}^{-1}$ . Although the increased conductivity would be



advantageous, particle attrition and crushing were detected within this range, indicating that the increased conductivity was due to increased contact points as a result of pore crushing within the GAC particles [235]. As this would negatively affect future adsorption processes within the GAC pores, this was not deemed to be an acceptable outcome. Thus, all regenerative trials conducted in this work were performed at a bed density of  $0.58 \text{ g/cm}^3$  to improve the electrochemical performance of the bed material without compromising its structural integrity. Furthermore, operating under such conditions gives the GAC bed a higher electrical conductivity in comparison to the implemented electrolytes, minimizing the potential drop across the bed of material. A bed conductivity of  $6.6 \times 10^{-2} \Omega^{-1}\text{cm}^{-1}$ , for example, is 7-times more conductive than a 0.1 M NaCl electrolyte used for promotion of the active chlorine pathway (e.g.  $9.2 \times 10^{-3} \Omega^{-1}\text{cm}^{-1}$  as shown in Appendix A.3); this reduces the amount of by-pass current passing through the electrolyte and allows a greater effective current to pass through the 3D electrode itself [12,238,239].

### 6.3.5 Electrochemical Regeneration

#### 6.3.5.1 Regenerative Treatments

As desorption processes were seen to have negligible effects on GAC regeneration, electrochemical reactions will be the leading mechanism for which the adsorptive capacity of the GAC is restored. To investigate their effect, the GAC was placed into the electrochemical reactor to act as a three-dimensional anode or cathode for promotion of the active chlorine and electro-Fenton pathways respectively. Sixty four trials of regeneration were carried out to determine the extent of regeneration that could be achieved under varying applied electric currents (0 – 500 mA) and treatment timeframes (0 – 8 hours) for each reaction.

##### 6.3.5.1.1 Effect of Applied Current

The effect of electric current was first assessed by promoting each reaction for two hours each at varying electric currents in the range of 0 and 500 mA. The results are shown in Figure 6.8, where both the active chlorine (AC) and electro-Fenton (EF) pathways promoted regeneration and ultimate restoration of adsorptive sites on the GAC surface. As desorption is understood to have negligible effects during treatment timeframes, this is a result of electrogenerated oxidizing species, active chlorine or hydroxyl radicals, attacking and degrading adsorbed naphthalene species. The direct oxidation of naphthalene species on the GAC surface was not assumed to be a major mechanism for adsorptive site recovery; this is due 1) Chapter 4 showing that active chlorine species are preferentially generated on carbonaceous electrodes over direct oxidation reactions, and 2) the literature supporting the notion that direct oxidation on GAC surfaces is not a major mechanism during the electrochemical degradation of organics as it has extremely slow kinetics and has poor yields (refer to Chapter 2).

As expected, increases in electric current resulted in greater regeneration efficiencies achieved for both reaction pathways. For example, the AC pathway reached regenerations of 16.9 %, 25.0 %, and 32.2 % when applying currents of 6 mA, 12 mA, and 25 mA, whilst the EF pathway reported regenerations of 18.3 %, 20.6 % and 24.7 % when operating at currents of 2 mA, 3 mA, and 6 mA. As discussed in Chapters 4 and 5 and stated by Faraday's Law,  $r = i/nF$ , this is due to the increased rate at which oxidizing species are electrogenerated when larger electric currents are introduced into the system; with more oxidizers present, the naphthalene will, in turn, be degraded at an increased rate.

It is also stated in the literature that larger electric currents and cell potentials increase regenerative outcomes due to the increased rates at which contaminants desorb from the GAC surface [22,49,91,145]. Although Sections 6.3.1 and 6.3.2 demonstrated that naphthalene is not susceptible to electrodesorption processes, it is possible that the electrochemically transformed by-products are susceptible to electrodesorption. This was assessed by regularly sampling the solution reservoir during regenerative runs; no naphthalene or by-product species were detected under any of the experimental conditions, indicating that oxidation reactions of naphthalene and its by-products sequentially occur on the GAC surface until adsorptive sites are restored.

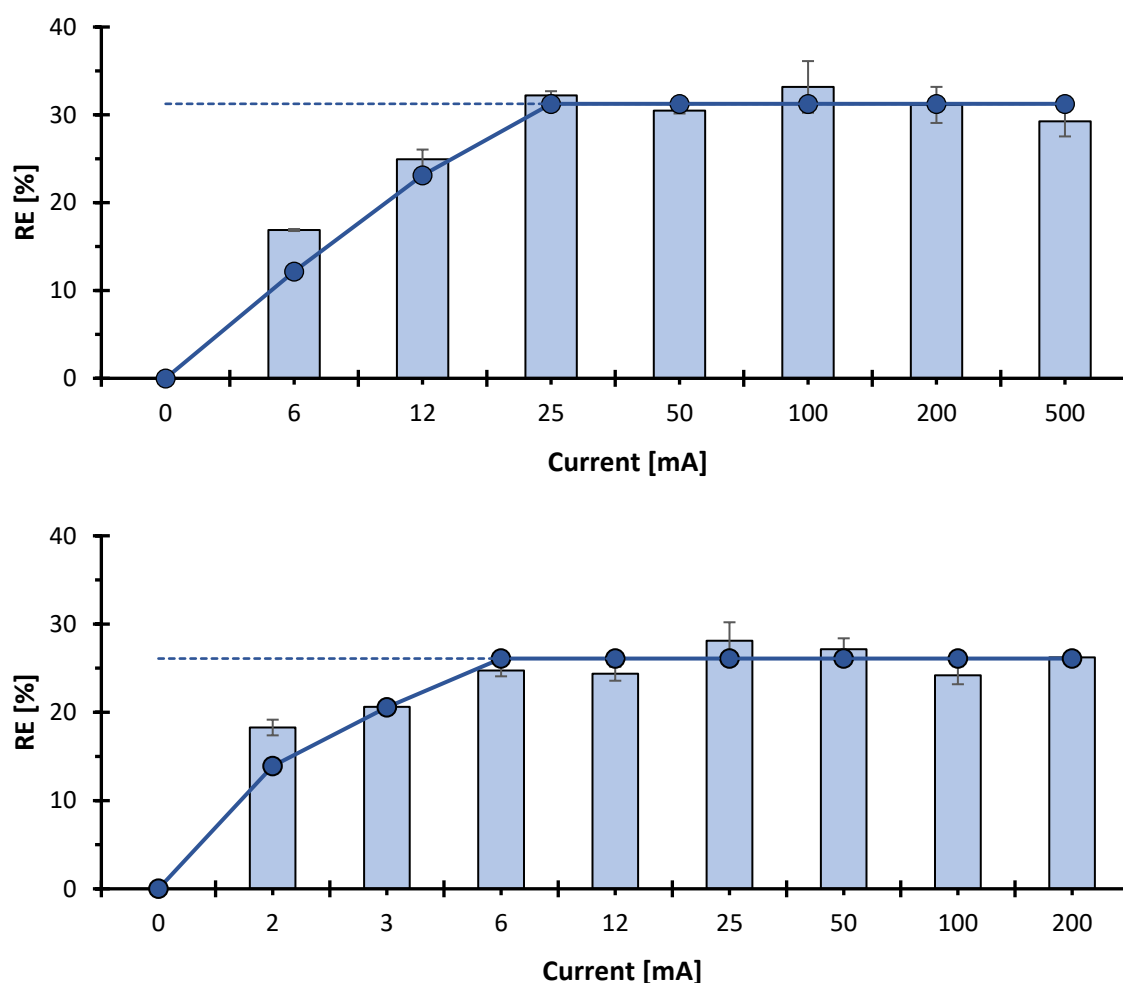


Figure 6.8: Regeneration efficiencies as a function of applied electric current for the (top) active chlorine and (bottom) electro-Fenton pathways when undergoing two hours of electrochemical treatment. Bars are experimental data, solid lines the kinetic model, and the dashed line is the average maximum regeneration achieved.

Unfortunately, currents greater than 25 mA and 6 mA for the AC and EF pathways respectively reported no further increases in regeneration. Despite increasing the current to 500 mA for the AC pathway and 200 mA for the EF pathway, regeneration efficiencies reached a maximum value nearing  $31.3 \pm 1.4\%$  and  $26.1 \pm 1.6\%$  for each reaction respectively, as illustrated in Figure 6.8. This suggests one of two things: 1) a limiting current has been reached, whereby the increased electric potentials associated with currents above 25 mA and 6 mA for the AC and EF pathways go towards side reactions such as the breakdown of water, instead of oxidant production [74],

or 2) a mass-transfer kinetic limitation has been reached whereby longer treatment times are required to allow electrogenerated oxidants to undergo intraparticle diffusion into the GAC pores [101]. Each of these possibilities can be overcome via operating the treatment for longer timeframes, addressed in Section 6.3.5.1.2.

Similar observations have been reported in the literature where increases in electric current have negligible, if not adverse, effects on regenerative outcomes [28,33,49,91,240]. Limited desorption from the GAC surface [28,47,145], by-products blocking pores and hindering access to oxidizing agents [49,240], and oxidation of the GAC surface and destroying active adsorptive sites [24,34,91,241] have all been hypothesized as causes of partial regeneration. Regarding surface oxidation, this current study has detected particle attrition of the GAC when operating the AC pathway at currents of 100 mA and higher, suggesting that oxidation of the GAC surface occurs at increased potentials; no visible attrition occurred at currents of 50 mA or lower. Similarly, no particle abrasion could be detected under any of the EF trials, theorized to be due to the GAC surface being cathodically protected from oxidation reactions, as free radicals preferentially attack adsorbed organic compounds rather than the GAC surface when it presents with a negative surface charge [24,38].

To investigate if active adsorptive sites were being destroyed during the applied treatments, two controls were conducted whereby clean, virgin GAC underwent regenerative treatments via the AC and EF pathways. A current of 50 mA was applied under each pathway for two hours, upon which the adsorptive capacity of the GAC was measured. Results showed that both the AC and EF treated GAC reached the adsorptive capacity predicted by the Freundlich isotherm in Section 6.3.3, suggesting that minimal changes to the GAC surface occur during the two hours of treatment. Passing greater quantities of charge, however, may cause surface alterations as particle attrition was observed when promoting the AC pathway at higher currents. This was assessed by performing another set of controls, but for an extended 6 hours of treatment; the resulting adsorptive capacities averaged 94.8 % of the initial material suggesting that small decreases in adsorptive capacity result with prolonged treatment timeframes.

#### 6.3.5.1.2 Effect of Treatment Time

As a limiting current or mass-transfer limitation can be overcome with prolonged treatment, the optimal currents for the AC and EF pathways, 25 mA and 6 mA respectively, were promoted for extended timeframes of up to 8 hours. The regenerative outcomes as a function of treatment time are shown in Figure 6.9.

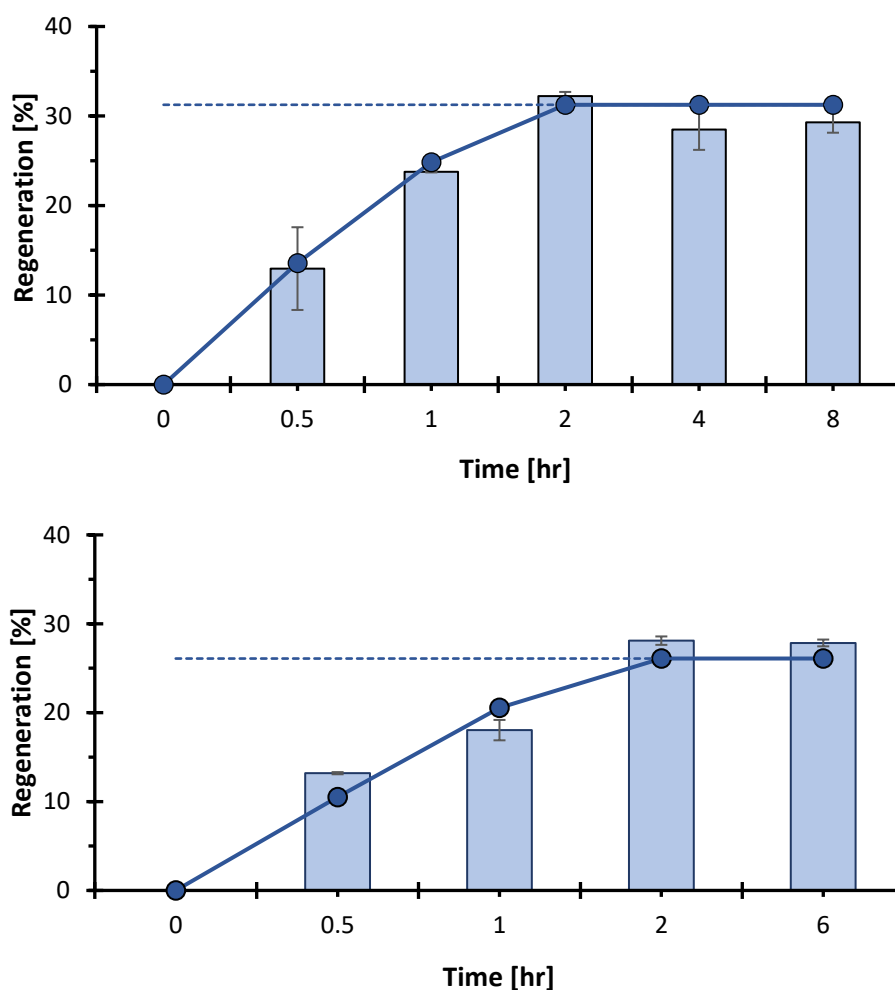


Figure 6.9: Regeneration efficiencies as a function of time for the (top) active chlorine and (bottom) electro-Fenton pathways. Bars are experimental data, solid lines the kinetic model, and the dashed line is the average maximum regeneration achieved.

As predicted, increasing treatment times from 0 to 2 hours resulted in increases in regeneration for both reaction pathways. For example, 0.5, 1, and 2 hours of treatment reported regenerations of 13.0 %, 23.8 %, and 32.3 % for the AC pathway, whilst regenerations of 13.2 %, 18.0 %, and 28.1 % resulted for the EF pathway. However, beyond two hours of treatment and regardless of the reaction pathway, no further regeneration was achieved. Despite introducing an additional charge of 540 C and 130 C for the AC and EF pathways respectively, regenerative outcomes tended towards their average maximum regeneration of  $31.3 \pm 1.4$  % and  $26.1 \pm 1.6$  % respectively. This indicates that 1) electrogenerated oxidizing agents reach a point where they can no longer assist in the regenerative process, and 2) that neither a limiting current nor mass-transfer limitation are the basis of the limited regeneration achieved in the previous section.

Partial regeneration efficiencies are commonly reported in the literature, where timeframes as short as 0.5 - 1 hour have reached maximum regenerative outcomes [44,240]; even if slight increases in regeneration can be achieved beyond this, a point is generally reached where adjustments in current and/or timeframe have negligible effects on treatment outcomes [143]. Narbaitz and Jashini [110], for example, reported minimal increases in regeneration when increasing the treatment timeframe from 5 to 25 hours; not being able to further improve regenerative outcomes was attributed to irreversible adsorption of the adsorbate species. As

discussed in Section 6.3.5.1.1, other investigators have hypothesized that incomplete regeneration is a result of oxidation of the GAC surface or blocked pores prohibiting oxidizing species from diffusing towards adsorbate compounds and aiding in their removal.

Xiao and Hill [242] assessed the argument for blocked pores in greater detail by examining how varying pore sizes within GAC substrates affect its ability to be chemically regenerated (i.e. externally adding oxidizing reagents rather than electrogenerating them *in situ*). GACs with varying degrees of microporosity were chemically regenerated under identical conditions for 8 hours. Following treatment, it was found that the achieved regenerations linearly decreased with increasing microporosity, whereby regenerations of 100 %, 40 % and 5 % were attained for GACs with microporosities of 5 %, 57 %, and 83 % respectively [242]; BET analysis showed that a majority of micropores with widths between 0.5 – 2 nm remained blocked after regenerative treatments. This was hypothesized to be due to adsorbates blocking access to oxidizing agents in narrow micropores, schematically shown in Figure 6.10, whilst larger mesopores provided greater area for oxidants to enter and attack adsorbate species.

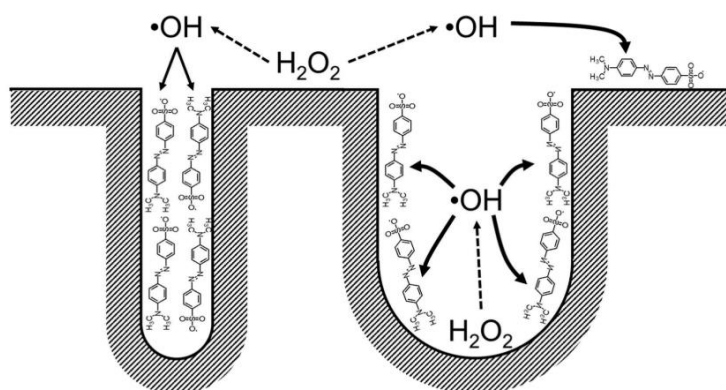


Figure 6.10: Schematic of hydroxyl radicals oxidizing adsorbed contaminants in a (left) micropore vs (right) mesopore [242].

Relating the results of Xiao and Hill [242] to the 100 % microporous GC1200 GAC used in this work, low regeneration outcomes would then be expected. It also suggests that the partial regenerations achieved in this study is due to the oxidation and removal of naphthalene species solely adsorbed on the GAC's external surface, leaving the interior micropores untouched.

To explore this theory further, the three-stage kinetic model proposed by Choi et al. [243] was used to determine the amount of naphthalene adsorbed on the GACs exterior prior to undergoing regenerative treatments. This model distinguishes between two types of adsorption sites on GAC substrates: Type 1, comprised of instantaneous, external surface adsorption, and Type 2, comprised of a more gradual, rate-limited adsorption due to the processes of intraparticle diffusion that occur within the GAC pores. An added benefit of this model is that it enables the two types of adsorption to be differentiated via a simple batch adsorption test.

The analytical solution of the proposed kinetic model [243] is described by Equation (6.68), where the normalized adsorbate concentration ( $C/C_0$ ) is characterized by four fitting parameters,  $\xi_1$ ,  $\xi_2$ ,  $\beta$ , and  $\gamma$ , each corresponding to a solid phase concentration associated with either Type 1 or Type 2 adsorption detailed by Equation (6.69). Here,  $M$  is the mass of GAC (kg),  $V$  is the volume of adsorptive solution (L),  $C_0$  is the initial aqueous phase concentration (mg/L),  $q_1(\infty)$  is the solid phase concentration associated with Type 1, external adsorption

(mg/kg), and  $q_2(\infty)$  is the solid phase concentration associated with Type 2, interior pore adsorption.

$$\frac{C(t)}{C_0} = \frac{(1 - \xi_1)(1 - \xi_1 - \beta\xi_2)}{(1 - \xi_1 - \beta\xi_2 e^{-\gamma t})} \quad (6.68)$$

$$\xi_1 = \frac{Mq_1(\infty)}{VC_0}, \quad \xi_2 = \frac{Mq_2(\infty)}{VC_0}, \quad \gamma = \frac{(1 - \xi_1 - \beta\xi_2)\alpha}{\beta\xi_2} \quad (6.69)$$

The normalized, batch adsorption data of naphthalene adsorbing onto GC1200 GAC was fitted to the kinetic model, Equation (6.68), to determine the amount of external adsorption occurring. As shown by Figure 6.11, naphthalene removal occurred in two distinct phases: an initial and instantaneous adsorption, associated with Type 1-external adsorption, followed by a more gradual removal, associated with a Type 2-interior adsorption. Even with the two phases present, the kinetic model fitted the data well and accurately captured each adsorptive region; an  $R^2$  of 0.998 resulted and the determined parameters of the kinetic model are detailed in Table 6.3.

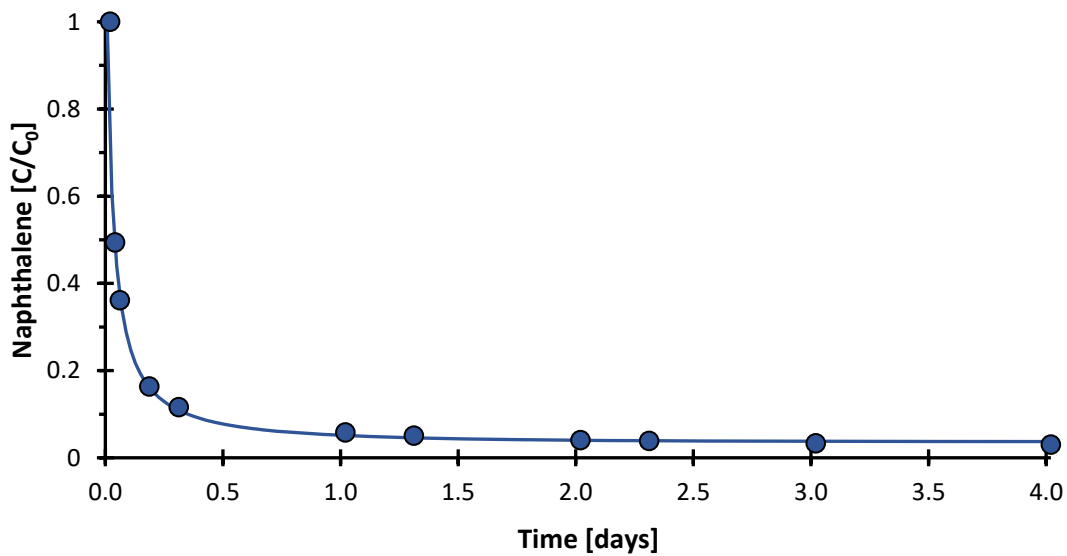


Figure 6.11: Naphthalene batch adsorption data fitted to the three-stage kinetic model.

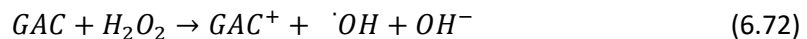
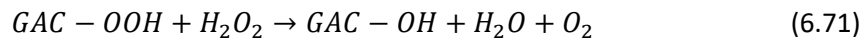
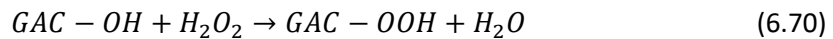
From the fitted model, the solid naphthalene concentration associated with Type 1, exterior adsorption,  $q_1(\infty)$ , was found to be 3,142.5 mg/kg. Given that the equilibrium solid phase naphthalene concentration achieved after the 96 hour loading period was 10,760 mg/kg, the exterior adsorptive sites were calculated to account for 29.2 % of the adsorbed naphthalene species. As this value proves to be within 1.5 % of the average regeneration achieved for both the active chlorine and electro-Fenton pathways,  $31.3 \pm 1.4$  % and  $26.1 \pm 1.6$  % respectively, it is plausible that only the exterior surface of the GAC is capable of being regenerated when utilizing microporous GAC substrates during electrochemical treatments. These results align with the analytical results of Xiao and Hill [242] that showed micropores remain blocked and filled with contaminants following chemical regenerative treatments.

Table 6.2: Determined parameters of the three-stage kinetic model and its goodness of fit to the experimental data, where SSE is the sum of squared errors.

$\xi_1$ [-]	$\xi_2$ [-]	$\beta$ [-]	$\gamma$ [-]	$q_1^{(\infty)}$ [mg/kg]	$q_2^{(\infty)}$ [mg/kg]	$R^2$ [-]	SSE [-]
0.28	0.80	0.85	1.24	3,142.5	8,952.5	0.998	0.002

The argument in support of blocked micropores, as suggested by Xiao and Hill [242], may explain why the interior micropores of the GAC are not regenerated during treatment: oxidizing agents simply cannot access and restore interior adsorptive sites. For this argument to apply, however, it is worth considering the relative sizes of the adsorbate and pores of the adsorbent employed in this work. Although micropores are narrow, characterized as having a diameter less than 2 nm, they still prove to be much larger than the electrogenerated oxidizing species generated in this study. For example, hydroxyl radicals have a molecular diameter nearing 0.11 nm [244], less than 6 % the diameter of a micropore; this contradicts the notion that micropores are too narrow for such reagents to diffuse within the porous structure of the GAC. This is particularly true since the much larger naphthalene species, having a molecular length and width of 0.92 and 0.74 nm [245], are able to migrate and adsorb within these regions; the relative molecular sizes of the oxidizing species generated in this work is schematically presented in Appendix A.3. This suggests that although narrow pores are plausible, they may not fully explain the inaccessibility of interior adsorptive sites towards oxidizing agents. Thus, a second argument can be made asserting that oxidizing agents are consumed by reactions with the GACs external surface prior to undertaking intraparticle diffusion within the GAC pores.

To investigate this theory, the reaction rate between hydrogen peroxide and GC1200 GAC was assessed to determine the extent that oxidizing products react with the GAC surface. It is known from the literature that  $H_2O_2$  reacts with either functional groups on the GAC, Equations (6.70) and (6.71), or be catalytically decomposed at the GAC surface, Equation (6.72) [246]. The rate at which these reactions occur with GC1200 GAC was examined by mixing varying amounts of GAC with aqueous, 20 mg/L hydrogen peroxide solutions and monitoring the  $H_2O_2$  decay as a function of time. The linearized first-order results are shown in Figure 6.12 where it is evident that hydrogen peroxide is rapidly consumed in the presence of GAC substrate. Increasing GAC concentrations resulted in a linear increase in the  $H_2O_2$  removal rate, where at the highest GAC concentration studied, 100 gGAC/L, about 85 % of the starting hydrogen peroxide had reacted away within 20 minutes of contact time.



Extending these results to the regenerative reactor used in this study, having a GAC concentration of 555 gGAC/L, Figure 6.12 predicts that hydrogen peroxide would be consumed by the GAC surface at a higher first-order rate of  $0.01 \text{ s}^{-1}$ . Considering that regenerative treatments commence with an oxidant concentration of zero, it is possible that electrogenerated oxidants are unable to reach a large bulk concentration and react with the GAC surface at a faster rate than diffusion processes through the GAC pores. In other words,

naphthalene adsorbed within the interior structure of the GAC may not be accessible to oxidants as they are consumed prior to undergoing intraparticle diffusion; this would result in only the exterior of the GAC surface being regenerated, as the results of this chapter have indicated.

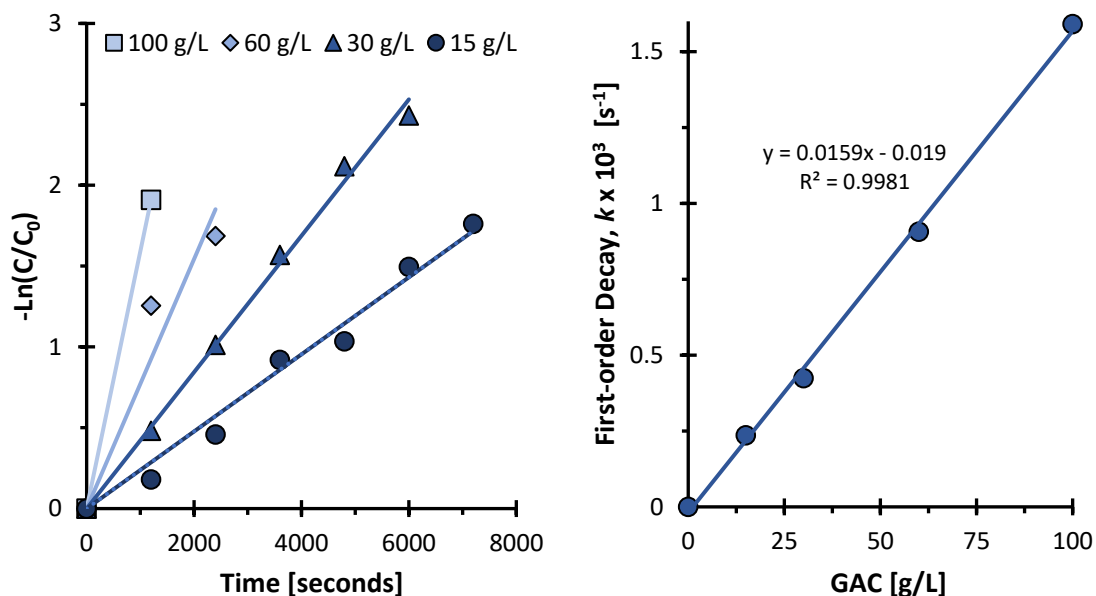
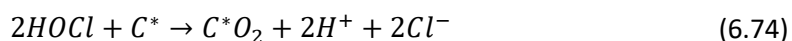
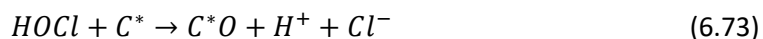


Figure 6.12: (Left) linearized, first-order decay rates of hydrogen peroxide against time in the presence of varying concentrations of GAC, and (right) the first-order decay rate as a function of GAC concentration.

Similar surface reactions are known to occur between active chlorine and GAC whereby the GAC surface,  $C^*$ , is rapidly oxidized via reactions (6.73) or (6.74) to an oxygenated form,  $C^*O$  or  $C^*O_2$  [247–250]; these compounds can present as surface oxides, altering the chemistry of the GAC surface, or be released into solution. Due to the rapid rate and efficacy for which active chlorine species react with GAC substrates, in the first-order range of  $0.1 - 0.02 \text{ s}^{-1}$  [251], they are commonly promoted in industrial applications as a means of dechlorinating processing streams [250]. Correspondingly, it is not surprising that the use of sodium chloride electrolytes during the electrochemical treatment of GAC has reported levels of surface oxidation that increase with increasing electric current and treatment time [252]. Similar surface reactions are known to occur between hydroxyl radicals and GAC surfaces, whereby the GAC quickly consumes hydroxyl radicals [24,246]; this has also been observed to oxidize and/or compromise the GAC surface during electrochemical treatments when the GAC is cathodically treated [34,49,91].



The occurrence of such reactions supports the notion that oxidation of the GAC surface may limit the amount of adsorbate species being oxidized, where oxidizing reagents are favourably consumed by the GAC surface. Interestingly, a study examining the reaction rate between free chlorine species and flow-through GAC beds concluded that GAC pores with a diameter less than 1.3 nm are not accessible to free chlorine species [251]. Although this was hypothesized to be due to water molecules blocking access at the pore mouth, it supports the theory that micropores are inaccessible to oxidizing reagents in the bulk solution.



As the results of this study suggest only the exterior GAC surface is capable of being regenerated, it is likely that mesoporous ( $2 > d_0 > 50$  nm), macroporous ( $d_0 > 50$  nm), or even non-porous GAC substrates would facilitate better regenerative outcomes. Increases in pore size, however, reduce the surface area available for adsorption processes and decrease the overall adsorptive capacity. This indicates there is a trade-off between overall adsorptive capacity and the ability for a carbon substrate to be regenerated.

### 6.3.5.1.3 Regenerative Cycles

The ultimate goal of this work was to increase the longevity for which GAC can perform within Antarctic PRBs. Thus, the number of effective regenerative cycles was assessed to see how many rounds of adsorption followed by regeneration the naphthalene loaded GAC could sustain. The GAC was cyclically regenerated via the AC and EF pathways at their optimal conditions, 25 mA and 6 mA for two hours respectively. The results of five cycles of regeneration are shown in Figure 6.13 where regenerative outcomes were observed to decrease with each cycle until minimal regeneration was achieved following four rounds of treatment. The AC pathway, for example, resulted in regenerations of 32.2 %, 22.8 %, 10.4 %, 4.8 %, and 0.02 % over the five cycles of treatment, while the EF pathway showed a similar trend having outcomes of 28.1 %, 19.6 %, 8.2 %, 4.3 %, and 1.3 %. Such results align with the concept that only the GAC exterior is able to be regenerated during electrochemical treatments. As the interior micropores are not saturated, inaccessible naphthalene continues to accumulate within them with each adsorptive cycle, causing the relative amount of externally adsorbed naphthalene to become less and less, ultimately decreasing regenerative outcomes.

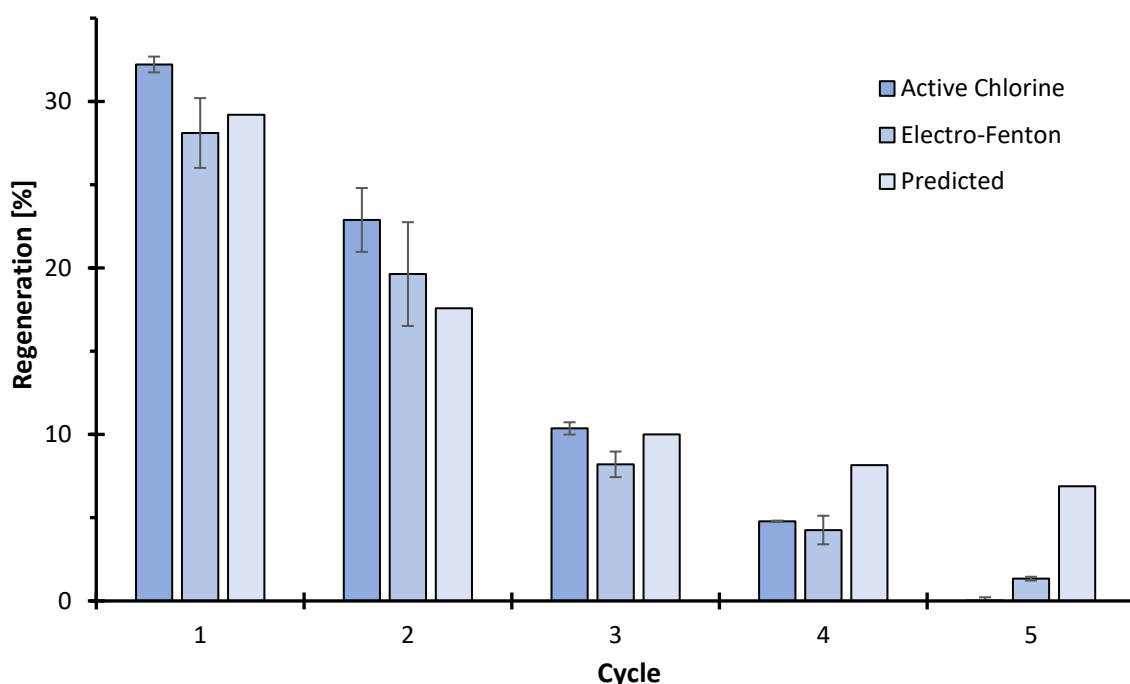


Figure 6.13: Regeneration over five cycles of adsorption followed by regeneration for the active chlorine and electro-Fenton reaction pathways. The predicted regeneration, assuming the same amount of externally adsorbed naphthalene is removed with each cycle, is also shown.

Assuming that the same amount of externally adsorbed naphthalene is removed with each cycle of electrochemical treatment, roughly 3,143 mg/kg as estimated by the three-stage kinetic

model, the theoretical regenerations efficiencies can be calculated for each consecutive cycle of treatment; these are shown in Figure 6.13. Due to continuous micropore filling, the theoretical regenerations gradually decrease with each cycle, reducing from 29.2 % to 6.9 %. Although anticipated, comparing the theoretical regenerations to the experimental results demonstrated that the actual regenerative outcomes decreased at a higher rate, where an average of 0.7 % regeneration was already obtained in the fifth cycle of treatment. This suggests that the observed reduction in regeneration is not only due to residual adsorbate remaining within the GAC micropores, but also due to a reduction in the overall adsorptive capacity of the GAC (i.e. a reduction in the isotherm due to losses in active adsorptive sites).

As discussed in Section 6.2.4.1, regeneration efficiency is calculated in reference to the adsorptive capacity of the starting material, where treatments aim to remove adsorbed pollutants without destroying the adsorbent itself [20,41]; when the physicochemical properties of the GAC are compromised, the calculated regeneration efficiency is reduced since the original adsorptive capacity cannot be restored. This phenomenon is illustrated in Figure 6.14, where a reduction in the isotherm post-treatment underestimates the amount of naphthalene removed from the GAC surface,  $\Delta q_{calculated}$  versus  $\Delta q_{actual}$ . In such a scenario, even if the exterior surface continues to be regenerated with each cycle of treatment, calculated regeneration efficiencies will decline due to a loss in overall adsorptive capacity. Due to the increased rate at which regenerations were seen to decrease in this current study, it is likely that the GAC structure and/or adsorptive sites were compromised with continuous and prolonged treatments. Similar conclusions have been reached by other studies, where regenerative outcomes have been observed to decline with additional cycles of treatment, claimed to be due to alteration of the GAC surface [36,91,240,253].

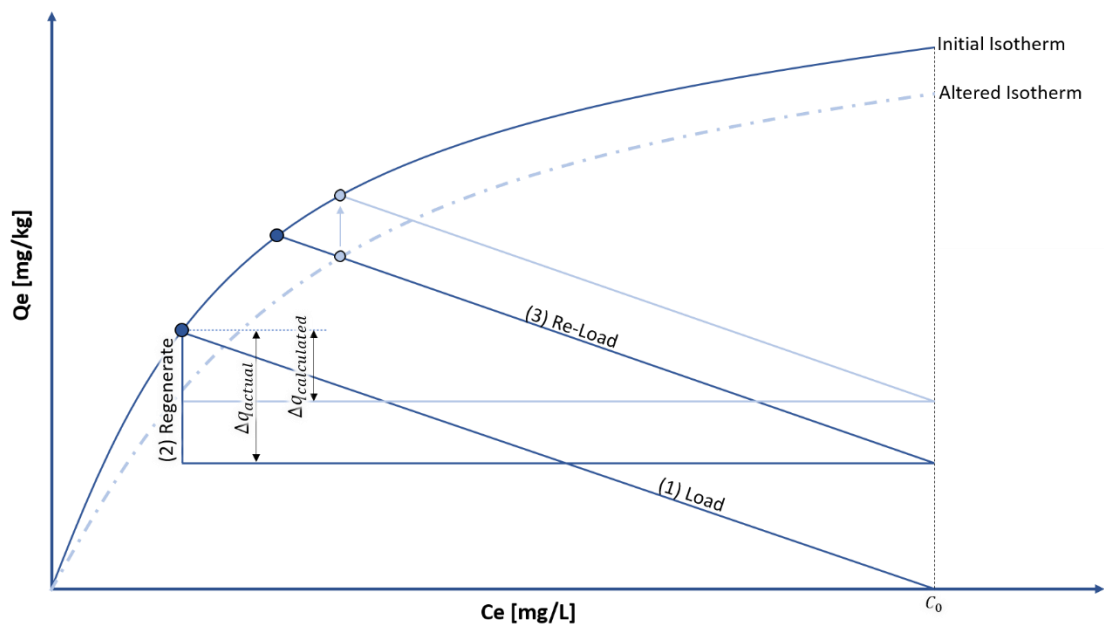


Figure 6.14: Schematic of how a reduced isotherm underestimates the amount of adsorbate removed from the GAC surface; the dark lines represent the actual amount of adsorbate removed,  $\Delta q_{actual}$ , whilst the light lines represent the calculated adsorbate removed,  $\Delta q_{calculated}$ , when the isotherm is altered.

Such losses in overall adsorptive capacity can occur when active adsorptive sites are oxidized, destroyed, or shielded by contaminant species. For example, Equations (6.70) - (6.74) show that

oxidation of the GAC surface is very likely during electrochemical treatments due to the continuous generation of powerful oxidizing agents. Such oxidation has been shown to significantly increase the oxygen content on GAC surfaces during electrochemical treatments [34,91,252], giving the GAC a hydrophilic surface that reduces its adsorptive selectivity towards hydrophobic compounds such as naphthalene [34]. This is a problematic result of regenerative treatments as the surface chemistry of GAC substrates has been shown to have more of an impact on adsorptive capacities than the physical structure itself. For example, a study by Deryło-Marczewska et al. [254] compared the adsorptive capacity of three activated carbons that were nearly identical in porous structure and surface area but presented with varying degrees of oxygenated surface groups; results showed that non-oxidized carbons had nearly double the adsorptive capacity towards organic compounds in comparison to oxidized carbon surfaces, despite having the same physical structure. This was attributed to oxygen surface groups decreasing the hydrophobicity of the surface and reducing the  $\pi$ -electron density in the graphene layers, limiting the interactive forces with solubilized organic compounds [254]. Extending this to the findings here, it is plausible that oxidation of the GAC surface may not only hinder the regeneration of micropores, but may also reduce the overall adsorptive capacity of the GAC substrate and result in reduced regenerative outcomes when cyclically treating the GAC.

Another possibility exists in what is termed the 'poisoning effect', or rather, fouling to the electrode surface. This is commonly observed with electrodes that have a high adsorptive capacities, and even more so when they are used for the treatment of aromatic organic compounds (i.e. GAC and naphthalene) [61,189,255]. The poisoning effect occurs when aromatic compounds react with the anode surface to form aromatic radicals that then react with each other to form long polymeric chains; as these polymeric films remain on the electrode surface, they decrease the catalytic activity of the electrode, and with regards to regeneration, may block adsorptive sites and lower the overall adsorptive capacity of the material. As such, this may also have been a reason for the decreased regeneration efficiencies achieved when cyclically treating the naphthalene loaded GAC substrate.

These results suggest that the use of an adsorptive/regenerative technology in engineering applications, such as *in situ* PRB regeneration, has a limited timeframe for which it is effective. Although 4 cycles of treatment will prolong the performance of GC1200 GAC, the bed will still require change out with fresh material when its saturation point is reached. Thus, improving upon regenerative outcomes (i.e. assessing GACs with lesser microporosity) should be the focus of further research. In contrast, a continuous treatment method may be more applicable for this technology, whereby continuous electrochemical reactions are promoted *in situ*, rather than an adsorption followed by regeneration approach. In this instance, the PRB material would act as an electrode surface to degrade incoming contaminants prior to them being adsorbed; the results of Chapter 4 and 5 have already shown that aqueous degradation is feasible and effective. Although alterations to the GAC surface chemistry would still result, its effect on future adsorptive performance would be irrelevant.

### 6.3.6 Kinetic Model

The results of this chapter have shown that desorption of naphthalene from the GAC surface is negligible during regenerative treatments. Rather, restoration of adsorptive sites occurs via oxidation of naphthalene species on the GAC surface where it is adsorbed. Thus, the

naphthalene removal rate previously described by Equations (6.59) and (6.60) become Equations (6.75) and (6.76) respectively.

$$\frac{dq_i}{dt} = -r_{oxidation,GAC} \quad (6.75)$$

$$\frac{dC_i}{dt} = 0 \quad (6.76)$$

As shown in Chapters 4 and 5, the rate of oxidation,  $r_{oxidation,GAC}$ , is dependent on the amount of oxidizing species present that are, in turn, electrogenerated at a rate proportional to the applied electric current; this is known to hold true for carbon packed-bed electrode systems [12,102,256,257]. Aligning with this, a simplified mathematical model proposed by Liu et al. [106] is used to describe the rate of naphthalene removal in the GAC bed system studied herein. The kinetic model, shown by Equation (6.77), states that the rate of naphthalene removal,  $N$  (g), is proportional to the applied current,  $I$  (C/s), where  $M_w$  is the molecular weight of naphthalene (g/mol),  $n$  is the number of electrons required for oxidant generation,  $F$  is Faraday's constant (C/mol), and  $\epsilon$  is the current efficiency describing the amount of effective current going towards naphthalene degradation.

$$\frac{dN}{dt} = -\frac{IM_w}{nF} \cdot \epsilon \quad (6.77)$$

As described by Liu et al. [106], the current efficiency,  $\epsilon$ , is assumed to be a function of the amount of naphthalene on the GAC surface: large naphthalene concentrations have high efficiencies and rapid removal rates, whilst small naphthalene concentrations have decreased efficiencies and reaction rates that asymptotically approach zero. This is represented by Equation (6.78) where  $N(t)$  is the amount of naphthalene in the system at any said time (g), and  $\alpha$  is an empirical fitting parameter used to describe a specified reaction. Such reduction in efficiency with decreasing concentration is analogous to the removal kinetics of Chapters 4 and 5 where the rate of naphthalene removal decrease with decreasing concentration,  $\frac{d[N]}{dt} = -k[Oxidant][N]$ .

$$\epsilon = \frac{N(t)}{N(t) + \alpha} \quad (6.78)$$

The obtained data sets in Sections 6.3.5.1.1 and 6.3.5.1.2 were fitted to the model equations, (6.77) and (6.78), using a non-linear least squares method treating  $\alpha$  as an adjustable parameter; the model equations were assumed to apply to regenerative outcomes up until the maximum regeneration efficiencies were reached for each pathway. Through fitting the model equations, the resulting efficiency values,  $\alpha$ , for the AC and EF pathways were determined to be 0.18 and 0.03 respectively, and the goodness of fit to the experimental data is detailed in Table 6.3; the kinetic model was seen to predict the resulting regenerative outcomes within 3 % in most cases as shown in Figure 6.8 and Figure 6.9.

Table 6.3: Efficiency parameter for the active chlorine and electro-Fenton pathways, and the root mean square error (RMSE) of the model when predicting treatment outcomes at varying currents and timeframes.

Reaction	$\alpha$ [g]	RMSE, current	RMSE, time
Active Chlorine	0.18	3.8	0.98
Electro-Fenton	0.026	2.6	3.0

The determined efficiency values indicated that the electro-Fenton reaction has a greater overall efficiency,  $\epsilon$ , signifying that a greater fraction of the applied current goes towards active site recovery. This is likely due to the non-competitive production of oxidizing agents in the EF pathway, whereby  $H_2O_2$  generation can occur in the absence of hydrogen gas evolution [172]. In contrast, the probability of parasitic side reactions occurring in the AC pathway is increased as the competitive and simultaneous production of both active chlorine and oxygen gas will reduce the effective current going towards naphthalene degradation [155]. Furthermore, Chapters 4 and 5 showed that hydroxyl radicals degrade naphthalene at a rate several orders of magnitude faster than active chlorine species, having second-order reaction rates of  $1.1 \times 10^8 M^{-1}s^{-1}$  and  $2.2 M^{-1}s^{-1}$  respectively; this suggests that electrogenerated oxidants in the EF pathway would recover active adsorptive sites at a heightened and more efficient rate in comparison to the AC pathway [242]. Further comparison of the reaction pathways showed that the EF pathway also required less energy input. Due to the lower potentials and currents required to regenerate the GAC, the EF pathway utilized 16 % of the energy required for the AC pathway to fully regenerate the GAC exterior, detailed in Table 6.4. Thus, although the same outcomes are achieved via either pathway, the EF reaction is, overall, more efficient.

Table 6.4: Average cell voltages and energy consumptions when regenerating the GAC for two hours.

Reaction	Average Cell Voltage [V]	Current [A]	Energy Consumption [Wh]
Active Chlorine	2.5	0.025	0.12
Electro-Fenton	1.7	0.006	0.02

#### 6.4 Conclusions

The results of this chapter have illustrated that enhanced desorption processes do not aid in the regeneration of naphthalene loaded GAC. However, promotion of the active chlorine and electro-Fenton reaction pathways enable a portion of the GAC to be regenerated; it is hypothesized that that only the exterior surface of the GAC was regenerated, leaving the interior adsorptive sites unaffected by electrochemical treatments. As interior micropores seem to be inaccessible to electrogenerated oxidizing agents, it is likely that macroporous or non-porous GAC substrates would better facilitate regenerative treatments.

Although only partial regeneration was achieved, it was demonstrated that the same proportion of GAC could be continually regenerated over four cycles of adsorption followed by regeneration. This suggests that the developed technology can increase the longevity for which GAC can perform in Antarctic PRBs. Following four cycles of treatment, however, minimal regeneration could be achieved, likely due to surface oxidation and physicochemical alterations to the GAC substrate, and/or polymeric films developing on the GAC surface. As this would negatively affect future adsorption processes, a continuous process may better suit environmental remediation efforts.

Although PRBs were the main consideration in this study, having the capability to adsorb and regenerate adsorbent materials within the same reactor extend well beyond this scope. Such a treatment would be largely beneficial for numerous industries encompassing adsorptive processes for the purification of processing streams.

---

# CHAPTER 7

---

## The Application of Electrochemical Treatments for the Regeneration of Granular Activated Carbons *in situ* of Permeable Reactive Barriers in the Antarctic

This chapter discusses how the electrochemical treatments studied within this thesis can be field deployed for the regeneration of granular activated carbon within permeable reactive barriers. The underlying calculations and reasonings of a field trial at Casey Station, Antarctica in 2018 is also discussed.

---

### 7.1 Background

In 1999, a storage tank near the Main Power House (MPH) at Casey Station, Antarctica leaked approximately 10,000 L of petroleum into the ground [5]. Upon examining the nearby soils, it was realized that several spills had historically occurred at that location prior to 1999, leaving soils and surface waters severely contaminated with a combination of hydrocarbons including special Antarctic blend (SAB) diesel, aviation turbine kerosene, and gasoline [2]. In order to contain the visible and migrating contaminant plume that resulted, a funnel-and-gate permeable reactive barrier (PRB) was installed in 2005 [19]; it is referred to as the Lower Main Power House (LMPH) PRB.

The PRB was initially designed so that investigators could evaluate the most effective flow-through system that could both capture and accelerate the biodegradation of adsorbed contaminants [19]. This resulted in 5 parallel treatments gates, depicted in Figure 7.1, each containing three zones intended for 1) nutrient release, comprised of fertilizers such as Zeopro or Maxbac, 2) hydrocarbon adsorption, containing GAC mixed with zeolite for additional structural integrity, and 3) capturing excess nutrients, comprised of zeolite.

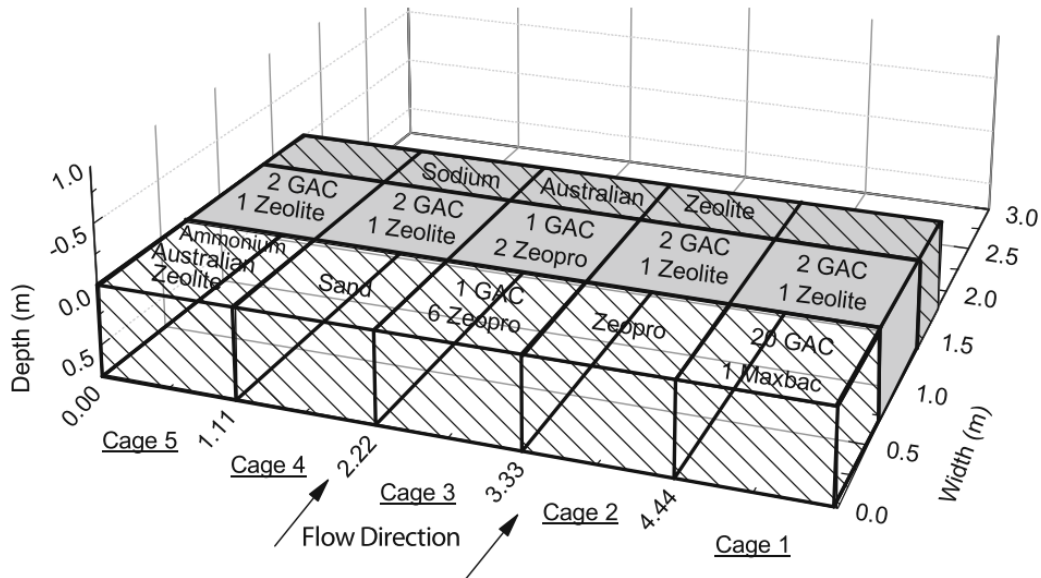


Figure 7.1: Schematic of the PRB indicating the materials used within each zone and the flow direction of ground water [10].

After 5 years of operation the PRB was sampled and shown to have successfully intercepted the migrating contaminant plume [10]. Analysis of the adsorptive granular activated carbon (GAC) in zone 1 of cage 1, for example, reported hydrocarbon concentrations of up to 6,373 mg total petroleum hydrocarbons (TPH) per kilogram of GAC, and no bed breakthrough could be detected [10]. To ensure the GAC bed did not near its saturation point with further operation, the PRB was excavated and re-filled with fresh materials; the updated zones and types of material that currently exist in the PRB are depicted in Figure 7.2.

The constant replacement of PRB material is manually difficult and not financially sustainable. Nonetheless, the PRB needs to remain in place as fuels in Antarctica migrate for decades following an initial spill due to the pulse of contaminants that arise with each summer snowmelt and thawing of the ground [2]; it is estimated that  $800 \pm 200 \text{ m}^3$  of water flow through this barrier annually [19]. Because of this, a long-term, sustainable, and *in situ* regenerative



treatment of the barrier is desired. This chapter presents how the electrochemical technology studied in this thesis can be applied for the *in situ* regeneration of materials within PRBs, using the LMPH PRB at Casey Station as a case study.

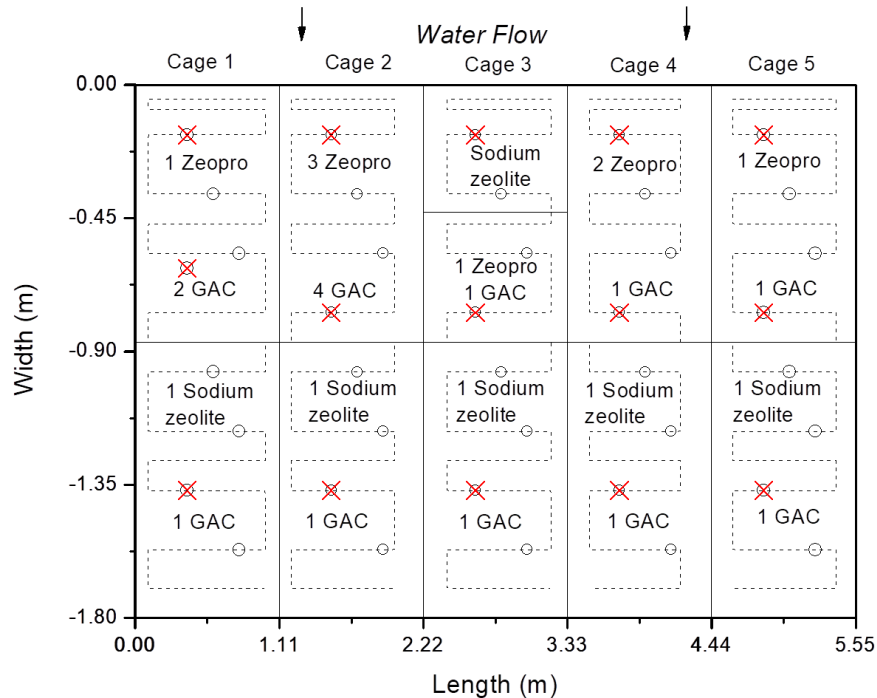


Figure 7.2: Updated zones and materials used within the PRB. The direction of groundwater flow is also specified.

## 7.2 Electrochemical Treatment Design

### 7.2.1 Initial Considerations

The following sections outline the main considerations that require attention prior to implementing an electrochemical treatment apparatus for the *in situ* regeneration of PRB materials.

#### 7.2.1.1 Seasonal Timing

The summer months at Casey Station, where temperatures top out near 5 °C, is limited to a 60 – 100 day window on an annual basis [5]; it is during this time that soils and surface waters thaw and migrate through the LMPH PRB. Once the summer ends, temperatures quickly decrease to temperatures averaging -34 °C, leaving the ground, inclusive of PRBs, frozen solid for the remainder of the year. As electrochemical regenerative treatments require a solid/liquid interface between the GAC surface and water within the PRB, it is imperative that treatments occur during the brief summer window before freezing occurs. This can be ensured in one of two ways:

- 1) When the summer thaw begins, manually install regenerative equipment within the PRB and commence treatment for the desired timeframe; the equipment can then be shut down and removed before the summer season ends, or
- 2) Pre-install weather-proof and temperature compliant equipment within the PRB that can be turned on remotely for *in situ* regeneration during the summer months; this scenario is ideal as it is low maintenance and minimizes manual labour on an annual basis.

### 7.2.1.2 Solid Contaminant Loading

Although saturation of the PRB GAC will not occur for several years, treatment should commence well before this point is reached. Three reasons for this are:

- 1) Avoiding GAC saturation preserves the number of electro-active sites on the GAC surface that can be used to promote electrochemical reactions; it has been shown that there is a direct correlation between the percent of adsorptive capacity reached and the number of active sites available for the electrogeneration of oxidizing species (i.e. active chlorine, hydrogen peroxide) [38].
- 2) Large solid concentrations, where contaminants are in close proximity to each other, can result in the polymerization of compounds on the GAC surface during electrochemical treatment. This has been shown to form high molecular weight compounds that not only take a longer time to break down, but also block pores and hinder future adsorption processes [258]; such an occurrence has not been observed when small solid concentrations are treated.
- 3) Keeping solid concentrations low will reduce treatment timeframes, a key consideration when working periods are limited to less than 60 days per year.

With these considerations, the *in situ* electrochemical regeneration of GAC within PRBs may be implemented in two ways:

- 1) Wait until a specified contaminant load is reached and then regenerate the GAC, or
- 2) Apply the treatment as a continuous process, destroying contaminants simultaneously to them being adsorbed within the barrier. This scenario may be ideal, especially if using sustainable energy sources such as solar power where daily regeneration can occur; this would prevent high-loadings from being reached and keep regeneration efficiencies high, as discussed in Chapter 6

### 7.2.1.3 Bed Conductivity

To ensure that a majority of the GAC is regenerated, a uniform electric current needs to pass through the bed material. As discussed in Chapter 6, increased electrical conductivity via improved particle-particle contact is required to achieve this; this also reduces the overall bed resistance and saves on energy usage [101].

Sufficient particle-particle contact is commonly achieved by applying external pressure to the bed. Although this is easily implemented within a PRB, where large volumes of GAC inherently compact the layers of GAC below it, an issue arises when the PRB has increased quantities of non-conductive materials such as zeolite, sand that has migrated into the barrier, and fertilizers. Whilst the introduction of non-conducting particles in GAC beds has been used in the literature as a means of avoiding short-circuiting, too high a content of non-conducting particles hinders treatment outcomes as electric current can no longer flow effectively [92,101]. With this in mind, PRB zones with higher proportions of GAC are the most appropriate for regenerative treatments. To demonstrate this, the electrochemical reactor in Chapter 6 was used to measure the resistivity of the GAC bed when mixed with varying amounts of zeolite. The results are shown in Figure 7.3 where the electrical resistance of the bed approaches infinity as the volumetric fraction of GAC approaches nil.

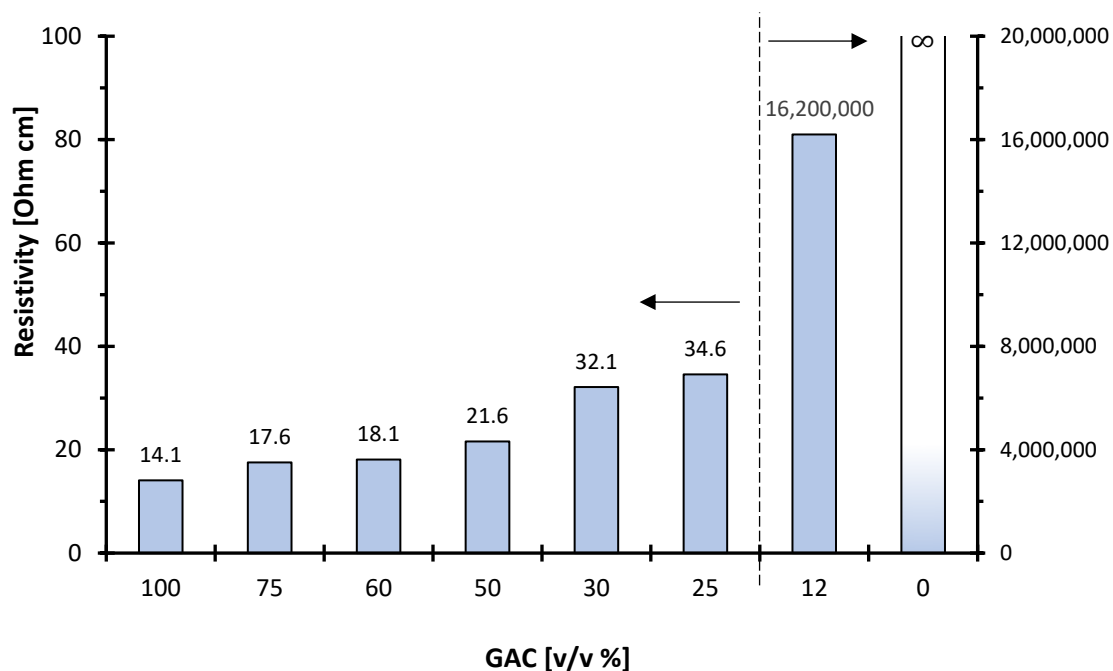


Figure 7.3: Resistivity of the GAC bed when mixed with varying amounts of zeolite.

#### 7.2.1.4 Electrochemical Reactions

Chapters 4 and 5 identified that both the active chlorine and electro-Fenton pathways can promote the *in situ* destruction of contaminants and fully remove them from the system, whilst Chapter 6 showed that both pathways are capable of regenerating the exterior surface of the GAC. Although the same outcomes are achieved with either reaction pathway, one reaction may be preferable over another based on the characterization of the site being treated (e.g. what reagents are naturally present, conditions of the groundwater/soils). Table 7.1 describes the varying conditions required to promote the active chlorine and electro-Fenton reaction pathways.

The regenerative treatment is designed such that GAC bed takes on a positive potential for promotion of the active chlorine pathway, or a negative potential for the promotion of the electro-Fenton pathway [143,232]. As demonstrated in Chapter 6, this is achieved by having the GAC bed in direct contact with only one of the externally applied electrodes. Thin separators such as fibrous fabrics, inert mesh, microporous and/or polymeric membranes inclusive of polypropylene, polyethylene, Teflon, polyvinylidene fluoride, and polyvinyl chloride can be used to separate the GAC from the opposing electrode; these materials prevent direct physical contact between the GAC bed and external electrode but allow the flow of electrolyte through them.

If the additional capital cost is too high or the manual step of installing a separator is too difficult, regenerative treatments may still occur when the bed is in contact with both the external anode and cathode. In this instance, the GAC becomes polarized and creates a cathodic and anodic terminal at each individual particle, allowing Faradaic reactions to occur at either end [103,136,143,259]; however, this setup requires larger applied potentials and increases the chances of short-circuiting that would reduce energy efficiency [196].

Table 7.1: Ideal operating conditions for promotion of the active chlorine and electro-Fenton reactions *in situ* of a PRB.

	Active Chlorine	Electro-Fenton
<b>Reagent</b>	Cl <sup>-</sup>	Fe <sup>2+</sup> , O <sub>2</sub>
<b>Reagent Source</b>	Naturally present or sourced via nearby seawater	Naturally present, sourced through the effluent of the water treatment container <sup>a</sup> , or manually introduced
<b>Reagent Concentration</b>	≥ 0.05 M (larger concentrations decrease energy consumption, smaller concentrations reduce energy efficiency and require longer treatment time)	0.01 – 0.5 mM (quantities outside this range work but reduce reaction efficiency)
<b>Potential (V vs SHE)<sup>b</sup></b>	1.4 ≤ V ≤ ~2.0 (potentials above this range work but lower energy efficiency as oxygen gas evolution commences)	0.7 ≤ V ≤ 0.83 (potentials above this range work but lower energy efficiency as hydrogen gas evolution commences)
<b>Charge (C/g GAC)</b>	~43.8	~10.5
<b>pH</b>	3 - 8	2 - 4
<b>Additional Comments</b>	Chapter 6 showed no desorption of contaminants or generated by-products during electrochemical treatment, however, having an adsorption zone downstream of treatment is recommended to completely rule out chlorinated compounds exiting the barrier	Acidic conditions are required which may not be appropriate for some applications. If necessary to avoid, possible options include, 1) neutralizing barrier effluent, 2) sequencing treatment within the barrier (e.g. produce acidic H <sup>+</sup> and alkaline OH <sup>-</sup> at barrier entrance and exit respectively with ion-exchange resins <sup>c</sup> ), 3) consider the heterogeneous electro-Fenton reaction that can take place at neutral pH <sup>d</sup>

<sup>a</sup>Casey Station has an *ex situ* pump-and-treat container that uses large quantities of iron for flocculation of contaminants, and its effluent is discharged at the entrance of the PRB, <sup>b</sup>Standard Hydrogen Electrode, <sup>c</sup>examples in the literature include [192,260], <sup>d</sup>examples in the literature include [261,262]

#### 7.2.1.5 Electrode Placement

The electrodes should be placed such that a uniform current passes through the bed. As shown in Figure 7.4, there are a variety of electrode configurations that can be implemented, whereby the most beneficial array will ensure an even distribution of current through the zone of material requiring treatment. With this in mind, conducting plates, Figure 7.4B and E, would be the most appropriate for installation within rectangular PRBs, whilst a circular array, for example, Figure 7.4C, would be most suited for cylindrical GAC adsorption columns.

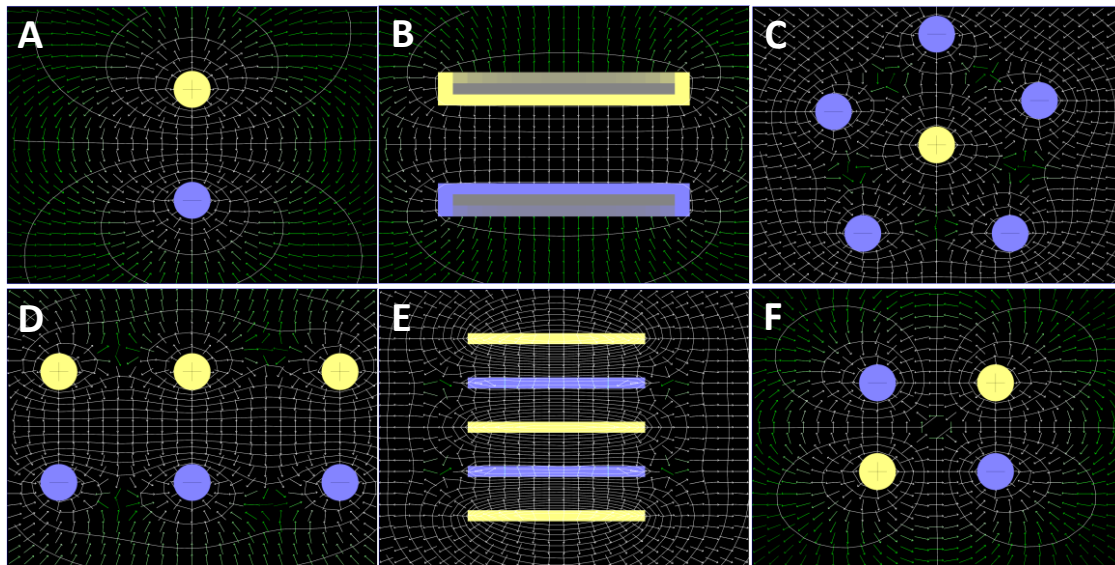


Figure 7.4: Electric fields for varying electrode arrangements (A) dipole charge, (B) conducting plates, (C) circular array, (D) face-to-face dipoles, (E) alternating conducting plates, and (F) quadrupole [263].

Once an appropriate electrode array is chosen, the interelectrode spacing needs careful consideration as it directly affects the bed resistance and overall energy consumption. Equation (7.79) shows that the bed resistance,  $R$  ( $\Omega$ ), increases with larger interelectrode gaps,  $l$  (cm), where  $A$  is the cross-sectional area of the bed ( $\text{cm}^2$ ) and  $\rho$  is the bed resistivity ( $\Omega \text{ cm}$ ), an intrinsic property that is only dependent on the material composition.

$$R = \rho \frac{l}{A} \quad (7.79)$$

Combining this understanding with Ohm's Law, Equation (7.80) where  $V$  is the applied cell voltage (V) and  $I$  is the applied current (A), larger electrode gaps require increased potentials to drive a desired current. As regenerative treatments of GAC will most likely be applied under galvanostatic, constant current conditions, there is an evident trade-off between capital expenditure (i.e. the number of electrodes required to maintain a specific interelectrode gap) and operating expenditure (i.e. the amount of energy required to drive the desired electric current and subsequent rate of electrochemical reactions).

$$R = \frac{V}{I} \quad (7.80)$$

The electrochemical reactor in Chapter 6, having a cross-sectional electrode area of  $4 \text{ cm}^2$  and a bed resistivity of  $14.3 \Omega \text{ cm}$ , was used to demonstrate these effects. It can be seen in Figure 7.5A that the bed resistance increases from  $0.4$  to nearly  $400 \Omega$  when increasing the interelectrode gap from  $0.1$  to  $100 \text{ cm}$ . Due to the increasing resistance that results with increasing bed length, heightened potentials are required to maintain a specific flow of current, as depicted in Figure 7.5B. For example, increasing the interelectrode gap from  $2$  and  $10 \text{ cm}$  increases the required cell voltage from  $4.5$  to  $18.5 \text{ V}$  to maintain a constant current of  $0.5 \text{ A}$ . Although these results are specific to the laboratory scale PRB in Chapter 6, Equations (7.79) - (7.80) and the resistivity values reported in Figure 7.3 can be used to predict the energy requirements when scaling up the technology for PRB implementation. In either case, smaller interelectrode gaps will always

have reduced energy consumption; they also have the added benefit of minimizing uneven distributions of current and potential along the length of the porous bed [101,264–266].

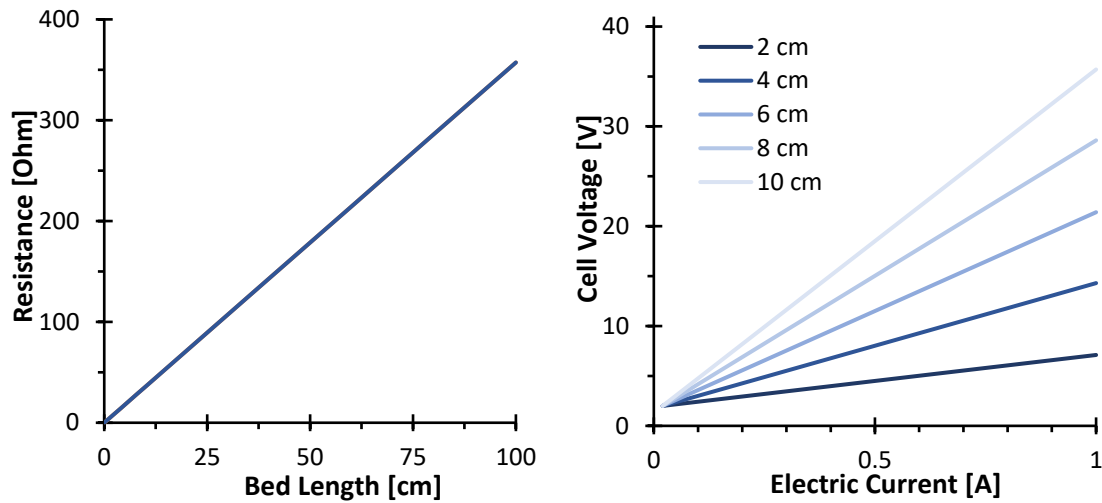


Figure 7.5: (Left) relationship between bed resistance and bed length, and (right) relationship between cell voltage and electric current at varying interelectrode distances.

Based on these considerations, an ideal electrode configuration for implementation within a PRB would be a line of alternating plate electrodes positioned parallel to the flow of groundwater such as shown in Figure 7.6; this would achieve the most uniform current through the bed, treat a large area of GAC, and not hinder the hydraulics of the barrier. Although an interelectrode gap of 10 cm is presented, larger electrode spacing can be utilized to minimize capital expenditure but will result in greater energy consumption as previously discussed. While not depicted, separators should also be used between the alternating plates of the electrode array, as discussed in Section 7.2.1.4, such that:

- 1) Short-circuiting and energy wastage are avoided,
- 2) The desired electrochemical reactions can be promoted and controlled (i.e. give the GAC bed either a positive or negative charge), and
- 3) The polarity of the bed can be easily reversed at the power supply if alternate electrochemical reactions are ever desired.

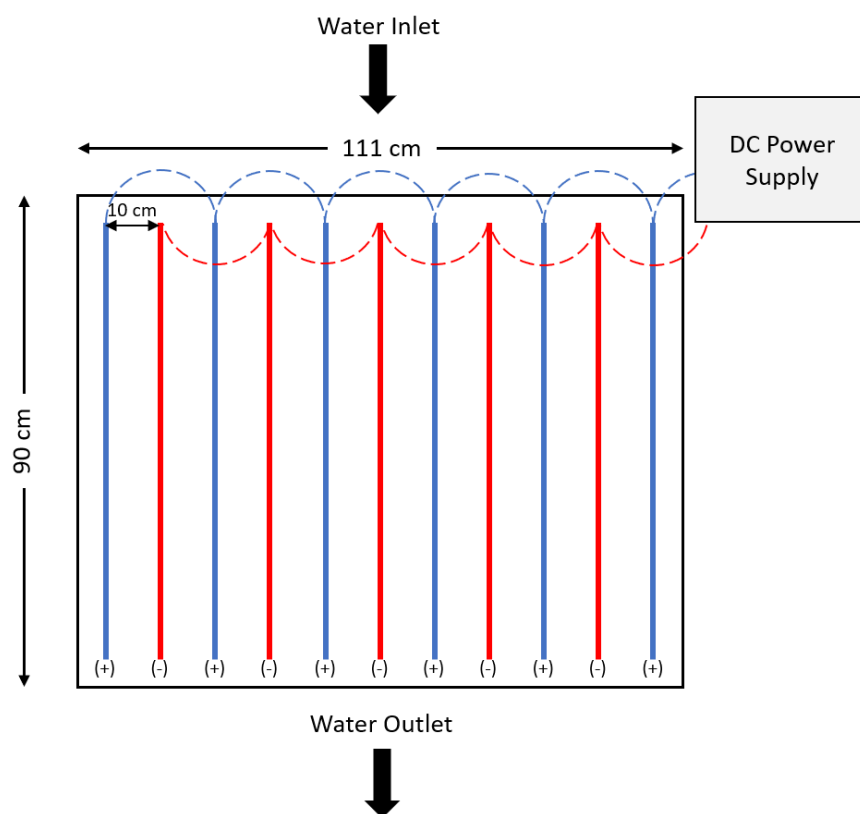


Figure 7.6: Ideal electrode array for obtaining uniform current distribution over a large volume of GAC *in situ* of a PRB.

### 7.3 Field Trial

This section describes a field trial of the described electrochemical technology conducted at Casey Station, Antarctica in February 2018.

#### 7.3.1 Methodology

##### 7.3.1.1 Media Sampling

Samples of PRB media were obtained using a 30 cm long steel drill bit fit to a steel shaft. Cores were taken in 15 cm increments at varying depths through the PRB; as groundwater flows at only the lower depths of the PRB, samples between 30 – 60 cm in depth were taken. Retrieved cores were stored in 120 ml amber glass jars at -20° C until returned to Australia (RTA) for analysis. Following RTA, each sample was thawed and homogenized prior to being analysed for total petroleum hydrocarbon concentrations (TPH) via Accelerated Solvent Extraction (ASE) as detailed in Chapter 3.

##### 7.3.1.2 Water Sampling

The water flowing through the PRB was sampled for TPH analysis through pre-installed multiports that were established during initial construction [19]; water could be drawn at depths of either 50 or 60 cm. Samples were collected in 500 ml amber glass bottles and stored at 4 °C. Upon RTA, 10 ml of dichloromethane (DCM) was added to the 500 ml sample bottle and hand shaken for 2 minutes. Following a 4 hour settling period, the organic layer was removed and a 1.5 ml aliquot was taken for analysis via GC-FID as detailed in Chapter 3. A 100 µl aliquot of internal standard mixture (comprising of 50 mg/L each of 1,4-dichlorobenzene, p-terphenyl, deuterated tetracosane (C<sub>24</sub>D<sub>50</sub>) and 250 mg/L of bromoeicosane and cyclooctane) was added to all samples prior to analysis to determine the TPH within the sample.

### 7.3.2 Construction

Zone 1 of cage 1 in Figure 7.2 was chosen to test the efficiency for which PRB GAC can be regenerated *in situ*. This cage was chosen for two reasons:

- 1) This zone had the highest GAC:Zeolite ratio (2:1) giving it good electrical conductivity that would allow for greater current efficiency, and
- 2) If any undesirable desorption of contaminants and/or by-products occurred during treatment they would be re-adsorbed in zone 2 of the cage (consisting of 1:1 GAC to Zeolite).

The active chlorine pathway was chosen to test the regenerative treatment. As the site is subject to periodic inundation of seawater during extreme high tides, surface waters are left with variable, and sometimes high, salinities [3,129]; this makes chloride ions as a naturally present catalyst within the PRB. Additionally, the active chlorine pathway is, in general, more easily implemented in comparison to the electro-Fenton pathway, as it can take place at the neutral pH present within the barrier and at an extremely wide range of saline concentrations (refer to Table 7.1). Thus, the inlet water of the PRB did not require modification.

Although alternating plate electrodes are ideal for PRB regeneration, these would need to be installed during initial PRB construction or during material change out as to avoid crushing large quantities of GAC; this would not only destroy the porous structure of the material and limit further adsorption but would also restrict hydraulic flow through the barrier. As this was not possible, two rows of electrode rods in a face-to-face dipole array were used. Prior to installing the electrodes, the PRB media was sampled in several locations to determine the hydrocarbon concentrations in the barrier prior to treatment; the sample locations are depicted in Figure 7.7.

As shown in Figure 7.7, a row of five anodes were placed perpendicular to the flow of water 10 cm from the PRB inlet and spaced 20 cm apart; a row of cathodes was placed 35 cm downstream from the anodes. To avoid short-circuiting, the cathodes were physically separated from the bed material by placing them within a thin piezometer casing filled with GAC; this prevented direct physical contact but allowed groundwater to flow through. Each electrode was fabricated from steel rebar, 1.2 cm in diameter, cut to a length of 90 cm. They were individually hammered down to the base of the PRB, 60 cm in depth, being careful not to pierce the underlying insulation. The remaining 30 cm of rebar was exposed at the surface allowing it to be connected to a power supply. As depicted in Figure 7.6, each row of electrodes was sequentially connected via a 10 mm<sup>2</sup> cross sectional annealed copper cable fabricated with a cold temperature compliant insulator; for each electrode, the cabling was stripped and connected to the exposed portion of the rebar with a hose tie, upon which heat shrink wire wrap was used to cover and hold the cabling in place. Each line of electrodes was then connected to a MP3087 (PowerTech) DC regulated power supply (0 – 32 V, 0 – 3 A).



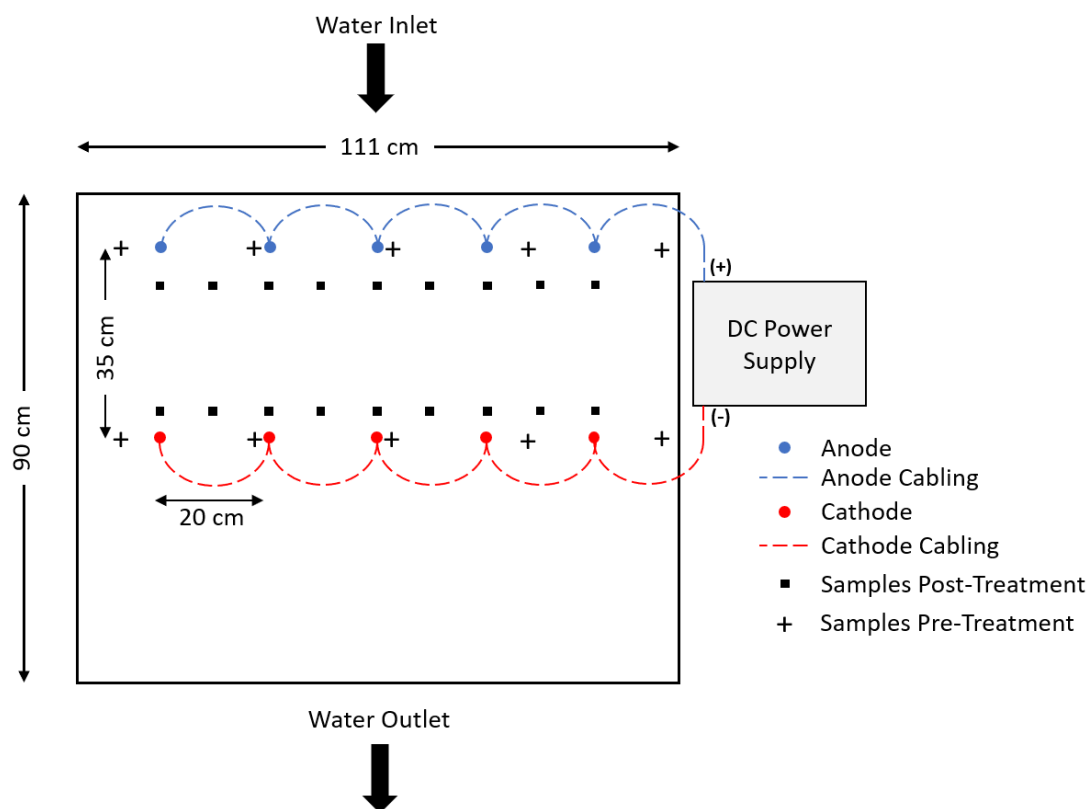


Figure 7.7: Layout and location of electrodes, electrical connections, and sample points pre- and post-treatment.

When scaling-up the electrochemical treatment of GAC, it has been demonstrated that the amount of charge passed per gram of GAC present should be maintained [101,110]. As per the results of Chapter 6, applying a current of 0.025 A for two hours was sufficient to fully regenerate the exterior surface of 4.0 g of GAC substrate; this equates to a charge passed of 45 C/g GAC. As the constructed electrode array had an interelectrode spacing of 35 cm, it was calculated (as described in Section 7.2.1.5) that an electric current near 1.2 A would result when applying a cell voltage of 10.0 V across the bed; this calculation considered a reduced bed conductivity due to the presence of zeolite as shown in Figure 7.3. Thus, based on the volume of GAC within the constructed array and assuming a water height of 10 cm in the barrier, the application of 1.2 A of current over an 8 day period would result in a passed charge of 62 C/g GAC, slightly above the desired amount. Accordingly, this was applied for 8 days, after which the GAC bed was resampled and compared to the solid contaminant concentration pre-treatment to determine the efficacy of the treatment.

#### 7.4 Results and Discussion

The concentrations of TPH and naphthalene in the PRB prior to being electrochemically treated are shown in Figure 7.8 and Figure 7.9 for PRB depths of 30 – 45 and 45 – 60 cm respectively. Due to the recent change-out of PRB material, the solid concentrations of TPH were relatively low; the maximum concentrations for TPH and naphthalene were detected at 727 and 0.392 mg/kg respectively. Although these readings are lower than those in previous years, it demonstrates that contaminants continue to be captured nearly 15 years after the PRB's initial installation.

At both depths considered, the most concentrated readings were detected on the “wing side” of the funnel-and-gate PRB entrance. This suggests that a majority of water flowing in from the

catchment is directed towards the PRB along the funnel-and-gate wing, primarily entering the PRB via cage 1, rather than being equally distributed along the width of the 5 cages. Coinciding with this, concentrations of TPH and naphthene were observed to gradually decline along the width of the cage in the direction of cage 2, further supporting the direction of flow through the barrier.

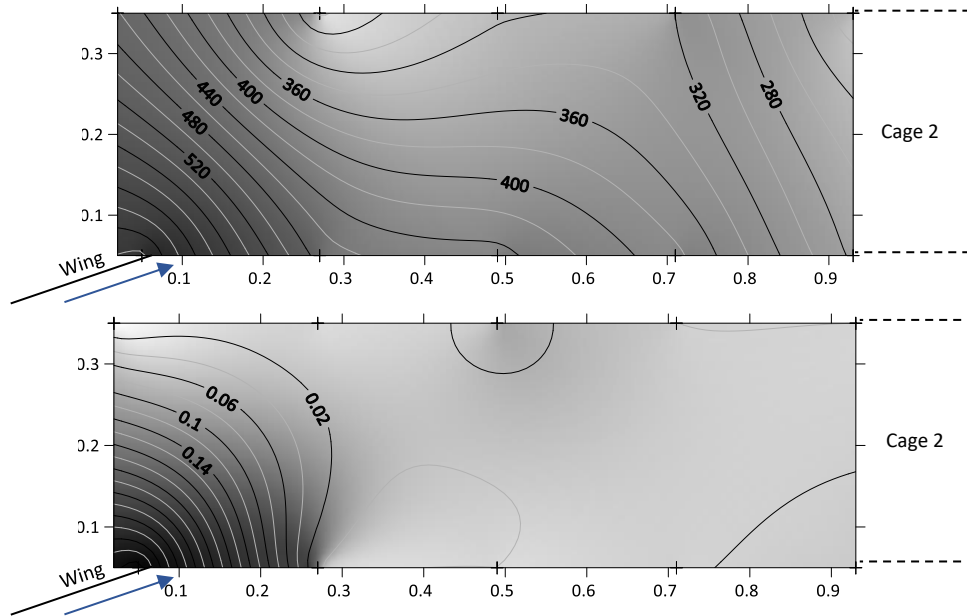


Figure 7.8: Pre-treatment solid loadings of (top) TPH and (bottom) naphthalene at a depth of 30 – 45 cm. The vertical axis is distance along the cage (m) and the horizontal axis is distance along the width of the PRB (m). The listed numbers are the solid concentration, mg/kg. The arrow represents the inflow of water alongside the PRB wing.

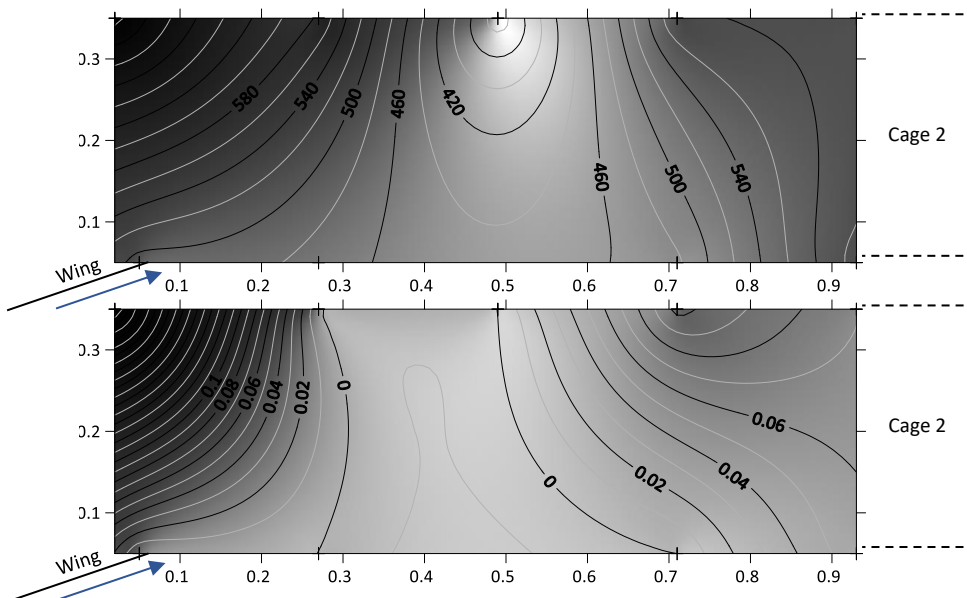


Figure 7.9: Pre-treatment solid loading of (top) TPH and (bottom) naphthalene at a depth of 45 – 60 cm. The vertical axis is distance along the cage (m) and the horizontal axis is distance along the width of the PRB (m). The listed numbers are the solid concentration, mg/kg. The arrow represents the inflow of water alongside the PRB wing.

Solid loadings at the base of the PRB, depths of 45 – 60 cm in Figure 7.9, had slightly higher concentrations than those at a depth of 30 – 45 cm. For example, the highest TPH concentrations

were 665 and 727 mg/kg for depths of 30 – 45 and 45 – 60 cm respectively; this is due to there being a higher flux of water through the lower portions of the PRB [10,11].

When the power supply was turned on to initiate the regeneration process, the electric current quickly jumped to 0.544 A, about half of the predicted value. Possible reasons for a lower-than-expected electric current include biological growth on the surface of the GAC, the infiltration of fines such as sand, the breakdown of GAC particles that have been subjected to diurnal and seasonal freeze/thaw events, or even a non-uniform distribution of GAC, zeolite, and/or weight distribution throughout the barrier; all of these things could vastly lower the electrical conductivity of the bed and reduce the anticipated electric current. Thus, a key consideration for future deployment scenarios would be to gain a better understanding of what the electrical conductivity of the bed is *in situ*, as it will not likely align with the pristine GAC studied within a laboratory setting.

Unfortunately, the current did not increase and rather slowly diminished over the coming hours and days, detailed in Table 7.2. Although the current seemed to reach a steady current of 0.03 A by the third day of treatment, this proved insufficient for the treatment of such a large volume of GAC. For reference, the application of 0.03 A over an 8 day period equates to a charge passed of 1.5 C/g GAC, only 3 % of the required charge to reach sufficient levels of regeneration.

Table 7.2: Fluctuations in electric current over the 8 days of treatment.

Treatment Time [hr]	Cell Voltage [V]	Current [mA]
0		0.544
1		0.519
19		0.112
23		0.093
48		0.050
71		0.037
89		0.031
96	10	0.031
112		0.025
120		0.025
136		0.027
144		0.025
160		0.025
167		0.025
190		0.025

Upon further investigation it was realized that by the time electrochemical treatments had started, water flow within the barrier was already starting to cease due to the lateness in the summer season; there proved to be insufficient amounts to even take a water sample. This was attributed to unavoidable delays in travel and weather that caused the trial to be conducted in mid-February whilst soils and groundwaters at Casey Station start to freeze in late January. With 8 days of inclement weather during the trial, and a 2-day period of constant snow fall, water flow in the barrier was observed to come to a complete halt; following the eighth day of the trial, several of the extracted, post-treatment PRB cores came out completely frozen. This becomes problematic, as discussed in Section 7.2.1.1, it is vital that a solid-liquid interface is present at the GAC surface in order for regenerative Faradaic reactions to commence. As most of the water within the barrier was frozen, leaving no interface for electrochemical reactions to

occur, it is likely that this was the main cause for which almost no electric current was passing through the barrier after 3 days of starting the trial.

Due to a lack of groundwater flowing through the barrier, the field trial was ultimately unsuccessful, and no sound conclusions could be drawn from the analysis of the post-treatment cores, shown in Appendix A. Although unfortunate, this highlights a consideration for future Antarctic seasons: as timing on station cannot always be guaranteed (i.e. weather conditions can delay travel to and from Antarctica, working outside is not always permitted), it is advantageous to have a simple regenerative system that can remain *in situ* between summer seasons that can be operated remotely. This field trial was the first step in attempting to construct such a system.

### 7.5 Conclusions

Although no comprehensive results could be drawn from the attempted 2018 field trial, it is still believed that this type of system would effectively aid in the regeneration of PRB materials if conducted earlier in the Antarctic season. This is supported by the results of Chapters 4 – 6 showing that promotion of the appropriate electrochemical reactions can regenerate petroleum hydrocarbon loaded GAC. This leaves scale-up and optimization, inclusive of a field trial, to future research.

---

# CHAPTER 8

---

## Concluding Remarks

This chapter summarizes the research findings of this thesis and discusses their significance towards the electrochemical regeneration of GAC. Recommendations for ongoing research are also discussed.

---



## 8.1 Thesis Summary

This thesis has demonstrated that electrochemical treatments represent a viable technology for the treatment of petroleum hydrocarbon contaminated waters commonly detected at Antarctic contaminated sites. Through a series of laboratory based assessments, it was shown that naphthalene contaminated waters can be treated via 1) indirect oxidation reactions in the bulk aqueous phase, or 2) adsorption onto granular activated carbons followed by electrochemical regeneration. Through this, the overarching objective of this thesis of determining whether electrochemical technologies can prolong the longevity of granular activated carbons *in situ* of permeable reactive barriers, has been answered in the affirmative.

Understanding the relevant electrochemical reactions that aid in GAC regeneration is key when attempting to electrochemically treat GAC substrates. As such, Chapters 4 and 5 investigated the efficacy of the active chlorine and electro-Fenton pathways towards naphthalene degradation; these specific reactions were considered due to the natural presence of chloride and iron compounds at the contaminated sites in the Antarctic and sub-Antarctic. Both reactions were shown to successfully obtain full naphthalene removal in as little as two hours of treatment. Despite the naphthalene being electrochemically transformed into species of lesser toxicity, chlorinated hydrocarbons presented during application of the active chlorine pathway. Similarly, small but recalcitrant quantities of 1,4-naphthoquinone presented during the electro-Fenton pathway. When applying such reactions in environmental remediation efforts, sufficient treatment timeframes will need to be ensured such that these compounds are subsequently removed from the system.

To aid in scalability and ultimate deployment of the electrochemical reactions, varying electric currents, reagent concentrations, and treatment timeframes were investigated. Through this, the underlying mechanisms of each pathway were determined, and dynamic kinetic models were developed that could predict treatment outcomes under a range of operating conditions. Similarly, ideal operating conditions were established and showed that each reaction pathway could achieve full naphthalene removal with minimal energy consumption, small enough to be run by solar power in remote regions. This is a key finding as resources in the Antarctic and sub-Antarctic are severely limited.

Due to the success of the active chlorine and electro-Fenton pathways degrading naphthalene within the aqueous phase, the reactions were applied to naphthalene loaded granular activated carbon. Although enhanced desorption processes had no effect on GAC regeneration, promotion of the appropriate electrochemical reactions on the GAC surface enabled a portion of the GAC to be regenerated. It is hypothesized that only the exterior surface of the GAC was regenerated, leaving interior adsorbate sites unaffected by electrochemical treatments. When cyclically treating the GAC it was shown that the same proportion of GAC was regenerated over four cycles of treatment, after which large losses in adsorptive capacity were observed; this is likely due to oxidation and/or the development of polymeric films on the GAC surface. This suggests that the developed technology can only slightly increase the longevity for which GAC can perform in Antarctic permeable reactive barriers; it is likely that a continuous process would be more suited for such an application.

To assess how the technology could be translated to implementation within permeable reactive barriers, a field trial was conducted at Casey Station in 2018. Due to poor seasonal timing, the field trial was unsuccessful. However, an ideal method for employing the technology in future

field seasons was developed. It is anticipated, based on the outcomes of Chapters 4 – 6, that this type of system would effectively aid in the regeneration of permeable reactive barrier materials.

Although permeable reactive barriers in the extreme polar environments of the Antarctic and sub-Antarctic were the main consideration of this study, having the capability to adsorb and regenerate adsorbent materials within the same reactor extend well beyond this scope; the rationale being that successful deployment under such harsh conditions would make translation to less extreme environments more likely to be successful. Such a treatment would be largely beneficial for numerous industries encompassing adsorptive processes for purification of processing streams. The results of this thesis can be used to inform and design such a treatment technology.

## 8.2 Recommendations for Future Work

Although the studies undertaken in this thesis have begun to address the research objectives initially established, a number of interesting research questions remain that should drive the direction of future research. They are outlined as follows:

- 1) In accordance with Chapters 4 and 5, it was shown that naphthalene could be fully removed via the active chlorine and electro-Fenton pathways. Although a number of the electrochemically transformed by-products were identified, a full mineralization pathway was not determined. Based on findings in the literature, it is expected that non-toxic and ring-opened products such as carboxylic acids, alcohols, and aldehydes are the end result, but it would be ideal to prove this prior to extensive field deployment applications.
- 2) Alternatively, mineralization efficiency could be assessed by measuring how the total organic content of the system is affected by electrochemical treatments. Chemical oxygen demand (COD), total organic carbon (TOC), and biochemical oxygen demand (BOD), for example, are commonly used to assess the efficacy of electrochemical treatment outcomes. Such measurements could be further used to assess how the biodegradability of the system contaminants evolve with treatment time, generally assessed via the BOD/COD ratio. It is anticipated that electrochemical treatments transform recalcitrant compounds, such as naphthalene, into a more biodegradable form. Thus, there is likely a positive synergy between electrochemical and microbial treatments whereby electrochemical reactions initiate microbial processes; this could ultimately save on energy requirements.
- 3) With further regard to microbial processes, previous works have focused on promoting *in situ* microbial regeneration of GAC within Antarctic PRBs (refer to Chapter 1). Although this method has been shown to have slow kinetics, it is still considered to be an important and effective process occurring within installed PRBs in the Antarctic and sub-Antarctic. With this in mind, it would be beneficial to gain an understanding of how the studied electrochemical treatments and their operating conditions affect the microbial communities within such barriers. This would also shed light on the possibility of utilizing a combined electrochemical / microbial treatment process.
- 4) In association with Chapter 5, the electro-Fenton reaction requires an acidic environment to commence and avoid iron precipitation. As this may not be appropriate in some environmental applications, the heterogeneous electro-Fenton reaction can be considered as an alternative. In this pathway, solubilized iron is replaced by insoluble iron-



containing solids such as goethite, magnetite, metallic iron, pyrite, or iron impregnated GAC and nanoparticles. Although the same sequence of reactions occur, the heterogenous pathway has the added benefit of being able to occur over a wide range of neutral pH conditions.

- 5) This thesis has demonstrated that the active chlorine and electro-Fenton reaction pathways can achieve full naphthalene removal, however, the contaminated sites in the Antarctic and sub-Antarctic present with a complex mixture of pollutant species. Thus, in order for these pathways to be successful in field deployment applications, it would be useful to investigate the efficacy of the reaction pathways to degrade alternative compounds such as alkanes, polar metabolites, kerosene oils, excess nutrients, or Special Antarctic Blend diesel.
- 6) Chapter 6 demonstrated that when applying the active chlorine and electro-Fenton reactions for the treatment of naphthalene loaded GAC, only the exterior surface substrate could be regenerated. As the micropores within the GAC were unaffected, it is possible that regenerative outcomes may be improved via implementing mesoporous, macroporous, or non-porous GAC substrates. This should be investigated further, as it may increase the efficiency at which GAC is regenerated, ultimately extending the lifetime for which it can perform in permeable reactive barriers.
- 7) It was further demonstrated that the GAC exterior could be continuously regenerated over four cycles of adsorption followed by regeneration. Beyond this, minimal regeneration could be achieved, possibly due to oxidation of the GAC surface that compromised its adsorptive capacity. It is recommended that future work assess how the applied electrochemical treatments affect the surface functional groups of the GAC, as well as if it can be prevented and/or reversed.
- 8) Similarly, due to the surface oxidation that results during electrochemical treatments, a continuous treatment method should be investigated whereby adsorption and regeneration occur simultaneously. The results described in Chapters 4 and 5 suggest this is a plausible option; rather than using external electrodes, instead use the GAC bed as a 3D electrode to degrade contaminants in the aqueous phase prior to adsorption on the GAC surface. Although surface oxidation would likely still occur, its effect on future adsorption processes would be irrelevant, extending the lifetime of the GAC even further.
- 9) All of the laboratory based experiments within this thesis, Chapters 4 – 6, were conducted at room temperature with an aim of determining the efficacy, mechanism, and mathematical modelling of the active chlorine and electro-Fenton pathways. As the ultimate goal is to promote such treatments in extreme environments, future work should investigate how decreased temperatures affect the resulting kinetics of the electrochemical treatments; it is anticipated that the mechanism and modelling will remain, but that lower temperatures will decelerate the reaction kinetics.
- 10) Lastly, due to the poor seasonal timing at which a field trial was conducted, it is recommended that further research go towards field scale testing and translating the laboratory based results to field deployment applications. This would ultimately

determine if such technology is applicable to permeable reactive barrier treatments, as well as to a range of industries that utilize activated carbons in their purification and processing streams.

---

## References

- [1] I. Hodgson-Johnston, A. Jackson, J. Jabour, A. Press, Cleaning up after human activity in Antarctica: Legal obligations and remediation realities, *Restor. Ecol.* 25 (2016) 135–139.
  - [2] I. Snape, S.H. Ferguson, P.M. Harvey, M.J. Riddle, Investigation of evaporation and biodegradation of fuel spills in Antarctica: II-Extent of natural attenuation at Casey Station, *Chemosphere.* 63 (2006) 89–98.
  - [3] I. Snape, M.J. Riddle, J.S. Stark, C.M. Cole, C.K. King, S. Duquesne, D.B. Gore, Management and remediation of contaminated sites at Casey Station, Antarctica, *Polar Rec. (Gr. Brit).* 37 (2001) 199–214.
  - [4] J.L. Rayner, I. Snape, J.L. Walworth, P.M. Harvey, S.H. Ferguson, Petroleum-hydrocarbon contamination and remediation by microbioventing at sub-Antarctic Macquarie Island, *Cold Reg. Sci. Technol.* 48 (2007) 139–153.
  - [5] R.S. McWatters, D. Wilkins, T. Spedding, G. Hince, B. Raymond, G. Lagerewskij, D. Terry, L. Wise, I. Snape, On site remediation of a fuel spill and soil reuse in Antarctica, *Sci. Total Environ.* 571 (2016) 963–973.
  - [6] Australian Antarctic Division, 2012/13 Annual Report, Fuel Spill Risk and Remediation Program, Macquarie Island, (2014).
  - [7] D.M. Filler, I. Snape, D.L. Barnes, *Bioremediation of petroleum hydrocarbons in cold regions*, Cambridge University Press, 2008.
  - [8] D.M. Filler, C.M. Reynolds, I. Snape, A.J. Daugulis, D.L. Barnes, P.J. Williams, Advances in Engineered Remediation for use in the Arctic and Antarctica, *Polar Rec. (Gr. Brit).* 42 (2006) 111–120.
  - [9] B.L. Freidman, D. Terry, D. Wilkins, T. Spedding, S.L. Gras, I. Snape, G.W. Stevens, K.A. Mumford, Permeable bio-reactive barriers to address petroleum hydrocarbon contamination at subantarctic Macquarie Island, *Chemosphere.* 174 (2017) 408–420.
  - [10] K.A. Mumford, S.M. Powell, J.L. Rayner, G. Hince, I. Snape, G.W. Stevens, Evaluation of a permeable reactive barrier to capture and degrade hydrocarbon contaminants, *Environ. Sci. Pollut. Res.* 22 (2015) 12298–12308.
  - [11] K.A. Mumford, J.L. Rayner, I. Snape, G.W. Stevens, Hydraulic performance of a permeable reactive barrier at Casey Station, Antarctica, *Chemosphere.* 117 (2014) 223–231.
  - [12] L. Wang, N. Balasubramanian, Electrochemical regeneration of granular activated carbon saturated with organic compounds, *Chem. Eng. J.* 155 (2009) 763–768.
  - [13] J. Wasley, T.J. Mooney, C.K. King, Soil invertebrate community change over fuel-contaminated sites on a subantarctic island: An ecological field-based line of evidence for site risk assessment, *Integr. Environ. Assess. Manag.* 12 (2016) 306–314.
  - [14] I.M. Cozzarelli, J.R. Mckelvie, A.L. Baehr, *Volatile Hydrocarbons and Fuel Oxygenates*, 2nd ed., Elsevier Ltd., 2013.
  - [15] D. Huguenot, E. Mousset, E.D. Van Hullebusch, M.A. Oturan, Combination of surfactant enhanced soil washing and electro-Fenton process for the treatment of soils contaminated by petroleum hydrocarbons, *J. Environ. Manage.* 153 (2015) 40–47.
  - [16] G. Hornig, K. Northcott, I. Snape, G. Stevens, Assessment of sorbent materials for treatment of hydrocarbon contaminated ground water in cold regions, *Cold Reg. Sci.*
-

- Technol. 53 (2008) 83–91.
- [17] I. Snape, C.E. Morris, C.M. Cole, The use of permeable reactive barriers to control contaminant dispersal during site remediation in Antarctica, *Cold Reg. Sci. Technol.* 32 (2001) 157–174.
- [18] T.M. Statham, S.C. Stark, I. Snape, G.W. Stevens, K.A. Mumford, A permeable reactive barrier (PRB) media sequence for the remediation of heavy metal and hydrocarbon contaminated water: A field assessment at Casey Station, Antarctica, *Chemosphere*. 147 (2016) 368–375.
- [19] K.A. Mumford, J.L. Rayner, I. Snape, S.C. Stark, G.W. Stevens, D.B. Gore, Design, installation and preliminary testing of a permeable reactive barrier for diesel fuel remediation at Casey Station, Antarctica, *Cold Reg. Sci. Technol.* 96 (2013) 96–107.
- [20] B.M. Van Vliet, The regeneration of activated carbon, *J. South. African Inst. Min. Metall.* 91 (1991) 159–167.
- [21] M. Sheintuch, Y.I. Matatov-Meytal, Comparison of catalytic processes with other regeneration methods of activated carbon, *Catal. Today*. 53 (1999) 73–80.
- [22] A. Bán, H. Schäfer, H. Wendt, Fundamentals of electrosorption on activated carbon for wastewater treatment of industrial effluents, *J. Electrochem.* 28 (1998) 227–236.
- [23] M.O. Omorogie, J.O. Babalola, E.I. Unuabonah, Regeneration strategies for spent solid matrices used in adsorption of organic pollutants from surface water: a critical review, *Desalin. Water Treat.* (2014) 1–27.
- [24] J.A. Bañuelos, O. García-Rodríguez, F.J. Rodríguez-Valadez, J. Manríquez, E. Bustos, A. Rodríguez, L.A. Godínez, Cathodic polarization effect on the electro-Fenton regeneration of activated carbon, *J. Appl. Electrochem.* 45 (2015) 523–531.
- [25] B. Ledesma, S. Román, A. Álvarez-Murillo, E. Sabio, J.F. González, Cyclic adsorption/thermal regeneration of activated carbons, *J. Anal. Appl. Pyrolysis*. 106 (2014) 112–117.
- [26] G. San Miguel, S.D. Lambert, N.J.D. Graham, The regeneration of field-spent granular-activated carbons, *Water Res.* 35 (2001) 2740–2748.
- [27] P.M. Álvarez, F.J. Beltrán, V. Gómez-Serrano, J. Jaramillo, E.M. Rodríguez, Comparison between thermal and ozone regenerations of spent activated carbon exhausted with phenol, *Water Res.* 38 (2004) 2155–2165.
- [28] R.M. Narbaitz, J. McEwen, Electrochemical regeneration of field spent GAC from two water treatment plants, *Water Res.* 46 (2012) 4852–4860.
- [29] R.J. Martin, W.J. Ng, Chemical Regeneration of Exhausted Activated Carbon - I, *Water Res.* 18 (1984) 59–73.
- [30] M.A. Ferro-García, J. Rivera-Utrilla, I. Bautista-Toledo, C. Moreno-Castilla, Chemical and Thermal Regeneration of an Activated Carbon Saturated with Chlorophenols, *J. Chem. Technol. Biotechnol.* 67 (1996) 183–189.
- [31] B.L. Freidman, S.L. Gras, I. Snape, G.W. Stevens, K.A. Mumford, Application of controlled nutrient release to permeable reactive barriers, *J. Environ. Manage.* 169 (2016) 145–154.
- [32] Ö. Aktaş, Ç. Ferhan, Bioregeneration of activated carbon: A review, *Int. Biodeterior. Biodegradation*. 59 (2007) 257–272.

- [33] R.M. Narbaitz, J. Cen, Electrochemical Regeneration of Granular Activated Carbon, *Water Res.* 28 (1994) 1771–1778.
- [34] M. García-Otón, F. Montilla, M.A. Lillo-Ródenas, E. Morallón, J.L. Vázquez, Electrochemical Regeneration of Activated Carbon Saturated with Toluene, *J. Appl. Electrochem.* 35 (2005) 319–325.
- [35] H. Sun, Z. Liu, Y. Wang, Y. Li, Electrochemical in situ regeneration of granular activated carbon using a three-dimensional reactor, *J. Environ. Sci.* 25 (2013) S77–S79.
- [36] M.H. Zhou, L.C. Lei, Electrochemical regeneration of activated carbon loaded with p-nitrophenol in a fluidized electrochemical reactor, *Electrochim. Acta.* 51 (2006) 4489–4496.
- [37] C.H. Weng, M.C. Hsu, Regeneration of granular activated carbon by an electrochemical process, *Sep. Purif. Technol.* 64 (2008) 227–236.
- [38] J.A. Bañuelos, F.J. Rodríguez, J. Manríquez Rocha, E. Bustos, A. Rodríguez, J.C. Cruz, L.G. Arriaga, L.A. Godínez, Novel electro-fenton approach for regeneration of activated carbon, *Environ. Sci. Technol.* 47 (2013) 7927–7933.
- [39] O. Zanella, I.C. Tessaro, L.A. Féris, Desorption- and Decomposition-Based Techniques for the Regeneration of Activated Carbon, *Chem. Eng. Technol.* 37 (2014) 1447–1459.
- [40] F. Salvador, N. Martin-Sanchez, R. Sanchez-Hernandez, M.J. Sanchez-Montero, C. Izquierdo, Regeneration of carbonaceous adsorbents. Part I: Thermal Regeneration, *Microporous Mesoporous Mater.* 202 (2015) 259–276.
- [41] F. Salvador, N. Martin-Sanchez, R. Sanchez-Hernandez, M.J. Sanchez-Montero, C. Izquierdo, Regeneration of carbonaceous adsorbents. Part II: Chemical, Microbiological and Vacuum Regeneration, *Microporous Mesoporous Mater.* 202 (2015) 277–296.
- [42] M. El Gamal, H.A. Mousa, M.H. El-Naas, R. Zacharia, S. Judd, Bio-regeneration of activated carbon: A comprehensive review, *Sep. Purif. Technol.* 197 (2018) 345–359.
- [43] R. Berenguer, J.P. Marco-Lozar, C. Quijada, D. Cazorla-amorós, E. Morallón, Comparison among Chemical, Thermal, and Electrochemical Regeneration of Phenol-Saturated Activated Carbon, *Energy Fuels.* 35 (2010) 3366–3372.
- [44] O. Zanella, D. Bilibio, W.L. Priamo, I.C. Tessaro, L.A. Féris, Electrochemical regeneration of phenol-saturated activated carbon – proposal of a reactor, *Environ. Technol.* 38 (2016) 549–557.
- [45] Y.B. Acar, A.N. Alshwabkeh, Principles of Electrokinetic Remediation, *Environ. Sci. Technol.* 27 (1993) 2638–2647.
- [46] A. Karimi-Jashni, R.M. Narbaitz, Electrochemical reactivation of granular activated carbon: pH dependence, *J. Environ. Eng. Sci.* 4 (2005) 187–194.
- [47] A. Karimi-Jashni, R.M. Narbaitz, Electrochemical Reactivation of Granular Activated Carbon: Effect of Electrolyte Mixing, *J. Environ. Eng.* 131 (2005) 443–450.
- [48] M.J. Semmens, A.B. Staples, G. Hohenstein, G.E. Norgaard, Influence of Coagulation on Removal of Organics By Granular Activated Carbon, *Am. Water Work. Assoc.* 78 (1986) 80–84.
- [49] R. Berenguer, J.P. Marco-Lozar, C. Quijada, D. Cazorla-Amorós, E. Morallón, Electrochemical regeneration and porosity recovery of phenol-saturated granular

- activated carbon in an alkaline medium, *Carbon N. Y.* 48 (2010) 2734–2745.
- [50] Y.B. Acar, R.J. Gale, A.N. Alshwabkeh, R.E. Marks, S. Puppala, M. Bricka, R. Parker, Electrokinetic remediation: Basics and technology status, *J. Hazard. Mater.* 40 (1995) 117–137.
- [51] H. Zhang, Regeneration of exhausted activated carbon by electrochemical method, *Chem. Eng. J.* 85 (2002) 81–85.
- [52] H. Zhang, L. Ye, H. Zhong, Regeneration of phenol-saturated activated carbon in an electrochemical reactor, *J. Chem. Technol. Biotechnol.* 1250 (2002) 1246–1250.
- [53] O. Savlak, B. Karabacakoğlu, Electrochemical Regeneration of Cr (VI) Saturated Granular and Powder Activated Carbon: Comparison of Regeneration Efficiency, *Ind. Eng. Chem. Res.* 53 (2014) 13171–13179.
- [54] H.A. Arafat, M. Franz, N.G. Pinto, Effect of salt on the mechanism of adsorption of aromatics on activated carbon, *Langmuir.* 15 (1999) 5997–6003.
- [55] L. Zou, G. Morris, D. Qi, Using activated carbon electrode in electrosorptive deionisation of brackish water, *Desalination.* 225 (2008) 329–340.
- [56] E.J. Bain, J.M. Calo, R. Spitz-steinberg, J. Kirchner, J. Ax, Electrosorption/Electrodesorption of Arsenic on a Granular Activated Carbon in the Presence of Other Heavy Metals, *Energy Fuels.* 24 (2010) 3415–3421.
- [57] P. Wu, L. Xia, M. Dai, L. Lin, S. Song, Electrosorption of fluoride on TiO<sub>2</sub>-loaded activated carbon in water, *Colloids Surfaces A Physicochem. Eng. Asp.* 502 (2016) 66–73.
- [58] J.-M. Beralus, R. Ruiz-Rosas, D. Cazorla-Amorós, E. Morallón, Electroadsorption of arsenic from natural water in granular activated carbon, *Front. Mater.* 1 (2014) 28.
- [59] C.C. Huang, Y.J. Su, Removal of copper ions from wastewater by adsorption/electrosorption on modified activated carbon cloths, *J. Hazard. Mater.* 175 (2010) 477–483.
- [60] J. Zou, X. Peng, M. Li, Y. Xiong, B. Wang, F. Dong, B. Wang, Electrochemical oxidation of COD from real textile wastewaters: Kinetic study and energy consumption, *Chemosphere.* 171 (2017) 332–338.
- [61] C. Comninellis, G. Chen, *Electrochemistry for the Environment*, Springer, London, 2010.
- [62] J.L. Wang, L.J. Xu, Advanced Oxidation Processes for Wastewater Treatment: Formation of Hydroxyl Radical and Application, *Crit. Rev. Environ. Sci. Technol.* 42 (2012) 251–325.
- [63] M. Panizza, G. Cerisola, Influence of anode material on the electrochemical oxidation of 2-naphthol: Part 1. Cyclic voltammetry and potential step experiments, *Electrochim. Acta.* 48 (2003) 3491–3497.
- [64] D. Rajkumar, K. Palanivelu, Electrochemical treatment of industrial wastewater, *J. Hazard. Mater.* 113 (2004) 123–129.
- [65] A. Urtiaga, I. Ortiz, A. Anglada, D. Mantzavinos, E. Diamadopoulos, Kinetic modeling of the electrochemical removal of ammonium and COD from landfill leachates, *J. Appl. Electrochem.* 42 (2012) 779–786.
- [66] A. Anglada, A. Urtiaga, I. Ortiz, Pilot scale performance of the electro-oxidation of landfill leachate at boron-doped diamond anodes, *Environ. Sci. Technol.* 43 (2009) 2035–2040.

- [67] J. Muff, E.G. Sjøgaard, Identification and fate of halogenated PAHs formed during electrochemical treatment of saline aqueous solutions, *J. Hazard. Mater.* 186 (2011) 1993–2000.
- [68] C. Zhang, Y. Jiang, Y. Li, Z. Hu, L. Zhou, M. Zhou, Three-dimensional electrochemical process for wastewater treatment: A general review, *Chem. Eng. J.* 228 (2013) 455–467.
- [69] A.M. Polcaro, M. Mascia, S.P. Palmas, A. Vacca, Kinetic study on the removal of organic pollutants by an electrochemical oxidation process, *Ind. Eng. Chem. Res.* 41 (2002) 2874–2881.
- [70] E. Brillas, I. Sires, M.A. Oturan, Electro-fenton process and related electrochemical technologies based on fenton's reaction chemistry, *Chem. Rev.* 109 (2009) 6570–6631.
- [71] C. Comninellis, Electrocatalysis in the Electrochemical Conversion / Combustion of Organic Pollutants, *Electrochim. Acta.* 39 (1994) 1857–1862.
- [72] G. Chen, Electrochemical technologies in wastewater treatment, *Sep. Purif. Technol.* 38 (2004) 11–41.
- [73] D. Wang, M. Zhou, Q. Dai, L. Lei, C. Ma, D. Wang, Long life modified lead dioxide anode for organic wastewater treatment: electrochemical characteristics and degradation mechanism, *Environ. Sci. Technol.* 39 (2005) 363–70.
- [74] A.J. Bard, L.R. Faulkner, *Electrochemical methods: fundamentals and applications.*, Wiley, New York, 2001.
- [75] J. Muff, H. Jepsen, E. Sjøgaard, Bench-Scale Study of Electrochemical Oxidation for On-Site Treatment of Polluted Groundwater, *J. Environ. Eng.* 138 (2012) 915–922.
- [76] C.A. Martínez-Huitle, M.A. Rodrigo, I. Sirés, O. Scialdone, Single and Coupled Electrochemical Processes and Reactors for the Abatement of Organic Water Pollutants: A Critical Review, *Chem. Rev.* 115 (2015) 13362–13407.
- [77] M. Deborde, U. von Gunten, Reactions of chlorine with inorganic and organic compounds during water treatment-Kinetics and mechanisms: A critical review, *Water Res.* 42 (2008) 13–51.
- [78] S. Sowmiya, R. Gandhimathi, S. Thanga, P. Ramesh, V. Nidheesh, Granular Activated Carbon as a Particle Electrode in Three-Dimensional Electrochemical Treatment of Reactive Black B from Aqueous Solution, *Environmental Prog. Sustain. Energy.* 35 (2016) 1616–1622.
- [79] R.L. Siegrist, M. Crimi, T.J. Simpkin, *In Situ Chemical Oxidation for Groundwater Remediation*, Springer, New York, 2011.
- [80] P. V. Nidheesh, R. Gandhimathi, Trends in electro-Fenton process for water and wastewater treatment: An overview, *Desalination.* 299 (2012) 1–15.
- [81] R.J. Watts, A.L. Teel, Chemistry of Modified Fenton's Reagent (Catalyzed H<sub>2</sub>O<sub>2</sub> Propagations-CHP) for In Situ Soil and Groundwater Remediation, *J. Environ. Eng.* 131 (2005) 612–622.
- [82] M. Panizza, G. Cerisola, Removal of organic pollutants from industrial wastewater by electrogenerated Fenton's reagent, *Water Res.* 35 (2001) 3987–3992.
- [83] K. Barbusiński, Fenton Reaction - Controversy Concerning the Chemistry, *Ecol. Chem. Eng. S.* 16 (2009) 347–358.

- [84] M. Zhou, L. Lei, The role of activated carbon on the removal of p-nitrophenol in an integrated three-phase electrochemical reactor, *Chemosphere*. 65 (2006) 1197–1203.
- [85] H.H. Huang, M.C. Lu, J.N. Chen, C. Te Lee, Catalytic decomposition of hydrogen peroxide and 4-chlorophenol in the presence of modified activated carbons, *Chemosphere*. 51 (2003) 935–943.
- [86] R. Tomat, A. Rigo, Electrochemical oxidation of toluene promoted by hydroxyl radicals, *J. Appl. Electrochem.* 14 (1984) 1–8.
- [87] R. Tomat, A. Rigo, Electrochemical oxidation of aliphatic hydrocarbons promoted by inorganic radicals. I. OH radicals, *J. Appl. Electrochem.* 15 (1985) 167–173.
- [88] G. Coria, I. Sirés, E. Brillas, J.L. Nava, Influence of the anode material on the degradation of naproxen by Fenton-based electrochemical processes, *Chem. Eng. J.* 304 (2016) 817–825.
- [89] E. Mousset, L. Frunzo, G. Esposito, E.D. va. Hullebusch, N. Oturan, M.A. Oturan, A complete phenol oxidation pathway obtained during electro-Fenton treatment and validated by a kinetic model study, *Appl. Catal. B Environ.* 180 (2016) 189–198.
- [90] H. Zazou, N. Oturan, M. Sönmez-Çelebi, M. Hamdani, M.A. Oturan, Mineralization of chlorobenzene in aqueous medium by anodic oxidation and electro-Fenton processes using Pt or BDD anode and carbon felt cathode, *J. Electroanal. Chem.* 774 (2016) 22–30.
- [91] J. Zhan, Y. Wang, H. Wang, W. Shen, X. Pan, J. Wang, G. Yu, Electro-peroxone regeneration of phenol-saturated activated carbon fiber: The effects of irreversible adsorption and operational parameters, *Carbon N. Y.* 109 (2016) 321–330.
- [92] L. Wei, S. Guo, G. Yan, C. Chen, X. Jiang, Electrochemical pretreatment of heavy oil refinery wastewater using a three-dimensional electrode reactor, *Electrochim. Acta.* 55 (2010) 8615–8620.
- [93] G. Lv, D. Wu, R. Fu, Performance of carbon aerogels particle electrodes for the aqueous phase electro-catalytic oxidation of simulated phenol wastewaters, *J. Hazard. Mater.* 165 (2009) 961–966.
- [94] C. He, T. An, X. Zhu, H. Karlsson, Removal of Formic Acid from Wastewater using Three-Phase Three-Dimensional Electrode Reactor, *Water Air Soil Pollut.* 144 (2003) 67–79.
- [95] J.A. Bañuelos, A. El-ghenymy, F.J. Rodríguez, J. Manríquez, E. Bustos, A. Rodríguez, E. Brillas, L.A. Godínez, Study of an Air Diffusion Activated Carbon Packed Electrode for an Electro-Fenton Wastewater Treatment, *Electrochim. Acta.* 140 (2014) 412–418.
- [96] A.M. Polcaro, S. Palmas, F. Renoldi, M. Mascia, Three-dimensional electrodes for the electrochemical combustion of organic pollutants, *Electrochim. Acta.* 46 (2000) 389–394.
- [97] I. Bouaziz, M. Hamza, A. Sellami, R. Abdelhedi, A. Savall, K. Groenen Serrano, New hybrid process combining adsorption on sawdust and electrooxidation using a BDD anode for the treatment of dilute wastewater, *Sep. Purif. Technol.* 175 (2017) 1–8.
- [98] P. Cañizares, J. Lobato, J. García-Gómez, M.A. Rodrigo, Combined adsorption and electrochemical processes for the treatment of acidic aqueous phenol wastes, *J. Appl. Electrochem.* 34 (2004) 111–117.
- [99] C. Gong, G. Shen, H. Huang, P. He, Z. Zhang, B. Ma, Removal and transformation of polycyclic aromatic hydrocarbons during electrocoagulation treatment of an industrial



- wastewater, *Chemosphere*. 168 (2017) 58–64.
- [100] B. Hou, H. Han, S. Jia, H. Zhuang, P. Xu, K. Li, Three-dimensional heterogeneous electro-Fenton oxidation of biologically pretreated coal gasification wastewater using sludge derived carbon as catalytic particle electrodes and catalyst, *J. Taiwan Inst. Chem. Eng.* 60 (2015) 352–360.
- [101] N.W. Brown, E.P.L. Roberts, A.A. Garforth, R.A.W. Dryfe, Electrochemical regeneration of a carbon-based adsorbent loaded with crystal violet dye, 49 (2004) 3269–3281.
- [102] L. Wang, Y. Hu, P. Li, Y. Zhang, Q. Yan, Y. Zhao, Electrochemical treatment of industrial wastewater using a novel layer-upon-layer bipolar electrode system (nLBPEs), *Chem. Eng. J.* 215–216 (2013) 157–161.
- [103] D. Rahner, G. Ludwig, J. Röhrs, Electrochemically induced reactions in soils — a new approach to the in-situ remediation of contaminated soils? Part 1: The microconductor principle, *Electrochim. Acta.* 47 (2002) 1395–1403.
- [104] F. Mavr e, R.K. Anand, D.R. Laws, K.F. Chow, B.Y. Chang, J.A. Crooks, R.M. Crooks, Bipolar electrodes: A useful tool for concentration, separation, and detection of analytes in microelectrochemical systems, *Anal. Chem.* 82 (2010) 8766–8774.
- [105] S.E. Fosdick, K.N. Knust, K. Scida, R.M. Crooks, Bipolar electrochemistry, *Angew. Chemie - Int. Ed.* 52 (2013) 10438–10456.
- [106] D. Liu, E.P.L. Roberts, A.D. Martin, S.M. Holmes, N.W. Brown, A.K. Campen, N. de las Heras, Electrochemical regeneration of a graphite adsorbent loaded with Acid Violet 17 in a spouted bed reactor, *Chem. Eng. J.* 304 (2016) 1–9.
- [107] R.M. Narbaitz, A. Karimi-jashni, Electrochemical reactivation of granular activated carbon: Impact of reactor configuration, *Chem. Eng. J.* 197 (2012) 414–423.
- [108] Y. Li, J.M. Kemper, G. Datuin, A. Akey, W.A. Mitch, R.G. Luthy, Reductive dehalogenation of disinfection byproducts by an activated carbon-based electrode system, *Water Res.* 98 (2016) 354–362.
- [109] X. Li, W. Zhu, C. Wang, L. Zhang, Y. Qian, F. Xue, Y. Wu, The electrochemical oxidation of biologically treated citric acid wastewater in a continuous-flow three-dimensional electrode reactor (CTDER), *Chem. Eng. J.* 232 (2013) 495–502.
- [110] R.M. Narbaitz, A. Karimi-Jashni, Electrochemical regeneration of granular activated carbons loaded with phenol and natural organic matter, *Environ. Technol.* 30 (2009) 27–36.
- [111] C.O. Ania, Electrochemical Regeneration of Activated Carbon Cloth Exhausted with Bentazone, *Environ. Sci. Technol.* 42 (2008) 4500–4506.
- [112] X.Y. You, L.Y. Chai, Y.Y. Wang, Y.R. Su, N. Zhao, Y. De Shu, Regeneration of activated carbon adsorbed EDTA by electrochemical method, *Trans. Nonferrous Met. Soc. China (English Ed.)* 23 (2013) 855–860.
- [113] Z. Hu, M. Beuret, H. Khan, P.A. Ariya, Development of a recyclable remediation system for gaseous BTEX: Combination of iron oxides nanoparticles adsorbents and electrochemistry, *ACS Sustain. Chem. Eng.* 2 (2014) 2739–2747.
- [114] N.W. Brown, E.P.L. Roberts, A. Chasiotis, T. Cherdron, N. Sanghrajka, Atrazine removal using adsorption and electrochemical regeneration, 38 (2004) 3067–3074.

- [115] B. Hou, H. Han, H. Zhuang, P. Xu, S. Jia, K. Li, A novel integration of three-dimensional electro-Fenton and biological activated carbon and its application in the advanced treatment of biologically pretreated Lurgi coal gasification wastewater, *Bioresour. Technol.* 196 (2015) 721–725.
- [116] L. Wang, Y. Zhao, J. Fu, The influence of TiO<sub>2</sub> and aeration on the kinetics of electrochemical oxidation of phenol in packed bed reactor, *J. Hazard. Mater.* 160 (2008) 608–613.
- [117] ArviaTechnology, Making Wastewater Safe to Resuse or Discharge, (2017). <http://www.arviatechnology.com/> (accessed October 14, 2017).
- [118] N.W. Brown, E.P.L. Roberts, Adsorption of Contaminants from Liquid and Electrochemical Regeneration of Adsorbent, WO2011058298 (A1), 2011.
- [119] N.W. Brown, E.P.L. Roberts, Treatment of Contaminated Liquids, US8936726 (B2), 2015.
- [120] N.W. Brown, E.P.L. Roberts, Apparatus for the Electrochemical Regeneration of Absorbents, WO2007125334 (A1), 2007.
- [121] S.N. Hussain, E.P.L. Roberts, H.M.A. Asghar, A.K. Campen, N.W. Brown, Oxidation of phenol and the adsorption of breakdown products using a graphite adsorbent with electrochemical regeneration, *Electrochim. Acta.* 92 (2013) 20–30.
- [122] N.W. Brown, E.P.L. Roberts, Electrochemical pre-treatment of effluents containing chlorinated compounds using an adsorbent, *J. Appl. Electrochem.* 37 (2007) 1329–1335.
- [123] N.W. Brown, E.P.L. Roberts, Combining adsorption with anodic oxidation as an innovative technique for removal and destruction of organics, *Water Sci. Technol.* 68 (2013) 1216–1222.
- [124] E. Lindberg, Improvement in and relating to the treatment of matrices and/or the contents of matrices, WO2016087461 (A1), 2016.
- [125] Eko Harden Technologies Oy, EKOGRID, Amplifying Remediat. Power Nat. (2020). <http://ekogrid.fi/> (accessed November 3, 2017).
- [126] F.R. Doring, N. Doring, Method and device for the elimination of toxic materials from, in particular, the topsoil, US5595644A, 1997.
- [127] J. Röhrs, G. Ludwig, D. Rahner, Electrochemically induced reactions in soils — a new approach to the in-situ remediation of contaminated soils? Part 2: remediation experiments with a natural soil containing highly chlorinated hydrocarbons, *Electrochem. Acta.* 47 (2002) 1405–1414.
- [128] B.L. Freidman, The Development and Contribution of Bio-Reactive Materials for Petroleum Hydrocarbon Remediation in the Antarctic, University of Melbourne, 2016.
- [129] P. Woodberry, G. Stevens, I. Snape, S. Stark, Removal of metal contaminants from saline waters at low temperature by an iminodiacetic acid ion-exchange resin, Thala Valley Tip, Casey Station, Antarctica, *Solvent Extr. Ion Exch.* 23 (2005) 289–306.
- [130] E. Brillas, C.A. Martínez-Huitle, Decontamination of wastewaters containing synthetic organic dyes by electrochemical methods. An updated review, *Appl. Catal. B Environ.* 166–167 (2015) 603–643.
- [131] C.A. Martínez-Huitle, S. Ferro, Electrochemical oxidation of organic pollutants for the wastewater treatment: direct and indirect processes, *Chem. Soc. Rev.* 35 (2006) 1324–

- 1340.
- [132] F.C. Moreira, R.A.R. Boaventura, E. Brillas, V.J.P. Vilar, Electrochemical advanced oxidation processes: A review on their application to synthetic and real wastewaters, *Appl. Catal. B Environ.* 202 (2017) 217–261.
- [133] M. Panizza, G. Cerisola, Direct And Mediated Anodic Oxidation of Organic Pollutants, *Chem. Rev.* 109 (2009) 6541–6569.
- [134] Y. Feng, L. Yang, J. Liu, B.E. Logan, Electrochemical technologies for wastewater treatment and resource reclamation, *Environ. Sci. Water Res. Technol.* 2 (2016) 800–831.
- [135] A.M. Sales Solano, C.K. Costa de Araújo, J. Vieira de Melo, J.M. Peralta-Hernandez, D. Ribeiro da Silva, C.A. Martínez-Huitle, Decontamination of real textile industrial effluent by strong oxidant species electrogenerated on diamond electrode: Viability and disadvantages of this electrochemical technology, *Appl. Catal. B Environ.* 130–131 (2013) 112–120.
- [136] N. Mohan, N. Balasubramanian, C.A. Basha, Electrochemical oxidation of textile wastewater and its reuse, *J. Hazard. Mater.* 147 (2007) 644–651.
- [137] Á. Anglada, A. Urtiaga, I. Ortiz, D. Mantzavinos, E. Diamadopoulos, Boron-doped diamond anodic treatment of landfill leachate: Evaluation of operating variables and formation of oxidation by-products, *Water Res.* 45 (2011) 828–838.
- [138] A. V. Moreno-Palacios, R.E. Palma-Goyes, J. Vazquez-Arenas, R.A. Torres-Palma, Bench-scale reactor for Cefadroxil oxidation and elimination of its antibiotic activity using electro-generated active chlorine, *J. Environ. Chem. Eng.* 7 (2019) 103173.
- [139] M. Mascia, A. Vacca, A.M. Polcaro, S. Palmas, J.R. Ruiz, A. Da Pozzo, Electrochemical treatment of phenolic waters in presence of chloride with boron-doped diamond (BDD) anodes: Experimental study and mathematical model, *J. Hazard. Mater.* 174 (2010) 314–322.
- [140] A.S. Fajardo, H.F. Seca, R.C. Martins, V.N. Corceiro, I.F. Freitas, M.E. Quinta-Ferreira, R.M. Quinta-Ferreira, Electrochemical oxidation of phenolic wastewaters using a batch-stirred reactor with NaCl electrolyte and Ti/RuO<sub>2</sub>anodes, *J. Electroanal. Chem.* 785 (2017) 180–189.
- [141] D.A. Szánto, S. Cleghorn, C. Ponce-De-León, F.C. Walsh, The Limiting Current for Reduction of Ferricyanide Ion at Nickel: The Importance of Experimental Conditions, *AIChE J.* 54 (2008) 802–810.
- [142] C. Ponce-De-León, C.T.J. Low, G. Kear, F.C. Walsh, Strategies for the determination of the convective-diffusion limiting current from steady state linear sweep voltammetry, *J. Appl. Electrochem.* 37 (2007) 1261–1270.
- [143] R. V. McQuillan, G.W. Stevens, K.A. Mumford, The electrochemical regeneration of granular activated carbons: A review, *J. Hazard. Mater.* 355 (2018) 34–49.
- [144] J. Muff, E.G. Sjøgaard, Electrochemical degradation of PAH compounds in process water: A kinetic study on model solutions and a proof of concept study on runoff water from harbour sediment purification, *Water Sci. Technol.* 61 (2010) 2043–2051.
- [145] Y. Xiao, J.M. Hill, Mechanistic insights for the electro-Fenton regeneration of carbon materials saturated with methyl orange: Dominance of electrodesorption, *J. Hazard. Mater.* 367 (2019) 59–67.

- [146] W. Zhou, L. Rajic, L. Chen, K. Kou, Y. Ding, X. Meng, Y. Wang, B. Mulaw, J. Gao, Y. Qin, A.N. Alshwabkeh, Activated carbon as effective cathode material in iron-free Electro-Fenton process: Integrated H<sub>2</sub> O<sub>2</sub> electrogeneration, activation, and pollutants adsorption, *Electrochim. Acta.* 296 (2019) 317–326.
- [147] H.I. Abdel-Shafy, M.S.M. Mansour, A review on polycyclic aromatic hydrocarbons: Source, environmental impact, effect on human health and remediation, *Egypt. J. Pet.* 25 (2016) 107–123.
- [148] W. Jury, W. Spencer, W. Farmer, Behavior Assessment Model for Trace Organics in Soil: III. Application of Screening Model, *J. Environ. Qual.* 13 (1984) 573–579.
- [149] National Water Quality Management Strategy, Australian and New Zealand Environment and Conservation Council and Agriculture and Resource Management Council of Australia and New Zealand, Canberra, 2000.
- [150] N.J. Bunce, L. Liu, J. Zhu, D.A. Lane, Reaction of naphthalene and its derivatives with hydroxyl radicals in the gas phase, *Environ. Sci. Technol.* 31 (1997) 2252–2259.
- [151] A.M. Polcaro, A. Vacca, M. Mascia, S. Palmas, J. Rodriguez Ruiz, Electrochemical treatment of waters with BDD anodes: Kinetics of the reactions involving chlorides, *J. Appl. Electrochem.* 39 (2009) 2083–2092.
- [152] Instrumental methods in electrochemistry., Chichester : E. Horwood ; New York : Halsted Press, 1985., 1985.
- [153] M.R. Cruz-Díaz, E.P. Rivero, F.A. Rodríguez, R. Domínguez-Bautista, Experimental study and mathematical modeling of the electrochemical degradation of dyeing wastewaters in presence of chloride ion with dimensional stable anodes (DSA) of expanded meshes in a FM01-LC reactor, *Electrochim. Acta.* 260 (2018) 726–737.
- [154] A. Özcan, M.A. Oturan, Degradation of picloram by the electro-Fenton process, *J. Hazard. Mater.* 153 (2008) 718–727.
- [155] J.G. Vos, Z. Liu, F.D. Speck, N. Perini, W. Fu, S. Cherevko, M.T.M. Koper, Selectivity Trends between Oxygen Evolution and Chlorine Evolution on Iridium-Based Double Perovskites in Acidic Media, *ACS Catal.* 9 (2019) 8561–8574.
- [156] J.H. Entwisle, Consumption of graphite anodes in chlorine manufacture by brine electrolysis \*, *J. Appl. Electrochem.* 4 (1974) 293–303.
- [157] V. Díaz, R. Ibáñez, P. Gómez, A.M. Urriaga, I. Ortiz, Kinetics of electro-oxidation of ammonia-N, nitrites and COD from a recirculating aquaculture saline water system using BDD anodes, *Water Res.* 45 (2011) 125–134.
- [158] A. Urriaga, P. Gómez, A. Arruti, I. Ortiz, Electrochemical removal of tetrahydrofuran from industrial wastewaters: Anode selection and process scale-up, *J. Chem. Technol. Biotechnol.* 89 (2014) 1243–1250.
- [159] K. Scott, Reactor modelling for electrochemical processes, *J. Chem. Technol. Biotechnol.* 54 (1992) 257–266.
- [160] G. Panizza, M; Bocca, C.; Cerisola, Electrochemical treatment of wastewater containing polyaromatic organic pollutants, *Water Res.* 34 (2000) 2601–2605.
- [161] P. Canizares, J. Garcia-Gomez, J. Lobato, M. a Rodrigo, Modeling of wastewater electro-oxidation processes part II. Application to active electrodes, *Ind. Eng. Chem. Res.* 43

- (2004) 1923–1931.
- [162] F. Walsh, G. Reade, Design and Performance of Electrochemical Reactors for Efficient Synthesis and Environmental Treatment Part 1. Electrode Geometry and Figures of Merit, *Analyst*. 119 (1994) 791–796.
- [163] M. Panizza, A. Kapalka, C. Comninellis, Oxidation of organic pollutants on BDD anodes using modulated current electrolysis, *Electrochim. Acta*. 53 (2008) 2289–2295.
- [164] J.M. Aquino, G.F. Pereira, R.C. Rocha-Filho, N. Bocchi, S.R. Biaggio, Electrochemical degradation of a real textile effluent using boron-doped diamond or  $\beta$ -PbO<sub>2</sub> as anode, *J. Hazard. Mater.* 192 (2011) 1275–1282.
- [165] L. Tran, P. Drogui, G. Mercier, J.-F. Blais, Comparison between Fenton oxidation process and electrochemical oxidation for PAH removal from an amphoteric surfactant solution, *J. Appl. Electrochem.* 40 (2010) 1493–1510.
- [166] S.N. Hussain, H.M.A. Asghar, H. Sattar, N.W. Brown, E.P.L. Roberts, Chlorinated breakdown products formed during oxidation of adsorbed phenol by electrochemical regeneration of a graphite intercalation compound, *J. Ind. Eng. Chem.* 30 (2015) 212–219.
- [167] X. Xu, R. Xiao, D.D. Dionysiou, R. Spinney, T. Fu, Q. Li, Z. Wang, D. Wang, Z. Wei, Kinetics and mechanisms of the formation of chlorinated and oxygenated polycyclic aromatic hydrocarbons during chlorination, *Chem. Eng. J.* 351 (2018) 248–257.
- [168] S.D. Boyce, J.F. Hornig, Reaction Pathways of Trihalomethane Formation from the Halogenation of Dihydroxyaromatic Model Compounds for Humic Acid, *Environ. Sci. Technol.* 17 (1983) 202–211.
- [169] J.J. Pignatello, E. Oliveros, A. MacKay, Advanced oxidation processes for organic contaminant destruction based on the fenton reaction and related chemistry, *Crit. Rev. Environ. Sci. Technol.* 36 (2006) 1–84.
- [170] X. Liu, Y. Zhou, J. Zhang, L. Luo, Y. Yang, H. Huang, H. Peng, L. Tang, Y. Mu, Insight into electro-Fenton and photo-Fenton for the degradation of antibiotics: Mechanism study and research gaps, *Chem. Eng. J.* 347 (2018) 379–397.
- [171] R.J. Watts, A.L. Teel, Treatment of contaminated soils and groundwater using ISCO, *Pract. Period. Hazardous, Toxic, Radioact. Waste Manag.* 10 (2006) 2–9.
- [172] N. Oturan, M.A. Oturan, *Electro-Fenton Process: Background, New Developments, and Applications*, Elsevier Inc., 2018.
- [173] I. Sirés, E. Brillas, M.A. Oturan, M.A. Rodrigo, M. Panizza, Electrochemical advanced oxidation processes: Today and tomorrow. A review, *Environ. Sci. Pollut. Res.* 21 (2014) 8336–8367.
- [174] H. Liu, X.Z. Li, Y.J. Leng, C. Wang, Kinetic modeling of electro-Fenton reaction in aqueous solution, *Water Res.* 41 (2007) 1161–1167.
- [175] E. Mousset, N. Oturan, E.D. Van Hullebusch, G. Guibaud, G. Esposito, M.A. Oturan, Influence of solubilizing agents ( cyclodextrin or surfactant ) on phenanthrene degradation by electro-Fenton process e Study of soil washing recycling possibilities and environmental impact, *Water Res.* 48 (2013) 306–316.
- [176] E. Petrucci, A. Da Pozzo, L. Di Palma, On the ability to electrogenerate hydrogen peroxide

- and to regenerate ferrous ions of three selected carbon-based cathodes for electro-Fenton processes, *Chem. Eng. J.* 283 (2016) 750–758.
- [177] M.A. Oturan, An ecologically effective water treatment technique using electrochemically generated hydroxyl radicals for in situ destruction of organic pollutants: Application to herbicide 2,4-D, *J. Appl. Electrochem.* 30 (2000) 475–482.
- [178] S. Qiu, D. He, J. Ma, T. Liu, T.D. Waite, Kinetic Modeling of the Electro-Fenton Process: Quantification of Reactive Oxygen Species Generation, *Electrochim. Acta.* 176 (2015) 51–58.
- [179] L. Yan, Y. Wang, J. Li, H. Ma, H. Liu, T. Li, Y. Zhang, Comparative study of different electrochemical methods for petroleum refinery wastewater treatment, *Desalination.* 341 (2014) 87–93.
- [180] I. Sirés, J.A. Garrido, R.M. Rodríguez, E. Brillas, N. Oturan, M.A. Oturan, Catalytic behavior of the Fe<sup>3+</sup>/Fe<sup>2+</sup> system in the electro-Fenton degradation of the antimicrobial chlorophene, *Appl. Catal. B Environ.* 72 (2007) 382–394.
- [181] C. Flox, S. Ammar, C. Arias, E. Brillas, A.V. Vargas-Zavala, R. Abdelhedi, Electro-Fenton and photoelectro-Fenton degradation of indigo carmine in acidic aqueous medium, *Appl. Catal. B Environ.* 67 (2006) 93–104.
- [182] M.M. Ghoneim, H.S. El-Desoky, N.M. Zidan, Electro-Fenton oxidation of Sunset Yellow FCF azo-dye in aqueous solutions, *Desalination.* 274 (2011) 22–30.
- [183] H.S. El-Desoky, M.M. Ghoneim, R. El-Sheikh, N.M. Zidan, Oxidation of Levafix CA reactive azo-dyes in industrial wastewater of textile dyeing by electro-generated Fenton's reagent, *J. Hazard. Mater.* 175 (2010) 858–865.
- [184] G. Xia, Y. Lu, H. Xu, Electrogeneration of hydrogen peroxide for electro-Fenton via oxygen reduction using polyacrylonitrile-based carbon fiber brush cathode, *Electrochim. Acta.* 158 (2015) 390–396.
- [185] A. Wang, J. Qu, J. Ru, H. Liu, J. Ge, Mineralization of an azo dye Acid Red 14 by electro-Fenton's reagent using an activated carbon fiber cathode, *Dye. Pigment.* 65 (2005) 227–233.
- [186] Y. Gong, J. Li, Y. Zhang, M. Zhang, X. Tian, A. Wang, Partial degradation of levofloxacin for biodegradability improvement by electro-Fenton process using an activated carbon fiber felt cathode, *J. Hazard. Mater.* 304 (2016) 320–328.
- [187] A. Özcan, Y. Şahin, A.S. Kopal, M.A. Oturan, A comparative study on the efficiency of electro-Fenton process in the removal of prophan from water, *Appl. Catal. B Environ.* 89 (2009) 620–626.
- [188] A. Özcan, Y. Şahin, A. Savaş Kopal, M.A. Oturan, Carbon sponge as a new cathode material for the electro-Fenton process: Comparison with carbon felt cathode and application to degradation of synthetic dye basic blue 3 in aqueous medium, *J. Electroanal. Chem.* 616 (2008) 71–78.
- [189] M. Panizza, G. Cerisola, Electro-Fenton degradation of synthetic dyes, *Water Res.* 43 (2009) 339–344.
- [190] H. Roth, Y. Gendel, P. Buzatu, O. David, M. Wessling, Tubular carbon nanotube-based gas diffusion electrode removes persistent organic pollutants by a cyclic adsorption - Electro-Fenton process, *J. Hazard. Mater.* 307 (2016) 1–6.

- 
- [191] N. Klidi, F. Proietto, F. Vicari, A. Galia, S. Ammar, A. Gadri, O. Scialdone, Electrochemical treatment of paper mill wastewater by electro-Fenton process, *J. Electroanal. Chem.* 841 (2019) 166–171.
- [192] G. Gao, Q. Zhang, Z. Hao, C.D. Vecitis, Carbon nanotube membrane stack for flow-through sequential regenerative electro-Fenton, *Environ. Sci. Technol.* 49 (2015) 2375–2383.
- [193] X. Zhang, J. Fu, Y. Zhang, L. Lei, A nitrogen functionalized carbon nanotube cathode for highly efficient electrocatalytic generation of H<sub>2</sub>O<sub>2</sub> in Electro-Fenton system, *Sep. Purif. Technol.* 64 (2008) 116–123.
- [194] J. Casado, Towards industrial implementation of Electro-Fenton and derived technologies for wastewater treatment: A review, *J. Environ. Chem. Eng.* 7 (2019) 102823.
- [195] Z. Lu, G. Chen, S. Siahrostami, Z. Chen, K. Liu, J. Xie, L. Liao, T. Wu, Di. Lin, Y. Liu, T.F. Jaramillo, J.K. Nørskov, Y. Cui, High-efficiency oxygen reduction to hydrogen peroxide catalysed by oxidized carbon materials, *Nat. Catal.* 1 (2018) 156–162.
- [196] R. V. McQuillan, G.W. Stevens, K.A. Mumford, Electrochemical removal of naphthalene from contaminated waters using carbon electrodes, and viability for environmental deployment, *J. Hazard. Mater.* 383 (2020).
- [197] R.L. Johnson, P.C. Johnson, D.B. McWhorter, R.E. Hincee, I. Goodman, An Overview of In Situ Air Sparging, *Groundw. Monit. Remediat.* 13 (1993) 127–135. .
- [198] W.C. Schumb, C.N. Satterfield, R.L. Wentworth, *Hydrogen Peroxide*, Reinhold Publishing Corporation, New York, 1955.
- [199] A.C. Kumoro, R. Ratnawati, D.S. Retnowati, Reaction and mass transfer kinetics model of hydrogen peroxide oxidation of starch under influence of ultraviolet irradiation, *Period. Polytech. Chem. Eng.* 61 (2017) 236–245.
- [200] W. Zhou, X. Meng, J. Gao, A.N. Alshwabkeh, Hydrogen peroxide generation from O<sub>2</sub> electroreduction for environmental remediation: A state-of-the-art review, *Chemosphere.* 225 (2019) 588–607.
- [201] G. Matyszczyk, A. Sędkowska, S. Kuś, Comparative degradation of Metanil Yellow in the electro-Fenton process with different catalysts: A simplified kinetic model study, *Dye. Pigment.* 174 (2020) 3–8.
- [202] E. Brillas, A review on the photoelectro-Fenton process as efficient electrochemical advanced oxidation for wastewater remediation. Treatment with UV light, sunlight, and coupling with conventional and other photo-assisted advanced technologies, *Chemosphere.* 250 (2020) 126198.
- [203] P. Kaur, V.K. Sangal, J.P. Kushwaha, Parametric study of electro-Fenton treatment for real textile wastewater, disposal study and its cost analysis, *Int. J. Environ. Sci. Technol.* 16 (2019) 801–810.
- [204] Y. Feng, L. Yang, J. Liu, B.E. Logan, Environmental technologies for wastewater treatment and resource reclamation, *Environ. Sci. Water Res. Technol.* 2 (2016) 800–831.
- [205] K. Cui, H. Yi, Z.J. Zhou, Q.F. Zhuo, Y.X. Bing, Q.W. Guo, Z.C. Xu, Fenton oxidation kinetics and intermediates of nonylphenol ethoxylates, *Environ. Eng. Sci.* 31 (2014) 217–224.

- [206] A. Babuponnusami, K. Muthukumar, A review on Fenton and improvements to the Fenton process for wastewater treatment, *J. Environ. Chem. Eng.* 2 (2014) 557–572.
- [207] F.J. Rivas, F.J. Beltrán, J. Frades, P. Buxeda, Oxidation of p-hydroxybenzoic acid by Fenton's reagent, *Water Res.* 35 (2001) 387–396.
- [208] S. Huo, D. Necas, F. Zhu, D. Chen, J. An, N. Zhou, L. Wang, Y. Cheng, Y. Liu, R. Ruan, Anaerobic digestion wastewater decolorization by H<sub>2</sub>O<sub>2</sub>-enhanced electro-Fenton coagulation following nutrients recovery via acid tolerant and protein-rich *Chlorella* production, *Chem. Eng. J.* (2020) 127160.
- [209] J.Y. Lee, D.A. Lane, Unique products from the reaction of naphthalene with the hydroxyl radical, *Atmos. Environ.* 43 (2009) 4886–4893.
- [210] M. Popescu, C. Sandu, E. Rosales, M. Pazos, G. Lazar, M.Á. Sanromán, Evaluation of different cathodes and reaction parameters on the enhancement of the electro-Fenton process, *J. Electroanal. Chem.* 808 (2018) 455–463.
- [211] A.A. Özcan, A. Özcan, Investigation of applicability of Electro-Fenton method for the mineralization of naphthol blue black in water, *Chemosphere.* 202 (2018) 618–625.
- [212] W. Yang, M. Zhou, N. Oturan, Y. Li, M.A. Oturan, Electrocatalytic destruction of pharmaceutical imatinib by electro-Fenton process with graphene-based cathode, *Electrochim. Acta.* 305 (2019) 285–294.
- [213] M. Pimentel, N. Oturan, M. Dezotti, M.A. Oturan, Phenol degradation by advanced electrochemical oxidation process electro-Fenton using a carbon felt cathode, *Appl. Catal. B Environ.* 83 (2008) 140–149.
- [214] Pubchem, Pubchem, (2020). <https://pubchem.ncbi.nlm.nih.gov/>.
- [215] H. Monteil, Y. Péchaud, N. Oturan, M.A. Oturan, A review on efficiency and cost effectiveness of electro- and bio-electro-Fenton processes: Application to the treatment of pharmaceutical pollutants in water, *Chem. Eng. J.* 376 (2019) 119577.
- [216] C. Rücker, W.M.M. Mahmoud, D. Schwartz, K. Kümmere, Biodegradation tests of mercaptocarboxylic acids, their esters, related divalent sulfur compounds and mercaptans, *Environ. Sci. Pollut. Res.* 25 (2018) 18393–18411.
- [217] K.Y. Foo, B.H. Hameed, Insights into the modeling of adsorption isotherm systems, *Chem. Eng. J.* 156 (2010) 2–10.
- [218] R.M. Narbaitz, J. Cen, Alternative methods for determining the percentage regeneration of activated carbon, *Water Res.* 31 (1997) 2532–2542.
- [219] A. Celzard, J.F. Maréché, F. Payot, G. Furdin, Electrical conductivity of carbonaceous powders, *Carbon N. Y.* 40 (2002) 2801–2815.
- [220] J.M. Montes, F.G. Cuevas, J. Cintas, Electrical resistivity of a titanium powder mass, *Granul. Matter.* 13 (2011) 439–446.
- [221] W.L. McCabe, J.C. Smith, P. Harriott, *Unit operations of chemical engineering.*, 7th ed. /, McGraw-Hill, 2005.
- [222] C.O. Ania, B. Cabal, J.B. Parra, A. Arenillas, B. Arias, J.J. Pis, Naphthalene adsorption on activated carbons using solvents of different polarity, *Adsorption.* 14 (2008) 343–355.
- [223] C.H. Giles, D. Smith, A. Huitson, *A General Treatment and Classification of the Solute*



- Adsorption Isotherm, *J. Colloid Interface Sci.* 47 (1974) 755–765.
- [224] R.L. Tseng, F.C. Wu, Inferring the favorable adsorption level and the concurrent multi-stage process with the Freundlich constant, *J. Hazard. Mater.* 155 (2008) 277–287.
- [225] J. Churchill, Remediation of contaminated meltwater in remote climates (Unpublished doctoral thesis), University of Melbourne, Australia, 2020.
- [226] A. Dąbrowski, P. Podkościelny, Z. Hubicki, M. Barczak, Adsorption of phenolic compounds by activated carbon - A critical review, *Chemosphere.* 58 (2005) 1049–1070.
- [227] K.A. Wilson, J.L. Kellie, S.D. Wetmore, DNA-protein  $\pi$ -interactions in nature: Abundance, structure, composition and strength of contacts between aromatic amino acids and DNA nucleobases or deoxyribose sugar, *Nucleic Acids Res.* 42 (2014) 6726–6741.
- [228] J.H. Deng, J. Luo, Y.L. Mao, S. Lai, Y.N. Gong, D.C. Zhong, T.B. Lu,  $\pi$ - $\pi$  stacking interactions: Non-negligible forces for stabilizing porous supramolecular frameworks, *Sci. Adv.* 6 (2020) 1–9.
- [229] I. Pikaar, A.A. Koelmans, P.C.M. van Noort, Sorption of organic compounds to activated carbons. Evaluation of isotherm models, *Chemosphere.* 65 (2006) 2343–2351.
- [230] M.A. Abdullah, L. Chiang, M. Nadeem, Comparative evaluation of adsorption kinetics and isotherms of a natural product removal by Amberlite polymeric adsorbents, *Chem. Eng. J.* 146 (2009) 370–376.
- [231] K.A. Northcott, J. Bacus, N. Taya, Y. Komatsu, J.M. Perera, G.W. Stevens, Synthesis and characterization of hydrophobic zeolite for the treatment of hydrocarbon contaminated ground water, *J. Hazard. Mater.* 183 (2010) 434–440.
- [232] N. Brown, E. Roberts, D. Eaton, A. Adeyemi, APPARATUS AND METHOD FOR AQUEOUS ORGANIC WASTE TREATMENT, US 2015/0191367 A1, 2015.
- [233] Y.-Y. Yu, D.-D. Zhai, R.-W. Si, J.-Z. Sun, X. Liu, Y.-C. Yong, Three-Dimensional Electrodes for High-Performance Bioelectrochemical Systems, *Int. J. Mol. Sci.* 18 (2017) 90.
- [234] A.I. Zárate-Guzmán, J. Manríquez-Rocha, R. Antaño-López, F.J. Rodríguez-Valadez, L.A. Godínez, Study of the Electrical Properties of a Packed Carbon Bed for Its Potential Application as a 3D-Cathode in Electrochemical Processes, *J. Electrochem. Soc.* 165 (2018) E460–E465.
- [235] B. Marinho, M. Ghislandi, E. Tkalya, C.E. Koning, G. de With, Electrical conductivity of compacts of graphene, multi-wall carbon nanotubes, carbon black, and graphite powder, *Powder Technol.* 221 (2012) 351–358.
- [236] T. Adinaveen, J.J. Vijaya, L.J. Kennedy, Comparative Study of Electrical Conductivity on Activated Carbons Prepared from Various Cellulose Materials, *Arab. J. Sci. Eng.* 41 (2016) 55–65.
- [237] L. Yan, H. Ma, B. Wang, Y. Wang, Y. Chen, Electrochemical treatment of petroleum refinery wastewater with three-dimensional multi-phase electrode, *Desalination.* 276 (2011) 397–402.
- [238] C.J.H. King, Current Distribution in a Thin Bipolar Electrode System, *Electrochim. Acta.* 22 (1977) 1135–1139.
- [239] L. Wang, Y. Zhao, Q. Gao, C. Qian, Y. Hu, A new strategy for determination of current efficiency during electro-oxidation of aromatic compounds in a packed-bed system,

- Water Sci. Technol. 63 (2011) 2685.
- [240] Z. Liu, B. Ren, H. Ding, H. He, H. Deng, C. Zhao, P. Wang, D.D. Dionysiou, Simultaneous regeneration of cathodic activated carbon fiber and mineralization of desorbed contaminations by electro-peroxydisulfate process: Advantages and limitations, *Water Res.* 171 (2020) 115456.
- [241] R. Berenguer, J.P. Marco-Lozar, C. Quijada, D. Cazorla-Amorós, E. Morallón, Effect of electrochemical treatments on the surface chemistry of activated carbon, *Carbon N. Y.* 47 (2009) 1018–1027.
- [242] Y. Xiao, J.M. Hill, Impact of Pore Size on Fenton Oxidation of Methyl Orange Adsorbed on Magnetic Carbon Materials: Trade-Off between Capacity and Regenerability, *Environ. Sci. Technol.* 51 (2017) 4567–4575.
- [243] J.W. Choi, N.C. Choi, S.J. Lee, D.J. Kim, Novel three-stage kinetic model for aqueous benzene adsorption on activated carbon, *J. Colloid Interface Sci.* 314 (2007) 367–372.
- [244] Y. Marcus, Volumes of aqueous hydrogen and hydroxide ions at 0 to 200 °c, *J. Chem. Phys.* 137 (2012) 0–5.
- [245] NIST Polycyclic Aromatic Hydrocarbon Structure Index, (2015).
- [246] Q. Chen, H. Liu, Z. Yang, D. Tan, Regeneration performance of spent granular activated carbon for tertiary treatment of dyeing wastewater by Fenton reagent and hydrogen peroxide, *J. Mater. Cycles Waste Manag.* 19 (2017) 256–264.
- [247] S.R. Qasim, G. Zhu, *Wastewater Treatment and Reuse Theory and Design Examples, Volume 2: Post-Treatment, Reuse, and Disposal*, CRC Press, Boca Raton, 2017.
- [248] F. Meng, G. Li, B. Zhang, J. Guo, Chemical kinetics and particle size effects of activated carbon for free chlorine removal from drinking water, *Water Pract. Technol.* 14 (2019) 19–26.
- [249] B. Li, H. Zhang, W. Zhang, L. Huang, J. Duan, J. Hu, W. Ying, Cost effective activated carbon treatment process for removing free chlorine from water, *Asia-Pacific J. Chem. Eng.* 5 (2010) 714–720. doi:10.1002/apj.
- [250] *Dechlorination with Activated Carbon*, Marshall, 1990.
- [251] B. Skibinski, C. Götze, E. Worch, W. Uhl, Pore diffusion limits removal of monochloramine in treatment of swimming pool water using granular activated carbon, *Water Res.* 132 (2018) 270–281.
- [252] R. Berenguer, J.P. Marco-Lozar, C. Quijada, D. Cazorla-Amorós, E. Morallón, A comparison between oxidation of activated carbon by electrochemical and chemical treatments, *Carbon N. Y.* 50 (2012) 1123–1134. doi:10.1016/j.carbon.2011.10.025.
- [253] J. Acuña-Bedoya, J.A. Comas-Cabrales, C.E. Alvarez-Pugliese, N. Marriaga-Cabrales, Evaluation of electrolytic reactor configuration for the regeneration of granular activated carbon saturated with methylene blue, *J. Environ. Chem. Eng.* 8 (2020) 104074.
- [254] A. Deryło-Marczewska, K. Skrzypczyńska, K. Kuśmierk, A. Świątkowski, M. Zienkiewicz-Strzałka, The adsorptive properties of oxidized activated carbons and their applications as carbon paste electrode modifiers, *Adsorption.* 25 (2019) 357–366.
- [255] M. Panizza, P. a. Michaud, G. Cerisola, C. Comninellis, Anodic oxidation of 2-naphthol at boron-doped diamond electrodes, *J. Electroanal. Chem.* 507 (2001) 206–214.

- 
- [256] L. Wang, Y. Hu, Y. Zhang, P. Li, Y. Zhao, A novel cost-saving strategy for electrochemical oxidation of organic matters by multi-current controlled operation, *Sep. Purif. Technol.* 109 (2013) 18–22.
- [257] L. Wang, B. Wu, P. Li, B. Zhang, N. Balasubramanian, Y. Zhao, Kinetics for electro-oxidation of organic pollutants by using a packed-bed electrode reactor (PBER), *Chem. Eng. J.* 284 (2016) 240–246.
- [258] O. Garcia-Rodriguez, A. Villot, H. Olvera-Vargas, C. Gerente, Y. Andres, O. Lefebvre, Impact of the saturation level on the electrochemical regeneration of activated carbon in a single sequential reactor, *Carbon N. Y.* 163 (2020) 265–275.
- [259] Y. Xiong, C. He, H.T. Karlsson, X. Zhu, Performance of three-phase three-dimensional electrode reactor for the reduction of COD in simulated wastewater-containing phenol, *Chemosphere.* 50 (2003) 131–136.
- [260] D. Fernández, I. Robles, F.J. Rodríguez-Valadez, L.A. Godínez, Novel arrangement for an electro-Fenton reactor that does not require addition of iron, acid and a final neutralization stage. Towards the development of a cost-effective technology for the treatment of wastewater., *Chemosphere.* 199 (2018) 251–255.
- [261] C. Zhang, M. Zhou, X. Yu, L. Ma, F. Yu, Modified iron-carbon as heterogeneous electro-Fenton catalyst for organic pollutant degradation in near neutral pH condition: Characterization, degradation activity and stability, *Electrochim. Acta.* 160 (2015) 254–262.
- [262] B. Hou, H. Han, S. Jia, H. Zhuang, P. Xu, D. Wang, Heterogeneous electro-Fenton oxidation of catechol catalyzed by nano-Fe<sub>3</sub>O<sub>4</sub>: Kinetics with the Fermi's equation, *J. Taiwan Inst. Chem. Eng.* 56 (2015) 138–147.
- [263] 2D Electrostatics Applet, (2020). <http://falstad.com/emstatic/index.html>.
- [264] J.L. Nava, M.T. Oropeza, C. Ponce de León, J. González-García, A.J. Frías-Ferrer, Determination of the effective thickness of a porous electrode in a flow-through reactor; effect of the specific surface area of stainless steel fibres, used as a porous cathode, during the deposition of Ag(I) ions, *Hydrometallurgy.* 91 (2008) 98–103.
- [265] L.A.M. Ruotolo, J.C. Gubulin, A mathematical model to predict the electrode potential profile inside a polyaniline-modified reticulate vitreous carbon electrode operating in the potentiostatic reduction of Cr(VI), *Chem. Eng. J.* 171 (2011) 1170–1177.
- [266] L.A.M. Ruotolo, J.C. Gubulin, A factorial-design study of the variables affecting the electrochemical reduction of Cr(VI) at polyaniline-modified electrodes, *Chem. Eng. J.* 110 (2005) 113–121.



---

# **Appendix A**

---

Supplementary Data

---

## A.1 Active Chlorine

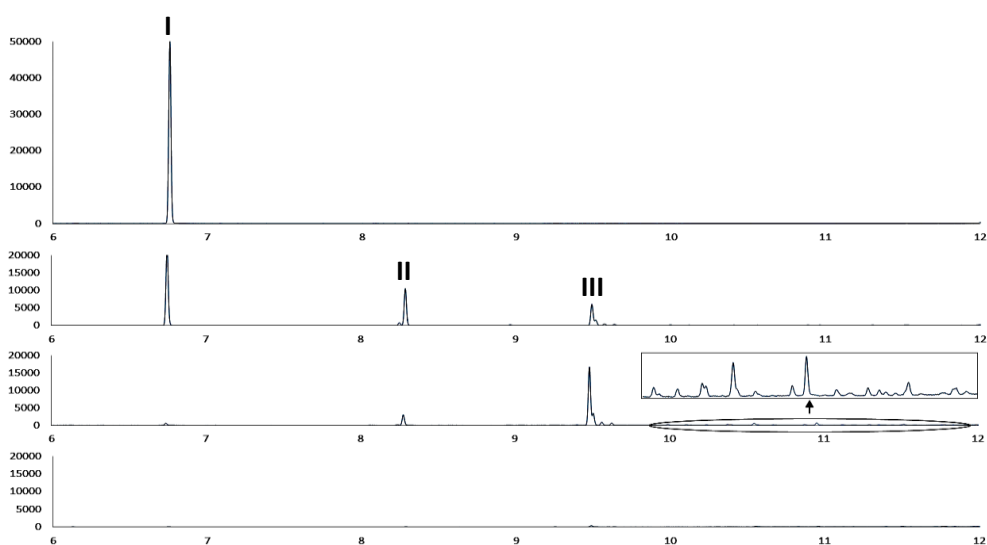


Figure A.1: GC-FID detection of active chlorine by-products at (from top to bottom), 0, 3, 15, and 120 minutes of treatment. Peak I - Naphthalene, Peak II - chloro-naphthalene, Peak III - dichloro-naphthalene.

## A.2 Electro-Fenton

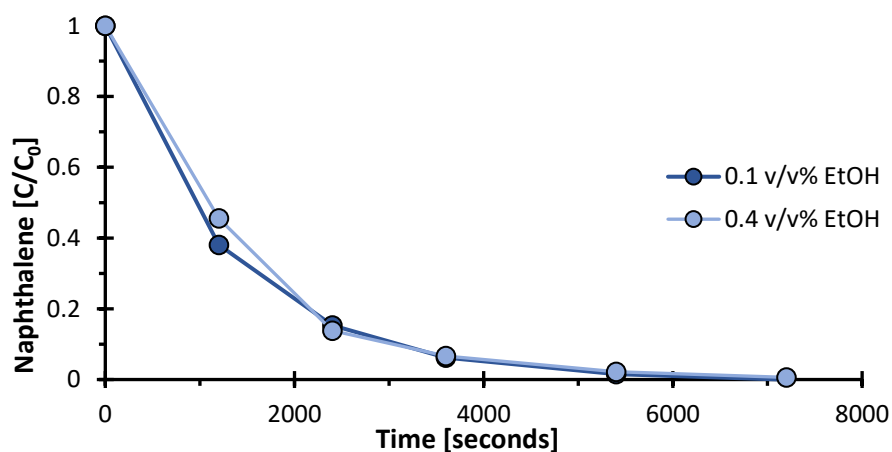


Figure A.2: Effect of ethanol concentration on naphthalene removal.

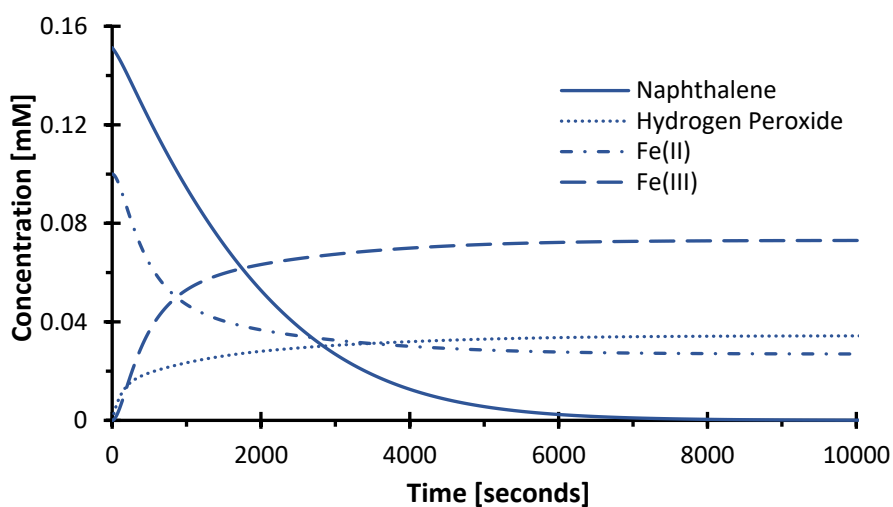


Figure A.3: Model predictions of species concentrations against time during the electro-Fenton reaction pathway.

## A.3 GAC Regeneration

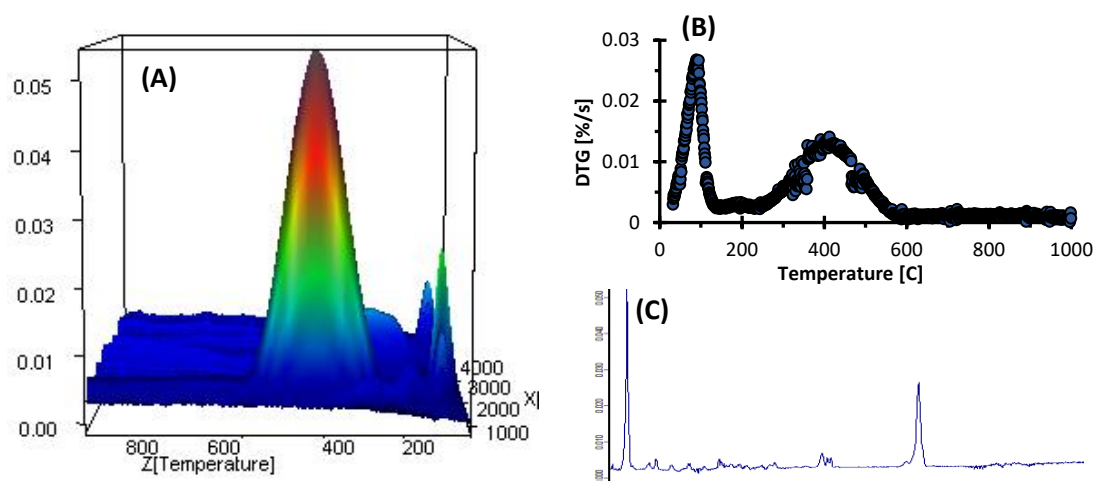


Figure A.4: Thermal gravimetric analysis – fourier transform infrared detection (TGA-FTIR) of naphthalene desorption from GC1200 GAC. (A) FTIR absorbance as a function of temperature, (B) Derivative thermogravimetric (DTG) curve, and (C) FTIR spectrum of naphthalene. Naphthalene is not seen to desorb until temperatures of 250 °C

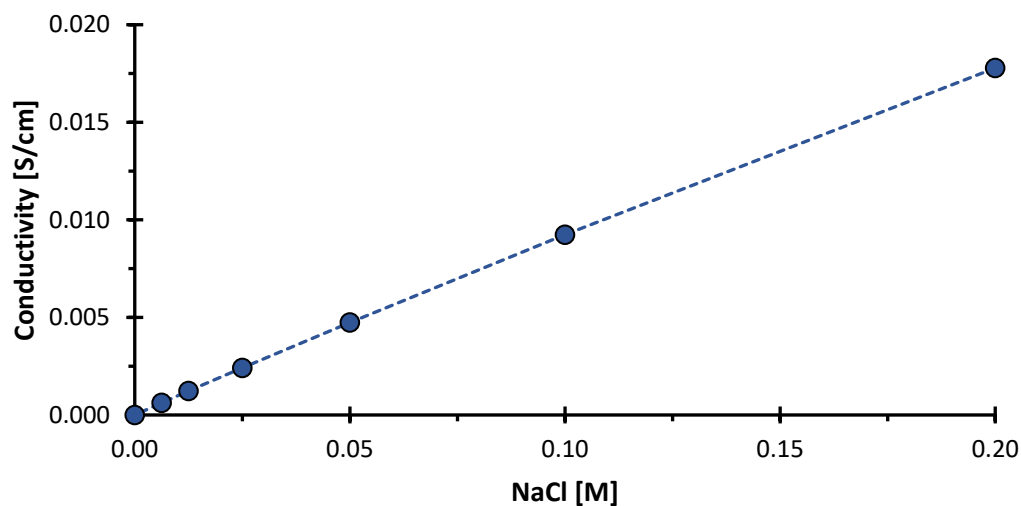


Figure A.5: Conductivity of aqueous NaCl solutions as a function of concentration at room temperature.

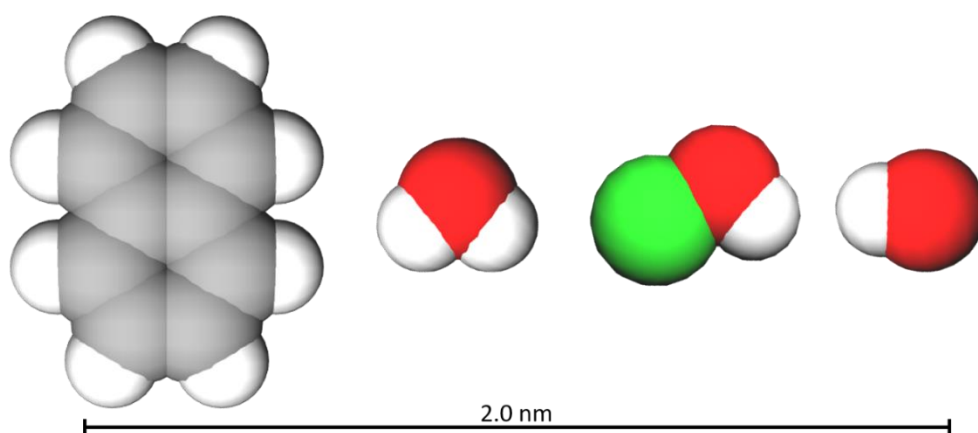


Figure A.6: Molecular structures and relative sizes of (left to right) naphthalene, water, hypochlorous acid, and hydroxyl radicals. The scale of a micropore (2 nm) is also shown.

A.4 Field Trial

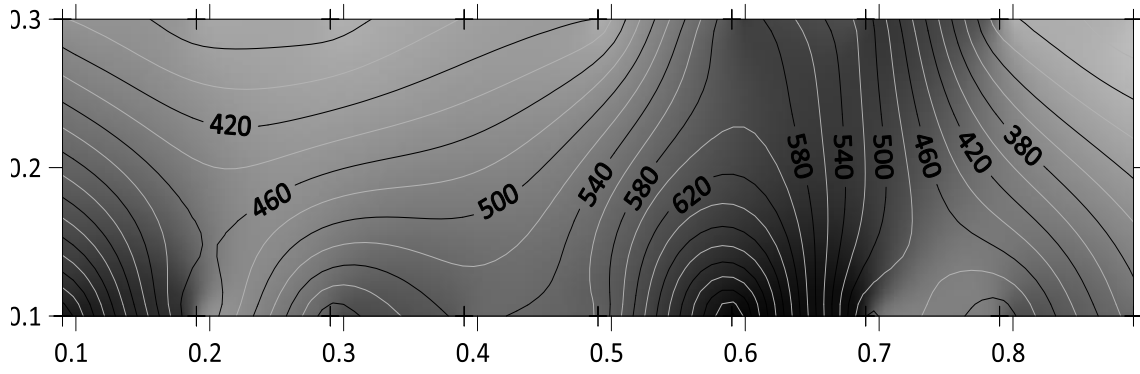


Figure A.7: Post-treatment solid TPH loadings (mg/kg) at a depth of 30 – 45 cm.

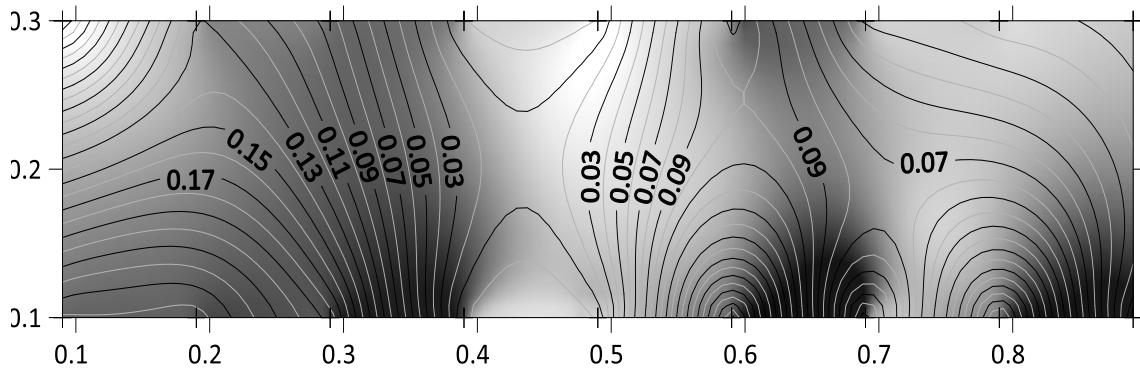


Figure A.8: Post-treatment solid naphthalene loadings (mg/kg) at a depth of 30 – 45 cm.

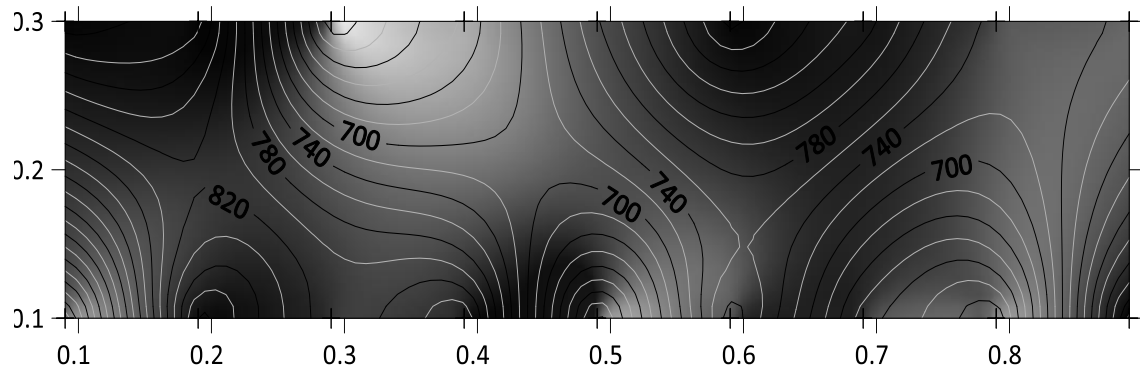


Figure A.9: Post-treatment solid TPH loadings (mg/kg) at a depth of 45 – 60 cm.

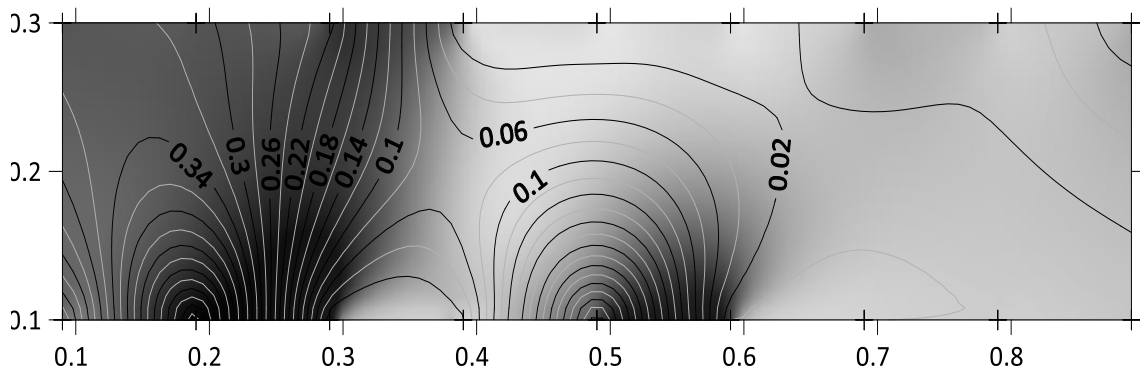


Figure A.10: Post-treatment solid naphthalene loadings (mg/kg) at a depth of 45 – 60 cm.



---

# **Appendix B**

---

Data Analysis

---

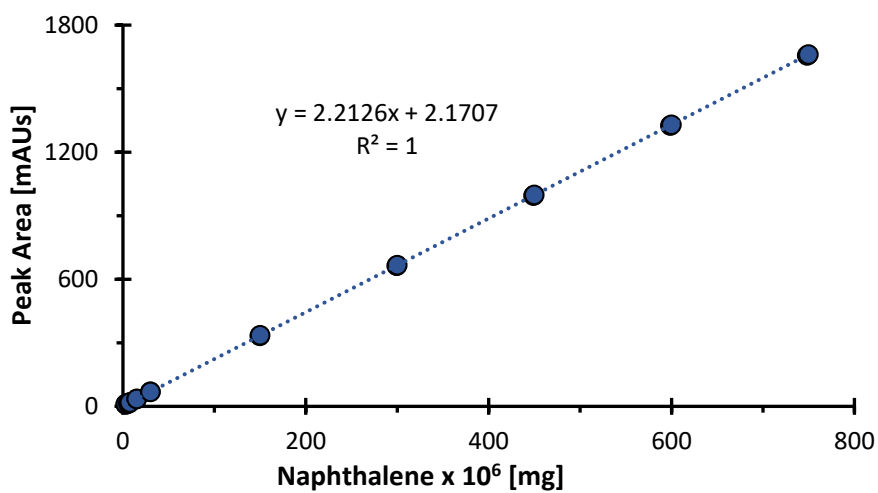


Figure B.1: Calibration curve for naphthalene detection via HPLC-DAD at 275 nm.

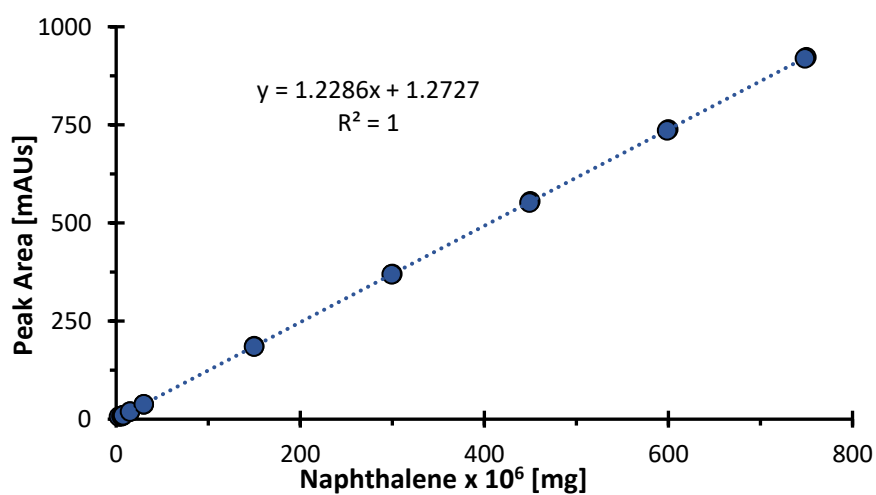


Figure B.2: Calibration curve for naphthalene detection via HPLC-DAD at 254 nm.

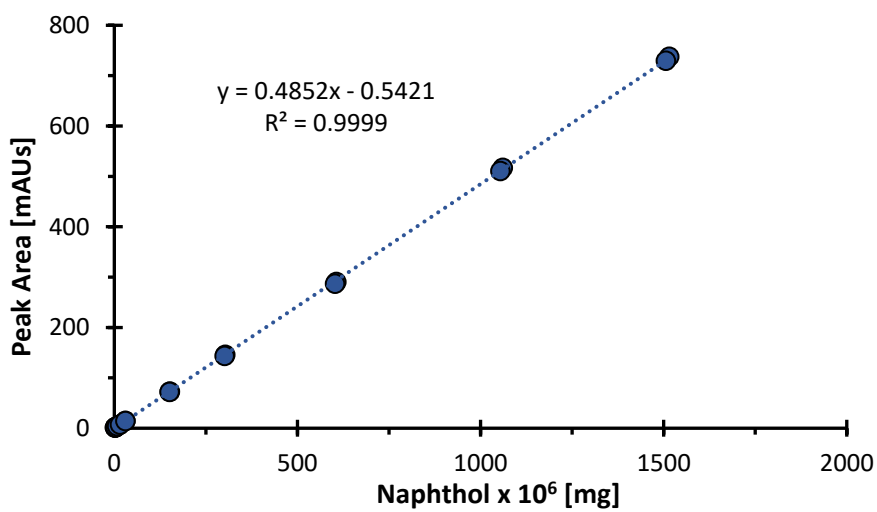


Figure B.3: Calibration curve for 1-naphthol detection via HPLC-DAD at 275 nm.

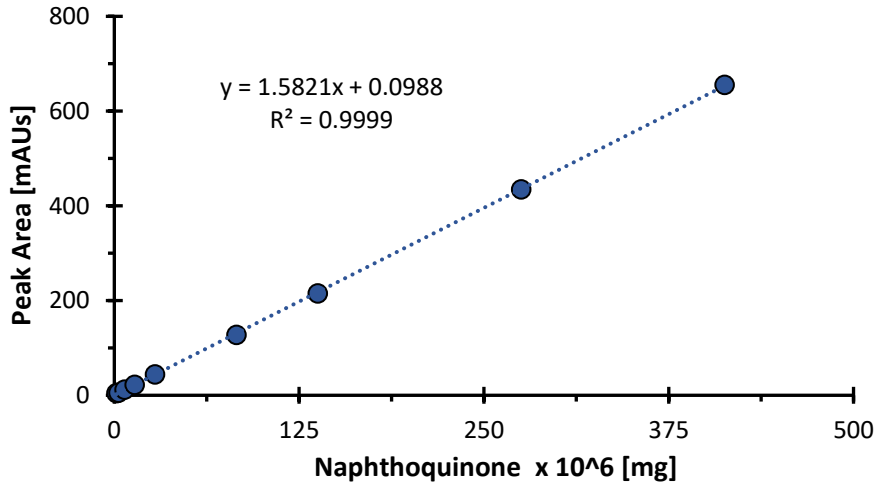


Figure B.4: Calibration curve for 1,4-naphthoquinone detection via HPLC-DAD at 230 nm.

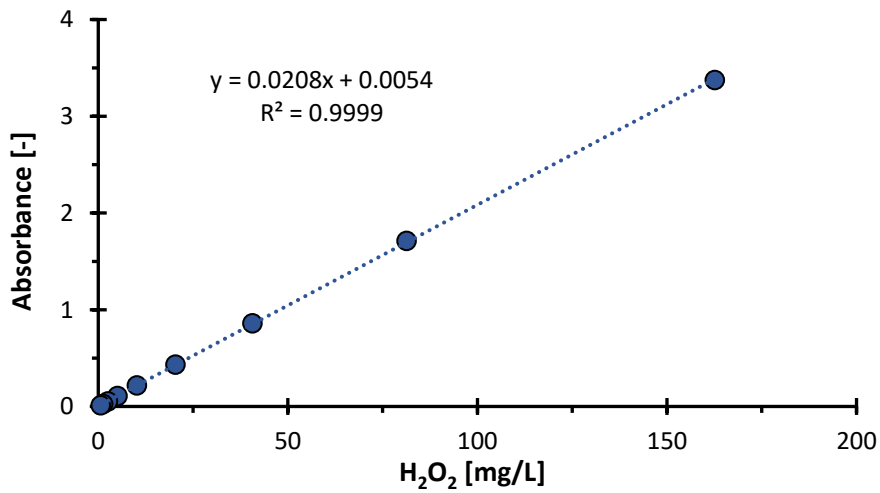


Figure B.5: Calibration curve for H<sub>2</sub>O<sub>2</sub> detection via UV/Vis at 409 nm.

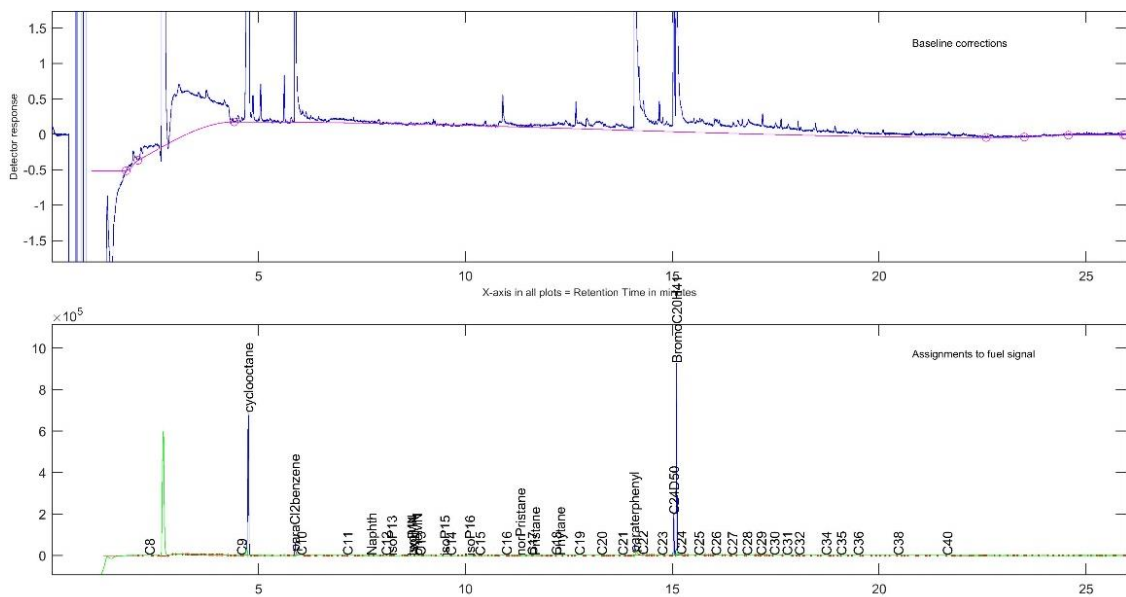


Figure B.6: GC-FID chromatogram for TPH detection - blank (SAB internal standard).

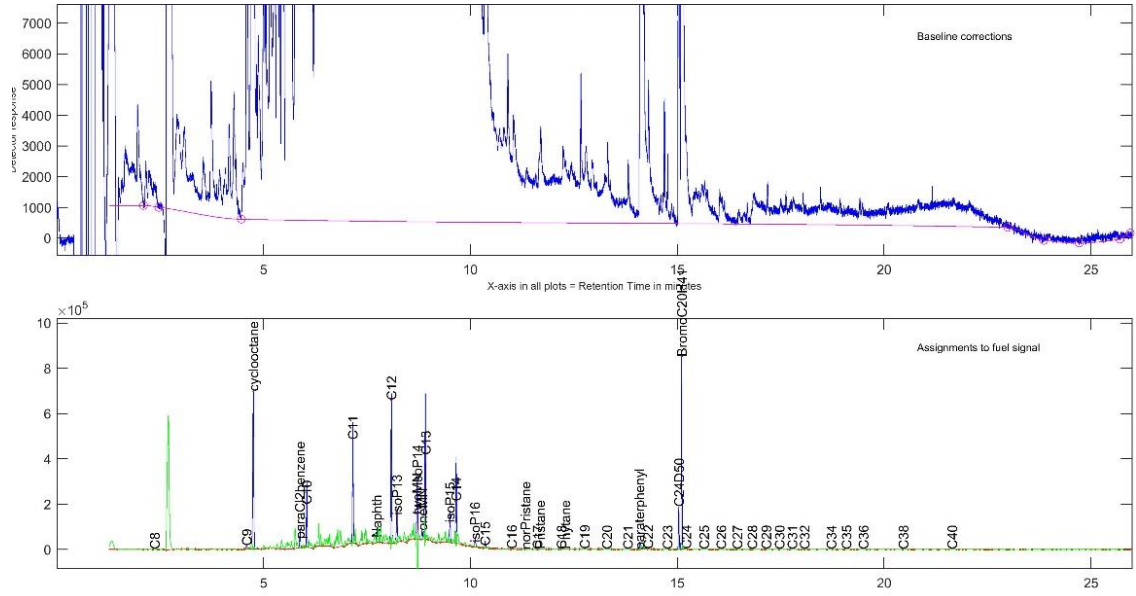


Figure B.7: GC-FID chromatogram for TPH detection – blank recovery (SAB internal standard + spike).

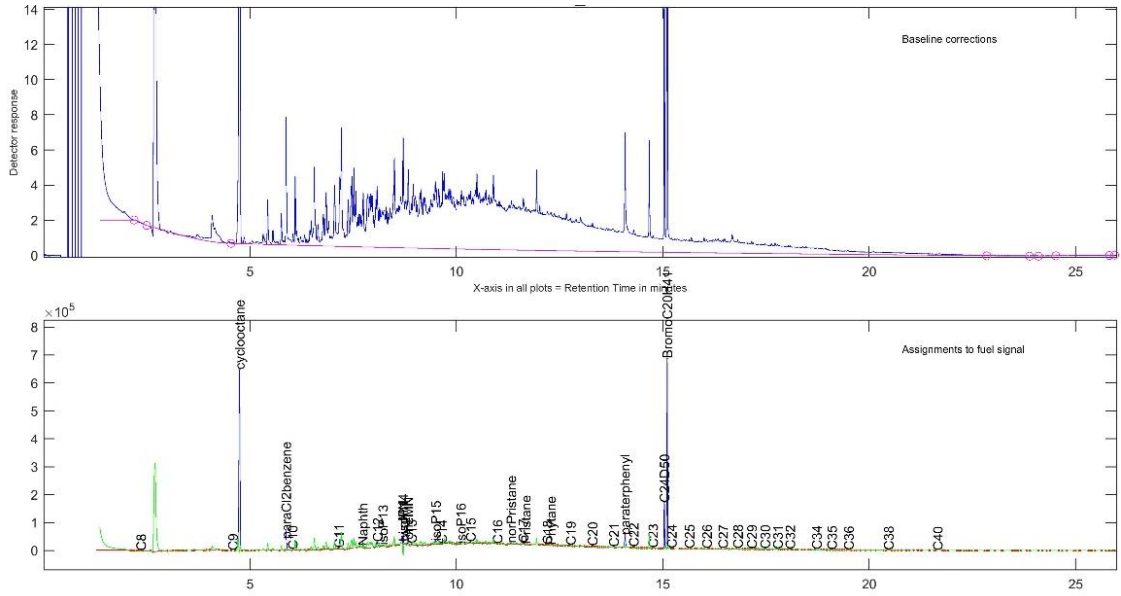


Figure B.8: GC-FID chromatogram for TPH detection – PRB sample.

---

# Appendix C

---

MATLAB Code

---

For Chapters 4 – 6 of this thesis, MATLAB was used to solve the relevant system of ordinary differential equations (ODEs). The ODE15S multistep solver was used to solve the ODEs, whilst the NLINFIT tool was used to minimize the difference between the experimental data and the model equations using a least squares method estimation; for each fitting parameter, initial guesses were made based on available literature values.

The following MATLAB code is an example of what was used to solve the ODEs and determine unknown parameters in the active chlorine study.

Running Script:

```
%import data from excel file-----
dataset = xlsread('ACData.xlsx', '100mA');

time = dataset(:,1);
naph = dataset(:,2);

plot(time, naph, 'o')

xlabel('Time [min]')
ylabel('C/Co')
title('Naphthalene Degradation')
axis([0 time(end) 0 1])

options = statset('Display', 'iter');
format long

[values] = nlinfit(time, naph, @ACRun, [2.2 1], options);

global epsilon alpha;
epsilon = values(1);
alpha = values(2);

Naph0 = 0.0001488847594254; % starting naphthalene concentration [mol/L]
[t,y] = ode15s('AC', [0:10:7200], [Naph0, 0]);

plot(t, y(:,1), '-b', time, naph, 'o', t, y(:,2), '-r');
```

---

```
function y = ACRun(a,x)
    global epsilon alpha;

    epsilon = a(1);
    alpha = a(2);

    Naph0 = 0.0001488847594254; % starting naphthalene concentration [mol/L]

    [t,y] = ode15s('AC', [0:10:7200], [Naph0, 0]);

    y = interp1(t, y(:,1), x);

end
```

---

```
function dx = AC(t,x)
    global epsilon alpha;

    % epsilon = current efficiency, [-]
    % alpha = reaction rate k[Naph][AC], [L mol-1 s-1]

    dx = [0; 0];
```

---

```

% CONSTANTS:
kvol = 0.0000729623; % volatilization rate of naphthalene [s-1]
n = 2; % electrons in oxidation of Cl to AC [-]
F = 96485; % Faraday's constant [C/mol]
V = 0.2; % reactor volume [L]
a = 5.15; % specific electrode area [m-1]
km = 0.0021; % mass transfer coefficient [m/s]
% VARIABLE INPUTS:
I = 0.1; % applied electric current [C/s]
NaCl0 = 0.1; % initial NaCl concentration [M]
% REACTION RATES:
r1 = alpha; % alpha = reaction rate k[Naph][AC], [L mol-1 s-1]
eff = epsilon; % epsilon = current efficiency, [-]

% x(1) = Naphthalene
% x(2) = AC

% eff = 14.53*NaCl0+0.14

dx(1) = -kvol*x(1) - r1*x(1)*x(2);
dx(2) = (eff*I)/(n*F*V) - a*km*x(2) - r1*x(1)*x(2);

```

```
end
```

Following parameter optimization and refinement, the fitness landscape around the solution was assessed to ensure valid initial guesses were used.

```

% Generate a 3D Mesh, one point at a time

for i=[1:101]
  for j=[1:101]
    % Transform alpha and epsilon into log-space
    a = 10^(.04*j-6);
    e = 10^(.04*i-6);

    % Get the estimates for the given alpha and epsilon
    points = ACrun([a e], time);

    % Calculate the error as the sum of the squared residuals
    error(i,j) = sum((naph - points).^2);
  end

  % Display a countdown as this is a long process.
  disp(180-i);
end

surface(error)

% Display the fitness landscape surface(error);

for i = [0:30]
  ang = 180 + 3*i; % rotate horizontally
  elv = 45 - 1.5*i; % rotate vertically
  view(ang, elv); % set the viewing angle

  % Create a new file name for the new frame
  name = sprintf('frames/frame-%02d.png', i);

  % Save the current figure as a png file using the file
  % name specified above.
  print('-dpng', name);
end

```







**Minerva Access is the Institutional Repository of The University of Melbourne**

**Author/s:**

McQuillan, Rebecca Victoria

**Title:**

The electrochemical regeneration of granular activated carbons in situ of permeable reactive barriers

**Date:**

2020

**Persistent Link:**

<http://hdl.handle.net/11343/265746>

**File Description:**

Final thesis file

**Terms and Conditions:**

Terms and Conditions: Copyright in works deposited in Minerva Access is retained by the copyright owner. The work may not be altered without permission from the copyright owner. Readers may only download, print and save electronic copies of whole works for their own personal non-commercial use. Any use that exceeds these limits requires permission from the copyright owner. Attribution is essential when quoting or paraphrasing from these works.